Selective ion separation by supported liquid membranes under electrodialysis conditions

Qian, Z.

Important note
To cite this publication, please use the final published version (if applicable).
Please check the document version above.

Selective ion separation by supported liquid membranes under electrodialysis conditions

Selective ion separation by supported liquid membranes under electrodialysis conditions

Dissertation

For the purpose of obtaining the degree of doctor
at Delft University of Technology
by the authority of the Rector Magnificus Prof. dr. ir
T.H.J.J. van der Hagen Chair of the Board for Doctorates
To be defended publicly on
Friday 16 September 2022 at 12:30 o'clock

Zexin Qian

Master of Science in Chemical Engineering,
University of Cincinnati, United States of America,
born in Xi'an, China

This dissertation has been approved by the promotor[s].

Composition of the doctoral committee:

Rector Magnificus,	Chairperson
Prof. dr. E.J.R. Sudhölter	Delft University of Technology, promoter
Dr. ir. L.C.P.M de Smet	Wageningen University & Research, promoter

Other member:

Dr. H. Miedema	Wetsus

Dr. H. Miedema has, as supervisor, contributed significantly to the preparation of this dissertation.

Independent members:

Prof. dr. ir. L.C. Rietveld	Delft University of Technology
Prof. dr. ir. R.G.H. Lammertink	University of Twente
Prof. dr. ir. E.R. Cornelissen	University of Ghent
Prof. T. He	Chinese Academy of Sciences

Water is the driving force of all nature.

- Leonardo da Vinci -

Table of Contents

Summary

Selective ion separation by supported liquid membranes under electrodialysis conditions

Electrodialysis (ED) is a membrane-based process in which ions are transported under the influence of an externally applied electrical potential. Ion-exchange membranes (IEMs) are key components in ED processes. There are two types of IEMs: (1) cation-exchange membranes (CEMs), which contain fixed, negatively charged groups, and (2) anion-exchange membranes (AEMs), which contain fixed, positively charged groups. ED processes have been widely applied for water desalination. This thesis investigates the application of ED in the treatment of drainage water of greenhouses. A key objective in sustainable greenhouse horticulture is the recirculation of drainage water, thereby minimizing the water volume used, which would otherwise be disposed into the environment.[1] The drainage water of greenhouses contains both K^+ and Na^+. Whereas K^+ is a valuable nutrient, Na^+ is detrimental for plant growth. Because of its toxicity, the Na^+ level should be controlled below the crop-specific threshold.[2-4] Because Na^+ is not taken up by plants, it accumulates and the excess needs to be removed. The main challenge here is to selectively separate and remove Na^+ without removing K^+ and other key nutrients like Ca^{2+} and Mg^{2+}. Na^+ and K^+ are two competitive cations ion separations as they have the same valence (+1), quite similar crystal and hydrated radii and a rather similar transport behavior (*i.e.* electrophoretic mobility), causing that separation by charge, size, and/or mobility is challenging. This thesis focusses on the development and characterization of a membrane-based process for the selective removal of Na^+.

An overview of this, related topics and challenges is given in Chapter 1.

In Chapter 2, a theoretical model, which is essentially based on mass balances, is presented for the Na^+ and K^+ concentrations in the irrigation and drainage water of greenhouses, in this case for cultivating tomatoes. The model not only describes the accumulation of Na^+, but also includes the implementation of a membrane-based unit for the selective removal of Na^+. Based on real-life greenhouse parameters, the model

calculates the Na^+ and K^+ concentrations at three reference points. These process parameters include the evapotranspiration, which is the process of transferring water from the soil to the surrounding environment by evaporation and transpiration by the plants, the K^+ uptake by the plants, the Na^+ and K^+ content of the fertilizer, the Na^+ leaching out from the hydroponic substrate material, and the assumed Na^+ and K^+ removal efficiency of the membrane unit. The prime aim of this initial study is to explore the requirements and to set future guidelines for the Na^+-selective membrane to-be-developed. It is concluded that in order to retain the Na^+ below the, for tomatoes, threshold of 20 mM, requires Na^+ over K^+ membrane selectivity of just 6. Economic aspects and ways of implementation of such a system are briefly discussed in this chapter.

In Chapter 3, a membrane is developed based on the concept of a supported liquid membrane (SLM). SLMs consist of a chemically inert porous polymer membrane support with an organic liquid phase immobilized in the pores, mainly by capillary forces. Lipophilic borate salts are added to the organic phase to promote the cation-over-anion selectivity of the membrane. The membrane selectivity mechanism for the separation of alkali metal cations (Li^+, Na^+ and K^+) has been investigated. It is concluded that the permeation selectivity of the two ionic species of the same charge is essentially based on differences in dehydration energy and electrophoretic mobility between the different alkali metal cations. The system favors the ionic species with the largest crystal radius, despite its lower electrophoretic mobility in the membrane. The reason is that the ionic species with the largest crystal radius have the lowest dehydration energy, and therefore, in this case, K^+ is more favorable for entering the membrane than Na^+. In mixtures of K^+ and Na^+, the SLM separates K^+ from Na^+ with a K^+ over Na^+ separation efficiency – which indicates the percentage of K^+ removed from the feed – ranging from ~20% to 90%, depending on the feed solution composition. With solutions containing either K^+ or Na^+ and Li^+, the K^+/Na^+ over Li^+ separation efficiency is nearly 100%. Addition of a cation-selective carrier, a crown ether, does not improve the SLM behavior, but slows down both the target and non-target ion transport. As a result, the current ratio of the two ionic species can be described exclusively in terms of their feed concentrations and crystal radii because the latter parameter defines both ion partitioning at the water-membrane interface and the electrophoretic mobility in the membrane.

In Chapter 4, the role of ion dehydration in the permeation and separation by an SLM under ED conditions is further investigated and extended to divalent cations (Ca^{2+} and Mg^{2+}). The electrophoretic mobility of the migrating cations, as determined

in single salt solutions, follows the order of $Na^+ > K^+ > Mg^{2+} > Ca^{2+}$. Because the calculated electrophoretic mobility accounts for ion charge already, the mobility order reflects the increasing size of the (partly hydrated) migrating cation. Given the crystal ion radii, this result indicates that divalent cations migrate through the SLM with (part of) the water shell still present. This conclusion is confirmed by water uptake measurements. Measurements involving divalent cations show a permeation selectivity of the SLM in the order of $K^+ > Na^+ > Ca^{2+} > Mg^{2+}$, quite different from the mobility order mentioned above. This difference between the electrophoretic mobility order and permeation selectivity order leads to the investigation of the ion-exchange selectivity. In the case of K^+/Na^+, this exchange selectivity is constant over the entire feed ratio range studied and close to the value predicted by the Born equation, assuming complete ion dehydration when crossing the water-membrane interface. This finding supports the conclusion in Chapter 3 that entering the membrane from the aqueous phase requires the total dehydration of Na^+ and K^+. The ion-exchange selectivity constant between water and membrane has the order of $K^+ > Ca^{2+} > Mg^{2+} \approx Na^+$. The ion exchange order and mobility order together determine the permeation selectivity order. For instance, apparently the relatively high K^+/Ca^{2+} ion-exchange selectivity cannot compensate for the relatively low Ca^{2+} mobility. On the same token, the high Na^+ mobility does compensate for the low K^+/Na^+ ion exchange.

Chapter 5 presents the implementation of a potential ED system by simulating the selective Na^+ removal from greenhouse drainage water. Because the SLM, as characterized in the previous chapters, preferably permeates K^+ (over Na^+), the selective removal of Na^+ requires a two-step treatment. The ED system to-be-developed requires a K^+-selective SLM and a monovalent cation-exchange membrane (CIMS). First, the membrane properties of the SLM and the CIMS, including ion permeation selectivity, transport number and limiting current density, were determined (and regarding the SLM, partly based on the findings of previous chapters). Real-life input parameters, provided by our industrial partner Van der Knaap, include the composition of the irrigation water entering and leaving the green house, volumetric flow, evapotranspiration rate by the tomato plants, target irrigation water Na^+ threshold value. Given the measured membrane characteristics and all other additional operational parameters, the two-step separation process is simulated. Two process scenarios are considered. One starting with treatment step by the SLM to separate K^+, followed by a CIMS treatment step to separate/remove Na^+. In the second

scenario, the two membrane types operate in reversed order. The simulations are evaluated for their ability to keep the Na^+ below the 4 mM threshold level and recover the other nutrients as much as possible. Even though both scenarios overall achieve the selective separation of Na^+, the most favorable one – in terms of the highest nutrient concentration and water recovery – is the one where CIMS follows SLM. This scenario results in the highest recovery rates for K^+, Ca^{2+} and Mg^{2+} (98%, 79% and 79%, respectively), as well as 80% water savings.

Finally, Chapter 6 summarizes the conclusions and provides an outlook based on the findings presented in this dissertation. Suggestions for further improvement on the mechanical stability of the SLM by surface modification with polymer (a sulfonated polyether ether ketone, sPEEK) and optimization of SLM functioning are discussed. Preliminary results over a period of 20 days indicate that the stability of the SLM can be enhanced by the addition of a surface polymer coating. Given its effect on the power consumption of any potential SLM-based ED system, ways to lower the resistance of the SLM are also discussed, *e.g.* by increasing the charge density in the SLM and/or reduce the SLM thickness. Two possible solutions can be investigated. 1). Increase the concentration of the negatively charged groups in the SLM. Another combination of organic solvent – lipophilic salt may allow the increase of the charge density of the SLM. 2). A reduction in membrane thickness will decrease the membrane resistance, *i.e.* from the current $100\,\mu m$ to $10\,\mu m$. The mechanical strength of such a thin membrane can be obtained by "sandwiching" the SLM between two polymer layers, given that such a double-sided coating hardly increases the resistance.

References

[1]   J.M. Costa, E. Berkmoes, E. Beerling, S. Nicol, J. Jose, J. Garcia, R. Cáceres. (2019). Water use in greenhouse horticulture: efficiency and circularity. (EPI-AGRI Focus Group-Circular horticulture Mini-paper). EIP-AGRI. https://ec.europa.eu/eip/agriculture/sites/agri-eip/files/fg27_mini-paper_water_2019_en.pdf.

[2]   J.L. Zhang, T.J. Flowers, S.M. Wang, Mechanisms of sodium uptake by roots of higher plants, Plant Soil. 326 (2010) 45–60. https://doi.org/10.1007/s11104-009-0076-0.

[3]   A.D. Blaylock, Cooperative Extension Service Soil Salinity, Salt Tolerance, and Growth Potential of Horticultural and Landscape Plants, 1994.

[4]   T.B. Kinraide, Interactions among Ca2+, Na+ and K+ in salinity toxicity: quantitative resolution of multiple toxic and ameliorative effects, J. Exp. Bot. 50 (1999) 1495–1505. https://doi.org/10.1093/jxb/50.338.1495.

Samenvatting

Selectieve ionscheiding onder electrodialyse met behulp van een vloeibaar membraan in een poreus polymeer support

Elektrodialyse (ED) is een membraanproces waarbij ionen worden getransporteerd onder invloed van een extern aangebrachte elektrische potentiaal. **Ionuitwisselingsmembranen of wel Ion-Exchange Membranes (IEMs)** zijn belangrijke componenten in ED-processen. Er zijn twee soorten IEMs: (1) kationuitwisselingsmembranen (CEMs) welke gefixeerde, negatief geladen groepen bevatten, en (2) anIonuitwisselingsmembranen (AEMs) welke gefixeerde, positief geladen groepen bevatten. ED-processen worden op grote schaal toegepast voor waterontzilting en worden in de glastuinbouw steeds vaker als een duurzame methode beschouwd. Een belangrijke doelstelling in de duurzame glastuinbouw is het maximaliseren van het hergebruik van afvalwater dat anders naar het milieu wordt afgevoerd, waarbij dan waardevolle voedingsstoffen verloren gaan.[1] Een grote uitdaging in het ED-zuiveringsproces van afvalwater van de glastuinbouw is de **selectieve scheiding** van ionen, met name de selectieve verwijdering van natrium. Voor de meeste planten is natrium (Na^+) schadelijk. Het wordt niet opgenomen door de plant en bij het hergebruik van irrigatiewater hoopt het zich daarom op. Het is dan ook zaak om het Na^+ niveau te controleren en beneden de gewasintolerantiegrens te houden. [2-4] Terwijl Na^+ dus toxisch is, is kalium (K^+) juist een waardevolle nutriënt voor de plant. In kasafvalwater zijn Na^+ en K^+ echter concurrerende kationen gedurende het scheidings- en terugwinningsproces, vanwege het hebben van dezelfde valentie (+1), een vergelijkbare (gehydrateerde) ionstraal en een vrij vergelijkbaar transportgedrag (*d.w.z.* de elektroforetische mobiliteit). Hierdoor is scheiding op lading, grootte en mobiliteit een uitdaging. Dit onderzoek richt zich op de ontwikkeling en karakterisering van een membraan voor de selectieve verwijdering

van Na$^+$. Een overzicht van dit onderwerp, gerelateerde aspecten en uitdagingen wordt gegeven in Hoofdstuk 1.

In Hoofdstuk 2 wordt een model, gebaseerd op massabalansen, gepresenteerd voor de concentraties van Na$^+$ en K$^+$ in het irrigatie- en drainagewater van kassen, specifiek voor de tomatenteelt. Het model beschrijft naast de accumulatie van Na$^+$, de implementatie van een membraanmodule voor de selectieve verwijdering van teveel Na$^+$. Op basis van actuele procesparameters, voor wat betreft de recirculatie van tuinbouwwater en afvalwaterbehandeling, berekent het model de Na$^+$ en K$^+$ concentraties op drie referentiepunten. Deze procesparameters omvatten de evapotranspiratie (de verdamping en transpiratie van de planten), de K$^+$ opname door de planten, het Na$^+$ en K$^+$-gehalte van de meststof, uitloging van Na$^+$ uit het hydroponische substraatmateriaal, dat is het material waarin de planten gekweekt worden (bijvoorbeeld kunstgrond, steenwol of kokossubstraat, en de Na$^+$ en K$^+$ verwijderingsefficiëntie van de membraaneenheid. In eerste instantie is het doel van deze studie om de vereisten te verkennen voor het te ontwikkelen van een Na$^+$-selectief membraan, met name voor wat betreft de Na$^+$ over K$^+$ selectiviteit. Het blijkt dat een Na$^+$ over K$^+$ selectiviteit van 6 of hoger voldoet om de Na$^+$ concentratie onder de (toxische) bovengrens (voor tomaten is dat 20 mM) te houden. Tevens wordt in dit hoofdstuk een aantal economische aspecten en manieren om een dergelijk systeem te implementeren kort besproken.

In Hoofdstuk 3 wordt een membraan ontwikkeld op basis van het concept van een zogenoemd **Supported Liquid Membrane (SLM)**. Een SLM bestaat uit een chemisch inerte, poreus polymeermembraan met een, voornamelijk door capillaire krachten geïmmobiliseerde, organische vloeibare fase in de poriën. Lipofiele boraat zouten zijn toegevoegd aan de organische fase om de kation-over-anion selectiviteit van het membraan te bevorderen. Het mechanisme van membraanselectiviteit voor de scheiding van alkalimetaalkationen (Li$^+$, Na$^+$ en K$^+$) is onderzocht. Geconcludeerd werd dat de permeatieselectiviteit hoofdzakelijk gebaseerd is op een verschil in de **dehydratie-energie** en de elektroforetische mobiliteit tussen de verschillende alkalimetaalkationen. In water zijn ionen gehydrateerd en omringd door een watermantel. Dehydratatie-energie is van belang omdat ionen alvorens vanuit het water naar de organische fase te kunnen overgaan, ze eerst de watermantel, of een deel ervan, kwijt moeten raken. Het SLM systeem begunstigt het ion met de grootste kristalradius, ondanks de lagere elektroforetische mobiliteit in het membraan. De reden hiervoor is dat het ion met de grootste kristalsradius de laagste dehydratie-energie heeft. In mengsels van K$^+$ en Na$^+$ scheidt de SLM K$^+$ van Na$^+$ met een

efficiëntie variërend van ~20% tot 90% afhankelijk van de samenstelling van de voedingsoplossing. Bij oplossingen die K^+ of Na^+ en Li^+ bevatten, is de K^+/Na^+ over Li^+ scheidingsefficiëntie bijna 100%. Toevoeging van een Na^+-selectieve component (*carrier*), een kroonether, verandert de SLM echter niet in een membraan dat meer Na^+ dan K^+ doorlaat. Dat is een gevolg van de veel hogere K^+ concentratie in de SLM, juist door de lagere dehydratatie-energie. Het idee om een kroonether toe te voegen werd daarom verlaten. De verhouding van de elektrische stromen gedragen door de twee monovalente kationen kan geheel worden beschreven door beide voedingsconcentraties en kristalradii, omdat de laatste parameter zowel ionenverdeling over de water en SLM fase alsmede de elektroforetische mobiliteit in het membraan bepaalt.

In Hoofdstuk 4 wordt de rol van ion-dehydratatie bij de permeatie en scheiding door het SLM onder ED-omstandigheden verder bestudeerd en uitgebreid naar de tweewaardige kationen Ca^{2+} en Mg^{2+}. De elektroforetische mobiliteit van de migrerende kationen, zoals bepaald in enkelvoudige zoutoplossingen, neemt af in de volgende volgorde: $Na^+ > K^+ > Mg^{2+} > Ca^{2+}$, hetgeen het verschil in totale grootte van de migrerende kationen weerspiegelt. Gezien de kristalradii van de ionen is geconcludeerd dat Ca^{2+} en Mg^{2+} gedeeltelijk gehydrateerd door de SLM migreren; dit dus in tegenstelling tot K^+ en Na^+, welke volledig gedehydrateerd zijn. Metingen van de wateropname bevestigen dit beeld. Metingen in de aanwezigheid van Ca^{2+} en Mg^{2+} tonen een permeatieselectiviteit aan van $K^+ > Na^+ > Ca^{2+} > Mg^{2+}$. Vanwege het verschil met de eerder genoemde volgorde voor de mobiliteit, is de selectiviteit van Ionuitwisseling over het water-membraan grensvlak nader bestudeerd, in zowel binaire als in multi-ion zoutoplossingen. In het geval dat alleen K^+ en Na^+ aanwezig zijn, is de uitwisselingsselectiviteit over de gehele bestudeerde concentratieverhouding constant en overeenkomend met de waarde die wordt voorspeld door de Born-vergelijking, uitgaande van volledige ion-dehydratie. Deze bevinding ondersteunt de conclusie van Hoofdstuk 3 dat de overgang van het water naar de SLM fase de volledige dehydratie van Na^+ en K^+ vereist. In aanwezigheid van Ca^{2+} en Mg^{2+} is de uitwisselingsselectiviteit: $K^+ > Ca^{2+} > Mg^{2+} \approx Na^+$. Als we deze drie selectiviteitsvolgordes vergelijken is de conclusie dat de permeatieselectiviteit van ionen wordt bepaald door een combinatie van de uitwisselingsselectiviteit en de elektroforetische mobiliteit.

Hoofdstuk 5 presenteert de (mogelijke) implementatie van een ED-systeem voor de selectieve Na^+ verwijdering uit drainagewater in de tuinbouw. Aangezien de SLM, zoals beschreven in de vorige hoofdstukken, bij voorkeur K^+ doorlaat (en niet Na^+),

vereis de selectieve verwijdering van Na^+ een tweestapsproces. Het ene om met behulp van een K^+-selectieve SLM K^+ terug te winnen en een tweede om met behulp van een monovalente CEM de andere kationen zo veel mogelijk terug te winnen en Na^+ af te scheiden. Het blijkt dat op basis van de membraaneigenschappen van de SLM en de monovalente CEM de ionenconcentraties in een oplossing van willekeurige samenstelling goed valt te voorspellen. Met dit gegeven is een simulatiemodel ontwikkeld voor Na^+ verwijdering uit tuinbouwwater met gebruikmaking van realistische operationele parameters, zoals aangeleverd door onze industriële partner Van der Knaap. Relevante parameters zijn bijvoorbeeld de samenstelling van het irrigatiewater dat de kas binnenkomt en verlaat, de volummetrische stroom en de evapotranspiratie van de tomatenplant. Er zijn twee processcenario's overwogen. Eén die begint met een behandeling door de SLM om K^+ te scheiden, gevolgd door een behandeling door de monovalente CEM om Na^+ te scheiden/verwijderen. Het tweede scenario start met de monovalente CEM, gevolgd door de SLM. Met beide scenario's is het zeer wel mogelijk om teveel Na^+ selectief af te scheiden en het Na^+ niveau beneden de vereiste 4 mM te reguleren. Het volgen van het eerste scenario resulteert echter in de hoogste terugwinningspercentages voor K^+, Ca^{2+} en Mg^{2+} (respectievelijk 98%, 79% en 79%), evenals 80% waterbesparing.

Tot slot vat Hoofdstuk 6 de conclusies samen en geeft het suggesties voor verder onderzoek op basis van de bevindingen in dit proefschrift. Een verbetering betreft de mechanische stabiliteit van de SLM door oppervlaktemodificatie met polymeer (een gesulfoneerd polyetherketon, sPEEK). Eerste testresultaten over een periode van 20 dagen zijn zeer positief. Een ander aspect dat aandacht verdient, is de hoge weerstand van de SLM. Aangezien het energieverbruik voor ED direct samenhangt met deze weerstand, is het essentieel om deze drastisch te verlagen. Twee mogelijke oplossingen dienen zich aan. Allereerst een hogere concentratie negatief geladen groepen in de SLM. De 50 mM boraat, die hier toegepast is, representeert de maximale oplosbaarheid van dit boraatzout in het gebruikte organische oplosmiddel NPOE. Een andere combinatie organisch oplosmiddel – lipofiel zout maakt het wellicht mogelijk de ladingsdichtheid van de SLM te verhogen. Ten tweede kan het membraan dunner worden gemaakt. Een tienvoudige reductie in dikte, van de huidige 100 μm naar 10 μm, zal de weerstand decimeren. De mechanische sterkte van een dergelijk dun membraan kan verkregen worden de SLM te 'sandwichen' tussen twee polymeerlagen, gegeven dat een dergelijke dubbelzijdige coating de weerstand nagenoeg niet verhoogt

X

Referenties

[1] J.M. Costa, E. Berkmoes, E. Beerling, S. Nicol, J. Jose, J. Garcia, R. Cáceres. (2019). Water use in greenhouse horticulture: efficiency and circularity. (EPI-AGRI Focus Group-Circular horticulture Mini-paper). EIP-AGRI. https://ec.europa.eu/eip/agriculture/sites/agri-eip/files/fg27_mini-paper_water_2019_en.pdf.

[2] J.L. Zhang, T.J. Flowers, S.M. Wang, Mechanisms of sodium uptake by roots of higher plants, Plant Soil. 326 (2010) 45–60. https://doi.org/10.1007/s11104-009-0076-0.

[3] A.D. Blaylock, Cooperative Extension Service Soil Salinity, Salt Tolerance, and Growth Potential of Horticultural and Landscape Plants, 1994.

[4] T.B. Kinraide, Interactions among Ca2+, Na+ and K+ in salinity toxicity: quantitative resolution of multiple toxic and ameliorative effects, J. Exp. Bot. 50 (1999) 1495–1505. https://doi.org/10.1093/jxb/50.338.1495.

Chapter 1

Introduction

1.1 Closing the loop of greenhouse irrigation water

The booming growth of the world population is continuously creating a higher demand of food production. One way to address this challenge is to achieve higher crop yields. Greenhouse horticulture serves as a powerful technology helping to fulfill that demand. Despite the advantages greenhouse horticulture brought over the last decades, the greenhouse industry was often criticized by the public for its heavy pollution of the environment by residuals of fertilizers, pesticides and other agrochemicals used. With an area of nearly 10,000 hectares the Netherlands has a much larger density of greenhouses than the other Northwest European countries.[1]

In 1994, the first legislation to reduce pollution of surface water in the Netherlands came into effect following the EU Nitrate Directive.[2] Due to the lack of control, for practicality reasons, and because of the growing number of enterprises and growers as well as the local conditions for cultivation, this legislation did not result in the intended improvements.[3] Therefore, in 2002, a new official Dutch agreement[4] was made defining specific obligations for greenhouse growers: (1) Mandatory collection and reuse of drain water, (2) Mandatory collection and storage of rain water for irrigation, (3) Permission to discharge drain water only if crop-specific Na^+ levels in drain water are exceeded or in case of emergencies (*i.e*. disease outbreak). The new regulation was released in 2010 based on an agreement between Dutch authorities and the growers' organization, aiming for (nearly) zero emission by greenhouse horticulture in 2027.[5,6]

For that reason, the concept of closed-loop agriculture was proposed. Closed-loop agriculture is a farming practice that aims for full recirculation of nutrients and returning water back to the soil or substrates where the crops grew in.[7] This type of agricultural practice preserves the nutrient levels within the soil as well as making full use of the water, and allows farming to be carried out in a sustainable way. High-tech greenhouses have begun to adopt closed-loop irrigation systems to reduce their environmental footprint.

1.2 Context of this research

Sodium ion accumulation is considered to be a major challenge for the large-scale implementation of water recirculation systems in greenhouses because of the intolerance most crops show towards high levels of sodium ions.[8–11]To reduce sodium ion levels and improve recycled water quality, horticulturists have started

piloting reverse osmosis (RO) or electrodialysis (ED) based irrigation water treatment.[12–14] Both technologies makes us of membranes: RO relies on the use of membranes that are only permeable for water and ED make use of ion-exchange membranes. When compared to RO, ED has the advantage of longer membrane life-times and less membrane fouling. Commonly used ED systems remove all ion constituents from the drainage water stream, not only the detrimental Na^+ but also various key plant nutrients, including K^+, NO_3^-, Ca^{2+}, Mg^{2+}, SO_4^{2-}, PO_4^{3-} ions, among others. Investigations have been done and reported regarding monovalent cation-selective electrodialysis (MSED) for treating greenhouse wastewater.[15,16] However, even though MSED enabled the separation of Na^+ from the multivalent ions Ca^{2+} and Mg^{2+}, the system still removes other monovalent cations, like K^+ as well. Therefore, in order to recover K^+ as well, Na^+ has to be removed from K^+.

These two ions share the same charge (+1), have similar crystal and hydrated radii[17] and a similar diffusion coefficient[18], which makes the separation by charge, size and mobility challenging. Nevertheless, consider their crystal radii (1.33 Å for K^+ and 0.95 Å for Na^+)[17], the difference translates in a substantial difference between the dehydration energy of the two ion species, 322 and 406 kJ·mol^{-1} for K^+ and Na^+[19,20], respectively.

Supported liquid membranes (SLM), which have an organic liquid phase immobilized in an inert polymer membrane support, enables ion separation based on the difference in dehydration energy of the permeating ion species. This thesis aims to investigate the mechanism of selective cation separation by a membrane based on the concept of a SLM operating under ED conditions and its potential implementation for achieving closed-loop greenhouse water irrigation.

1.3 Electrodialysis

ED is an electro-membrane process based on the use of ion-exchange membranes (IEMs).[21–24] The principles of ED are well known for more than 100 years,[25] but large-scale applications in the fields of industrial or agricultural water treatment were only achieved after the development of multi-cell stacks and the possibility for the production of stable IEMs showing permeation selectivity. Compared with RO, ED is generally considered to be too energy intensive[26,27] as the required energy for desalination is proportional to the required amount of salt that needs to be removed. Instead, for RO the required energy depends on the amount of desalinated water. Therefore, ED is most favorable at relatively low salt concentration in the feed

4

solution, requiring lower current densities. Additional advantages of ED over RO are less membrane fouling and the absence of a high cross-membrane pressure.[26] As for the pressure over the membrane, ED can result in higher brine concentrations as no pressure limitation exists for overcoming the osmotic pressure difference over the membrane. Current IEMs demonstrate excellent chemical and mechanical stability that enables longer membrane lifetimes, even under rather aggressive and oxidizing conditions in the feed waters.[28]

Figure 1.1 schematically illustrates the principle of ED. Anion-exchange membranes (AEMs), which selectively transport anions, and cation-exchange membranes (CEMs), which selectively transport cations are placed in an alternating configuration between the two electrodes.
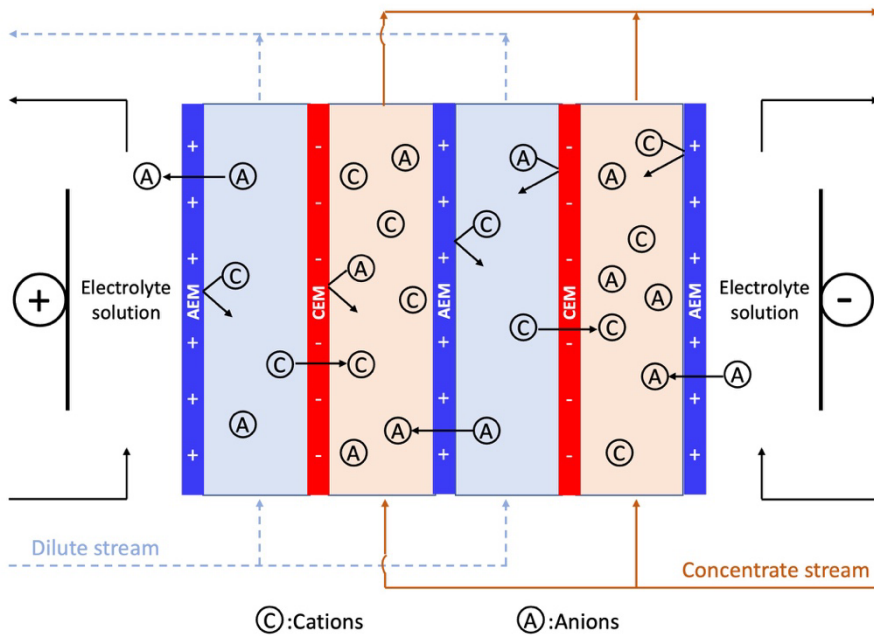
Figure 1.1 Schematic illustration of the ED principle. The transport of cations (C) and anions (A) reflect the selective nature of the Ion Exchange Membranes or IEMs. Cations and anions move in opposite direction, as a result, the incoming stream is divided into a concentrated and dilute stream.

In the conventional ED cell, the membranes are separated by non-conductive spacers (for flat membranes) to obtain the feed water channels.[26] In these channels,

electrolyte solutions are pumped through. The main driving force for ion transport over each membrane is the electrochemical potential which is dominated by the electrical potential. Because of the applied electrical potential, cations migrate towards the cathode and pass through the CEMs, but they are retained by the AEMs. Likewise, the anions migrate towards the anode and pass through the AEMs, but are retained by the CEMs. As a result, the electrolyte stream through the channels becomes alternatingly concentrated or depleted for its ionic components. The depleted solution is generally referred to as the dilute and the concentrated solution as the brine or the concentrate.[29]

The reactions that generally occur in the outer electrode compartments in ED involve the reaction at the cathode:

$$2H_2O + 2e^- \rightarrow H_2(g) + 2OH^-$$ (1.1)

And at the anode:

$$H_2O \rightarrow 2H^+ + \frac{1}{2}O_2(g) + 2e^-$$ (1.2)
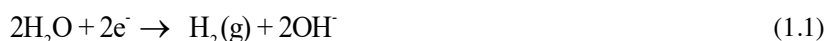
If the solution contains dissolved chloride ions, formation of Cl_2 gas can occur by:

$$2Cl^- \rightarrow Cl_2 + 2e^-$$ (1.3)

To minimize the effect of acidification or alkalinization of the electrolyte solutions, the same solution is continuously mixed and recirculated in a closed loop.

1.4 Ion-exchange membranes

As shown in Figure 1.1, IEMs are key elements in the ED process because they make it possible to re-distribute the salt ions over a concentrated and diluted stream, *i.e.*, to desalinate the water. The application of IEMs can be found in many other processes, such as fuel cells, reverse electrodialysis (RED), Donnan dialysis and the chlor-alkali process.[30] The two types of IEMs, which are made from polymers, used in the ED process are[31]:

- CEM or Cation-Exchange Membranes: possess fixed negatively charged moieties, *e.g.* carboxylic acid groups (for weakly basic membranes) or sulfonic acid groups (for strongly acidic membranes).

6

- AEM or Anion-Exchange membranes: possess fixed positively charged moieties, *e.g.* tertiary ammonium groups (for weakly basic membranes) or quaternary ammonium groups (for strongly basic membranes).
  Both types of membranes can be divided into two categories[32]:
- Homogeneous membranes, where the fixed charged groups are evenly distributed over the membrane polymer matrix.
- Heterogeneous membranes, where charged resins are blended with uncharged polymers. This results in the formation of ion-conductive domains dispersed in a non-conductive matrix.
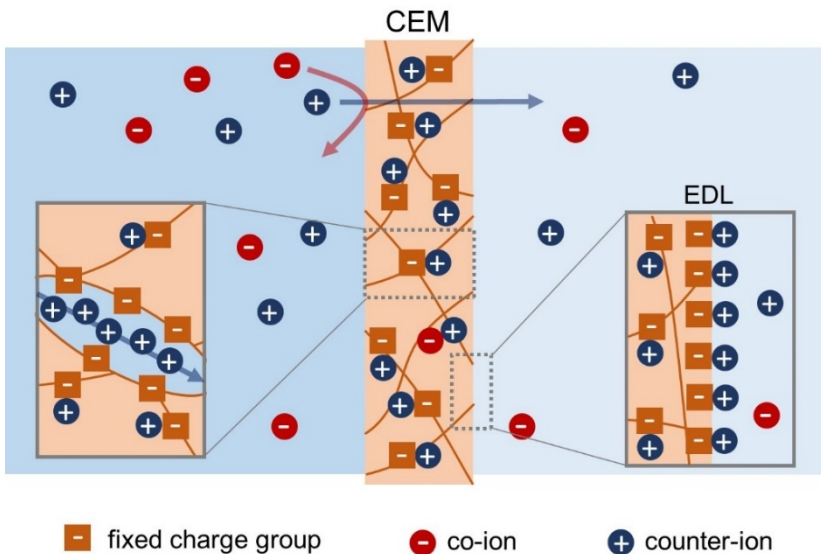
Figure 1.2 Schematic presentation of a Cation-Exchange Membrane (CEM) and ion transport under a potential difference. Indicated are the fixed immobile negative charges in the membrane as well as the mobile cations passing the membrane, the solid lines represent the polymer backbones. On the right, a very schematic view of the Electrical Double Layer (EDL).

Commonly, ion-exchange membranes contain a high concentration of fixed charged groups (negative charges in the case of a CEM as shown in Figure 1.2). When brought into contact with a salt solution, the membrane rejects the ions with the same charge (co-ions) due to Donnan exclusion, while it attracts the ions with the opposite charge (counter-ions) to their surface. At the water – membrane interface, an electrical

double layer (EDL) (Figure 1.2) is formed, a concentration profile composed of two layers of opposite polarity.[29] When a potential difference as the driving force is applied to the ion-exchange membrane, counter-ions are transported through the membrane as a result of Donnan exclusion. The membrane electrical resistance is a macroscopic parameter representing the resistance ions experience when moving through the membrane upon the application of an electric field. The resistance depends on the concentration of mobile charge carriers, their valence and mobility. Noteworthy, the ion mobility may be affected by an interaction between the mobile ion passing and the fixed, immobile charge in the membrane. Similarly, the electrolyte resistance also depends on the concentration, valence and mobility of the particular ion species present. In addition, temperature will have an effect (higher temperature is known to reduce the electrolyte resistance).[33] Because of the concentration dependence, the electrolyte resistance, notably the one of the dilute stream, is in general (much) higher than the membrane resistance and considered to be a significant parameter in the design of an electrochemical cell.

1.5 Membrane selectivity

A selective membrane can be interpreted as "a selective barrier that separates and/or contacts two phases and allows or promotes the exchange of matter between the phases".[34] The selectivity of an ion-exchange membrane can be divided into two categories as permselectivity and permeation selectivity. The term permselectivity is related to the nature of an ion-exchange membrane of permeating counter-ions and repelling co-ions. Membrane permeation selectivity is a measure of the flux or current ratio of the permeable ions over the ion-exchange membrane. Even though the two different measures of selectivity are related, the experimental conditions under which they are determined are essentially different. Whereas perm selectivity is determined under zero-current or flux conditions, the permeation selectivity represents a current or flux ratio of two permeating ion species. They both present key properties and as such are instrumental in the evaluation of membrane performance.[35,36]

As explained in section 1.4, in polymeric membranes, selectivity can be invoked by adding fixed or immobile charge moieties to the polymer matrix. Selectivity is achieved because co-ions, carrying the same charge as the immobile charge, are repelled, a mechanism referred to as Donnan exclusion. The partitioning of ions in case of Na^+ over solution and membrane phase can be express as:

8

$$Na_m \times Cl_m = K \times Na_s \times Cl_s \qquad (1.4)$$

Here, Na_m represents the Na^+ concentration in the membrane, Cl_m the Cl^- concentration in the membrane and K the equilibrium constant of the partitioning of NaCl.

Because of electro neutrality and in case the fixed charge (A) is negative, the concentration of the cations in the membrane (Na_m) equals the sum of A and the concentration of anions in the membrane (Cl_m):

$$Na_m = A + Cl_m \qquad (1.5)$$

Based on chemical potential arguments:

$$Na_m \times Cl_m = K \times c^2 \qquad (1.6)$$

Here, c represents the salt concentration of the solution. Substitution of Eq. 1.4 into Eq. 1.5 renders an (implicit) expression of Cl_m:

$$Cl_m = \frac{K \times c^2}{A + Cl_m} \qquad (1.7)$$

In the particular case of $A \gg Cl_m$, Eq. 1.6 can be simplified to:

$$Cl_m = \frac{K \times c^2}{A} \qquad (1.8)$$

In all other cases, Cl_m is given by the (positive) root of $Cl_m^2 + A \times Cl_m - K \times c^2 = 0$. The efficiency of Donnan exclusion, and hence the extent of charge permeation selectivity, thus depends on the fixed charge density in the membrane in relation to the salt concentration of the solution. The lower the salt concentration of the solution compared to the concentration of immobile charge in the membrane, the higher the membrane selectivity.

Determination of the membrane permselectivity is performed under zero-current conditions and measures the potential difference due to a concentration gradient of the permeable ion species over the ion-exchange membrane. The potential developed by an ideal, 100% selective membrane is given by the Nernst equation:

$$\phi = \frac{RT}{F} \times \ln \frac{C_1}{C_2} \qquad (1.9)$$

where R is the gas constant (8.314 J·mol⁻¹·K⁻¹), F the Faraday constant (96485 C·mol⁻¹), T the temperature (K), C_1 and C_2 are the concentrations of the salt solutions on both sides of the membrane (mol·m⁻³).

The permselectivity is then expressed as the ratio of measured potential and the theoretical Nernst potential predicted by Eq. 1.9.

The determination of the permeation selectivity is based on the counter-ion flux across the membrane. The flux J_i of ion species i (in mol·m⁻²·s⁻¹) is defined by:

$$J_i = \frac{V(C_i^1 - C_i^0)}{A \times t} \tag{1.10}$$

where V is the volume of the solution (L), C_i^t is the concentration of counter-ion at time t (mol·L⁻¹), C_i^0 is the initial counter-ion concentration (mol·L⁻¹), A is the membrane surface area (m²) and t the time elapsed after the start of the experiment (s).

Following Sata[37] and Tanaka[38], the membrane permeation selectivity can be expressed as the product of the flux ratio and feed concentration ratio:

$$P_A^B = \frac{J_B}{J_A} \times \frac{C_A}{C_B} \tag{1.11}$$

In terms of ion currents, Eq. 1.6 reads:

$$P_A^B = \frac{z_A I_B}{z_B I_A} \times \frac{C_A}{C_B} \tag{1.12}$$

The application of IEMs for the separation of monovalent from divalent or multivalent ions have been widely reported.[39–43] Commercially available Neosepta, Fuji and Nafion cation-exchange membranes have a monovalent over divalent cation selectivity ranging from 0.5-2.[44,45] Surface modifications of the standard CEMs were reported to be effective improving the membrane selectivity of ions with different valence.[44,46–48] However, it is still highly challenging to selectively separate two ions that have the same valence and have similar chemical properties, *i.e.* the separation of monovalent (K⁺/Li⁺, K⁺/Na⁺ and Na⁺/Li⁺) or divalent cations (Ca²⁺/Mg²⁺). Table 1.1 summarizes the reported values of membrane selectivity of cations with the same valence under ED conditions in literature.

10

Ref.	Membrane	Permeation selectivity			
		K^+/Li^+	K^+/Na^+	Na^+/Li^+	Ca^{2+}/Mg^{2+}
[49]	(PAH/PSS)₅PAH-Nafion [a]	2.3	-	-	-
[50]	M-12C4-0.50-PEI [b]	2.69	-	-	-
[51]	DA-ACE-SPSF [c]	2.87	1.45	-	-
[52]	SPEEK	-	1.31	-	-
	CMX	-	1.43	-	-
[53]	Neosepta CM-1	1.60	-	1.25	-
[54]	OH-MMT [d]	-	-	-	2.04

Table 1.1 Summary of reported membrane selectivity of cations with the same valence (K^+/Li^+, K^+/Na^+, Na^+/Li^+ and Ca^{2+}/Mg^{2+}) all determined under ED conditions. [a]: Nafion membrane coated with polyelectrolyte layers; b: sulfonated polysulfone (SPSF) membrane coated with polyethyleneimine and crown ether; [c]: SPSF membrane coated with dopamine and crown ether; [d]; heterogenous CEM with addition of protonated Montmorillonite (MMT) nanoparticles.

In addition to the most reported modification approaches (*i.e.* surface modification by layer by layer (LbL) assembly and composite membrane with additional selective component) of the CEMs for achieving an ion selectivity, recent research also points to the role of ion dehydration in the selective transport of ions across IEMs.[46,55–58]

1.6 Evaluation aspects for the implementation of ED system in water treatment

The energy consumption of ED is substantial. One reason is the increasing internal transport resistance due to the decreasing salt concentration in the dilute compartments. With a constant current or voltage applied to the electrodes, the changing conditions can lead to an uneven distribution of ionic current in the ED system. This uneven distribution is more significant at the membrane interface of the dilute compartment because of ion depletion. This happens whenever the limiting current density (LCD) is exceeded. The LCD is resulted from salt depletion at the diffusion boundary layer at the membrane interface of the dilute compartment. This, in turn, lead to lower ion transport numbers in solutions compared to those in the membrane. It is also referred to as concentration polarization [59,60]. With the

desalination of the dilute stream proceeding, the lowered salt concentration may, at a certain point, give rise to a lower LCD. If not anticipated by a lower applied current density, water splitting may occur, resulting in lower transport numbers of the ion species of interest.

Another key element regarding implementation of an ED system includes an analysis of the economics, *e.g.*, the capital costs, energy consumption, membrane lifetime, replacement costs and other operating costs (*i.e.* system maintenance).

The energy consumption $E_{desalination}$ (kWh·m^{-3}) required for desalination is calculated as:

$$E_{desalination} = \frac{I \times V_{cp} \times N}{Q_{dilute}}$$
(1.13)

where I is the applied current (A), V_{cp} is the cell pair voltage (V), N is the number of cell pairs and Q_{dilute} the dilute stream flow rate (m^3·h^{-1}). The general reported energy consumption for brine desalination with low salinity using ED ranges from 0.6-1.8 kWh·m^{-3}.[61,62]

Besides the energy consumption for ED, energy is also required consumed for pumping the concentrate and dilute streams through the ED system. The pumping energy E_{pump}(kWh·m^{-3}) is calculated as:

$$E_{pump} = \frac{\Delta p_{dil} \times Q_{dil} + \Delta p_{conc} \times Q_{conc}}{\eta \times Q_{dil}}$$
(1.14)

in which Δp is the differential pressure (Pa) between the inlet and outlet of the stack for the dilute (*dil*) and concentrate (*conc*) compartments, Q the flow rate (m^3·h^{-1}) in the dilute or concentrate compartments and η the pump efficiency (%). As for the space in between the membranes, the design of an ED stack requires a delicate balance in which a short distance lowers the electrical resistance but increases the hydraulic resistance.

1.7 Supported liquid membranes

Supported liquid membranes (SLMs) are commonly reported to be used in the fields of analytical chemistry, biotechnology, chemical engineering and biomedical engineering.[63–66] The reported and traditional use of SLMs offers advantages of low operational energy requirements, low capital and operating costs. In general, an

SLM consists of a liquid membrane phase which, due to capillary forces, is immobilized in a porous inert polymer support (*i.e.* polypropylene made ACCUREL or Celgard) (Figure 1.3). The SLM separation process can be described as a combination of solvent extraction and a stripping process (re-extraction).[67] The chemical or, in the case of ED, electrochemical potential gradient serves as the driving force for the ion/charged molecules permeation from the feed phase to the strip phase. In order to improve the selectivity of the system, a selective carrier can be included in the organic solvent phase to interact with the target ion/compound (Figure 1.3). Carrier-facilitated transport is achieved by a complexation reaction between the target ion/compound and the carrier and the subsequent diffusion of the complex through the membrane phase.

Crown ethers and their derivatives are well-known to the sensor community for their application in (affinity) coatings of potentiometric ion-selective electrodes (ISEs), *e.g.*, the K⁺-selective 18-crown-6 and 15-crown-5.[68,69] A key difference between a typical separation membrane and a potentiometric membrane is that the latter operates under zero-current conditions. Crown ethers or other carrier molecules in general can also be used in SLMs for selective ion separation.[70,71] If applied in a separation membrane with substantial ion fluxes passing, it is of key importance that the complexation reaction between the carrier and target ion is reversible. Stated otherwise, selectivity requires an interaction and the complexation should be fast but not too strong. A too slow-release step impairs the flux over the membrane.
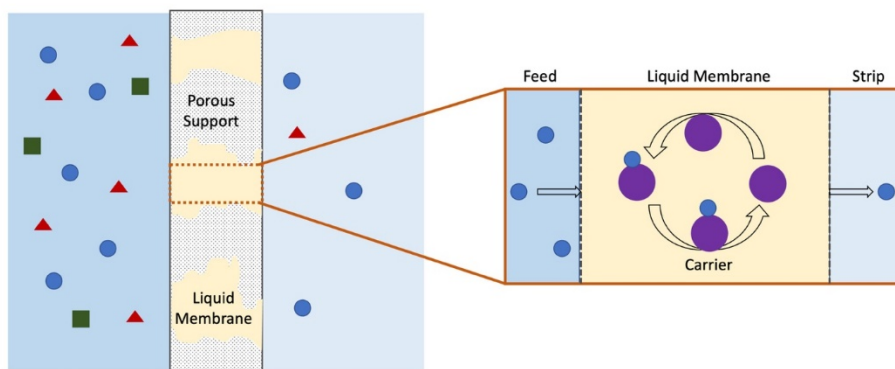

Figure 1.3 Left panel: Schematic configuration of a porous support impregnated with an organic phase, resulting in a supported liquid membrane (SLM). Right panel: the mechanism of carrier-facilitated membrane transport.

1.8 Supported liquid membranes in ED

Studies have reported the promoted extraction and separation across the SLM by the use of electrical fields.[71–73] However, different from the typical IEMs with their high concentration of fixed charge sites in the membrane matrix, the SLM with low solubility of salt holds a much higher membrane resistance. Lipophilic salts have been widely used as ion exchangers in polymeric membranes to provide a good working performance.[74–76] Adding, for instance, lipophilic anions to the organic phase improves the cation over anion selectivity and, in addition, lowers the electrical resistance by increasing the concentration of mobile charge carriers, in this case cations, in the SLM. However, due to the limited solubility of lipophilic anion moieties in the organic solvent phase, the ion-exchange capacity of an SLM (for the borate/NPOE combination in this thesis estimated to be 0.085 mEq·g⁻¹) is much lower than those of commercially available monovalent cation-exchange membranes (CIMS), typically 1.5-1.8 mEq· g⁻¹ [77,78]. As a result, the membrane resistance of the SLM is much higher than the resistance of commercial CIMS.

1.9 Ion partitioning and mobility in the SLM

Because of the electrostatic interaction between ions and water molecules (with high dipole moment), ions in water are hydrated, *i.e.*, they are surrounded by a so-called water shell. When such a hydrated ion moves from the aqueous phase (with high permittivity) to a more hydrophobic phase (with lower permittivity), the ion needs to be (partly) dehydrated. The ΔG and ΔH of dehydration (both >0) are equal in magnitude but of opposite sign as the ΔG and ΔH of hydration (both <0). The Born equation, based on electrostatic solvation models[79,80], gives the ΔG required to transfer an ion species of charge z and crystal radius r_c (Å)from a phase with permittivity ε_1 to another phase with permittivity ε_2.

$$\Delta G = \frac{N_A z^2 e^2}{8\pi\varepsilon_0 r}\left(\frac{1}{\varepsilon_2} - \frac{1}{\varepsilon_1}\right)$$
(1.15)

with ΔG in kJ mol⁻¹, N_A Avogadro's number (6.02×10²³), e the elementary charge (1.6022×10⁻¹⁹ C) and ε_0 the permittivity of vacuum (8,854×10⁻¹² F·m⁻¹). Note that if $\varepsilon_1 > \varepsilon_2$, $\Delta G > 0$. With a ε-value of 78 F·m⁻¹ (at RT), water has a very high relative permittivity. By implication, the transfer of (a hydrated) charge from the aqueous phase to most other phases (*e.g.* a more hydrophobic membrane) involves, with

$\Delta G{>}0$, an energy "barrier", *i.e.* the energy required for the (partly) dehydration of the particular charge. Of two ions that have the same valence, the smallest one has the highest dehydration energy because of its higher charge density. Also note the strong dependency of ΔG on the valence of the particular ion species. As a result, the ΔG of a divalent ion species is approximately a factor four larger than the ΔG of its monovalent equivalent of similar size. Reported dehydration values, *e.g.* the 322 and 406 kJ mol^{-1} for K$^+$ and Na$^+$, respectively, commonly refer to the biphasic system water – vacuum, *i.e.* they refer to the energy required for complete dehydration with all hydration water removed.

The Born energy change, in turn, affects the partitioning of an ion species over the water and membrane phase. Figure 1.4 schematically depicts the application of an SLM, using 2-nitrophenyl-n-octyl ether (NPOE) as the organic liquid membrane phase, for the separation of K$^+$ and Na$^+$ under ED conditions. In the absence of any interaction between the immobile charge in the membrane (not indicated) and the mobile Na$^+$ and K$^+$ passing the membrane, the partitioning of Na$^+$ and K$^+$ over the aqueous phase and the organic liquid membrane phase is defined by a Boltzmann distribution. Consequently, the ratio of K$^+$ and Na$^+$ concentration in the membrane is given by:

$$\frac{\mathrm{K_m}}{\mathrm{Na_m}} = \frac{\mathrm{K_s}}{\mathrm{Na_s}} \exp(\frac{\Delta G_{Na} - \Delta G_K}{RT}) \qquad (1.16)$$

where ΔG_K and ΔG_{Na} refer to the molar Born energy of K$^+$ and Na$^+$ and indices m ans s refer to the membrane and solution phase, respectively. Note that because $\Delta G_{Na}{>}\Delta G_K$, $\mathrm{K_m} > \mathrm{Na_m}$.

Because the mobility of an ion is related to its radius, (de)hydration also effects its mobility. The ion species with the smaller crystal radius has the larger hydrated radius and with that the lower mobility. Table 1.2 shows for a number of ion species their crystal radius (Å), hydrated radius (Å), molar dehydration energy ΔG (kJ·mol^{-1}) and ionic mobility in water at 298 K and NPOE (m^{-2}·V^{-1}·s^{-1}). Note the two orders of magnitude difference in mobility in water and in NPOE.
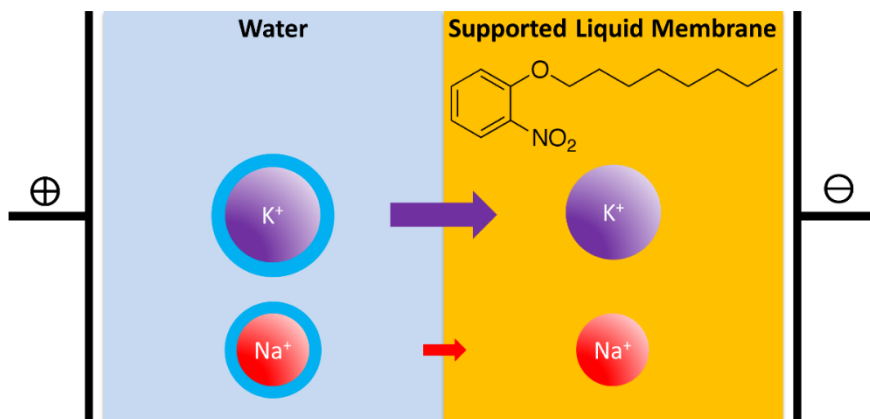
Figure 1.4 Selective transport of K^{+} based on dielectric exclusion. Both K^{+} and Na^{+} require dehydration before entering the membrane. Because the dehydration energy of K^{+} is lower, the system favors this ion species (as indicated by the size of the arrows). The dark blue ring represents the hydration shell.

Ion species	Crystal radius (Å)[17]	Hydrated radius (Å)[17]	Dehydration energy ΔG (kJ·mol^{-1}) [19,20,81]	Ionic mobility in water at 298 K ($\times 10^8$ m²·s^{-1}·V[-1])[82]	Ionic mobility in NPOE ($\times 10^{10}$ m²·s^{-1}·V[-1]) [83,84]
Na^{+}	0.95	3.58	406	5.19	3.61
K^{+}	1.33	3.31	322	7.62	2.17
Mg^{2+}	0.65	4.28	1921	5.5	2.26
Ca^{2+}	0.99	4.12	1577	6.17	1.53
Cl^{-}	1.81	3.32	363	7.64	N/A

Table 1.2 Summary of the crystal radius (Å)[17], hydrated radius (Å)[17], molar dehydration energy ΔG (kJ·mol^{-1})[19,20,81]and ionic mobility in water at 298 K[82] and NPOE[83,84] (m[-2]·V[-1]·s^{-1}) of Na^{+}, K^{+}, Mg^{2+}, Ca^{2+} and Cl^{-} N/A refers to as 'not available'.

1.10 Aim of the thesis

Summarized, the aim of this thesis is: to provide more insight into the membrane selectivity required for the selective removal of Na^{+} from greenhouse irrigation water with the other ion species recovered as much as possible. In more detail:

- Gain our understanding of ion-exchange and ion-transport processes through SLMs under ED conditions.
- Understanding the role of ion-selective carriers in the SLM under ED conditions.
- Validate a promising strategy to selectively separate cations using the concept of SLM.
- Develop a simulation model that assists in defining a number of key operational parameters for water treatment process design.

1.11 Outline of the thesis

Figure 1.5 provides a schematic outline of this dissertation.
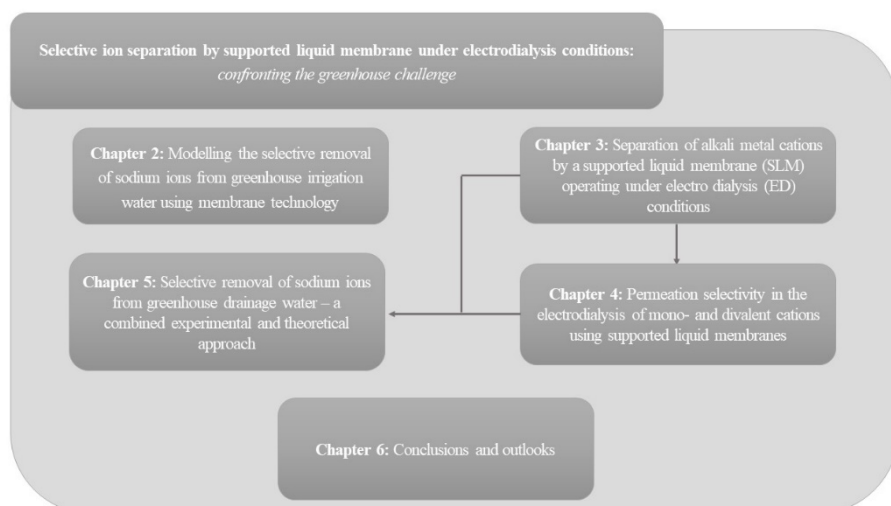
Figure 1.5 Graphical outline of the thesis, presenting the relationship between some of the chapters.

After this introduction, Chapter 2 presents the modelling of the Na$^+$ and K$^+$ concentration in the recycled closed-loop irrigation and drainage water of greenhouses, specifically those cultivating tomatoes. The model estimates the required minimum selectivity of the membrane-to-be-developed to keep the Na$^+$ level below its detrimental threshold.

Chapter 3 demonstrates the effective separation of alkali metal cations using a supported liquid membrane (SLM) under electrodialysis (ED) conditions and investigates the working mechanism of the membrane.

Chapter 4 is an extension of Chapter 3, now including the divalent cations Ca^{2+} and Mg^{2+} as well.

Chapter 5 investigates the design and implementation of an ED system using a combination of the SLM and a monovalent cation-selective membrane for the treatment of greenhouse drainage water.

Finally, Chapter 6 presents the conclusions and outlooks with recommendations for future SLM developments.

1

References

[1]   M. Raaphorst, Quantitative Information for Greenhouse Horticulture, Report GTB-5154, Wageningen, 2017.

[2]   EU-ND, Nitrate Directive, Council Directive of 12 December 1991 concerning the protection of waters against pollution caused by nitrates from agricultural sources (91/676/EEC), Official Journal of the European Communities. L 375/1-8 (1992).

[3]   C. van der Salm, W. Voogt, E. Beerling, J. van Ruijven, E. van Os, Minimising emissions to water bodies from NW European greenhouses; with focus on Dutch vegetable cultivation, Agricultural Water Management. 242 (2020). https://doi.org/10.1016/j.agwat.2020.106398.

[4]   Besluit Glastuinbouw, Regulation Greenhouse Horticulture, (2002). https://wetten.overheid.nl/BWBR0013430/2012-01-01.

[5]   EU-WFD, Water Framework Directive, Directive 2000/60/EC of the European Parliament and of the Council of 23 October 2000 establishing a framework for Community action in the field of water policy, Official Journal of the European Communities. L327/1-72 (2000).

[6]   E.A.M. Beerling, C. Blok, A.A. Van Der Maas, E.A. Van Os, Closing the water and nutrient cycles in soilless cultivation systems, Acta Horticulturae. 1034 (2014) 49–55. https://doi.org/10.17660/ActaHortic.2014.1034.4.

[7]   F. Harty, Closed Loop Agriculture for Envitonmental Enhancement: Returning Biomass and Nutrients from Humanure and Urine to Agriculture, 2016.

[8]   W. Voogt, E.A. Van Os, Strategies to manage chemical water quality related problems in closed hydroponic systems, in: Acta Horticulturae, International Society for Horticultural Science, 2012: pp. 949–956. https://doi.org/10.17660/actahortic.2012.927.117.

[9]   J.L. Zhang, T.J. Flowers, S.M. Wang, Mechanisms of sodium uptake by roots of higher plants, Plant and Soil. 326 (2010) 45–60. https://doi.org/10.1007/s11104-009-0076-0.

[10]   A.D. Blaylock, Cooperative Extension Service Soil Salinity, Salt Tolerance, and Growth Potential of Horticultural and Landscape Plants, 1994.

[11]   A. Läuchli, S.R. Grattan, Plant growth and development under salinity stress, in: Advances in Molecular Breeding Toward Drought and Salt Tolerant Crops, Springer Netherlands, 2007: pp. 1–32. https://doi.org/10.1007/978-1-4020-5578-2_1.

[12]   N. Gruyer, M. Dorais, B.W. Alsanius, G.J. Zagury, Simultaneous Removal of Nitrate and Sulfate from Greenhouse Wastewater by Constructed Wetlands, Journal of Environmental Quality. 42 (2013) 1256–1266. https://doi.org/10.2134/jeq2012.0306.

[13]   C. Fritzmann, J. Löwenberg, T. Wintgens, T. Melin, State-of-the-art of reverse osmosis desalination, Desalination. 216 (2007) 1–76. https://doi.org/10.1016/j.desal.2006.12.009.

[14]   E. Farrell, M.I. Hassan, R.A. Tufa, A. Tuomiranta, A.H. Avci, A. Politano, E. Curcio, H.A. Arafat, Reverse electrodialysis powered greenhouse concept for water- and energy-self-sufficient agriculture, Applied Energy. 187 (2017) 390–409. https://doi.org/10.1016/j.apenergy.2016.11.069.

[15]   Y.D. Ahdab, G. Schücking, D. Rehman, J.H. Lienhard, Treatment of greenhouse wastewater for reuse or disposal using monovalent selective electrodialysis, Desalination. 507 (2021) 115037. https://doi.org/10.1016/j.desal.2021.115037.

[16]   Y.D. Ahdab, D. Rehman, J.H. Lienhard, Brackish water desalination for greenhouses: Improving groundwater quality for irrigation using monovalent selective electrodialysis reversal, Journal of Membrane Science. 610 (2020) 118072. https://doi.org/10.1016/j.memsci.2020.118072.

[17]   E.R. Nightingale, Phenomenological theory of ion solvation. Effective radii of hydrated ions, Journal of Physical Chemistry. 63 (1959) 1381–1387. https://doi.org/10.1021/j150579a011.

[18]   J. Rumble, ed., Handbook of Chemistry and Physics, 101st ed., CRC Press, 2020.

[19]   L. Zhang, X. Lu, X. Liu, J. Zhou, H. Zhou, Hydration and mobility of interlayer ions of (Nax, Cay)-montmorillonite: A molecular dynamics study, Journal of Physical Chemistry C. 118 (2014) 29811–29821. https://doi.org/10.1021/JP508427C/SUPPL_FILE/JP508427C_SI_001.PDF.

[20]   J. Lee, S.M. Park, E.K. Jeon, K. Baek, Selective and irreversible adsorption mechanism of cesium on illite, Applied Geochemistry. 85 (2017) 188–193. https://doi.org/10.1016/J.APGEOCHEM.2017.05.019.

[21]   Y. Tanaka, Electrodialysis, in: Progress in Filtration and Separation, Elsevier Ltd, 2015: pp. 207–284. https://doi.org/10.1016/B978-0-12-384746-1.00006-9.

[22]   T. Uragami, Introduction to Membrane Science and Technology, in: Science and Technology of Separation Membranes, 2017: pp. 1–12. https://doi.org/10.1002/9781118932551.ch1.

20

[23] H. Strathmann, Membrane separation processes, Journal of Membrane Science. 9 (1981) 121–189. https://doi.org/10.1016/S0376-7388(00)85121-2.

[24] H. Strathmann, Electrodialysis, in: Synthetic Membranes: Science, Engineering and Applications, Springer Netherlands, Dordrecht, 1986: pp. 197–223. https://doi.org/10.1007/978-94-009-4712-2_8.

[25] T. Scarazzato, K.S. Barros, T. Benvenuti, M.A.S. Rodrigues, D.C.R. Espinosa, A.M.B. Bernardes, F.D.R. Amado, V. Pérez-Herranz, Achievements in electrodialysis processes for wastewater and water treatment, in: Current Trends and Future Developments on (Bio-) Membranes, Elsevier, 2020: pp. 127–160. https://doi.org/10.1016/b978-0-12-817378-7.00005-7.

[26] H. Strathmann, Electrodialysis, a mature technology with a multitude of new applications, Desalination. 264 (2010) 268–288. https://doi.org/10.1016/j.desal.2010.04.069.

[27] A.M. Lopez, M. Williams, M. Paiva, D. Demydov, T.D. Do, J.L. Fairey, Y.P.J. Lin, J.A. Hestekin, Potential of electrodialytic techniques in brackish desalination and recovery of industrial process water for reuse, Desalination. 409 (2017) 108–114. https://doi.org/10.1016/j.desal.2017.01.010.

[28] H. Strathmann, A. Grabowski, G. Eigenberger, Ion-Exchange Membranes in the Chemical Process Industry, Industrial and Engineering Chemistry Research. 52 (2013) 10364–10379. https://doi.org/10.1021/IE4002102.

[29] H. Strathmann, Ion-Exchange Membrane Separation Processes, 2004. https://doi.org/10.1007/s13398-014-0173-7.2.

[30] J. Veerman, The effect of the NaCl bulk concentration on the resistance of ion exchange membranes-measuring and modeling, Energies. 13 (2020) 1946. https://doi.org/10.3390/en13081946.

[31] H. Strathmann, Ion-exchange membrane separation processes, Elsevier, Amsterdam, 2004. https://doi.org/10.1007/s13398-014-0173-7.2.

[32] P. Długołecki, K. Nymeijer, S. Metz, M. Wessling, Current status of ion exchange membranes for power generation from salinity gradients, Journal of Membrane Science. 319 (2008) 214–222. https://doi.org/10.1016/j.memsci.2008.03.037.

[33] P. Długołecki, P. Ogonowski, S.J. Metz, M. Saakes, K. Nijmeijer, M. Wessling, On the resistances of membrane, diffusion boundary layer and double layer in ion exchange membrane transport, Journal of Membrane Science. 349 (2010) 369–379. https://doi.org/10.1016/J.MEMSCI.2009.11.069.

[34] M. Mulder, Basic principles of membrane technology, 2nd ed., Springer Netherlands, Dordrecht, 1996. https://doi.org/10.1007/978-94-009-1766-8_1.

[35] L. Marder, E.M. Ortega Navarro, V. Pérez-Herranz, A.M. Bernardes, J.Z. Ferreira, Evaluation of transition metals transport properties through a cation-exchange membrane by chronopotentiometry, Journal of Membrane Science. 284 (2006) 267–275. https://doi.org/10.1016/j.memsci.2006.07.039.

[36] S. Koter, Transport number of counterions in ion-exchange membranes, Separation and Purification Technology. 22–23 (2001) 643–654. https://doi.org/10.1016/S1383-5866(00)00160-X.

[37] T. Sata, Theory of Membrane Phenomena in Ion Exchange Membranes, in: Ion Exchange Membranes, Royal Society of Chemistry, 2007: pp. 7–34. https://doi.org/10.1039/9781847551177-00007.

[38] Y. Tanaka, Fundamental Properties of Ion Exchange Membranes, in: Ion Exchange Membranes, Elsevier, 2015: pp. 29–65. https://doi.org/10.1016/b978-0-444-63319-4.00002-x.

[39] M. Sadrzadeh, A. Razmi, T. Mohammadi, Separation of different ions from wastewater at various operating conditions using electrodialysis, Separation and Purification Technology. 54 (2007) 147–156. https://doi.org/10.1016/j.seppur.2006.08.023.

[40] A.H. Galama, M. Saakes, H. Bruning, H.H.M. Rijnaarts, J.W. Post, Seawater predesalination with electrodialysis, Desalination. 342 (2014) 61–69. https://doi.org/10.1016/j.desal.2013.07.012.

[41] Y. Zhang, S. Paepen, L. Pinoy, B. Meesschaert, B. Van Der Bruggen, Selectrodialysis: Fractionation of divalent ions from monovalent ions in a novel electrodialysis stack, Separation and Purification Technology. 88 (2012) 191–201. https://doi.org/10.1016/j.seppur.2011.12.017.

[42] X.Y. Nie, S.Y. Sun, Z. Sun, X. Song, J.G. Yu, Ion-fractionation of lithium ions from magnesium ions by electrodialysis using monovalent selective ion-exchange membranes, Desalination. 403 (2017) 128–135. https://doi.org/10.1016/j.desal.2016.05.010.

[43] M. Kumar, M.A. Khan, Z.A. AlOthman, M.R. Siddiqui, Polyaniline modified organic-inorganic hybrid cation-exchange membranes for the separation of monovalent and multivalent ions, Desalination. 325 (2013) 95–103. https://doi.org/10.1016/j.desal.2013.06.022.

[44] Y. Zhu, M. Ahmad, L. Yang, M. Misovich, A. Yaroshchuk, M.L. Bruening, Adsorption of polyelectrolyte multilayers imparts high monovalent/divalent cation selectivity to aliphatic polyamide cation-exchange membranes, Journal of Membrane Science. 537 (2017) 177–185. https://doi.org/10.1016/J.MEMSCI.2017.05.043.

[45] T. Luo, S. Abdu, M. Wessling, Selectivity of ion exchange membranes: A review, Journal of Membrane Science. 555 (2018) 429–454. https://doi.org/10.1016/j.memsci.2018.03.051.

[46] S. Yang, Y. Liu, J. Liao, H. Liu, Y. Jiang, B. Van Der Bruggen, J. Shen, C. Gao, Codeposition modification of cation exchange membranes with dopamine and crown ether to achieve high K+ electrodialysis selectivity, ACS Applied Materials and Interfaces. 11 (2019) 17730–17741. https://doi.org/10.1021/acsami.8b21031.

[47] S. Sahin, J.E. Dykstra, H. Zuilhof, R.L. Zornitta, L.C.P.M. De Smet, Modification of cation-exchange membranes with polyelectrolyte multilayers to tune ion selectivity in capacitive deionization, ACS Applied Materials and Interfaces. 12 (2020) 34746–34754. https://doi.org/10.1021/ACSAMI.0C05664.

[48] E.N. Durmaz, S. Sahin, E. Virga, S. de Beer, L.C.P.M. de Smet, W.M. de Vos, Polyelectrolytes as Building Blocks for Next-Generation Membranes with Advanced Functionalities, ACS Applied Polymer Materials. 3 (2021) 4347–4374. https://doi.org/10.1021/ACSAPM.1C00654.

[49] L. Yang, C. Tang, M. Ahmad, A. Yaroshchuk, M.L. Bruening, High selectivities among monovalent cations in dialysis through Cation-Exchange Membranes coated with polyelectrolyte multilayers, ACS Applied Materials and Interfaces. 10 (2018) 44134–44143. https://doi.org/10.1021/acsami.8b16434.

[50] S. Yang, S. Yu, L. Yu, Y. Liu, J. Liao, J. Shen, C. Gao, Cation Exchange Membranes Coated with Polyethyleneimine and Crown Ether to Improve Monovalent Cation Electrodialytic Selectivity, Membranes 2021, Vol. 11, Page 351. 11 (2021) 351. https://doi.org/10.3390/MEMBRANES11050351.

[51] S. Yang, Y. Liu, J. Liao, H. Liu, Y. Jiang, B. Van Der Bruggen, J. Shen, C. Gao, Codeposition Modification of Cation Exchange Membranes with Dopamine and Crown Ether to Achieve High K+ Electrodialysis Selectivity, ACS Applied Materials and Interfaces. 11 (2019) 17730–17741. https://doi.org/10.1021/acsami.8b21031.

[52] T. Luo, F. Roghmans, M. Wessling, Ion mobility and partition determine the counter-ion selectivity of ion exchange membranes, Journal of Membrane Science. 597 (2020) 117645. https://doi.org/10.1016/j.memsci.2019.117645.

[53] G.P.T. Cruz, P.A.D. Gaspillo, K. Takahashi, Selective transport of Li–Na and Li–K binary systems across a cation exchange membrane under an electric field, Separation and Purification Technology. 19 (2000) 21–26. https://doi.org/10.1016/S1383-5866(99)00077-5.

[54] F. Radmanesh, T. Rijnaarts, A. Moheb, M. Sadeghi, W.M. de Vos, Enhanced selectivity and performance of heterogeneous cation exchange membranes through addition of sulfonated and protonated Montmorillonite, Journal of Colloid and Interface Science. 533 (2019) 658–670. https://doi.org/10.1016/J.JCIS.2018.08.100.

[55] R. Epsztein, E. Shaulsky, M. Qin, M. Elimelech, Activation behavior for ion permeation in ion-exchange membranes: Role of ion dehydration in selective transport, Journal of Membrane Science. 580 (2019) 316–326. https://doi.org/10.1016/j.memsci.2019.02.009.

[56] Z. Qian, H. Miedema, S. Sahin, L.C.P.M. de Smet, E.J.R. Sudhölter, Separation of alkali metal cations by a supported liquid membrane (SLM) operating under electro dialysis (ED) conditions, Desalination. 495 (2020) 114631. https://doi.org/10.1016/j.desal.2020.114631.

[57] F. Gallucci, Encyclopedia of Membranes, Springer Berlin Heidelberg, 2016. https://doi.org/10.1007/978-3-662-44324-8.

[58] S. Chaudhury, A. Bhattacharyya, A. Goswami, Electrodriven Ion Transport through Crown Ether–Nafion Composite Membrane: Enhanced Selectivity of Cs $^+$ over Na $^+$ by Ion Gating at the Surface, Industrial & Engineering Chemistry Research. 53 (2014) 8804–8809. https://doi.org/10.1021/ie500934v.

[59] M. La Cerva, L. Gurreri, M. Tedesco, A. Cipollina, M. Ciofalo, A. Tamburini, G. Micale, Determination of limiting current density and current efficiency in electrodialysis units, Desalination. 445 (2018) 138–148. https://doi.org/10.1016/j.desal.2018.07.028.

[60] V. V. Nikonenko, N.D. Pismenskaya, E.I. Belova, P. Sistat, P. Huguet, G. Pourcelly, C. Larchet, Intensive current transfer in membrane systems: Modelling, mechanisms and application in electrodialysis, Advances in Colloid and Interface Science. 160 (2010) 101–123. https://doi.org/10.1016/j.cis.2010.08.001.

[61] R.K. McGovern, A.M. Weiner, L. Sun, C.G. Chambers, S.M. Zubair, J.H. Lienhard V, On the cost of electrodialysis for the desalination of high salinity feeds, Applied Energy. 136 (2014) 649–661. https://doi.org/10.1016/j.apenergy.2014.09.050.

24

[62] L.M. Camacho, L. Dumée, J. Zhang, J. de Li, M. Duke, J. Gomez, S. Gray, Advances in membrane distillation for water desalination and purification applications, Water (Switzerland). 5 (2013) 94–196. https://doi.org/10.3390/w5010094.

[63] A.C. Ghosh, M.M. Bora, N.N. Dutta, Developments in liquid membrane separation of beta-lactam antibiotics, Bioseparation. 6 (1996) 91–105.

[64] J. De Gyves, E.R. De San Miguel, Metal ion separations by supported liquid membranes, Industrial and Engineering Chemistry Research. 38 (1999) 2182–2202. https://doi.org/10.1021/ie980374p.

[65] M.H. Al Marzouqi, M.A. Abdulkarim, S.A. Marzouk, M.H. El-Naas, H.M. Hasanain, Facilitated transport of CO2 through immobilized liquid membrane, Industrial and Engineering Chemistry Research. 44 (2005) 9273–9278. https://doi.org/10.1021/ie050526y.

[66] Q. Yang, N.M. Kocherginsky, Copper recovery and spent ammoniacal etchant regeneration based on hollow fiber supported liquid membrane technology: From bench-scale to pilot-scale tests, Journal of Membrane Science. 286 (2006) 301–309. https://doi.org/10.1016/j.memsci.2006.10.012.

[67] P. Dzygiel, P.P. Wieczorek, Supported liquid membranes and their modifications: Definition, classification, theory, stability, application and perspectives, in: Liquid Membranes, Elsevier, 2010: pp. 73–140. https://doi.org/10.1016/B978-0-444-53218-3.00003-9.

[68] T. Guinovart, D. Hernández-Alonso, L. Adriaenssens, P. Blondeau, F.X. Rius, P. Ballester, F.J. Andrade, Characterization of a new ionophore-based ion-selective electrode for the potentiometric determination of creatinine in urine, Biosensors and Bioelectronics. 87 (2017) 587–592. https://doi.org/10.1016/J.BIOS.2016.08.025.

[69] J. Bobacka, A. Ivaska, A. Lewenstam, Potentiometric ion sensors, Chemical Reviews. 108 (2008) 329–351. https://doi.org/10.1021/cr068100w.

[70] Y. Nakatsuji, S. Fujimoto, M. Nakamura, M. Muraoka, Supported liquid membrane transport of alkali metal cations by monoazacryptand with a partially fluorinated sidearm and the corresponding monoazacrown ethers, Journal of Oleo Science. 59 (2010) 369–373. https://doi.org/10.5650/jos.59.369.

[71] A. Šlampová, P. Kubáň, P. Boček, Fine-tuning of electromembrane extraction selectivity using 18-crown-6 ethers as supported liquid membrane modifiers, ELECTROPHORESIS. 35 (2014) 3317–3320. https://doi.org/10.1002/elps.201400372.

[72] S. Pedersen-Bjergaard, K.E. Rasmussen, Extraction across supported liquid membranes by use of electrical fields, Analytical and Bioanalytical Chemistry. 388 (2007) 521–523. https://doi.org/10.1007/s00216-007-1142-1.

[73] A. Gjelstad, K.E. Rasmussen, S. Pedersen-Bjergaard, Electrokinetic migration across artificial liquid membranes: Tuning the membrane chemistry to different types of drug substances, Journal of Chromatography A. 1124 (2006) 29–34. https://doi.org/10.1016/J.CHROMA.2006.04.039.

[74] T. Rosatzin, E. Bakker, K. Suzuki, W. Simon, Lipophilic and immobilized anionic additives in solvent polymeric membranes of cation-selective chemical sensors, Analytica Chimica Acta. 280 (1993) 197–208. https://doi.org/10.1016/0003-2670(93)85122-Z.

[75] E. Bakker, E. Pretsch, Lipophilicity of tetraphenylborate derivatives as anionic sites in neutral carrier-based solvent polymeric membranes and lifetime of corresponding ion-selective electrochemical and optical sensors, Analytica Chimica Acta. 309 (1995) 7–17. https://doi.org/10.1016/0003-2670(95)00077-D.

[76] F.G. Bănică, Chemical Sensors and Biosensors: Fundamentals and Applications, John Wiley and Sons, Chichester, UK, 2012. https://doi.org/10.1002/9781118354162.

[77] Y. Asensio, C.M. Fernandez-Marchante, J. Lobato, P. Cañizares, M.A. Rodrigo, Influence of the ion-exchange membrane on the performance of double-compartment microbial fuel cells, (n.d.).

[78] Jingwei Zhou, Han Kuang, Wei Zhuang, Yong Chen, Dong Liu, Hanjie Ying, Jinglan Wu, Application of electrodialysis to extract 5′-ribonucleotides from hydrolysate: efficient decolorization and membrane fouling, RSC Advances. 8 (2018) 29115–29128. https://doi.org/10.1039/C8RA02550A.

[79] M. Born, Volumen und Hydratationswärme der Ionen, Zeitschrift Für Physik. 1 (1920) 45–48. https://doi.org/10.1007/BF01881023.

[80] M.H. Abraham, J. Liszi, E. Papp, Calculations on ionic solvation. Part 6. - Structure-making and structure-breaking effects of alkali halide ions from electrostatic entropies of solvation. Correlation with viscosity B-coefficients, nuclear magnetic resonance B′-coefficients and partial molal volumes, Journal of the Chemical Society, Faraday Transactions 1: Physical Chemistry in Condensed Phases. 78 (1982) 197–211. https://doi.org/10.1039/F19827800197.

[81]   M. Patra, M. Karttunen, Systematic comparison of force fields for microscopic simulations of NaCl in aqueous solutions: Diffusion, free energy of hydration, and structural properties, Journal of Computational Chemistry. 25 (2004) 678–689. https://doi.org/10.1002/JCC.10417.

[82]   M.J. Kadhim, M.I. Gamaj, Estimation of the Diffusion Coefficient and Hydrodynamic Radius (Stokes Radius) for Inorganic Ions in Solution Depending on Molar Conductivity as Electro-Analytical Technique-A Review, Journal of Chemical Reviews. 2 (2020) 182–188. https://doi.org/10.22034/JCR.2020.106910.

[83]   Z. Qian, H. Miedema, S. Sahin, L.C.P.M. de Smet, E.J.R. Sudhölter, Separation of alkali metal cations by a supported liquid membrane (SLM) operating under electro dialysis (ED) conditions, Desalination. 495 (2020) 114631. https://doi.org/10.1016/j.desal.2020.114631.

[84]   Z. Qian, H. Miedema, L.C.P.M. de Smet, E.J.R. Sudhölter, Permeation selectivity in the electro-dialysis of mono- and divalent cations using supported liquid membranes, Desalination. 521 (2022) 115398. https://doi.org/10.1016/j.desal.2021.115398.

Chapter 2

Modelling the selective removal of sodium ions from greenhouse irrigation water using membrane technology

Abstract

A model is presented for the Na^+ and K^+ levels in the irrigation water of greenhouses, specifically those for the cultivation of tomato. The model, essentially based on mass balances, not only describes the accumulation of Na^+ but includes a membrane unit for the selective removal of Na^+ as well. As determined by the membrane properties, some of the K^+ is removed as well. Based on real-life process parameters, the model calculates the Na^+ and K^+ concentration at three reference points. These process parameters include the evapotranspiration rate, the K^+ uptake by the plants, the Na^+ and K^+ content of the fertilizer, the Na^+ leaching out from the hydroponic substrate material, and the Na^+ and K^+ removal efficiency of the membrane unit. Using these parameters and given a constant K^+ concentration of the irrigation water entering the greenhouse of 6.6 mM (resulting in the optimal K^+ concentration for tomato cultivation), the composition of the solution is completely defined at all three reference points per irrigation cycle. Prime aim of this investigation is to explore the requirements for the selective membrane that currently is developed in our lab. It is found that even for a limited Na^+ over K^+ selectivity of 6, after a number of cycles the Na^+ level reaches steady state at a level below the upper (toxic) threshold for tomato cultivation (20 mM). Economic aspects and ways of implementation of such a system are briefly discussed.

2.1 Introduction

Closed-loop soilless or hydroponic systems are already widely used if not, at least in certain countries *e.g*. The Netherlands, common practice in horticulture.[1] Nutrients and water are supplied continuously to the irrigation water (IW) to compensate for nutrient uptake by the plants and water loss due to evapotranspiration. Ideally, the nutrient and water supply are fine-tuned such that the nutrient concentration and the osmotic pressure of the drainage solution remain (fairly) constant. Consequently, nutrients, which are present but are not taken up by the plant, accumulate in the IW.[2] Na^+ is a typical example of an ion that over time builds up in the IW. High Na^+ levels inhibit plant growth directly or indirectly by hampering the uptake of other nutrients.[3–6] Because of the detrimental effects of high Na^+, the IW Na^+ level has been subject of numerous studies already.[7–9] These studies are restricted however to simulation studies, validated or not by monitoring the actual Na^+ level in the IW during crop growth. Despite the detrimental effects at higher levels, plants do show a certain tolerance for Na^+. Reported Na^+ threshold values for tomato vary somewhat but levels above 5 dS m^{-1}, equivalent to 50 mM, prove to inhibit growth and yield[10]. The threshold value might depend on the tomato species; the value used in the present study is 20 mM. As soon as Na^+ exceeds the threshold level, the IW is discharged and needs to be renewed. After replenishing the system with freshly prepared IW the entire process of Na^+ building up starts all over again. Our goal is, apart from monitoring, to develop a (membrane-based) system that selectively removes accumulated Na^+ from the IW. A complication arises from the fact that K^+, an essential plant nutrient, has very similar physicochemical properties as Na^+. Both (alkali metal) ion species have the same valence (+1) and are similar in size with ionic radii of 0.95 and 1.33 Ångstrom for Na^+ and K^+, respectively. However, a key (physiological) difference between the two ion species is that Na^+ is hardly taken up by the plant and is the major cause of salinity toxicity.[11,12] Excess Na^+ thus needs to be removed, either by resin-based absorbance technology or membrane technology. The latter is preferred because it circumvents the necessity of resin regeneration once it has become saturated with Na^+.

The fact that Na^+ and K^+ behave very much the same because they share similar physicochemical properties is exactly the reason that there are no commercial *separation* membranes available yet that discriminate between the two ion species. Here separation refers to a membrane that allows high fluxes. Selective membranes for ion selective electrodes (ISE) do exist already. However, ion fluxes over such

potentiometric membranes are by definition essentially zero.[13,14] Ceramic NASICON-based membranes do selectively transport Na^+.[15] However, only harsh operational conditions like high temperature or high acidity or alkalinity justify their use because of the high price. In addition, the high conductivity demonstrated in battery applications remains relatively low compared to the conductivity of typical polymeric ion exchange membranes.[16]

To impose selectivity on a polymeric or Supported Liquid Membrane (SLM), a compound is blended in with the membrane polymer or a mobile carrier is added to the organic phase of the SLM.[17–19] Na^+ selective carriers include natural monensin and the synthetic crown ether 15-crown-5. Monensin has been used for ISE applications as well as for Na^+ extraction by ionic liquids enriched with monensin.[20,21] Current focus of our lab is on developing a SLM-based system with the organic phase supplemented with 15-crown-5.

The technological challenge thus is to develop a separation membrane that permeates Na^+ but not, or at least to a much lower extent, K^+. Obviously, the less permeable for K^+, the less K^+ needs to be re-supplied to compensate for this loss. Therefore, a key question for the membrane-to-be-developed concerns its required Na^+ over K^+ permeation selectivity. Crucial here to realize is that there is no need to remove all Na^+. Instead, all that needs to be achieved is a (steady-state) concentration of Na^+ below the threshold for, in this case, tomato cultivation. Apart from the fact that total Na^+ removal is technologically hardly feasible, it can be expected as a rule of thumb that the higher the membrane selectivity, the higher the investment costs will be. On the other hand, the higher the selectivity the lower the costs for K^+ re-supply and, evenly important, the more sustainable the overall technology. Prime aim of the present study is to explore the required membrane specifications in terms of Na^+ over K^+ permeation selectivity and K^+ and Na^+ permeability and flux, given real-life operational process parameters (*e.g.*, K^+ uptake by tomato, optimal K^+ level in the IW, evapotranspiration). The simulation study presented here is based on the calculation of the K^+ and Na^+ levels at three different reference locations in the IW system and during subsequent cycles of operation. The prime criteria for the optimal membrane characteristics will essentially be based on the largest number of cycles the system can operate continuously at the lowest possible discharge of K^+. The membrane specifications resulting from the present analysis will guide us in the currently performed investigation to actually fabricate such a membrane system.

2.2 Material and methods

2.2.1 System and model design

The greenhouse recycling system considered in the present study is schematically shown in Figure 2.1. The fresh water source is accumulated rainwater whereas dissolved fertilizer is added as stock solution with a composition adjusted to the requirement of the particular greenhouse crop. Also indicated in Figure 2.1 is the membrane unit responsible for Na^+ removal and producing a waste stream of Na^+. Depending on the membrane selectivity, this waste stream is to a more or lesser extent contaminated with K^+. Along the process line, three reference points are distinguished: point #0 where fresh water, stock solution and recycled drain water are mixed forming fresh (*i.e.*, next cycle) irrigation water entering the greenhouse; #1 the drain water leaving the greenhouse before it enters the membrane module and #2 the drain water after filtration by the membrane unit. The model aims to calculate the Na^+ and K^+ concentrations during each cycle (n) at the three reference points indicated. The nomenclature practiced throughout this study is based on the use of two indices, the first representing the reference point, the second the cycle number. For instance, $[K^+]_{2,3}$ refers to the K^+ concentration at reference point #2 during the third cycle.
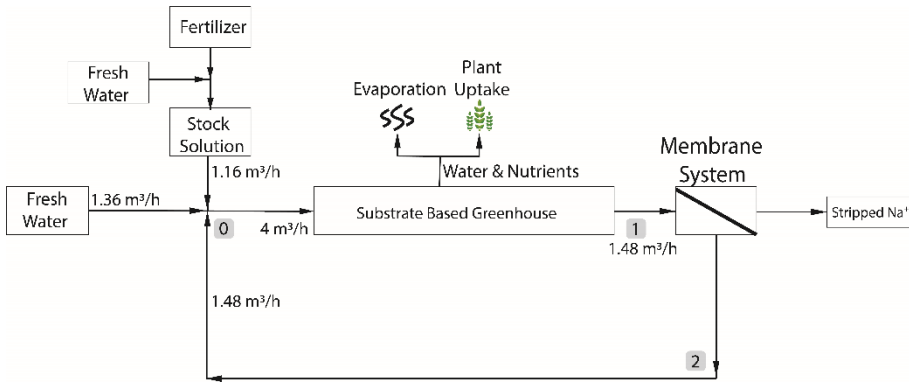

Figure 2.1 Outline of a substrate-based greenhouse irrigation water system with the drain water recycled and including a membrane unit for the selective removal of Na^+. Reference points #0-2 are indicated as well as the relevant (steady-state) volumetric flows while assuming a K^+ loss of 10% (i.e., $\beta=0.1$).

2.2.2 Process parameters

The greenhouse crop data used in the simulations were provided by Van der Knaap (The Netherlands) and (the Dutch branch of) Yara International. Van der Knaap exploits greenhouses, cultivating tomatoes; Yara is manufacturer of fertilizer. Taking into account K^+ uptake by the tomato plants and evapotranspiration, the optimal K^+ concentration of the IW entering the greenhouse is 6.6 mM whereas the (detrimental) threshold Na^+ level of the IW in the greenhouse is set at 20 mM.

Fertilizer stock solution. Nutrients are added as dissolved salts. The fertilizer stock solution contains 9.5 mM K^+ and 2.7 mM Na^+ (Van der Knaap, personal communication).

Fresh water. Since rainwater is used as fresh water source at reference point #0, three sets of samples were collected during September-October-2017 at Wetsus in Leeuwarden, the Netherlands. The K^+ and Na^+ levels were analyzed using inductively coupled plasma optical emission spectrometry (ICP-OES, Perkin Elmer Optima 5000 Series). All required dilutions were carried out with ultrapure water (Millipore purification unit). The average K^+ and Na^+ concentration in rain water was 158 μg/l and 2587 μg/l, resulting in background concentrations of 4 μM and 112.5 μM for K^+ and Na^+, respectively.

Water loss (evapotranspiration). Based on a weekly analysis of their irrigation data, over the year 2016 the average evapotranspiration in the tomato greenhouse of Van der Knaap was 63%, implying the volumetric flow at point #1 (and #2 as well with the assumption of zero water transportation through the membrane during treatment) equals 0.37 times the volumetric flow leaving point #0 and entering the greenhouse.

K^+ concentration. K^+ enters the system from two potential sources:
1) The background K^+ concentration in fresh water (4 μM), and
2) The K^+ content of the fertilizer stream (9.5 mM).

Furthermore, K^+ leaves the system at two locations. Firstly, the nutritional K^+ uptake by the crops and, secondly, the loss through the membrane unit due to the given Na^+ over K^+ permeation selectivity of the membrane. Given the optimal K^+ concentration in the IW entering the greenhouse (6.6 mM) and the (fixed) total water loss of 63%, the fraction of added fertilizer at point #0 is adjusted to this value of 6.6 mM. The fraction of K^+ uptake by the plants (μ) has been determined experimentally by measuring the K^+ concentrations of the drain water leaving the greenhouse, i.e., at

reference point #1. From the measured value of 11.4 mM and the average concentration of K^+ entering the greenhouse (6.6 mM):

$$\mu = 1 - \frac{11.4 \times (1-0.63)}{6.6} = 0.36$$

Na^+ concentration. Na^+ enters the system from three potential sources:
1) The background Na^+ concentration in fresh water (112.5 μM),
2) The Na^+ content of the fertilizer (2.7 mM), and
3) The Na^+ leaching from the (coconut-based) substrate material used in the greenhouse, leads to a Na+ enrichment of the irrigation water (vide infra).

Because Na^+ is not taken up by the plants, it leaves the system only at the membrane unit. At the start of the first irrigation cycle the Na^+ concentration in the irrigation water is 1.9 mM (resulting from the background Na^+ concentrations in both fresh water and fertilizer and fixing the K^+ concentration at point #0 at 6.6 mM). The Na^+ leaching from the substrate was determined by measuring the Na^+ concentration at point #1, and found to be 13.5 mM, resulting in a concentration increase (L) of: 13.5×(1-0.63)-1.9=3.1 mM. Even though over time the Na^+ is washed out the substrate, the present study assumes a constant degree of leaching during the consecutive cycles of operation.

The membrane unit needs to remove Na^+ to meet a (steady-state) Na^+ concentration level in the irrigation water <20 mM, *i.e.*, the upper tolerance level for Na^+ of tomato cultivation. Noteworthy, the model assumes that the membrane unit does not remove any water. The reason is that the SLM under development is composed of a hydrophobic support impregnated with a hydrophobic solvent containing the Na^+ selective carrier 15-crown-5. Prior to entering this organic phase, ions need to be dehydrated with the free energy (ΔG) of dehydration (>0) is compensated for by the ΔG of ion coordination by the 15-crown-5(<0). The water permeation through such SLM systems is negligible.

2.2.3 Mass balances

At the start of each new cycle, the addition of fresh water and fertilizer at reference point #0 has to compensate for the total water loss due to evapotranspiration and K^+ losses due to plant uptake and removal by the membrane unit. Together with the recycled fraction entering point #0, the fractions of added fresh water and stock solution are adjusted such that the K^+ concentration of the irrigation water entering

the greenhouse at point #0 is 6.6 mM. Given this fixed value of 6.6 mM, adjustment is possible because the total fraction of fresh water and stock solution at point #0 is known to be 1.0 for the first cycle ($n=1$), and 0.63 for all subsequent cycles ($n>1$). The calculation of all parameters is thus based on the fraction of fertilizer stock solution (ε) added at point #0. For that reason, we designated ε the master variable in our simulations. On the same token, K^+ is the master ionic species, dictating, by means of ε, the concentration of the slave ionic species Na^+ at point #0 at the start of each new cycle. Once ε has been calculated from the mass (or volumetric flow) balance at point #0, the Na^+ concentration can be calculated as well.

For the very first water cycle, only stock solution and fresh water will meet at point #0. From the second cycle on, however, recycled drain water will join these two water streams at point #0. For this reason, the calculation of the first and the following cycles should be considered separately.
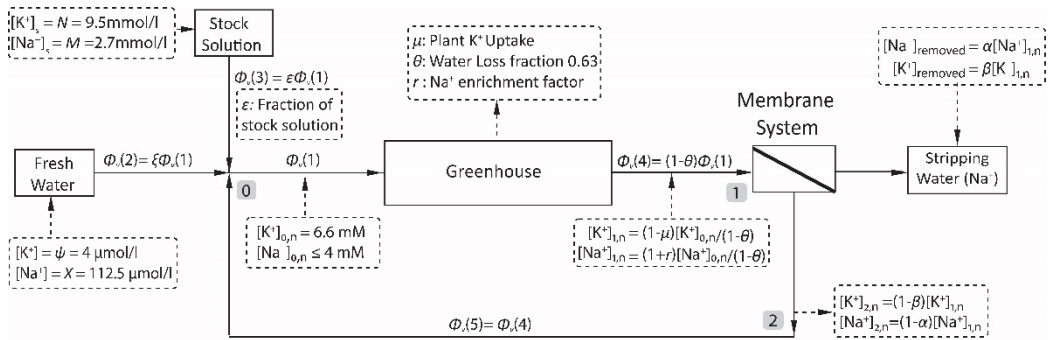
Figure 2.2 Outline of Figure 2.1 complemented with the volumetric flows $\Phi_v(1)$- $\Phi_v(5)$ and the process parameters indicated.

2.2.3.1 Volumetric flow balance for the first two cycles

2.2.3.1.1 First irrigation cycle (n=1)

Figure 2.2 shows the basic outline of Figure 2.1 but complemented with all relevant parameters referred to in this study. Table 1 lists all these parameters as well as their numerical value as used in this study.

Variables		Values
$\Phi_v(1)$	Volumetric flow entering the greenhouse	$4\ \text{m}^3\,\text{h}^{-1}$
Ψ	K^+ concentration in fresh water	$4\ \mu M$
X	Na^+ concentration in fresh water	$112.5\ \mu M$
N	K^+ concentration in fertilizer stock solution	9.5 mM
M	Na^+ concentration in fertilizer stock solution	2.7 mM
ξ	fraction of fresh water added at point #0	
ε	fraction of fertilizer stock solution added at point #0	
μ	fraction of K^+ entering the greenhouse taken up by the crop	0.36
L	Na^+ concentration increase due to Na^+ leaching out from the coconut-based substrate	3.1 mM
θ	fraction of $\Phi v(1)$ lost due to evapotranspiration	0.63
α	fraction of Na^+ removed from the drain water leaving the greenhouse	0-1
β	fraction of K^+ removed from the drain water leaving the greenhouse	0-1
γ	Na^+ over K^+ permeation selectivity of the membrane unit	α/β

Table 2.1 Description of the parameters used throughout this study, corresponding to Figures. 2.1 and 2.2.

Volumetric flows (Φ_v) are presented as fraction of the flow entering the greenhouse, $\Phi_v(1)$ with ε the fraction of the stock solution and ξ the fraction of fresh water. Flows $\Phi_v(2)$ and $\Phi_v(3)$ represent the volumetric flow of fresh water and stock solution added at point #0, respectively.

Reference point #0

As mentioned, given the optimal K^+ concentration for tomato and taken into account K^+ uptake and evapotranspiration, the K^+ concentration at point #0 is set at 6.6 mM. The Na^+ threshold of 20 mM is the maximum acceptable Na^+ level of the IW leaving the greenhouse. Given the Na^+ leaching out the substrate (3.1 mM) and the evapotranspiration (0.67), the 20 mM translates into a Na^+ of the IW entering the

greenhouse of 20×0.37-3.1=4.3 mM. Throughout this study the threshold Na$^+$ level at point #0 of the incoming IW is set at 4 mM.

The volumetric flow balance reads:

$$\Phi_v(1) = \Phi_v(2) + \Phi_v(3) = \xi_1\Phi_v(1) + \varepsilon_1\Phi_v(1) \tag{2.1}$$

Suppose Ψ and N are the K$^+$ concentration in the fresh water and in the fertilizer stock solution, respectively. Then, according to Eq. 2.1, the K$^+$ mass balance equals:

$$[K^+]_{0,1} \times \Phi_v(1) = \Psi \times \xi_1\Phi_v(1) + N \times \varepsilon_1\Phi_v(1) \tag{2.2}$$

Because $\xi_1 + \varepsilon_1 = 1$ and dividing by $\Phi_v(1)$ renders for the K$^+$ concentration:

$$[K^+]_{0,1} = (1 - \varepsilon_1)\Psi + \varepsilon_1(N - \Psi) + \Psi \tag{2.3}$$

The fraction of stock solution thus is:

$$\varepsilon_1 = ([K^+]_{0,1} - \Psi) / (N - \Psi) \tag{2.4}$$

With $[K^+]_{0,1} = 6.6\ mM$ and Ψ and N being known, the value of ε_1 is defined. Once ε_1 is known, the Na$^+$ concentration for the first cycle can be calculated by:

$$[Na^+]_{0,1} = \xi_1 X + \varepsilon_1 M = \varepsilon_1(M - X) + X \tag{2.5}$$

Where M and X are the Na$^+$ concentration of the stock solution and fresh water, respectively.

Compared to the K$^+$ concentration at point #0, the K$^+$ concentration at point #1 will be different due to K$^+$ uptake by the plants and evapotranspiration. Because $[K^+]_{0,n}$ is fixed at 6.6 mM, $[K^+]_{1,n}$ is directly proportional to $[K^+]_{0,n}$. Let μ be the fraction of K$^+$ taken up by the plants and θ the fraction of water loss due to evapotranspiration. Then, $[K^+]_{1,1}$ is given by:

$$[K^+]_{1,1} = \frac{(1 - \mu)[K^+]_{0,1}}{1 - \theta} \tag{2.6}$$

The Na$^+$ concentration will also change, firstly, because of evapotranspiration, secondly because of the Na$^+$ that leaches out of the coconut-based substrate used, causing an increase of the Na$^+$ concentration, represented by L. Then $[Na^+]_{1,1}$ is given by:

$$[Na^+]_{1,1} = \frac{[Na^+]_{0,1} + L}{1 - \theta} \qquad (2.7)$$

Reference point #2

Reference point #2 is located downstream the membrane unit (permeate side) and calculation of the K^+ and Na^+ concentration at this point therefore requires implementation of the membrane characteristics. Let α be the fraction of Na^+ (compared to reference point #1) that permeates the membrane (and with that removed from the system) and β the fraction of K^+ that permeates the membrane (also removed from the system). Then the K^+ and Na^+ concentrations are given by $[K^+]_{2,1}=(1-\beta)[K^+]_{1,1}$ and $[Na^+]_{2,1}=(1-\alpha)[Na^+]_{1,1}$, respectively.

2.2.3.1.2 Second irrigation cycle (n=2)

The calculations for the second cycle are essentially the same as those for the first cycle. The main difference concerns the starting point, *i.e.*, the volumetric flow balance at point #0, now given by:

$$\Phi_v(1) = \Phi_v(2) + \Phi_v(3) + \Phi_v(5) \qquad (2.8)$$

Expressed in terms of $\Phi_v(1)$, Eq. 2.8 equals :

$$\Phi_v(1) = \xi_2\Phi_v(1) + \varepsilon_2\Phi_v(1) + (1-\theta)\Phi_v(1) \qquad (2.9)$$

Given $\xi_2 + \varepsilon_2 + (1-\theta) = 1$ and therefore $\xi_2 = \theta - \varepsilon_2$, Eq. 2.9 reads:

$$\Phi_v(1) = (\theta - \varepsilon_2)\Phi_v(1) + \varepsilon_2\Phi_v(1) + (1-\theta)\Phi_v(1) \qquad (2.10)$$

In analogy with Eq. 2.2, Eq. 2.10 results in a K^+ concentration and ε_2 at point #0 of:

$$[K^+]_{0,2} = \xi_2\Psi + \varepsilon_2 N + (1-\theta)[K^+]_{0,2} = (\theta - \varepsilon_2)\Psi + \varepsilon_2 N + (1-\theta)[K^+]_{0,2}$$

$$(2.11)$$

$$\varepsilon_2 = \frac{[K^+]_{0,2} - (1-\theta)[K^+]_{2,1} - \theta \times \Psi}{N - \Psi} \qquad (2.12)$$

Once ε_2 has been determined, $[Na^+]$ at each point can be calculated:

$$[Na^+]_{0,2} = \varepsilon_2(M-X) + \theta X + (1-\theta)[Na^+]_{2,1} \tag{2.13}$$

$$[Na^+]_{1,2} = \frac{\varepsilon_2(M-X) + \theta X + L}{1-\theta} + [Na^+]_{2,1} \tag{2.14}$$

$$[Na^+]_{2,2} = \frac{1-\alpha}{1-\theta}[\varepsilon_2(M-X)] + \theta X + L \times (1-\alpha)[Na^+]_{2,1} \tag{2.15}$$

Apart from the fact that $[K^+]_{0,n}$ remains constant for n>1 (6.6 mM), $[K^+]_{1,n}$ and $[K^+]_{2,n}$ are constant as well having (if assuming β=0.1) a value of 11.4 and 10.3 mM, respectively. In addition, from the second cycle onwards ε_n remains constant as well and independent of n. This can be seen after, first, substituting ε_1 into $[K^+]_{2,1}$ followed by substituting $[K^+]_{2,1}$ into ε_2, resulting in:

$$\varepsilon_n = \frac{[K^+]_{0,n}[1-(1-\beta)(1-\mu)] - \theta \times \Psi}{N - \Psi} \tag{2.16}$$

According to the parameter values in Table 1.1, ε_n adopts a numerical value expressed in terms of β of $0.25 + 0.44\beta$ (=0.29 for β=0.1).

2.2.3.1.3 Generalized expressions

As evident from Eqs. 2.3-2.5, for the first cycle ε and by implication the $[K^+]$ and $[Na^+]$ as well can all be expressed exclusively in terms of the known process parameters $[K^+]_{0,1}$, α, β, μ, θ, r, N, M, X and Ψ. The same is actually true for the second cycle. This can readily be seen after substituting the expression for $[Na^+]_{2,1}$ into Eqs. 2.13, 2.14 and 2.15. Because of this, generalized expressions can be derived for $[Na^+]$ at each reference point as function of known process parameters and the cycle number n. The advantage of these generalized expressions is that they allow the direct calculation of $[Na^+]$ during the nth cycle at each reference point without the need to know (calculate) the concentrations during the previous cycles. As an example but also because Figures 2.3 and 2.4 were constructed using these expressions, the generalized expression for $[Na^+]_{0,n}$ and $[Na^+]_{1,n}$ from the 2nd cycle on are given below (for their derivation, *see* Supplementary Information).

$$[Na^+]_{0,n} = (M-X)\sum_{i=1}^{n}[\varepsilon_i(1-\alpha)^{n-1}] + (X\theta+L)\sum_{i=1}^{n-2}[(1-\alpha)^i] + (X+L)(1-\alpha)^{(n-1)} + X\theta \tag{2.17}$$

$$[\text{Na}^+]_{1,n} = \frac{1}{1-\theta} \times$$

$$\left((M-X)\sum_{i=1}^{n}[\varepsilon_i(1-\alpha)^{n-i}] + (X\theta+L)\sum_{i=1}^{n-1}(1-\alpha)^{i-1} + (1-\alpha)^{n-1}(X+L) \right)$$

<div align="right">(2.18)</div>

Note that for $n=2$ and after a number of repeated substitutions, Eqs. 2.17 and 2.18 reduce to Eqs. 2.13 and 2.14, respectively.

2.3 Results and discussion

2.3.1 Membrane selectivity

The Na$^+$ over K$^+$ permeation selectivity also is an intrinsic membrane property. As stated previously, one of our prime goals is to determine the minimum membrane selectivity (γ) required to maintain the Na$^+$ concentration in the IW below the upper tolerance level of 4-5 mM. Because the membrane selectivity (γ) is defined as the ratio of its permeability towards Na$^+$ (α) and its permeability towards K$^+$ (β), the permeation of both ion species is coupled. With both β and γ set at a fixed value, α can be calculated and with that the Na$^+$ level at point #2, which, in turn, allows the calculation of the Na$^+$ level at point #0 at the start of a new cycle.

To compromise between minimizing K$^+$ loss and dealing with a finite membrane selectivity, the value of β is set (arbitrarily) at 0.1, implying that 10% of K$^+$ is removed together with Na$^+$. In combination with a membrane that does not discriminate between K$^+$ and Na$^+$ ($\gamma = 1$) this results in a Na$^+$ removal of also 10%. In this case it is expected to see a dramatic Na$^+$ accumulation in the IW. Figure 2.3 confirms this expectation showing the Na$^+$ level in the IW after 10 cycles of operation and for a Na$^+$ over K$^+$ selectivity ranging from $\gamma = 1$ to 9. Note that $\gamma = 1$ indeed results in staggering Na$^+$ concentrations after 10 cycles of operation.
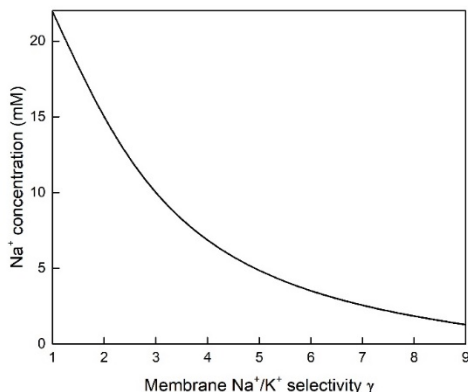
Figure 2.3 Accumulation of Na$^+$ in the irrigation water entering the greenhouse (i.e., at point #0) after 10 cycles of operation for a membrane with a Na$^+$/K$^+$ selectivity ranging from 1 to 9 and a K$^+$ permeability β of 0.1, *i.e.*, with 10% - 90% of the Na$^+$ and 10% of the K$^+$ removed.

Figure 2.4 explores the relationship between membrane selectivity and the Na$^+$ level at points #0 and #1 during 15 subsequent cycles of operation, given the 10% removal of K$^+$ ($\beta = 0.1$) and for a Na$^+$ over K$^+$ membrane permeability selectivity ranging from 5 to 9. A membrane selectivity of 5 does not suffice to achieve a steady-state [Na$^+$] below the threshold of 4 mM at point #0 (a) and of 20 mM at point #1 (b). Indeed, it requires at least a selectivity of 6 to accomplish steady-state levels remaining below these thresholds. As indicated in Figure 2.2, Na$^+$ is entering the system from three sources, the fresh water, the fertilizer content and the Na$^+$ leaching from the coconut-based substrate used. As already remarked, from the second cycle on ε_n adopts a constant numerical value of $0.25 + 0.44\beta$, *i.e.*, 0.29 for $\beta = 0.1$. Given $\theta=0.63$, ξ equals 0.34, implying that the amount of Na$^+$ entering the system from the fresh water and fertilizer is 3 and 72 g h^{-1}, respectively. The Na$^+$ concentration increase due to leaching equals 3.1 mM, resulting in 285 g h^{-1}. Evidently, at steady state the total amount of 360 g h^{-1} equals the amount of Na$^+$ that needs to be removed by the membrane unit.
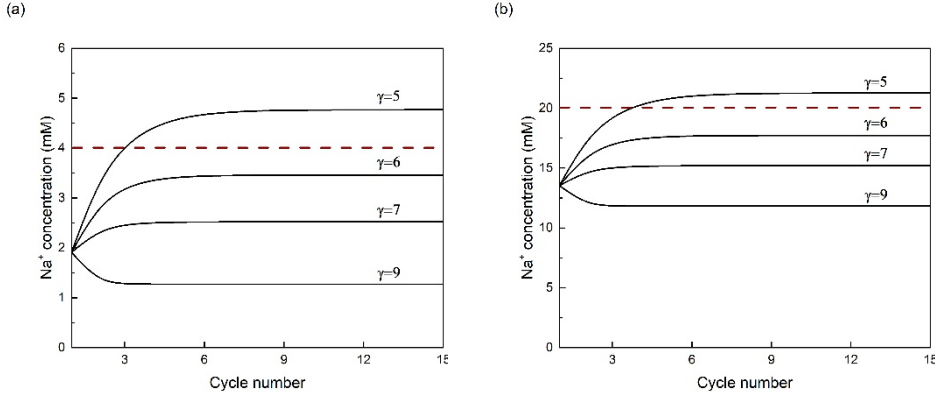
42

Figure 2.4 (a). Na$^+$ concentration in the irrigation water entering the greenhouse at point #0; (b). Na$^+$ concentration in the irrigation water leaving the greenhouse at point #1 during 15 cycles of operation, for a Na$^+$/K$^+$ membrane selectivity ranging from 5 to 9 and a K$^+$ permeability β of 0.1, i.e., with 50% - 90% of the Na$^+$ and 10% of the K$^+$ removed. Dotted lines represent the threshold of 4 mM of the Na$^+$ content of the IW entering the greenhouse (a) and the physiological tolerance threshold for tomato of 20 mM (b).

In order to maintain a steady-state K$^+$ concentration in the IW of 6.6 mM, the added amount of K$^+$, originating from the fertilizer, equals $\varepsilon_n \times N \times \Phi_v(1)$=430 g h^{-1}.

2.3.2 Implementation

As argued in the previous paragraph, Na$^+$ leaching from the substrate contributes most to the amount of Na$^+$ entering the IW system, even if considering that over time this amount reduces. So even if the Na$^+$ content of the fertilizer could be drastically reduced, Na$^+$ still accumulates in the (recycled) IW but at a lower rate.

We envision implementing the membrane-to-be-developed in an electro dialysis (ED)-like setting, operating under constant current conditions. From the view point of capital costs, a key parameter is the total required membrane surface area (A), given the amount of Na$^+$ that need to be removed. Eq. 2.19 gives the value of A as a function of volumetric flow through the membrane module Q, the Faraday constant F (96485 C/mol), the Na$^+$ concentration difference between the water entering and leaving the membrane module, the current density (i) and the current utilization factor (f)[22]:

$$A = \frac{Q \times F \times ([Na^+]_{1,ns} - [Na^+]_{2,ns})}{i \times f} \tag{2.19}$$

Where $[Na^+]_{1,ns}$ and $[Na^+]_{2,ns}$ are the Na^+ concentration at point 1 and 2 at steady state. The volumetric flow Q equals $\Phi_v(4)=0.37\times\Phi_v(1)=4.1\times10^{-4}$ m³ s⁻¹. As mentioned before, any water flow arising from either osmosis or electro osmosis is ignored, given the strong hydrophobic nature of the SLM system. According to Figure 2.2 and given $\alpha=0.6$ and $\beta=0.1$ (Figure 2.4a with $\gamma=6$), $[Na^+]_{0,n}$ reaches a steady-state value of 3.45 mM. The difference between the Na^+ concentration of the solution entering and leaving the membrane then is $0.6\times(3.5+3.1)/0.37=10.7$ mM. Note that this concentration difference results in $10.7\times10^{-3}\times23\times4000\times0.37=365$ gr Na^+/hr that needs to be removed, essentially the same amount as previously derived from the amount of Na^+ entering the system. As for the current density, we take a 'typical' value for ion exchange membranes given a total ionic strength of the incoming water of around 25-30 mM, $i.e.$, 10 A m⁻² [23]. Further, as a rather conservative estimate the current utilization factor (f) is assumed to be 0.6, implying that 60% of the current is actually carried by Na^+, the remaining 40% by K^+ and other ion species present. Substituting these numbers in Eq. 2.19 renders a membrane surface area of 70 m². In practice, this could be achieved by constructing ED stacks with a number of cells in series. For instance, three ED modules, each comprising of a stack of 12 cells with a membrane surface area of 2 m² each.

So far, our analysis has been based on average parameter values over one entire year, thereby ignoring seasonal variations. In any real-life application, the level of evapotranspiration and nutrient uptake will depend on time of the year and crop growth. This asks for a dynamic rather than static nutrient control. One option could be to monitor the water conductivity at point #1 and use this signal as input parameter for the electro dialysis unit. This way, the recorded conductivity (as measure of the Na^+ content) allows fine tuning of the constant current magnitude applied during operation, and with that the amount of Na^+ (and K^+) removed per unit time. Evidently, the implication of such dynamic control is that ε_n requires re-adjustment as well.

2.3.3 Economics perspective

The specifications of the membrane-to-be developed, $e.g.$ regarding membrane thickness and the required density of the crown ethers (as carrier molecules) in the membrane, remain elusive and await further study. Nevertheless, despite these uncertainties a few general remarks can be put forward.

Firstly, the capital cost of the SLM currently developed and validated is to a large extent dominated by the amount of 15-crown-5 needed. When purchased from TCI-

Chemicals and given the 15-crown-5 density (0.2 M), the membrane thickness (100 μm) and a support porosity of 50% the estimated cost price amounts to 500-800 euro per m^2. To put this number in perspective, the price of typical commercially available ion exchange membranes is around 300 euro per m^2. The most promising options to bring the price from the SLM down, seem a thinner membrane and upscaling 15-crown-5 (in-house) synthesis. It should be mentioned however that the (at this moment unknown and therefore not considered here) manufacturing cost contribute significantly to if not dominate the cost prize (Fuji Film, Netherlands; personal communication).

Secondly, the operational costs on the other hand will be dominated by the power needed to run the system. Based on the specifications of a typical ED system and given the salt concentration in the feed, the power consumption will be in the range 0.6-1.8 kWh m^{-3} [24]. The power consumption is linear with the applied current density [22] and as evident from Eq. 2.19, there are essentially three ways to reduce the required total membrane surface area: by reducing the volumetric flow through the system, by increasing the current utilization factor or by increasing the current density. Reduction of the volumetric flow could (possibly) be accomplished by a different configuration altogether. For instance, by positioning the membrane module not in the main stream (as in Figures 2.1 and 2.2) but instead in a bypass. This option will be explored in more detail once we (experimentally) obtained the actual specifications of our membrane under development. Improving the current utilization factor implies a higher Na$^+$ over K$^+$ membrane selectivity. Even though the cost for re-supplementing the IW with K$^+$ will go down, the membrane itself will (probably) be more expensive due to the higher density of crown ethers required. Finally, a higher current density will reduce the total membrane surface area needed but increase the power needed during operation. As pointed out by Strathmann [22], the opposite effect of current density on required membrane surface area and energy cost may translate in an optimal current density, resulting in the lowest overall costs.

Apart from the foregoing discussion and as remarked earlier on, the prime incentive for the current analysis was inspired more by environmental issues than by economics, even though at a certain point both types of arguments might become intertwined. For instance, (European) legislation becomes more stringent and might even aim for zero discharge in 2027, with discharge allowed only at high(er) cost [25,26]. For now, it remains speculative how including such discharge cost will affect the overall balance.

2.4 Conclusion

Excess Na^+ in irrigation water needs to be removed to a level dictated by the tolerance threshold specific for the particular crop, for tomato 20 mM. The closed-loop irrigation water system described here includes a membrane-based module to remove excess Na^+ while preserving the (nutrient) K^+ as much as possible. Based on real-life process parameters, the present study indicates that a Na^+ over K^+ membrane permeation selectivity of 6 already suffices to remain the Na^+ level the plants are exposed to below 20 mM, at least if accepted that 10% of the K^+ is removed as well. If implemented in an electro dialysis set-up while assuming a constant current density of 10 A m^{-2}, the estimated total membrane surface is 70 m^2. Considering the opposite effect of current density on required membrane surface area and energy cost, an optimum current density is hypothesized, resulting in a minimum of overall cost.

Supporting information

As in the manuscript, the nomenclature practiced is based on the use of two indices, the first representing the reference point, the second the cycle number. For instance, $[Na^+]_{2,3}$ refers to the Na^+ concentration at point #2 during the third cycle.

The manuscript gives the equations for ε and the K^+ and Na^+ concentrations during the 1st and 2nd cycle of operation. Here the expressions for the Na^+ concentrations at the three reference points during the 2nd cycle are given again but, in contrast to the manuscript, this time exclusively in terms of known parameters, as required to derive the generalized expressions.

$$[Na^+]_{0,2} = (M - X)\big(\varepsilon_2 + \varepsilon_1(1-\alpha)\big) + (X+L)(1-\alpha) + \theta X \qquad (S2.1)$$

$$[Na^+]_{1,2} = \frac{(M-X)\big(\varepsilon_2 + \varepsilon_1(1-\alpha)\big) + (X+L)(1-\alpha) + \theta X + L}{1-\theta} \qquad (S2.2)$$

$$[Na^+]_{2,2} = \frac{(M-X)\big(\varepsilon_2(1-\alpha) + \varepsilon_1(1-\alpha)^2\big) + (X+L)(1-\alpha)^2 + (\theta X + L)(1-\alpha)}{1-\theta}$$

$$(S2.3)$$

As shown in the manuscript (Eq. 2.16), from the 2nd cycle on ε_n becomes constant:

$$\varepsilon_n = \frac{[K^+]_{0,n} \times \big(1 - (1-\beta)(1-\mu)\big) - \theta \times \Psi}{N - \Psi} \qquad (S2.4)$$

Apart from the fact that $[K^+]_{0,n}$ remains constant for $n>1$ (6.6 mM), $[K^+]_{1,n}$ and $[K^+]_{2,n}$ are constant as well having (if assuming β=0.1) a value of 11.4 and 10.3 mM, respectively. For this reason, this Supplement is restricted to the Na^+ level at each reference point for $n>2$.

Mass Balance for the third irrigation cycle (n=3)

Reference point #0

In analogy with Eq. 2.13 in the manuscript, once ε_3 is known, $[Na^+]_{0,3}$ is given by:

$$[Na^+]_{0,3} = \varepsilon_3(M - X) + \varepsilon_2(M-X)(1-\alpha) + \varepsilon_1(M-X)(1-\alpha)^2$$
$$+ (X+L)(1-\alpha)^2 + (X\theta + L)(1-\alpha) + X\theta \qquad (S2.5)$$

Reference point #1

Likewise, in analogy with Eq. 2.14 in the manuscript, $[Na^+]_{1,3}$ reads:

$$[Na^+]_{1,3} = \frac{(M-X)\left(\varepsilon_3 + \varepsilon_2(1-\alpha) + \varepsilon_1(1-\alpha)^2\right) + (1-\alpha)^2(X+L)}{1-\theta}$$
$$+ \frac{(1-\alpha)(X\theta+L) + X\theta + L}{1-\theta} \tag{S2.6}$$

Reference point #2

In analogy with $[Na^+]_{2,1}=(1-\alpha)[Na^+]_{1,1}$, the $[Na^+]_{2,3}$ reads:

$$[Na^+]_{2,3} = \frac{(M-X)\left(\varepsilon_3(1-\alpha) + \varepsilon_2(1-\alpha)^2 + \varepsilon_1(1-\alpha)^3\right)}{1-\theta}$$
$$+ \frac{(1-\alpha)^3(X+L) + (1-\alpha)^2(X\theta+L) + (1-\alpha)(X\theta+L)}{1-\theta} \tag{S2.7}$$

Mass Balance for the fourth irrigation cycle (n=4)

Reference point #0

$$[Na^+]_{0,4} = (M-X)\left(\varepsilon_4 + \varepsilon_3(1-\alpha) + \varepsilon_2(1-\alpha)^2 + \varepsilon_1(1-\alpha)^3\right) + (1-\alpha)^3(X+L)$$
$$+ (1-\alpha)^2(X\theta+L) + (1-\alpha)(X\theta+L) + X\theta \tag{S2.8}$$

Reference point #1

$$[Na^+]_{1,4} = \frac{(M-X)\left(\varepsilon_4 + \varepsilon_3(1-\alpha) + \varepsilon_2(1-\alpha)^2 + \varepsilon_1(1-\alpha)^3\right) + (1-\alpha)^3(X+L)}{1-\theta}$$
$$+ \frac{(1-\alpha)^2(X\theta+L) + (1-\alpha)(X\theta+L) + X\theta + L}{1-\theta} \tag{S2.9}$$

48

Reference point #2

$$[Na^+]_{2,4} = \frac{(M-X)\left(\varepsilon_4(1-\alpha) + \varepsilon_3(1-\alpha)^2 + \varepsilon_2(1-\alpha)^3 + \varepsilon_1(1-\alpha)^4\right) + (1-\alpha)^4(X+L)}{1-\theta}$$

$$+ \frac{(1-\alpha)^3(X\theta+L) + (1-\alpha)^2(X\theta+L) + (1-\alpha)(X\theta+L)}{1-\theta}$$

(S2.10)

Mass Balance for the fifth irrigation cycle (n=5)

Reference point #0

$$[Na^+]_{0,5} = (M-X)\left(\varepsilon_5 + \varepsilon_4(1-\alpha) + \varepsilon_3(1-\alpha)^2 + \varepsilon_2(1-\alpha)^3 + \varepsilon_1(1-\alpha)^4\right)$$

$$+ (1-\alpha)^4(X+L) + (1-\alpha)^3(X\theta+L) + (1-\alpha)^2(X\theta+L)$$

$$+ (1-\alpha)(X\theta+L) + X\theta$$

(S2.11)

Reference point #1

$$[Na^+]_{1,5} = \frac{(M-X)\left(\varepsilon_5 + \varepsilon_4(1-\alpha) + \varepsilon_3(1-\alpha)^2 + \varepsilon_2(1-\alpha)^3 + \varepsilon_1(1-\alpha)^4\right)}{1-\theta}$$

$$+ \frac{(1-\alpha)^4(X+L) + (1-\alpha)^3(X\theta+L) + (1-\alpha)^2(X\theta+L)}{1-\theta}$$

$$+ \frac{(1-\alpha)(X\theta+L) + X\theta+L}{1-\theta}$$

(S2.12)

Reference point #2

$$[Na^+]_{2,5} = \frac{(M-X)\left(\varepsilon_5(1-\alpha) + \varepsilon_4(1-\alpha)^2 + \varepsilon_3(1-\alpha)^3 + \varepsilon_2(1-\alpha)^4 + \varepsilon_1(1-\alpha)^5\right)}{1-\theta}$$

$$+ \frac{(1-\alpha)^5(X+L) + (1-\alpha)^4(X\theta+L)}{1-\theta}$$

$$+ \frac{(1-\alpha)^3(X\theta+L) + (1-\alpha)^2(X\theta+L) + (1-\alpha)(X\theta+L)}{1-\theta}$$

(S2.13)

49

Generalized expressions for the nth irrigation cycle (n≥2)

When comparing Eqs. S2.1, S2.5, S2.8 and S2.11, the resemblance in the form of the expressions becomes evident. This resemblance allows the formulation of a generalized expression for $[\text{Na}^+]_{0,n}$ as function of n:

$$[\text{Na}^+]_{0,n} = (M - X)\sum_{i=1}^{n}[\varepsilon_i(1-\alpha)^{n-1}] + (X\theta + L)\sum_{i=1}^{n-2}[(1-\alpha)^i]$$
$$+ (X + L)(1-\alpha)^{(n-1)} + X\theta \qquad \text{(S2.14)}$$

Using the generalized form of Eq. 2.7 in the manuscript:

$$[\text{Na}^+]_{1,1} = \frac{([\text{Na}^+]_{0,1} + L)}{(1-\theta)} \quad \text{the generalized expression for } [\text{Na}^+]_{1,n} \text{ is:}$$

$$[\text{Na}^+]_{1,n} = \frac{1}{1-\theta} \times$$
$$\left((M - X)\sum_{i=1}^{n}[\varepsilon_i(1-\alpha)^{n-i}] + (X\theta + L)\sum_{i=1}^{n-1}(1-\alpha)^{i-1} + (1-\alpha)^{n-1}(X+L)\right)$$
$$\text{(S2.15)}$$

Finally, using $[\text{Na}^+]_{2,n} = (1-\alpha)[\text{Na}^+]_{1,n}$, the generalized expression for $[\text{Na}^+]_{2,n}$ becomes:

$$[\text{Na}^+]_{2,n} = \frac{1}{1-\theta} \times$$
$$\left((M - X)\sum_{i=1}^{n}[\varepsilon_i(1-\alpha)^{n-i+1}] + (X\theta + L)\sum_{i=1}^{n-1}(1-\alpha)^i + (1-\alpha)^n(X+L)\right)$$
$$\text{(S2.16)}$$

References

[1] C. Sonneveld, Effects of salinity on substrate grown vegetables and ornamentals in greenhouse horticulture, Wageningen University and Research, 2004.

[2] A.M.S. Abdul Qados, Effect of salt stress on plant growth and metabolism of bean plant Vicia faba (L.), J. Saudi Soc. Agric. Sci. 10 (2011) 7–15. https://doi.org/10.1016/j.jssas.2010.06.002.

[3] J.L. Zhang, T.J. Flowers, S.M. Wang, Mechanisms of sodium uptake by roots of higher plants, Plant Soil. 326 (2010) 45–60. https://doi.org/10.1007/s11104-009-0076-0.

[4] A.D. Blaylock, Cooperative Extension Service Soil Salinity, Salt Tolerance, and Growth Potential of Horticultural and Landscape Plants, 1994.

[5] A. Läuchli, S.R. Grattan, Plant growth and development under salinity stress, in: Adv. Mol. Breed. Towar. Drought Salt Toler. Crop., Springer Netherlands, 2007: pp. 1–32. https://doi.org/10.1007/978-1-4020-5578-2_1.

[6] T.B. Kinraide, Interactions among Ca2+, Na+ and K+ in salinity toxicity: quantitative resolution of multiple toxic and ameliorative effects, J. Exp. Bot. 50 (1999) 1495–1505. https://doi.org/10.1093/jxb/50.338.1495.

[7] D. Savvas, E. Chatzieustratiou, G. Pervolaraki, G. Gizas, N. Sigrimis, Modelling Na and Cl concentrations in the recycling nutrient solution of a closed-cycle pepper cultivation, Biosyst. Eng. 99 (2008) 282–291. https://doi.org/10.1016/J.BIOSYSTEMSENG.2007.10.008.

[8] D. Savvas, N. Mantzos, P.E. Barouchas, I.L. Tsirogiannis, C. Olympios, H.C. Passam, Modelling salt accumulation by a bean crop grown in a closed hydroponic system in relation to water uptake, Sci. Hortic. (Amsterdam). 111 (2007) 311–318. https://doi.org/10.1016/J.SCIENTA.2006.10.033.

[9] G. Carmassi, L. Incrocci, R. Maggini, F. Malorgio, F. Tognoni, A. Pardossi, Modeling Salinity Build-Up in Recirculating Nutrient Solution Culture, Http://Dx.Doi.Org/10.1081/PLN-200049163. 28 (2007) 431–445. https://doi.org/10.1081/PLN-200049163.

[10] P. Zhang, M. Senge, Y. Dai, EFFECTS OF SALINITY STRESS ON GROWTH, YIELD, FRUIT QUALITY AND WATER USE EFFICIENCY OF TOMATO UNDER HYDROPONICS SYSTEM, Rev. Agric. Sci. 4 (2016) 46–55. https://doi.org/10.7831/RAS.4.46.

[11] J.M. Pardo, F.J. Quintero, Plants and sodium ions: Keeping company with the enemy, Genome Biol. 3 (2002) 1–4. https://doi.org/10.1186/GB-2002-3-6-REVIEWS1017/FIGURES/1.

[12] F.J.M. Maathuis, I. Ahmad, J. Patishtan, Regulation of Na+ fluxes in plants, Front. Plant Sci. 5 (2014) 467. https://doi.org/10.3389/FPLS.2014.00467/BIBTEX.

[13] J. Bobacka, A. Ivaska, A. Lewenstam, Potentiometric ion sensors, Chem. Rev. 108 (2008) 329–351. https://doi.org/10.1021/cr068100w.

[14] T. Guinovart, D. Hernández-Alonso, L. Adriaenssens, P. Blondeau, F.X. Rius, P. Ballester, F.J. Andrade, Characterization of a new ionophore-based ion-selective electrode for the potentiometric determination of creatinine in urine, Biosens. Bioelectron. 87 (2017) 587–592. https://doi.org/10.1016/J.BIOS.2016.08.025.

[15] S. Song, H.M. Duong, A.M. Korsunsky, N. Hu, L. Lu, A Na+ Superionic Conductor for Room-Temperature Sodium Batteries, Sci. Rep. 6 (2016) 32330. https://doi.org/10.1038/srep32330.

[16] A.H. Galama, N.A. Hoog, D.R. Yntema, Method for determining ion exchange membrane resistance for electrodialysis systems, Desalination. 380 (2016) 1–11. https://doi.org/10.1016/J.DESAL.2015.11.018.

[17] M. Akieh-Pirkanniemi, G. Lisak, J. Arroyo, J. Bobacka, A. Ivaska, Tuned ionophore-based bi-membranes for selective transport of target ions, J. Memb. Sci. 511 (2016) 76–83. https://doi.org/10.1016/J.MEMSCI.2016.03.042.

[18] W. Walkowiak, C.A. Kozlowski, Macrocycle carriers for separation of metal ions in liquid membrane processes-a review, Desalination. 240 (2009) 186–197. https://doi.org/10.1016/j.desal.2007.12.041.

[19] S.D. Alexandratos, C.L. Stine, Synthesis of ion-selective polymer-supported crown ethers: a review, React. Funct. Polym. 60 (2004) 3–16. https://doi.org/10.1016/J.REACTFUNCTPOLYM.2004.02.006.

[20] D. Parmentier, M. Lavenas, E. Güler, S.J. Metz, M.C. Kroon, Selective removal of sodium from alkali-metal solutions with tetraoctylammonium monensin, Desalination. 399 (2016) 124–127. https://doi.org/10.1016/j.desal.2016.08.018.

[21] K. Tohda, K. Suzuki, N. Kosuge, H. Nagashima, K. Watanabe, H. Inoue, T. Shirai, A Sodium Ion Selective Electrode Based on a Highly Lipophilic Monensin Derivative and Its Application to the Measurement of Sodium Ion Concentrations in Serum, Anal. Sci. 6 (1990) 227–232. https://doi.org/10.2116/ANALSCI.6.227.

[22] H. Strathmann, Electrodialysis, a mature technology with a multitude of new applications, Desalination. 264 (2010) 268–288. https://doi.org/10.1016/j.desal.2010.04.069.

52

[23]   H.J. Lee, F. Sarfert, H. Strathmann, S.H. Moon, Designing of an
        electrodialysis desalination plant, Desalination. 142 (2002) 267–286.
        https://doi.org/10.1016/S0011-9164(02)00208-4.

[24]   A. Al-Karaghouli, L.L. Kazmerski, Energy consumption and water
        production cost of conventional and renewable-energy-powered desalination
        processes, Renew. Sustain. Energy Rev. 24 (2013) 343–356.
        https://doi.org/10.1016/J.RSER.2012.12.064.

[25]   European Commision, The EU Nitrate Directive, 2010.

[26]   European Commision, Water Framework Directive, 2010.

2

Chapter 3

Separation of alkali metal cations by a supported liquid membrane operating under electrodialysis conditions

Abstract

This study demonstrates the effective separation of alkali metal cations using a Supported Liquid Membrane (SLM) containing lipophilic, negatively charged borate moieties, operating under electro dialysis conditions. The selectivity of the membrane is essentially based on differences in dehydration energy and mobility between ion species. The system favors the ion species with the largest crystal radius, despite its lower mobility. In mixtures of K^+ and Na^+, the SLM separates K^+ from Na^+ with a separation efficiency ranging from ~20% to 90%, depending on the feed solution composition. With solutions containing either K^+ or Na^+ and Li^+, the K^+/Na^+ over Li^+ separation efficiency is nearly 100%. Addition of 15-crown-5 derivative does not improve SLM behavior, but slows down the K^+ current by approximately 30% whereas the Na^+ current remains unaffected. As supported by simulations, the free K^+ and Na^+ ratio in the membrane (and with that the current ratio) is entirely defined by partitioning and the feed concentration ratio, regardless the presence of 15-crown-5. As a result, the current ratio of two ion species can be described exclusively in terms of their feed concentrations and crystal radii because the latter parameter defines both partitioning and mobility.

3.1 Introduction

The underlying working mechanism of different types of membranes varies. The ability to discriminate between different components may be based on, for instance, charge, sieving, partitioning (effected by charge and size), mobility or the affinity between a guest and membrane-based host compound. In nanofiltration (NF) membranes, for instance, sieving properties dominate whereas in ion-exchange membranes (IEMs) charge is the predominant separation parameter. Most membranes exploit however a combination of two or more of these parameters. In IEMs, apart from charge, the interaction between a host and guest molecule as well as the mobility of the (partly dehydrated) ionic species may play a role.

The combination of IEMs with electro dialysis (ED) as applied in sea or waste water desalination has been widely reported [1–6]. There are two main reasons why this combination proved to be so fruitful. Firstly, transport enhancement by an electrical field is so much more efficient than a concentration gradient as driving force [7]. Secondly, currently existing IEMs possess a rather high selectivity in that they are quite well able to discriminate between cations and anions [8–10]. The fixed immobile charge inside the membrane effectively excludes co-ions (of the same sign of charge as the fixed charge inside), thereby preventing them entering the membrane. This concept, known as Donnan exclusion, works especially well as long as the concentration of co-ions in the surrounding solution is much lower than the fixed charges inside the membrane. The separation of two positively charged or two negatively charged ion species is also possible, at least if they differ in their valence, for instance, monovalent from divalent [11]. A membrane covered with, for instance, a positively charged top layer may repel divalent cations just strong enough, while meanwhile passing the monovalent cations [10]. It has been demonstrated that (co)polymer and nanofibers membranes can be used for the removal of Cu^{2+} ions from waste water [12–14].

A very challenging endeavor is the separation of two ionic species of the same charge, even more so if the two ion species are very similar in size. Once feasible, this possibility will open the way to novel applications in the field of selective element removal and element recovery, the former in the context of more severe legislation for discharge, the latter because of element scarcity. Because of its potential impact, the present study addresses this challenge. A previous study of this lab focused on the removal of Na^+ from the drainage water of greenhouses also containing K^+ [15]. Due to the salination of ground water and the fact that Na^+ is not taken up by plants,

Na⁺ accumulates in the (recycled) irrigation water. Whereas K⁺ is an essential nutrient for plants, too high levels of Na⁺ are toxic for most plants [16–18]. The challenge thus is to selectively remove Na⁺ while leaving K⁺ untouched as much as possible. Worth to mention is that the sensor community is familiar for decades already with artificial membranes capable of distinguishing between ionic species of the same charge. The (potentiometric) membranes of Ion Selective Electrodes (ISE) contain carrier molecules (*e.g*. crown ethers) with a high specific affinity for one particular ionic species [19,20]. A key difference between an ISE membrane and a typical separation membrane (the aim of the present study) is however that the fluxes over the ISE membrane are, or ideally should be, by definition essentially zero as any ion movement over the membrane will compromise the response sensitivity of the ISE.

The starting point of the present study is the so-called Supported Liquid Membrane or SLM. In short, in an SLM an organic phase is immobilized into an inert porous support, offering mechanical strength [21,22]. The SLM represents a three-phase extraction process where solutes can be extracted from one aqueous phase into another meanwhile passing the organic liquid phase in between. One reason to select the SLM as our membrane type of choice is the flexibility to add or adjust specific components to the organic phase [23]. The potential of SLM's in water desalination has been pointed out in [24]. Lipophilic salts have been widely reported to be used as ion exchanger in polymeric membranes for a good working performance [25–27]. Therefore, in order to improve its cation-over-anion selectivity and lower its ionic resistance, lipophilic anions are added to the SLM. These anionic sites are essentially the functional equivalent of the fixed permeant charge in typical ion-exchange membranes.

The present study reports on a SLM system implemented in an ED setting able to selectively enrich Na⁺ from a solution also containing K⁺. To generalize the concept of the SLM used, Li⁺ is included in this study as well. Generally, SLM's contain specific carrier molecules to improve the membrane selectivity during the separation process [28–31]. For that reason, we explored the effect of inclusion of 15-crown-5 on SLM behavior. Finally, the application of the technology outlined here in green houses is briefly addressed including a test using a synthetic solution with the same composition as drainage irrigation water and a (brief) comment on the economic feasibility of the technology.

3.2 Materials and methods

3.2.1 Chemicals

All chemicals used were of analytical grade. The ACCUREL support (polypropylene, thickness: 100 µm, pore size: 0.1 µm) was purchased from MEMBRANA; the non-ionic base molecule for the synthesis of the lipophilic crown ether used as ion carrier, 2-hydroxymethyl-15-crown-5, from TCI Chemicals. All other chemicals were from Sigma-Aldrich: the organic solvent used for impregnating the ACCUREL support, 2-nitrophenly-n-octyl ether (NPOE); the lipophilic backbone hydride-terminated poly(dimethylsiloxane), the catalyst chloride tris (triphenylphosphane)rhodium(I) (Wilkinson's catalyst); the solvent toluene (anhydrous); the lipophilic anion sodium tetrakis[3,5-bis(trifluoromethyl)phenyl]borate (NaBArF) and the salts, KCl, NaCl, LiCl and Na_2SO_4.

3.2.2 Crown Ether Synthesis

In order to prevent leaching out, 15-crown-5 was covalently attached to a rather bulky lipophilic backbone, *i.e.*, hydride-terminated poly(dimethylsiloxane) (PDMS), resulting in 1,8-(polydimethysily)propyloxymethyl-15-crown-5 (PSCE). Figure 3.1 schematically shows the synthesis route of PSCE, a more detailed recipe and characterization can be found in the Supplementary Information.
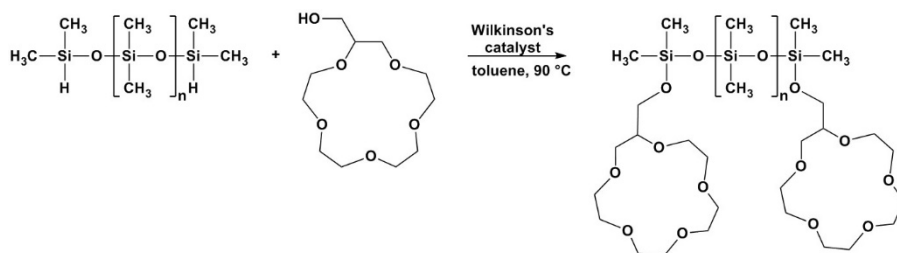

Figure 3.1 Schematically depicted synthesis route of polysiloxane-bound crown ether (PSCE)

3.2.3 Membrane preparation & stability

All experiments were performed with freshly prepared SLMs. The membrane support (ACCUREL) was submerged in the organic solvent mixture for 30 min, at RT. Due to capillary forces, the ACCUREL pores are filled up with solvent.

Afterwards, excess solvent was removed by gently tissue wiping the membrane. The organic solvent mixture consisted of different combinations of NPOE, NaBArF and crown ether. If present, the NaBArF concentration always was fixed at 0.05 M. The crown ether concentration, as established by NMR, (see Supplementary Information), always was 0.13 M, a value close to its maximal solubility in NPOE [29].

As for membrane stability, the morphology of the membrane support and the obtained SLM before and after an ED experiment were assessed by SEM. No obvious changes were visible (see Supplementary Information).

3.2.4 Membrane characterization

3.2.4.1 Membrane selectivity

The membrane selectivity under zero-current conditions was assessed in a two-compartment measuring cell. For the cation over anion selectivity, one compartment was continually perfused with 0.5 M KCl solution, the other one with 0.005 M KCl. For the K^+ over Na^+ selectivity, the SLM separated a 0.1 M KCl solution from a 0.1 M NaCl solution. Two double-junction Ag/AgCl reference electrodes recorded the potential difference over the SLM. The effective membrane surface area under investigation was 10.15 cm^2. All experiments were performed at room temperature $(25 \pm 0.2$ °C. Following the protocol of Długołecki et al. [32], all membranes were conditioned in the solution of lower salt concentration (0.005M KCl or 0.1M NaCl solutions) for 24 h. Membrane potentials were measured 30 min after the start of perfusion the measuring cell with the proper solutions [32].

The reversal, equilibrium or zero-current potential (E_{rev}) of a membrane permeable for both monovalent cations and anions, *e.g.* K^+ and Cl^-, is given by the Goldman-Huxley-Katz or GHK equation:

$$E_{rev} = \frac{RT}{F} \ln \frac{P_K \times K_{feed} - P_{Cl} \times Cl_{receiving}}{P_K \times K_{receiving} - P_{Cl} \times Cl_{feed}} \qquad (3.1)$$

R is the gas constant (8.314 J K^{-1} mol^{-1}), T is the temperature (K) and F is the Faraday constant (96485 C mol^{-1}), P_K and P_{Cl} are the permeability coefficient (m^2/s) for K^+ and Cl^-, respectively, and with [K] and [Cl] in terms of activity rather than concentration.

Dividing the right term by P_{Cl} and after rearranging terms renders the expression for P_K/P_{Cl}:

$$\frac{P_{\mathrm{K}}}{P_{\mathrm{Cl}}} = \frac{\phi \times \mathrm{Cl}_{\mathrm{feed}} - \mathrm{Cl}_{\mathrm{receiving}}}{\mathrm{K}_{\mathrm{feed}} - \phi \times \mathrm{K}_{\mathrm{receiving}}} \quad (3.2)$$

with ϕ as a constant is defined by:

$$\phi = \exp\left(\frac{FE_{\mathrm{rev}}}{RT}\right) \quad (3.3)$$

For a membrane 100% selective for monovalent cations, $e.g.$ K$^+$, Eq. 3.1 is reduced to the Nernst equation:

$$E_{\mathrm{rev}} = E_N = \frac{RT}{F}\ln\frac{\mathrm{K}_{\mathrm{feed}}}{\mathrm{K}_{\mathrm{receiving}}} \quad (3.4)$$

The monovalent cation over monovalent cation selectivity, $e.g.$ K$^+$ over Na$^+$, can be assessed under bi-ionic conditions with equimolar amounts of KCl and NaCl in the feed and receiving compartment, respectively [33,34]. Then, Eq. 3.1 reads:

$$E_{\mathrm{rev}} = \frac{RT}{F}\ln\frac{P_{\mathrm{K}} \times \mathrm{K}_{\mathrm{feed}}}{P_{\mathrm{Na}} \times \mathrm{Na}_{\mathrm{receiving}}} \quad (3.5)$$

with the permeability ratio of P_{K} and P_{Na} given by:

$$\frac{P_K}{P_{Na}} = \phi\frac{[K]_{\mathrm{feed}}}{[Na]_{\mathrm{receiving}}} \quad (3.6)$$

3.2.4.2 Electrodialysis (ED)

Apart from the behavior (selectivity) of the SLM under zero-current conditions, selectivity can be expressed in terms of transport numbers, a measure of the selectivity under non-zero current conditions and representing the current contribution of one particular ion species to the (forced) total current over the membrane. Ion transport across the SLMs were evaluated under ED conditions. Experiments were carried out in a six-compartment cell equipped with a platinum electrode (54 mm in diameter) in both outer compartments, as shown in Figure 3.2. This way, possible redox reactions occurring in the two outer compartments do not affect the concentrations of the

permeable ion species present in the two inner compartments directly facing the SLM. Also note the position of cation-exchange membranes (CEM from Neosepta) and anion-exchange membranes (AEM from Neosepta) separating the several compartments. In effect, changes in concentration in the two inner compartments can be attributed exclusively to ion transport over the SLM.
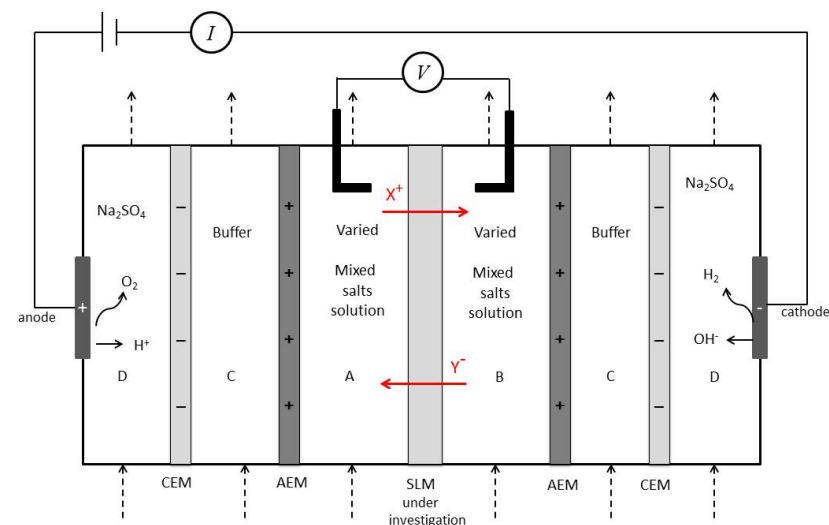
Figure 3.2 Configuration of the six-compartment cell used during the electro dialysis experiments. Compartments C and D as well as the position of the CEM and AEM ensure that the concentration changes in the two inner measuring compartments arise solely from ion fluxes over the SLM.

The effective surface area and thickness of the SLMs under investigation was 10.15 cm² and 100 μm, respectively. The feed compartment A and receiving compartment B were filled with (different) KCl or NaCl solution, depending on the type of selectivity assessed. Both C compartments were perfused with a recirculating buffer (1 L) solution with the same salt concentration as in A and B. The two outer D compartments recirculated an electrolyte solution containing 0.05 M Na_2SO_4 solution. Prior to use, SLMs were pre-conditioned for 24 h in the measuring solution of lowest salt concentration. Using a water bath, the temperature of all solutions was controlled at 25 ± 0.2 °C. A potentiostat (Ivium Technologies, Vertex. One, Eindhoven, The Netherlands) was employed as power source for applying a constant current (density). In order to monitor the voltage drop over the membrane, two Haber-Luggin capillaries

were positioned directly adjacent to the SLM (Figure 3.2) and connected to two reservoirs containing 3 M KCl-filled Ag/AgCl reference electrodes (QM711X, QIS, The Netherlands). Typically, a constant current of 10 mA (corresponding to a current density of 10 A m^{-2}) was applied during a time period of 24 (for single salt experiments) or 48 h (for all mixed salt experiments).

3.2.5 Transport Numbers & Mobility

Determination of transport numbers requires recording of the concentration changes in compartments A or B but preferably in both. Therefore, during the experiments every hour samples of 1 mL were taken from both compartments, with the ion concentrations determined by ion chromatography (IC, Metrohm Compact IC 761), at a confidence level >95%.

The transport number t_i for monovalent ion species i is given by:

$$t_i = \frac{FV\frac{\Delta C}{\Delta t}}{I_{tot}A}$$

(3.7)

where V is the volume (L) of the feed and receiving compartment, A the effective membrane surface area (m^2), and I_{tot} the (constant) externally applied current density (A m^{-2}). The number of moles transferred over the SLM per unit time, $\Delta C/\Delta t$ (mol m^{-3} s^{-1}), was calculated from the change in concentration in both compartments A and B: $\Delta C = (C_{B,t} - C_{A,t})/2$ (mol m^{-3}).

During single-salt experiments (aiming to assess the ion mobility in the membrane), compartments A and B contained either symmetrical 0.1 M KCl, NaCl or LiCl. A constant (absolute) current of 10 A m^{-2} was applied during 24 h experimental time. The ion mobility u_i of ion species i is given by:

$$u_i = \frac{t_i I_{tot}}{c_i F \frac{E_m}{d}}$$

(3.8)

Here, c_i represents the free cation concentration in the membrane (in mol m^{-3}). Because of electro neutrality, c_i equals the concentration of immobilized lipophilic anions A in the membrane. Equating c_i with A presumes that ion pair formation between the free cations and A can be neglected. The electric field strength in the

membrane (E_m/d) is defined as the ratio of recorded voltage drop over the SLM and its thickness (d).

3.2.6 Ion Partitioning

The Born equation gives the ΔG of the transfer of an ion species of charge z and crystal radius r (in Å) from phase 1 with permittivity ε_1 to phase 2 with permittivity ε_2:

$$\Delta G = \frac{N_A z^2 e^2}{8\pi\varepsilon_0 r}\left(\frac{1}{\varepsilon_2}-\frac{1}{\varepsilon_1}\right) = \frac{695}{r}\left(\frac{1}{\varepsilon_2}-\frac{1}{\varepsilon_1}\right) = \frac{20.3}{r} \tag{3.9}$$

with ΔG in kJ mol^{-1}, N_A Avogadro's number (6.02×10^{23}), e the elementary charge (1.6022×10^{-19} C) and ε_0 the permittivity of vacuum (8.854×10^{-12} F m^{-1}). The pre-factors 695 and 20.3 in Eq. 3.9 result from transferring a monovalent cation ($z = 1$) from the aqueous ($\varepsilon_1 = 80$) into the NPOE/membrane phase ($\varepsilon_2 = 24$) [35].

Table 3.1 lists the crystal radii and the ΔG calculated according to the Born equation of the three monovalent cations used in this study.

	Crystal radius (in Å) [36,37]	ΔG (in kJ mol^{-1})	Ion pairs	α
Li$^+$	0.60	33.8	K$^+$/Na$^+$	11.7
Na$^+$	0.95	21.4	Na$^+$/Li$^+$	150.4
K$^+$	1.33	15.3	K$^+$/Li$^+$	1771.5

Table 3.1 Crystal radii (in Å) of Li$^+$, Na$^+$ and K$^+$, as well as the Calculated Born ΔG (in kJ mol^{-1}) required for the transport of the particular ionic species from the aqueous into the NPOE/membrane phase. The value of α in the most-right column refers to Eq. 3.10.

The partitioning of both ion species over the (feed) aqueous and NPOE/membrane phase is defined by a Boltzmann distribution. In the case of K$^+$ and Na$^+$, the ratio of free K$^+$ and free Na$^+$ in the membrane, K$_m$/Na$_m$, equals:

$$\frac{K_m}{Na_m} = \frac{K_f}{Na_f}\exp\left(\frac{\Delta G_{Na}-\Delta G_K}{RT}\right) = \alpha\frac{[K]_f}{[Na]_f} \tag{3.10}$$

with $[K]_f$ and $[Na]_f$ the (time-dependent) K$^+$ and Na$^+$ concentration in the feed solution. After substituting the ΔG values for K$^+$ and Na$^+$ from Table 3.1, the

numerical value of α turns out to be 11.7. For ion pairs Na$^+$/Li$^+$ and K$^+$/Li$^+$ the value of α equals 150.4 and 1771.5, respectively.

3.2.7 Membrane Resistance

For the membrane resistance measurements, the configuration of the six-compartment cell as shown in Figure 3.2 was slightly adapted in that all AEMs were replaced by CEMs. The SLM resistance was measured in (circulating) symmetrical 0.5 M NaCl solutions in compartments A and B. Prior to the actual recording, membranes were conditioned in 0.5 M NaCl solution for 24 h. All resistance measurements were performed at room temperature of 25 ± 0.2 °C. A potentiostat (Autolab AUT85567, The Netherlands) served as constant-current supply. The protocol followed was a step-wise increase of the current density, ranging from 0 – 2.5 A m^{-2}. The slope of the current density (A m^{-2}) *versus* voltage drops over the membrane (E_m) gives the (apparent) membrane resistance. The actual resistance of solely the SLM requires a resistance measurement of just the electrolyte solution as well. Subtraction of the latter from the former measurement renders the pure membrane resistance (Ω cm^2).

3.3. Results & Discussion

3.3.1 Mass and charge balances

In order to investigate whether the ion concentration changes in the two inner compartments of the six-compartment cell in Figure 3.2 can be exclusively ascribed to transport over the central membrane separating chambers A and B, mass and charge balances were set up. Ideally, the changes of one particular ionic species in both compartments are the same but of opposite sign; stated otherwise, their summation add up to zero. In addition, in order to retain electro neutrality, the total charge in each compartment also adds up to zero. As Table 3.2 shows, the mass and charge balance for both single and mixed salts solutions were indeed essentially closed. The same is true for the 'Total' balance taking into account all compartments. This bookkeeping gives credit to the concentration measurement of all ionic species involved by IC and ICP.

	Single 0.1 M KCl			Single 0.1 M NaCl			Mixed 0.05 M KCl + 0.05 M NaCl		
	A	B	Total	A	B	Total	A	B	Total
ΔK (mmol)	-8.39	8.26	-0.86	N/A	N/A	-0.01	-13.30	11.51	-1.18
ΔNa (mmol)	N/A	N/A	-0.33	-7.05	7.07	-0.02	-4.95	4.80	0.19
ΔCl (mmol)	-8.52	8.51	-1.09	-7.64	7.68	0.04	-17.15	15.16	0.99
ΔCharge (mmol e)	0.01	0	-0.04	0.56	-0.61	-0.01	-1.13	-1.15	0

Table 3.2 Mass and charge balance of compartments A and B, where charge balance refers to the net charge of the solution after accounting for the measured ion concentration changes. The third column, labelled Total, refers to the balances including all compartments A, B, C and D. Balances were calculated from measurements in either single-salt 0.1 M KCl and NaCl solutions or a mixed solution containing 0.05 M KCl and 0.05 M NaCl. N/A=Not Applicable.

Careful analysis revealed that the discrepancy between the mass leaving the feed and entering the receiving phase as well as the non-zero total net charge are not due to ion accumulation inside the membrane. It is concluded that any deviation, *i.e.* non-zero value, falls in the error-range of ion concentration measurement by IC or ICP, typically ±5%.

3.3.2 Membrane selectivity and membrane electrical resistance

First, the cation over anion selectivity of the SLM was assessed, as measured in asymmetrical 0.5/0.005 M KCl solutions, summarized in Table 3.3. With a P_K/P_{Cl} value of 357, the standard SLM, defined as a membrane containing both the solvent NPOE and lipophilic anion borate (A), clearly is cation selective in nature.

	K$^+$ *vs.* Cl$^-$ Selectivity	K$^+$ *vs.* Na$^+$ selectivity	Membrane resistance (Ω cm^{-2})
	P_K/P_{Cl}	P_K/P_{Na}	R
SLM (=NPOE + A)	357	30	440
SLM – A	0	19	12142
SLM + PSCE	3069	59	3760
SLM + PSCE – A	12	76	4391

Table 3.3 Effect of excluding the lipophilic anion (A) or including the crown-ether (PSCE) on the K$^+$ over Cl$^-$ selectivity, the K$^+$ over Na$^+$ selectivity and membrane resistance of the SLM.

Taking out the lipophilic anion (SLM-A) turned the SLM in an essentially non-selective membrane, indicating that the observed K$^+$ over Cl$^-$ selectivity of the SLM is solely due to the presence of A. Next, we investigated the effect of the inclusion of polysiloxane bound 15-crown-5 (SLM+PSCE). Supplementing the SLM with PSCE drastically increased the selectivity to >3000, almost a factor ten higher than the selectivity of the standard SLM. Even though this result may suggest a possible synergetic effect of A and PSCE, it should be realized that in this range, calculated permeability ratios are extremely sensitive to the measured reversal potential with large effects already upon shifts of merely a few mV's. The reason is both that the measured E_{rev} values asymptotically approach the theoretical Nernst potential of, in this case, K$^+$ (109 mV) and that the calculated P_K/P_{Cl} scales exponentially with E_{rev} (Eq. 3.2). The P_K/P_{Cl} of a membrane containing PSCE but not A reduced to 12, emphasizing the predominant role of A in the cation over anion selectivity of the SLM with just a marginal contribution of PSCE, if any at all.

The next question concerned the membrane selectivity under bi-ionic conditions, with one chamber containing 0.1 M NaCl and the other 0.1 M KCl. As both solutions contain the common anion at the same concentration, any contribution of anion permeability to the recorded E_{rev} can be safely dismissed (Eq. 3.6). Apart from the fact that all membranes tested clearly demonstrate K$^+$ over Na$^+$ selectivity, differences are less profound as seen in the charge selectivity previously discussed. With theoretical Nernst potentials of K$^+$ and Na$^+$ of +/- ∞, this observation also relates to the fact that measured E_{rev} values fall in a range where calculated P_K/P_{Na} values are relatively insensitive to E_{rev}. The picture that arises from the values of P_K/P_{Cl} and

P_K/P_{Na} is that the lipophilic anion is responsible for the cation-over-anion selectivity, whereas the presence of PSCE only slightly improves the K^+ over Na^+ selectivity of the SLM. The slight improvement is possibly caused by the cation complexing properties of the PSCE and its higher affinity towards K^+.

The last column of Table 3.3 refers to the measured membrane resistance, as assessed in symmetrical 0.5 M NaCl. Most remarkable is the low resistance of the standard SLM and the high resistance of a membrane lacking the lipophilic anion A. Adding PSCE to the standard SLM increases the resistance nearly tenfold, an effect suggesting an interaction between the permeant cation and the hardly mobile PSCE, resulting in a lower mobility of the permeant cation.

3.3.3 Single-Salt Solutions: Transfer Numbers & Mobility

Starting point are flux measurements in symmetrical 0.1 M KCl, NaCl or LiCl solutions over the SLM solely containing NPOE and A. Figure 3.3 shows the normalized K^+, Na^+ and Li^+ concentration over time, *i.e.* the ratio of measured cation concentration and the initial cation concentration in feed compartment A (closed symbols). Note that in symmetrical solutions the minimum value of this normalized concentration is zero. For all three alkali metal ions, the relative cation concentration shows a similar linear decrease with time.
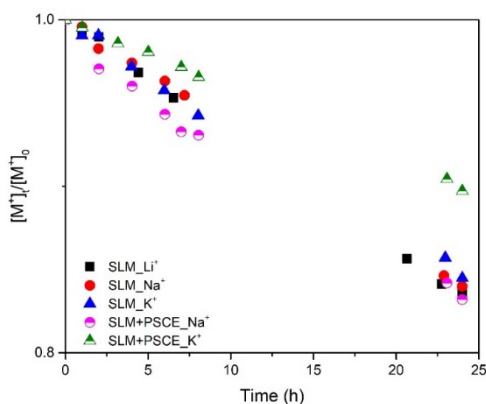

Figure 3.3 Normalized K^+, Na^+ and Li^+ concentration in feed compartment A, recorded over time in symmetrical 0.1 M KCl, NaCl or LiCl solutions (closed symbols). Also shown, the effect of PSCE as determined in KCl and NaCl solutions (half open symbols).

The transport numbers of K^+ and Na^+ (Eq. 3.7) and the absolute amount of transported K^+ and Na^+ over the SLM can be derived from the data in Figure 3.3. Once the transport number has been determined and together with the simultaneously recorded voltage drop over the SLM (E_m), the slope of Figure 3.3 allows the calculation of the cation mobility (u) in the membrane, assuming that, due to overall electro neutrality, the free cation concentration in the membrane equals the concentration of lipophilic anion A (Eq. 3.8). Table 3.4 summarizes the calculations based on data plotted in Figure 3.3: ion transport number (t), membrane potential (E_m), absolute amount being transferred (in mmol) and ion mobility (u). Regarding the SLM data, the amount of salt transported as well as the transport number are very similar for K^+, Na^+ and Li^+, indicating that the current is predominantly cationic in nature, consistent with the high cation over anion selectivity of the SLM discussed in the previous paragraph. Also note that the mobility of Na^+ and Li^+ are quite similar and significantly higher than the mobility of K^+. Even though the ion mobility is directly calculated from the recorded voltage drop over the membrane (Eq. 3.8), the ratio of measured E_m (slightly) deviates from the reciprocal ratio of mobility values. For example, due to a small difference in transport number, the K^+/Na^+ E_m ratio of 2.78/1.6=1.74, is close but not identical to the Na^+/K^+ mobility ratio of 1.66.

0.1 M KCl	t_{ion}	E_m (V)	[K] (mmol)	$u_i \times 10^{-11}$ (m^2 V^{-1} s^{-1})
SLM	0.97	2.78	8.39	7.2
SLM+PSCE	0.73	1.01	6.03	5.4
0.1 M NaCl	t_{ion}	E_m (V)	[Na] (mmol)	$u_i \times 10^{-11}$ (m^2 V^{-1} s^{-1})
SLM	0.93	1.60	8.16	12.0
SLM+PSCE	0.96	1.89	8.43	12.4
0.1 M LiCl	t_{ion}	E_m (V)	[Li] (mmol)	$u_i \times 10^{-11}$ (m^2 V^{-1} s^{-1})
SLM	0.93	1.33	8.42	14.5

Table 3.4 Transport numbers of K^+, Na^+ and Li^+ (t_{ion}), recorded membrane potential (E_m), absolute amount of transported cation from feed to receiving compartment and the ion mobility in the membrane (u_{ion}), all derived from single salt measurements.

Assuming that the ion can freely move within the SLM, the mobility of a completely dehydrated ion species is expected to be directly proportional to its reciprocal crystal radius. By approximation, this is indeed observed. First exemplified

for K^+ and Na^+, the experimentally obtained Na^+/K^+ mobility ratio of 1.66 is indeed in reasonable agreement with the reciprocal ratio of their crystal radii of 1.4 (Table 3.1). For Li^+/Na^+ and Li^+/K^+ the measured mobility ratio is 1.21 and 2.09, respectively *versus* a reciprocal crystal radii ratio of 1.58 and 2.22, respectively. This observation supports the view that the charge carrier in the SLM is the dehydrated cation species, in agreement with the rather low permittivity of NPOE of 24. Small differences between the calculated mobility ratio and the reciprocal ratio of crystal radii may point to a possible (ion species-dependent) interaction between the permeant cation and the lipophilic anion.

3.3.4 Single-Salt Solutions: Effect of Crown Ether

Next, the addition of PSCE on SLM behavior was investigated, corresponding to the SLM + PSCE data in Table 3.4 and the half open symbols in Figure 3.3, showing how the presence of PSCE affects the K^+ concentration changes. The presence of PSCE clearly has a distinct effect when recorded in either K^+ or Na^+ solution. Whereas the K^+ transport number drops from 0.97 to 0.73 and the recorded E_m from 2.78 to 1.01 V, inclusion of PSCE hardly affects Na^+ transport, despite its recorded effect on E_m as listed in Table 3.3. This differential effect on K^+ and Na^+ transport indicates that K^+ (but not Na^+) interacts with the (rather immobile) PSCE, resulting in an overall reduced K^+ mobility. Note that the reduced E_m of 1.01 V in the presence of PSCE should not be interpret in terms of a reduced membrane resistance. The latter is defined by the slope of the IV-plot rather than the recorded voltage at one particular current density (as is the case here).

The reduced transport number of 0.73 raises the question about the identity of the ion species responsible for the remaining 0.27 part. Based on (changes in) measured pH values, H^+ as charge carrier can be excluded. The only candidate left is Cl^-, moving in opposite direction. Apparently, the constant applied current forces the SLM, despite its high cation selectivity, to the transport of Cl^-, all resulting from the reduced mobility of that part of K^+ interacting with PSCE and because transport numbers should add up to unity. The current carried by each ion species is directly proportional to both its concentration and its mobility in the membrane. As will be discussed in more detail later on, K^+ and Na^+ may interact with the lipophilic anion A. Because such interaction between Cl^- and A can be safely dismissed, the mobility of Cl^- might be (significantly) higher than the mobility of K^+ and Na^+. By implication, even though, in the case of KCl in the feed solution, Cl^- transport accounts for 27%

of the total current, the actual number of Cl⁻ ions transported over the membrane might still be limited compared to that of K⁺. Unfortunately, because of the configuration of the six-compartment cell with an AEM separating compartments A and B from C, quantifying the Cl⁻ current is impossible because of Cl⁻ entering from compartment C (Figure 3.2). To compensate for the presence of Cl⁻ in the membrane, the actual K⁺ concentration is expected to be (slightly) higher than the concentration in the absence of PSCE. Finally, the calculated mobility of K⁺ in the presence of PSCE is an average value with contributions of both free K⁺ and K⁺/PSCE complex. Consistent with the conclusion that PSCE interacts with K⁺, but not with Na⁺, in K⁺ this average value is lower than the value observed in a pure K⁺ solution, whereas its value in a pure Na⁺ solution remained unaffected.

3.3.5 Mixed Salt Solutions

Even though measurements in pure salt solutions, as described in the previous paragraph, may already point to a different SLM behavior in KCl and NaCl solutions, the selectivity observed in mixed salt solutions is essentially different in nature. Because the total number of cations cannot exceed the number of lipophilic anions, K⁺ and Na⁺ will actually compete to enter and/or move within the SLM. Therefore, transport studies were conducted in 1:1 solutions containing 0.05 M KCl and 0.05 M NaCl. Figure 3.4a shows the measured (normalized) Na⁺ and K⁺ concentration in feed compartment A and ionic current over a time span of 48 h.
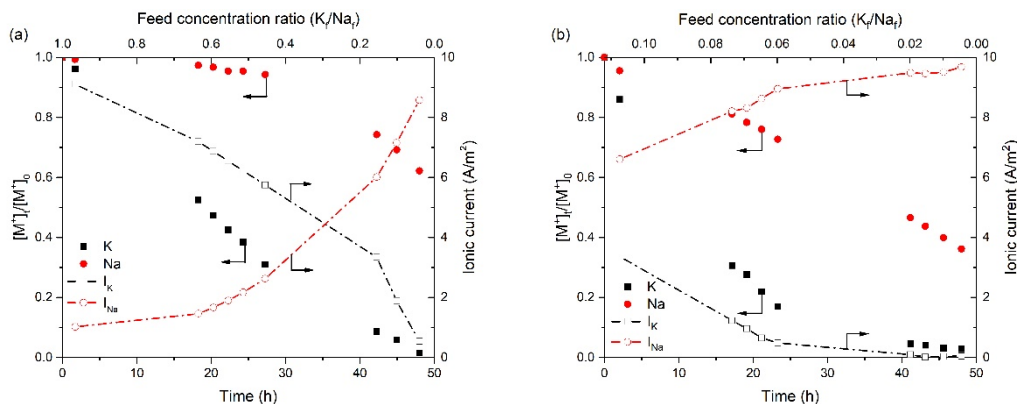
Figure 3.4 Normalized K⁺ and Na⁺ concentrations and ionic current over time in symmetrical mixed salt solutions of either 0.05 M NaCl + 0.05 M KCl (a) or 0.09 M NaCl + 0.01 M KCL (b). Note that the top axis indicates the corresponding K⁺ over Na⁺ feed concentration ratio over time.

In 1:1 solutions (Figure 3.4a), K⁺ is transported right from the start with the K⁺ carried current gradually decreasing over time. In contrast, initially Na⁺ is hardly transported at all, but gradually increases over time with a stronger increase only after around 50% of the K⁺ has already been removed from the feed solution. The initial Na⁺ transport rate is forced to a higher level by increasing the (initial) Na⁺/K⁺ concentration ratio in the feed solution to 9:1, an effect shown in Figure 3.4b. With 0.09 M NaCl and 0.01 M KCl present in the feed, Na⁺ and K⁺ transport start out simultaneously with the K⁺ current decreasing and the Na⁺ increasing over time. As evident from Figure 3.4b, whereas the K current eventually completely vanishes, the Na⁺ current reaches to near saturation level halfway the duration of the experiment. Apparently, with high Na⁺ in the feed, the Na⁺ level in the membrane reaches steady-state after about 25 h of forced ED. The summed up transport numbers of K⁺ and Na⁺ calculated for the 1:1 and 9:1 mixed salt solutions are 0.97 and 0.92, respectively, indicating that also under these conditions the current is predominantly carried by cations.

3.3.6 Separation Efficiency

Following Van der Bruggen *et al*. [38], the efficiency of the separation (*S*) of two components *A* and *B* (as function of time) is expressed by:

$$S(t) = \frac{\dfrac{[A]_t}{[A]_0} - \dfrac{[B]_t}{[B]_0}}{\left(1 - \dfrac{[A]_t}{[A]_0}\right) + \left(1 - \dfrac{[B]_t}{[B]_0}\right)} \times 100\% \qquad (3.11)$$

with $[A]_t$ and $[A]_0$ the concentration of component A in the dilute compartment (here the feed) at time t and time zero, respectively. Likewise for component B. In order to prevent calculating a value of $S(t)<0$, Eq. 3.11 only holds in the case component A is the one species moving the slowest. Figure 3.5a shows the separation factor S(K/Na) (is K^+ over Na^+ separation efficiency) as function of the normalized feed concentration ratio belonging to the data shown in Figure 3.4. The initial rise from 70% to 90% for the 1:1 NaCl/KCl mixture and from 50% to ~55% for the 9:1 NaCl/KCl mixture, most likely reflects the exchange of Na^+ for K^+ because the membranes were equilibrated in NaCl. As expected, the K^+ over Na^+ separation efficiency decreases with increasing the feed Na^+/K^+ concentration ratio even though the shape of the two curves in 1:1 and 9:1 solutions are identical. Figure 3.5b shows the separation efficiency data for mixed 1:1 salt solutions of NaCl/LiCl and KCl/LiCl. Compared to S(K/Na) show in Figure 3.5a, both the Na^+ over Li^+, S(Na/Li), and K^+ over Li^+ separation efficiency, S(K/Li), are not only higher but remain over time near the 95-100% level with only S(Na/Li) dropping to 80% at Na/Li feed concentrations<0.1.
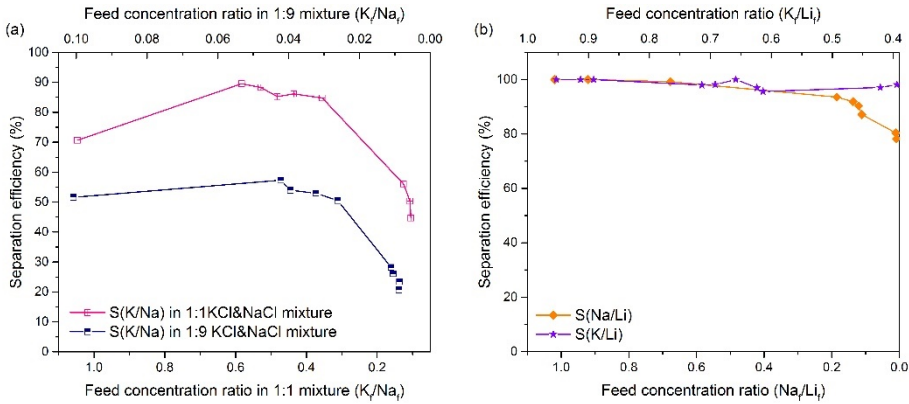

Figure 3.5 Calculated separation factors derived from measurements in either symmetrical 1:1 (0.05 M NaCl + 0.05 M KCl) or 9:1 (0.09 M NaCl + 0.01 M KCL) solutions (a) or in symmetrical 1:1 (0.05 M NaCl + 0.05 M LiCl) or (0.05 M KCl + 0.05 M LiCl) solutions (b).

3.3.7 Mechanism of Selectivity

This paragraph explores the possible role of the (difference in) dehydration energy between two ion species in the observed selectivity of the SLM. As for K^+ and Na^+, the K^+/Na^+ current ratio (at any time) can be derived from Figure 3.4 as the ratio of both normalized concentration *versus* time slope values. Starting from the general expression $I=zcuFE_m/d$ (with c the concentration of the particular ion species in the membrane), the current ratio of K^+ and Na^+ (I_K/I_{Na}) is directly proportional to the product of the mobility ratio of both ion species u_{Na}/u_K and the ratio of the K^+ and Na^+ concentration in the membrane. The former has already been obtained from the single-salt measurements (=1.66, see Table 3.4), rendering the membrane concentration ratio K_m/Na_m given by:

$$\frac{K_m}{Na_m} = \frac{u_{Na}}{u_K} \times \frac{I_K}{I_{Na}} = 1.66 \times \frac{I_K}{I_{Na}} \qquad (3.12)$$

Eq. 3.12 gives the experimentally obtained value of K_m/Na_m as function of time in relation to the (time-dependent) value of I_K/I_{Na}. Eq. 3.10, on the other hand, predicts the theoretical value of K_m/Na_m. Figures 3.6a plots the experimentally obtained value of K_m/Na_m versus the calculated theoretically predicted value, both as function of the time-dependent K_f/Na_f and starting in either 1:1 or 9:1 NaCl:KCl solutions. As visible guidance, the dotted line in Figure 3.6 represents the line of equality with a slope of unity ($\alpha=1$), *i.e.*, the ideal case in which experimental and predicted values are identical.
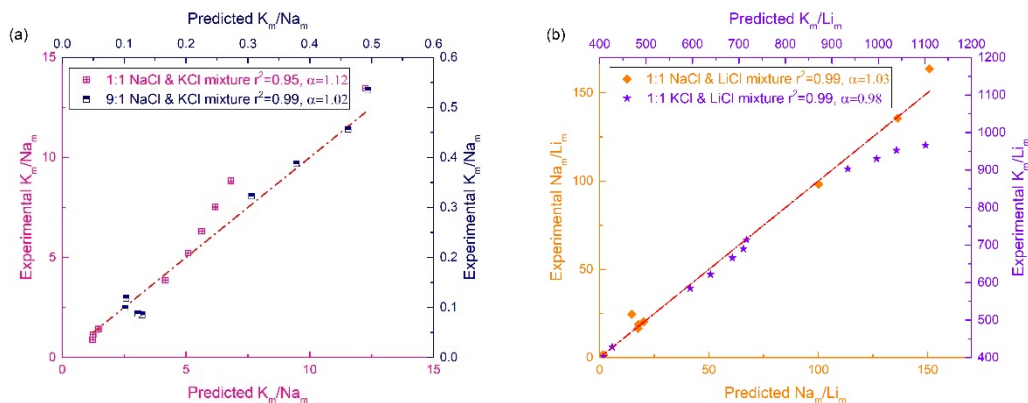
Figure 3.6 Comparison between experimentally obtained and theoretically predicted membrane concentration ratios starting in symmetrical 1:1 and 9:1 NaCl:KCl solutions (a) or 1:1 KCl:LiCl and NaCl:LiCl solutions (b). The slope (α) and regression coefficient (r^2) for each data set (actual regression lines not shown) are indicated. The calculated α and r^2 values for the 1:1 KCl:LiCl solution is based on the linear part of the data set with $K_m/Li_m < 800$. The dotted line, added as visible guidance, represents the line of equality with $\alpha = 1$.

The slopes (α) experimentally obtained from linear fits (not shown) of the date sets of Figure 3.6 are: 1.12 for 1:1 Na/K; 1.02 for 9:1 Na/K; 1.03 for Na/Li and 0.98 for K/Li. These values are close (enough) to the ideal case of $\alpha = 1$. This result justifies the conclusion that Figure 3.6 provides evidence that the SLM has a preference for the ion species with the largest crystal radius, an effect due to the fact that a larger crystal radius pairs with a lower dehydration energy. The hypothesis that dehydration dictates the current ratio of the two ion species is supported by measurements in mixed salt solutions of either NaCl and LiCl or KCl and LiCl. Figure 3.6b shows similar data as Figure 3.6a but for 1:1 Na^+/Li^+ and K^+/Li^+ mixtures. Because of its crystal radius, Na^+ (0.95 Å) outcompetes the smaller Li^+ (0.60 Å) for exactly the same reason as K^+ (1.33 Å) is able to outcompete the smaller Na^+. Note the difference in range of membrane concentration ratio between panels (a) and (b) of Figure 3.6. Including the Li^+ data of Figure 3.6b extrapolates the validity of the argument to membrane concentration ratios up to a value of 150 for the Na/Li mixture to ~800-900 for the K/Li mixture (with a deviation of linearity at larger ratios).

In agreement with the above-mentioned observations, with a large difference in crystal radii of 0.73 Å, the separation efficiency shown in Figure 3.5 is highest for K^+ and Li^+ compared to those recorded in either K^+/Na^+ or Na^+/Li^+ mixtures.

Combining Eqs. 3.9, 3.10 and 3.12 results in an expression of the current ratio exclusively in terms of the crystal radii of both ion species and the feed concentration ratio. For instance, the current ratio I_K/I_{Na} in the K^+/Na^+ solution is given by:

$$\frac{I_K}{I_{Na}} = \frac{r_{Na}}{r_K} \exp\left(\frac{20300}{RT} \left(\frac{1}{r_{Na}} - \frac{1}{r_K} \right) \right) \frac{K_f}{Na_f} = \beta \frac{K_f}{Na_f} \qquad (3.13)$$

with β adopting the value of 8.4, implying that only at Na^+ concentrations in the feed exceeding the K^+ concentration by a factor 8.4, will the Na^+ flux be larger than the K^+ flux over the membrane. This is the reason that in symmetrical 1:1 solutions K^+ is the dominant ion species transported whereas in 9:1 mixtures the current is initially carried by both K^+ and Na^+. For ion combinations Na^+/Li^+ and K^+/Li^+, the value of β is 97.3 and 819.9, respectively. Eq. 3.13 predicts a linear relationship between the current ratio and the feed concentration ratio, which is indeed observed experimentally. Figure 3.7 shows for all three ion combinations the measured current ratio as function of the (time-dependent) feed concentration ratio. The dotted lines in Figure 3.7 are based on the theoretical β values and the current ratio predicted by Eq. 3.13. Any deviation between the experimental (actual regression lines not shown) and theoretical curves may relate to effects not taken into account by Eq. 3.13, for example, an interaction between the permeating cation and the lipophilic borate or an ion permeation mechanism requiring partial dehydration only, leading to an underestimation of the actual ion radius and hence overestimation of both its dehydration energy and mobility. However, despite the shortcomings of the very simplified view expressed by Eq. 3.13, as Figure 3.7 shows, with increasing size difference between the two ion species (*e.g.* for K^+ and Li^+), ion radius starts to dominate SLM behavior.
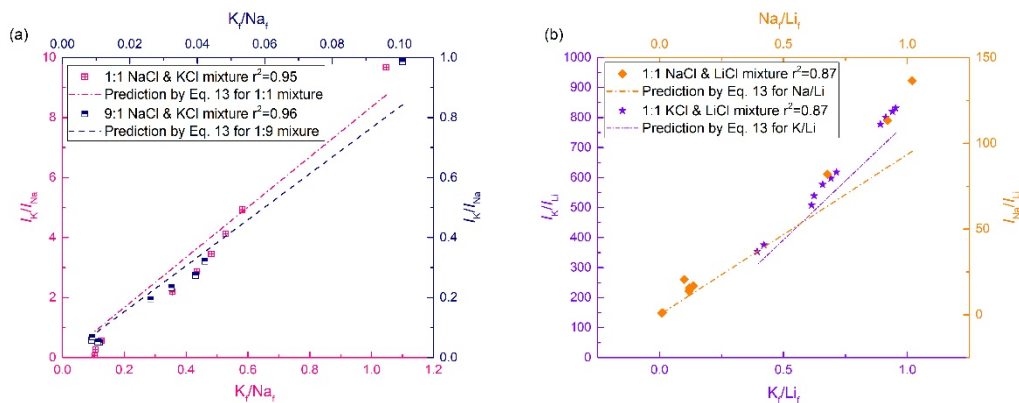
Figure 3.7 Experimentally obtained current ratio plotted as function of the (time-dependent) feed concentration ratio. Dashed lines are based on theoretical values of β according to Eq. 3.13. Data based on recordings in symmetrical 1:1 or 9:1 NaCl:KCl solutions (a) or 1:1 KCl:LiCl and NaCl:LiCl solutions (b). The regression coefficient (r^2) for each data set (actual regression lines not shown) is indicated.

Finally, a word on the difference between the selectivity measured under zero-current and bi-ionic conditions (Table 3.3) and the selectivity reflected by the current ratio as shown in Figure 3.7. The K^+ over Na^+ selectivity of 30 shown in Table 3.3 is about three times the value of ~10 following from the ED measurement with equal feed concentrations, *i.e.*, $K_f/Na_f=1$ (Figure 3.7a). Apart from differences in ionic conditions, one reason for the difference in selectivity may the role of mobility. Whereas this parameter plays no role in the equilibrium potential established during the zero-current measurement, during ED it works against the larger K^+, the ion species that is favored because of partitioning reasons. This effect may indeed lower the K^+ over Na^+ selectivity under ED conditions. The observation that different types of selectivity measurements may lead to a different outcome has also been reported by [34], in which selectivity determination by Donnan dialysis has been compared with an assessment by ED.

3.3.8 Interaction between K^+/Na^+ and CE

The idea behind adding a crown ether is that cation coordination by crown ether oxygens compensates for the energy penalty due to the required ion dehydration for entering the membrane. As a result, the CE enhances the partitioning of the particular ion species over the membrane phase. Given the cavity size of 15-crown-5, it was

actually anticipated that 15-crown-5 would predominantly interact with Na^+ rather than with K^+ [39]. However, as shown in Figure 3.3, addition of modified 15-crown-5 (PSCE) affects the transport of K^+ but not of Na^+. An explanation for the observed effect on the K^+ current is that (in this particular case) ring size is actually not the defining parameter because the ion is possibly sandwiched between two (or more) crown ether molecules due to the lower interaction energy compared the interaction energy with only a single crown involved [40–42]. Alternatively, 15-crown-5 may indeed show a higher affinity for Na^+ but this effect is obscured by the effect on the K^+ current because the latter ion species is present at a higher concentration, due to the favored partitioning discussed in previous paragraphs. It is this second possibility that will be explored here in more detail. Therefore, we modelled the interaction between CE and K^+/Na^+ using set values for the equilibrium affinity constants (K_K and K_{Na}) of the CE - metal ion complexes, CE-K and CE-Na. Let K_m and Na_m be the free K^+ and Na^+ concentration in the membrane, A the lipophilic anion concentration, CE_{tot} is the total CE concentration, being the sum of free CE, CE_0 (*i.e.* not complexed with K^+ or Na^+) and complexed CE-K and CE-Na. The following set of equations fully describes the system in terms of fixed total amount of CE (Eq. 3.14), electro neutrality (Eq. 3.15), affinity constants of CE for K^+ and Na^+ (Eqs. 3.16 and 3.17) and ion partitioning (Eqs. 3.10 and 3.18).

$$CE_{tot} = CE_0 + CE\text{-}K + CE\text{-}Na \qquad (3.14)$$

$$A = K_m + Na_m + CE\text{-}K + CE\text{-}Na \qquad (3.15)$$

$$CE\text{-}K = K_K \times K_m \times CE_0 \qquad (3.16)$$

$$CE\text{-}Na = K_K \times Na_m \times CE_0 \qquad (3.17)$$

$$K_m = \alpha \times Na_m \times \frac{K_f}{Na_f} \qquad (3.18)$$

Combining Eqs. 3.14 - 3.17 renders:

$$K_m + Na_m = A - \frac{CE_{tot} \times (K_K K_m + K_{Na} Na_m)}{1 + K_K K_m + K_{Na} Na_m} \qquad (3.19)$$

Substitution of Eq. 3.18 in Eq. 3.19 results in an implicit expression for Na_m which can be solved for Na_m using, for instance, the Solver function in Excel, giving a unique

solution independent of the starting value of Na_m. With CE covalently attached to the bulky siloxane-based polymer, the concentration of free Na^+ in the membrane is of particular interest because this is the species responsible for the Na^+ carried current over the membrane. Figure 3.8 plots the free Na^+ and K^+ concentrations as function of the ratio of the two equilibrium interaction constants K_K/K_{Na}, in symmetrical 1:1 (a) and asymmetrical 9:1 (Na^+:K^+) solutions. For an equimolar feed solution and with the affinity constants of CE-K and CE-Na set at 0.0025 M^{-1} and at a value < 0.001 M^{-1}, respectively (with $K_K/K_{Na}{>}25$), the K^+ current reduction is around 30%, *i.e.* the reduction observed is in the single-salt KCl measurements in the presence of CE (Figure 3.3). Increasing K_{Na} and decreasing K_K, resulting in $K_K/K_{Na}{=}0.01$, strongly affects the free membrane concentration of both K^+ and Na^+; however, their ratio remains the same.
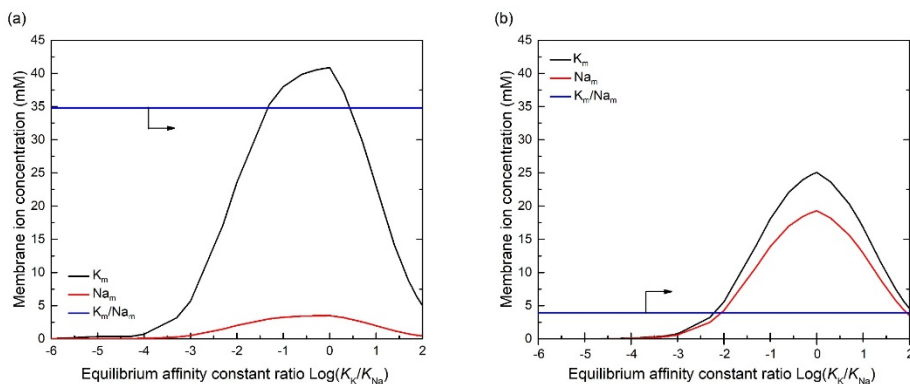
Figure 3.8 Simulated free K^+ and Na^+ concentrations in the membrane (in mM) as function of the ratio of the (arbitrary set) equilibrium affinity constants K_K/K_{Na} in a feed solution of either 1:1 (a) or 9:1 (b) NaCl & KCl. The total amount of lipophilic anion and total amount of 15-crown-5 is 0.05 M and 0.13 M, respectively.

Given that ion partitioning occurs at a much faster time scale than complexation, this result is inherently hidden in the model. Figure 3.7, showing a current ratio closely following the (time-dependent) feed concentration, both in 1:1 and 9:1 Na^+/K^+ solution, supports this view. If correct, this observation also implies that ion currents are exclusively carried by the free ion species in the membrane. In summary, for a (SLM) system as described in this study, in which the ion partitioning over the aqueous and membrane phase dictates the ratio of free K^+ and Na^+ concentrations in

the membrane, the current ratio closely follows the concentration ratio in the feed solution.

3.3.9 Implementation

A first requirement for implementation is membrane stability and longevity. Therefore, in addition to the morphology test as described in the Supplementary Information, a functionality test over time has been performed. To this end, the same ED experiment was repeated twice using the same SLM and fresh solutions each time. The K^+ over Na^+ separation efficiency, S(K/Na), was assessed in symmetrical solutions containing 0.05 M KCl and 0.05M NaCl and under the same experimental conditions as described in the main text for the other ED experiments. Figure 3.9 shows for each run the calculated S(K/Na) as a function of the normalized feed concentration ratio. Even though the curves not fully overlap, in both runs S(K/Na) follows the same trend with respect to the feed concentration ratio. Despite the observed shift, the loss in separation efficiency, as recorded over a total time period of 96 hrs, remains limited to 5-10%. Current investigations include strategies to further improve the SLM stability over time.

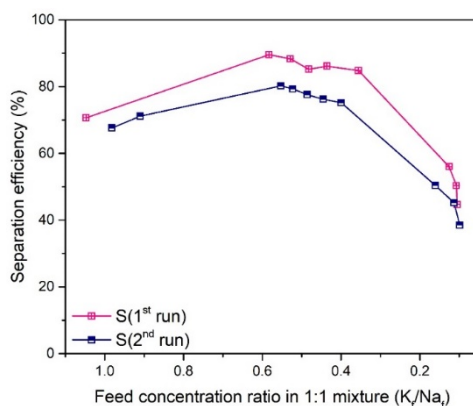Figure 3.9. Calculated K^+ over Na^+ separation efficiency of two ED experiments in series over a total time period of 96 hrs using the same membrane and fresh solutions each time and measured in symmetrical 0.05 M NaCl + 0.05 M KCl solutions.

The conclusions drawn in previous paragraphs have implications for the application we aim for, *i.e.*, the selective removal of Na^+ from the drainage water of

greenhouses (major cations present are K^+, Na^+, Ca^{2+} and Mg^{2+}) and process design. Firstly, as can be concluded from Figure 3.5, the K^+ over Na^+ separation efficiency can be optimized by controlling the feed concentration ratio within a certain range. Secondly, the Na^+/K^+ concentration ratio of the drainage water leaving the greenhouse typically is 1-1.5. As remarked, as long as Na^+/K^+ concentration ratio <8.4 will K^+ be the dominant ion species to be removed. The actual drainage water leaving the greenhouse contains about the same concentration of K^+ and Na^+. Therefore, in order to extent our findings to the real-life situation, Figure 3.10 shows the result of a preliminary ED experiment using a synthetic salt solution with, regarding the four most prominent cationic constituents, the same composition as natural drainage irrigation water: Na^+: 13.8 mM, K^+: 11.9 mM, Ca^{2+}: 6.4 mM and Mg^{2+}: 5 mM (data provided by Van der Knaap). As shown in Figure 3.9, with more or less the same K^+ and Na^+ concentration (12-14 mM) and in the presence of Ca^{2+} and Mg^{2+}, K^+ transport clearly is favoured by the SLM under ED conditions.
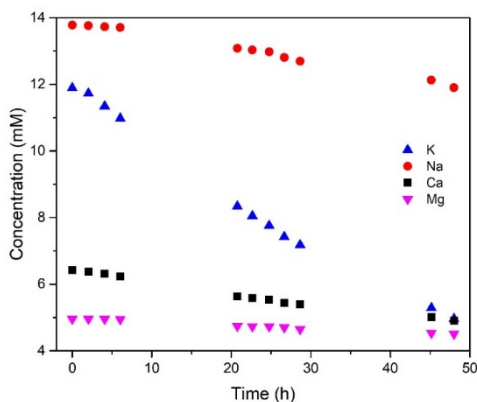
Figure 3.10 K^+, Na^+, Ca^{2+}, Mg^{2+} concentrations changes over time in symmetrical synthetic drainage irrigation water.

Consequently, the implementation of this technology for the intended greenhouse application of selectively removing Na^+ requires a two-step cleaning process. Figure 3.11 schematically outlines two different process designs based on the use of two types of membranes, the SLM developed here and a standard monovalent over divalent cation selective membrane. In the first option, as shown in Figure 3.11a using the SLM, K^+ is selectively removed first, followed by a second step which removes

the remaining Na^+ from the retentate. The second option as shown in Figure 3.11b starts out with the removal of both K^+ and Na^+, followed by the selective separation of K^+ from this permeate using the SLM. In both scenarios, afterwards the recovered K^+ is re-combined with the divalent cation-containing solution.
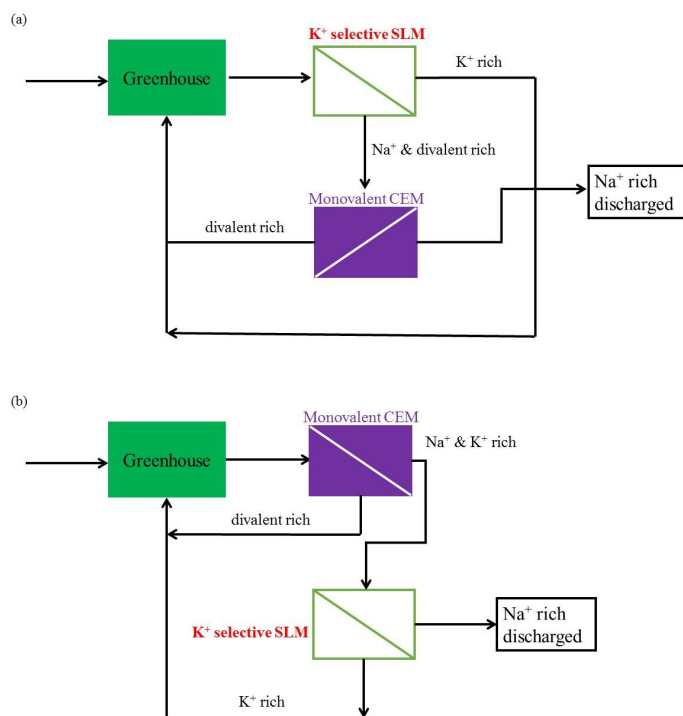
Figure 3.11 Two different process designs for the removal of excess Na^+ from (circulated) greenhouse drainage water. Both two-step processes are based on the use of the SLM developed here and a membrane with a monovalent over divalent cation selectivity.

Finally, a brief comment on the economic feasibility of the technology outlined here. In a previous study of this lab this issue has been addressed [15]. However, in that entirely theoretical exercise we anticipated the mandatory inclusion of crown-ether in the SLM. The conclusion then was that the capital cost of the SLM was dominated by the price of crown-ether. Evidently, the experimental results shown in the present study point to the fact that an effective separation does not require the presence of crown ether. In the absence of crown ether, borate determines to a large extent the price of the SLM resulting in (an estimated) price per m^2 of 828 euro. This still is almost three times the price of a typical ion exchange membrane of Neosepta

(300 euro per m²; EURODIA, 2019). However, in order to achieve similar selectivity properties than described here for the SLM requires the Neosepta membrane to be chemically modified, which will force its price upwards. As for the operational costs of the SLM, notably the power consumption, the reader is referred to [15].

3.4 Final Remarks

Studies reporting the efficient separation of a monovalent cation species from a solution containing other monovalent cation species as well remain scarce, even more so for (binary) K^+/Na^+ solutions. But based on what has been reported and to the best of our knowledge, the performance of the SLM system described here ranks rather high regarding its selectivity. For instance, using a dopamine-covered sulfonated polysulfone membrane resulted in K^+ over Li^+ selectivity of 2.9, as assessed under ED conditions [42]. A similar result, *i.e.*, a K^+ over Li^+ selectivity of 2.3 (also under ED conditions), was found when using a polyelectrolyte-coated Nafion membrane instead [34]. These numbers are rather modest compared to the K^+/Li^+ selectivity values shown in Figure 3.7b, indeed even with the K^+/Na^+ selectivity shown in Figure 3.7a (both at 1:1 feed concentrations). Adding a crown ether may enhance the selectivity properties of the system [43] but this often is at the expense ion mobility, resulting in higher membrane resistances [42]. Interestingly, Guo and co-workers report on a rather high discrimination between K^+ and Li^+ applying a polymer/metal-organic framework composite [44]. However, the Li^+ over Na^+/K^+ selectivity of 35-67 reflects an inversed selectivity in which the smallest ion species is favored, thereby pointing to a selectivity mechanism based on sieving rather than partitioning.

The SLM system described here shows a permeation preference for the ionic species with the largest crystal radius ($K^+>Na^+>Li^+$) with, by definition, the lowest dehydration energy. To quantify dehydration, the Born equation was used instead of the Gibbs free energy of dehydration. The reason is that in our case, describing ion transfer from water into NPOE, the Born approach is more realistic as the standard Gibbs free energy of dehydration refers to the transfer from water to vacuum (see also Luo *et al*.) [10]. As argued, the ion radius plays a key role in the behavior of the SLM, as expressed by Eq. 3.13 and shown in Figure 3.7. Even though reported crystal radii slightly vary (*e.g*. Atkins[45] lists Na^+ and K^+ radii of 1.02 Å and 1.38 Å, respectively), those differences do not affect the overall observed trends in the membrane separation performance.

As shown, the calculated mobility ratio of two ion species in the SLM is directly proportional to the inverse ratio of both crystal radii, in the same way as the mobility ratio in water relates to the ratio of the (hydrated) Stokes radius of the two ion species. Despite this relationship, the calculated absolute mobility values are an order of two smaller than those measured in water, despite their smaller radius. One explanation is that the permeating cation (somehow) interacts with NPOE, for example, via cation-π interaction or, alternatively, interacts with the lipophilic anions dissolved in NPOE [46]. In addition, the higher viscosity of NPOE (13.8 mPa.s versus 0.89 mPa.s of water) [47,48] may impede ion movement.

Regarding a possible interaction between the permeant cation and the lipophilic anion, given the borate concentration of 0.05 M, the average distance between two borate sites is 3.2 nm. Apparently, the (temporal) interaction between the cation and the borate anion slows down the overall mobility but the mobility required to jump (or hop) from one site to another still is inversely proportional to the crystal radius of the ion. As remarked before, such cation – borate interaction could (partly) explain the deviation of SLM behavior from theoretical prediction (Figure 3.7). The relatively low borate concentration of 0.05 M is related to the observed relatively high SLM resistance. Even though the addition of borate to the NPOE significantly decreases the membrane resistance and transforms the SLM into a highly cation selective membrane, the resistance still is relatively high compared to that of existing commercially available ion-exchange membranes, typically 1-2 Ω cm^{-2}. The reason for the high resistance of the SLM reflects its limited ion-exchange capacity (IEC) of 0.05 M, compared to 1 M for typical ion exchange membranes. As remarked already, ions may move through the membrane by hopping from borate site to borate site, with these sites located 3.2 nm apart from each other. A prerequisite of such hopping mechanism is a high enough borate density and by implication a not too large mutual distance between adjacent sites. The percolation theory provides a theoretical frame work of this concept. Tongwen *et al*. [49], presented a general percolation model applicable to all kinds of ionomeric systems. Only when the IEC exceeds a certain threshold value are conductive channels formed allowing an effective flow of ions. The (generic) IEC threshold reported Tongwen *et al*. ranges from 0.54 to 1.07 mEq per gram dry membrane. Assuming a zero-water content of our SLM, the 0.05 M borate applied translates to an IEC value of 0.085 mEq g^{-1} of NPOE/membrane, at least almost a factor 10 lower than the abovementioned value. This may indeed (partly) explain the high resistance observed. Unfortunately, the applied 0.05 M

lipophilic borate represents already the maximal solubility of NaBArF in NPOE, hampering us to test our hypothesis by increasing the borate concentration.

Lastly, regarding the relatively lower resistances of other membrane systems, one should bear in mind that the (efficient) transport of one particular ion species and ion selectivity are two related but nevertheless different issues. For instance, ceramic NASICON-based membranes show high Na^+ transport rates but only in the absence of K^+[50–52]. Evidently, under free K^+ conditions there is no need for a high Na^+ over K^+ membrane selectivity. The same holds for all types of Li^+ selective membrane as applied in lithium battery technology where Li^+ is the only monovalent cation present.[51] As soon as selectivity is required, one encounters the frequently reported trade-off seen in membrane transport studies in which increased selectivity pairs with decreased flux and *vice versa* [53,54].

3.5. Conclusions

This study shows the ability to separate two ion species that are very similar regarding charge and size. The novel aspect of the present study is, firstly, the high separation efficiency (up to ~90% for K^+ over Na^+ to ~100% for K^+ over Li^+) and, secondly, that achieving such high separation does not require the presence of carrier molecules in the membrane. Essentially, the working mechanism of the supported liquid membrane used comes back entirely to the radii of the two ion species involved. Entering the hydrophobic NPOE containing membrane (permittivity = 24) requires the ions to be (partly) dehydrated. According to the Born equation, the larger the crystal ion radius, the lower this dehydration energy. The partitioning ratio in turn, dictated by Boltzmann distributions, scales exponentially with the difference in dehydration energy. The lower mobility of the largest ion species in the SLM cannot compensate for this dehydration/partitioning effect, consequently the SLM favors the largest ion species. Together with the concentration ratio in the feed solution, these basic physico-chemical principles suffice to adequately describe the behavior of the SLM.

Supporting information

3.S1 Synthesis of polysiloxane-bound 15-crown-5 (PSCE)[55]

In a Schlenk tube, 15 mL of dry toluene was degassed by four freeze-pump-thaw cycles and sealed under argon with molecular sieves and stored for later use. In a 10 mL round-bottom flask, chloridotris(triphenylphosphane)rhodium(I) (Wilkinson's catalyst, 0.08 mmol) was dissolved in degassed toluene (5 mL), followed by (i) 2-hydroxymethyl-15-crown-5 (CE) (4.4 mmol, 1.1 g), (ii) poly(dimethylsiloxane) (2 mmol, 1.16 g) (PDMS) under stirring. The mixture was heated up to 90 ºC. The dark brown color of the catalyst disappeared within 30 minutes after starting the heating and the color of the reaction mixture turned into homogeneously light yellow, and further changed into orange upon further proceeding the reaction. When the reaction was completed, the color of the mixture turned back to dark brown. The organic solution was filtered through a membrane filter (0.2 μm Nylon syringe filter). Afterwards the excess toluene was evaporated with rotavap to obtain the raw product. Extraction with ethyl acetate and water mixture was performed three times to remove unreacted CE. Then the organic phase was dried with anhydrous magnesium sulfate and filtered with a filter paper. The final product was obtained as a light-yellow viscous liquid after evaporation of ethyl acetate, with a yield of 67%.

The product was characterized by ^{1}H-NMR (Bruker AVANCE III NMR) and FT-IR spectroscopy (Bruker Tensor 27).

3.S2 Characterization of polysiloxane bound 15-crown-5 (PSCE)

The spectra of ^{1}H-NMR and FT-IR are given in Figures 3.S1 and 3.S2 and indicate the structure proposed as the reaction product.
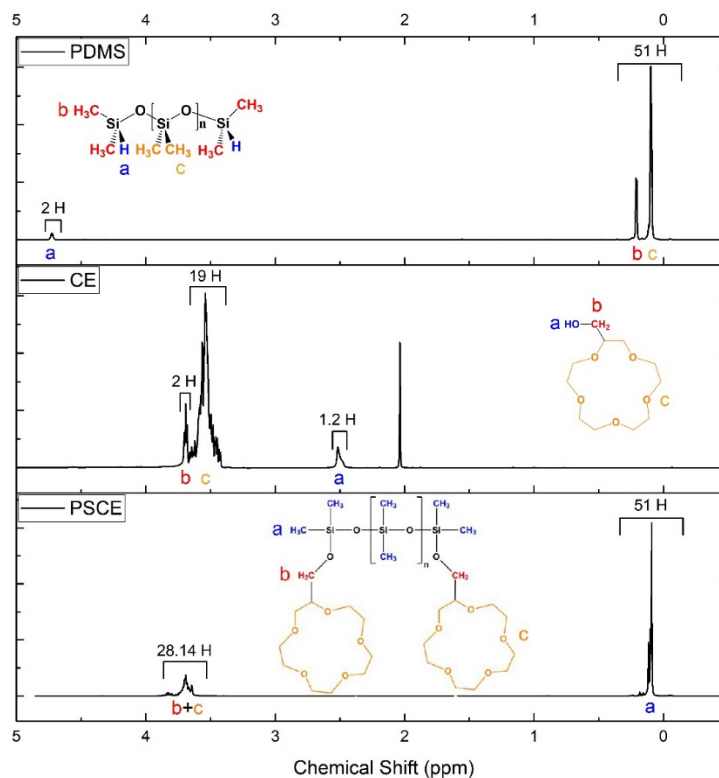

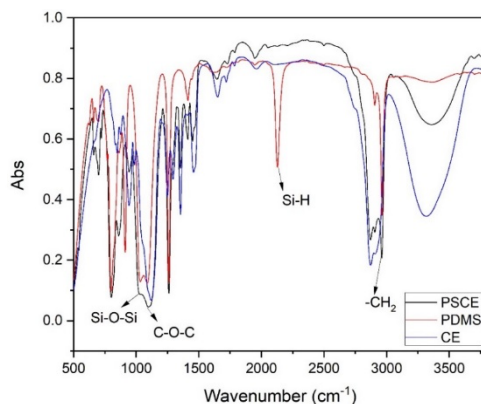Figure 3.S1 ^{1}H-NMR spectrum of the final product PSCE.

Figure 3.S2 FTIR spectrum of the final product PSCE.

In more detail, in the ^{1}H-NMR spectrum of PDMS backbone, we observed a chemical shift at $\delta = 4.7$ ppm as well as a shift around $\delta = 0$ ppm, which can be assigned to the Si-H and Si-CH$_3$ proton, respectively. The ratio of integral values of these shifts of the PDMS backbone was found to be Si-CH$_3$:Si-H = 51:2. The relative integral values related to the resonances of protons that are part of the 2-hydroxymethyl-15-crown-5 (CE) moiety is, within the accuracy of NMR, also in line with the structure. It is noted that in the ^{1}H-NMR spectrum of the product, the chemical shift at $\delta = 4.7$ ppm (assigned to the Si-H proton) disappeared just like the wavenumber around 2100 cm^{-1} (assigned to stretching vibration of the Si-H bond), suggesting the completion of the reaction. When we set the integration of Si-CH$_3$ ($\delta = 0$ ppm) to 51 H (as obtained from the spectrum of PDMS) integration of the peak related to the crown ether protons was found to be 28.14. The ratio of integration of CE (28.14 H) to the theoretical value (21 H) gives us a modification ratio of 1:1.3 modification in the product, *i.e.* 1.3 CEs per molecule.

3.S3 Membrane stability

3.S3.1 Assessment of morphology

Figures 3.S3(a) and (b) show the ACCUREL support before (a) and after the pores have been completely impregnated by NPOE (b). The same membrane shown in (b) is shown in Figure 3.S3(c) but after 48 hours of electro dialysis. Based on visible inspection, the SLMs were not brittle and retained their stability during the entire

experimental period. It is also clear from (c) that during ED the ACCUREL support remained fully impregnated with NPOE.
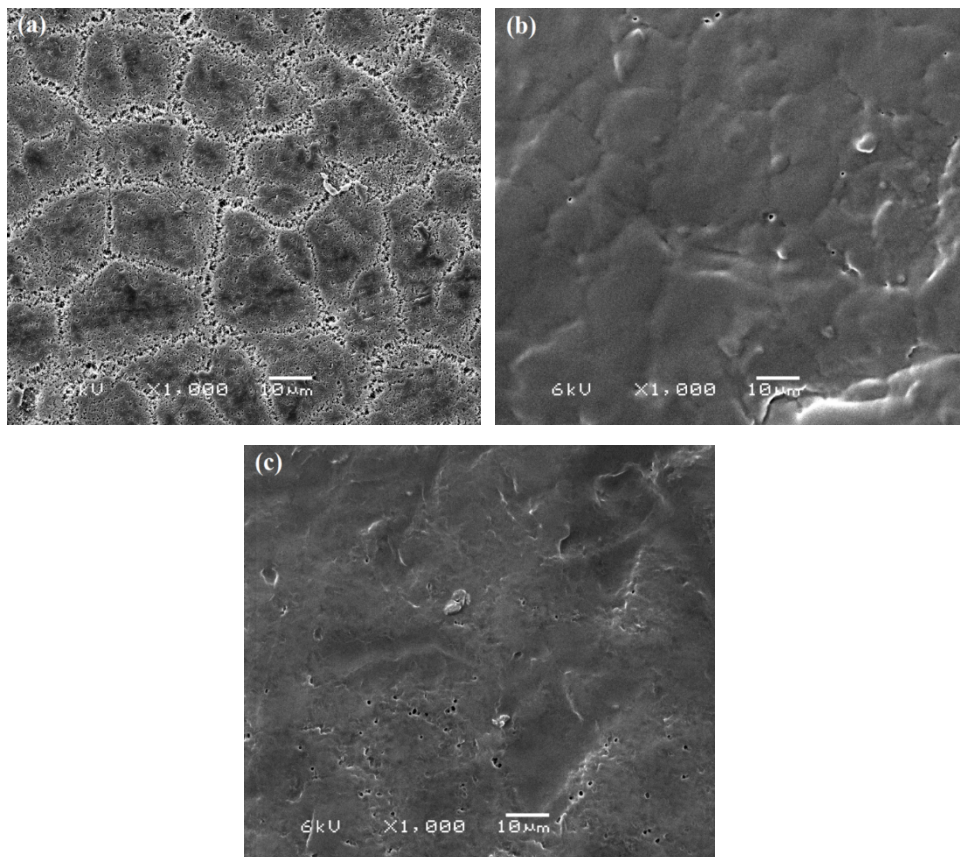

Figure 3.S3 SEM images of the SLM: (a). ACCUREL membrane support before impregnation with NPOE, (b) freshly prepared SLM (ACCREL impregnated with NPOE), (c). SLM after applying 48 hours of electro dialysis.

Reference

[1]   M. Sadrzadeh, T. Mohammadi, Sea water desalination using electrodialysis, Desalination. 221 (2008) 440–447. https://doi.org/10.1016/J.DESAL.2007.01.103.

[2]   A.H. Galama, M. Saakes, H. Bruning, H.H.M. Rijnaarts, J.W. Post, Seawater predesalination with electrodialysis, Desalination. 342 (2014) 61–69. https://doi.org/10.1016/j.desal.2013.07.012.

[3]   T. Chakrabarty, A.M. Rajesh, A. Jasti, A.K. Thakur, A.K. Singh, S. Prakash, V. Kulshrestha, V.K. Shahi, Stable ion-exchange membranes for water desalination by electrodialysis, Desalination. 282 (2011) 2–8. https://doi.org/10.1016/j.desal.2011.08.009.

[4]   H. Strathmann, Electrodialysis, a mature technology with a multitude of new applications, Desalination. 264 (2010) 268–288. https://doi.org/10.1016/j.desal.2010.04.069.

[5]   Y. Tanaka, Ion-exchange membrane electrodialysis program and its application to multi-stage continuous saline water desalination, Desalination. 301 (2012) 10–25. https://doi.org/10.1016/j.desal.2012.06.007.

[6]   G.J. Doornbusch, M. Tedesco, J.W. Post, Z. Borneman, K. Nijmeijer, Experimental investigation of multistage electrodialysis for seawater desalination, Desalination. 464 (2019) 105–114. https://doi.org/10.1016/j.desal.2019.04.025.

[7]   M. Mulder, Basic principles of membrane technology, 2nd ed., Springer Netherlands, Dordrecht, 1996. https://doi.org/10.1007/978-94-009-1766-8_1.

[8]   H. Strathmann, Membrane separation processes, J. Memb. Sci. 9 (1981) 121–189. https://doi.org/10.1016/S0376-7388(00)85121-2.

[9]   H. Strathmann, Ion-exchange membrane separation processes, Elsevier, Amsterdam, 2004. https://doi.org/10.1007/s13398-014-0173-7.2.

[10]   T. Luo, S. Abdu, M. Wessling, Selectivity of ion exchange membranes: A review, J. Memb. Sci. 555 (2018) 429–454. https://doi.org/10.1016/j.memsci.2018.03.051.

[11]   M. Irfan, Y. Wang, T. Xu, Novel electrodialysis membranes with hydrophobic alkyl spacers and zwitterion structure enable high monovalent/divalent cation selectivity, Chem. Eng. J. 383 (2019) 123171. https://doi.org/10.1016/j.cej.2019.123171.

3

[12]   S. Caprarescu, M.C. Corobea, V. Purcar, C.I. Spataru, R. Ianchis, G. Vasilievici, Z. Vuluga, San copolymer membranes with ion exchangers for Cu(II) removal from synthetic wastewater by electrodialysis, J. Environ. Sci. (China). 35 (2015) 27–37. https://doi.org/10.1016/j.jes.2015.02.005.

[13]   S. Caprarescu, A.L. Radu, V. Purcar, A. Sarbu, D.I. Vaireanu, R. Ianchis, M. Ghiurea, Removal of copper ions from simulated wastewaters using different bicomponent polymer membranes, Water. Air. Soil Pollut. 225 (2014) 1–12. https://doi.org/10.1007/s11270-014-2079-6.

[14]   C.Y. Foong, M.D.H. Wirzal, M.A. Bustam, A review on nanofibers membrane with amino-based ionic liquid for heavy metal removal, J. Mol. Liq. 297 (2020) 111793. https://doi.org/10.1016/j.molliq.2019.111793.

[15]   Z. Qian, H. Miedema, L.C.P.M. de Smet, E.J.R. Sudhölter, Modelling the selective removal of sodium ions from greenhouse irrigation water using membrane technology, Chem. Eng. Res. Des. 134 (2018) 154–161. https://doi.org/10.1016/j.cherd.2018.03.040.

[16]   F.J.M. Maathuis, A. Amtmann, K+ nutrition and Na+ toxicity: The basis of cellular K+/Na+ ratios, Ann. Bot. 84 (1999) 123–133. https://doi.org/10.1006/anbo.1999.0912.

[17]   E. Blumwald, Sodium transport and salt tolerance in plants, Curr. Opin. Cell Biol. 12 (2000) 431–434. https://doi.org/10.1016/S0955-0674(00)00112-5.

[18]   J.L. Zhang, T.J. Flowers, S.M. Wang, Mechanisms of sodium uptake by roots of higher plants, Plant Soil. 326 (2010) 45–60. https://doi.org/10.1007/s11104-009-0076-0.

[19]   J. Bobacka, A. Ivaska, A. Lewenstam, Potentiometric ion sensors, Chem. Rev. 108 (2008) 329–351. https://doi.org/10.1021/cr068100w.

[20]   T. Guinovart, D. Hernández-Alonso, L. Adriaenssens, P. Blondeau, F.X. Rius, P. Ballester, F.J. Andrade, Characterization of a new ionophore-based ion-selective electrode for the potentiometric determination of creatinine in urine, Biosens. Bioelectron. 87 (2017) 587–592. https://doi.org/10.1016/j.bios.2016.08.025.

[21]   N.M. Kocherginsky, Q. Yang, L. Seelam, Recent advances in supported liquid membrane technology, Sep. Purif. Technol. 53 (2007) 171–177. https://doi.org/10.1016/j.seppur.2006.06.022.

[22]   P.K. Parhi, Supported Liquid Membrane Principle and Its Practices: A Short Review, J. Chem. 2013 (2013) 1–11. https://doi.org/10.1155/2013/618236.

[23]   R.A. Bartsch, J.D. Way, Chemical Separations with Liquid Membranes: An Overview, American Chemical Society Washington, 1996. https://doi.org/10.1021/bk-1996-0642.ch001.

3

[24] M.M. Naim, A.A. Monir, Desalination using supported liquid membranes, Desalination. 153 (2003) 361–369. https://doi.org/10.1016/S0011-9164(02)01129-3.

[25] T. Rosatzin, E. Bakker, K. Suzuki, W. Simon, Lipophilic and immobilized anionic additives in solvent polymeric membranes of cation-selective chemical sensors, Anal. Chim. Acta. 280 (1993) 197–208. https://doi.org/10.1016/0003-2670(93)85122-Z.

[26] E. Bakker, E. Pretsch, Lipophilicity of tetraphenylborate derivatives as anionic sites in neutral carrier-based solvent polymeric membranes and lifetime of corresponding ion-selective electrochemical and optical sensors, Anal. Chim. Acta. 309 (1995) 7–17. https://doi.org/10.1016/0003-2670(95)00077-D.

[27] F.G. Bănică, Chemical Sensors and Biosensors: Fundamentals and Applications, John Wiley and Sons, Chichester, UK, 2012. https://doi.org/10.1002/9781118354162.

[28] W. Walkowiak, C.A. Kozlowski, Macrocycle carriers for separation of metal ions in liquid membrane processes-a review, Desalination. 240 (2009) 186–197. https://doi.org/10.1016/j.desal.2007.12.041.

[29] M.M. Wienk, T.B. Stolwijk, E.J.R. Sudhölter, D.N. Reinhoudt, Stabilization of crown ether containing supported liquid membranes, J. Am. Chem. Soc. 112 (1990) 797–801. https://doi.org/10.1021/ja00158a046.

[30] A. Šlampová, P. Kubáň, P. Boček, Fine-tuning of electromembrane extraction selectivity using 18-crown-6 ethers as supported liquid membrane modifiers, Electrophoresis. 35 (2014) 3317–3320. https://doi.org/10.1002/elps.201400372.

[31] A. Oberta, J. Wasilewski, R. Wódzki, Selective lead(II) transport in a liquid membrane system with octylsulfanylacetic acid ionophore, Desalination. 252 (2010) 40–45. https://doi.org/10.1016/j.desal.2009.11.004.

[32] P. Długołecki, K. Nymeijer, S. Metz, M. Wessling, Current status of ion exchange membranes for power generation from salinity gradients, J. Memb. Sci. 319 (2008) 214–222. https://doi.org/10.1016/j.memsci.2008.03.037.

[33] J.A. Ibáñez-Mengual, J. García-Gamuz, R.P. Valerdi-Pérez, Bi-ionic potential: Experimental measurements and diffusion coefficients determinations, Desalin. Water Treat. 36 (2011) 81–88. https://doi.org/10.5004/dwt.2011.2072.

3

[34]   L. Yang, C. Tang, M. Ahmad, A. Yaroshchuk, M.L. Bruening, High selectivities among monovalent cations in dialysis through Cation-Exchange Membranes coated with polyelectrolyte multilayers, ACS Appl. Mater. Interfaces. 10 (2018) 44134–44143. https://doi.org/10.1021/acsami.8b16434.

[35]   A. Kumar, P.S.H. Rizvi, A.M.S. Requena, Handbook of Membrane Separations: chemical, pharmaceutical, food, and biotechnological applications, 2nd ed., CRC Press, 2015.

[36]   E.R. Nightingale, Phenomenological theory of ion solvation. Effective radii of hydrated ions, J. Phys. Chem. 63 (1959) 1381–1387. https://doi.org/10.1021/j150579a011.

[37]   R.A. Robinson, R.H. Stokes, Electrolyte solutions, 2nd ed., Dover Publications, 2002.

[38]   B. Van Der Bruggen, A. Koninckx, C. Vandecasteele, Separation of monovalent and divalent ions from aqueous solution by electrodialysis and nanofiltration, Water Res. 38 (2004) 1347–1353. https://doi.org/10.1016/j.watres.2003.11.008.

[39]   L. Torun, New crown ether compounds and their alkali metal ion complexation, Texas Tech University, 1994. http://hdl.handle.net/2346/15105.

[40]   Y. Liu, L.H. Tong, S. Huang, B.Z. Tian, Y. Inoue, T. Hakushi, Complexation thermodynamics of bis(crown ether)s. 4. Calorimetric titration of intramolecular sandwich complexation of thallium and sodium ions with bis(15-crown-5)s and bis(12-crown-4)s: enthalpy-entropy compensation, J. Phys. Chem. 94 (1990) 2666–2670. https://doi.org/10.1021/j100369a079.

[41]   J. Kim, M. Shamsipur, S.Z. Huang, R.H. Huang, J.L. Dye, Sandwich and mixed sandwich complexes of the cesium ion with crown ethers in nitromethane, J. Phys. Chem. A. 103 (1999) 5615–5620. https://doi.org/10.1021/jp990685t.

[42]   S. Yang, Y. Liu, J. Liao, H. Liu, Y. Jiang, B. Van Der Bruggen, J. Shen, C. Gao, Codeposition modification of cation exchange membranes with dopamine and crown ether to achieve high K+ electrodialysis selectivity, ACS Appl. Mater. Interfaces. 11 (2019) 17730–17741. https://doi.org/10.1021/acsami.8b21031.

[43]   S. Chaudhury, A. Bhattacharyya, A. Goswami, Electrodriven Ion Transport through Crown Ether–Nafion Composite Membrane: Enhanced Selectivity of Cs^+ over Na^+ by Ion Gating at the Surface, Ind. Eng. Chem. Res. 53 (2014) 8804–8809. https://doi.org/10.1021/ie500934v.

3

[44]   Y. Guo, Y. Ying, Y. Mao, X. Peng, B. Chen, Polystyrene Sulfonate
        Threaded through a Metal-Organic Framework Membrane for Fast and
        Selective Lithium-Ion Separation, Angew. Chemie Int. Ed. 55 (2016)
        15120–15124. https://doi.org/10.1002/anie.201607329.

[45]   P. Atkins, T. Overton, J. Rourke, M. Weller, F. Armstrong, Shriver and
        Atkins' Inorganic Chemistry, Oxford University Press, 2009.
        http://www.amazon.co.uk/Shriver-Atkins-Inorganic-Chemistry-
        Peter/dp/0199236178.

[46]   C. Miller, Ionic hopping defended, J. Gen. Physiol. 113 (1999) 783–787.
        https://doi.org/10.1085/jgp.113.6.783.

[47]   Z. Samec, J. Langmaier, A. Trojánek, E. Samcová, J. Málek, Transfer of
        protonated anesthetics across the water| o-nitrophenyl octyl ether interface:
        effect of the ion structure on the transfer kinetics and pharmacological
        activity, Anal. Sci. 14 (1998) 35–41.
        https://doi.org/https://doi.org/10.2116/analsci.14.35.

[48]   J.C. Crittenden, R.R. Trussell, D.W. Hand, K.J. Howe, G. Tchobanoglous,
        MWH's Water Treatment: Principles and Design, 3rd ed., John Wiley and
        Sons, 2012. https://doi.org/10.1002/9781118131473.

[49]   X. Tongwen, Y. Weihua, H. Binglin, Ionic conductivity threshold in
        sulfonated poly (phenylene oxide) matrices: A combination of three-phase
        model and percolation theory, Chem. Eng. Sci. 56 (2001) 5343–5350.
        https://doi.org/10.1016/S0009-2509(01)00242-1.

[50]   J. Bartrolí, L. Alerm, P. Fabry, E. Siebert, Conductive epoxy-graphite
        composite as a solid internal reference in a NASICON-based sodium ion-
        selective electrode for flow-injection analysis, Anal. Chim. Acta. 308
        (1995) 102–108. https://doi.org/10.1016/0003-2670(94)00655-6.

[51]   M. Cretin, P. Fabry, Comparative study of lithium ion conductors in the
        system Li1+xAlxA2-xIV (PO4)3 with AIV=Ti or Ge and 0≤ x ≤0·7 for use
        as Li+ sensitive membranes, J. Eur. Ceram. Soc. 19 (1999) 2931–2940.
        https://doi.org/10.1016/s0955-2219(99)00055-2.

[52]   S. Balagopal, T. Landro, S. Zecevic, D. Sutija, S. Elangovan, A. Khandkar,
        Selective sodium removal from aqueous waste streams with NaSICON
        ceramics, Sep. Purif. Technol. 15 (1999) 231–237.
        https://doi.org/10.1016/S1383-5866(98)00104-X.

[53]   H.B. Park, J. Kamcev, L.M. Robeson, M. Elimelech, B.D. Freeman,
        Maximizing the right stuff: The trade-off between membrane permeability
        and selectivity, Science (80-.). 356 (2017) 1138–1148.
        https://doi.org/10.1126/science.aab0530.

[54]   B.D. Freeman, Basis of permeability/selectivity trade-off relations in polymeric gas separation membranes, Macromolecules. 32 (1999) 375–380. https://doi.org/10.1021/ma9814548.

[55]   B.P.S. Chauhan, P. Boudjouk, New neutral carrier-type ion sensors. Crown ether derivatives of poly(methylhydrosiloxane), Tetrahedron Lett. 40 (1999) 4123–4126. https://doi.org/10.1016/S0040-4039(99)00722-4.

3

Chapter 4

Permeation selectivity in the electrodialysis of mono- and divalent cations using supported liquid membranes

Abstract

We investigated in detail the permeation selectivity in the electro-dialysis of Na^+, K^+, Mg^{2+} and Ca^{2+} in both binary and quaternary mixtures using a supported liquid membrane (SLM). The SLM consisted of the organic liquid 2-nitrophenyl octyl ether (NPOE) containing a lipophilic anion, *i.e.* tetrakis[3,5-bis(trifluoromethyl)phenyl]borate, as the cation-exchanging site, which was used to fill the pores of the supporting membrane Accurel^R. We first determined the electro-phoretic mobilities of the migrating cations in single salt solutions, yielding: $Na^+ > K^+ > Mg^{2+} > Ca^{2+}$. This order reflects the different size of the migrating cations. The monovalent cations Na^+ and K^+ migrate in the dehydrated state and the divalent cations Ca^{2+} and Mg^{2+} migrate in a (partly) hydrated state, a conclusion was supported by Karl Fisher titrations.

Both binary and quaternary salt experiments showed a permeation selectivity in the following order: $K^+ > Na^+ > Ca^{2+} > Mg^{2+}$. Since this order does not correlate with the order of electro-phoretic mobilities, we have determined the ion-exchange selectivity constant (K_{ex}) and found: $K^+ > Ca^{2+} > Mg^{2+} \approx Na^+$. We conclude that the overall permeation selectivity is determined by the combination of ion-exchange selectivity and electro-phoretic mobility of the cations present in the membrane.

4.1 Introduction

Electrodialysis (ED) is a mature electrochemical separation process that has been applied to wastewater treatment and to the production of clean water for more than 70 years.[1] For certain applications with specific requirements for ion separation, water and ion recovery or for operation under harsh conditions, ED has become one of the state-of-art technologies.[2,3] In ED an applied electrical field is used to enhance the transport of ions from one solution through ion-exchange membranes (IEMs) into another solution, making it possible to separate a salt stream into desalinated water and brine. IEMs are the core components in such a separation process as they are permselective for cations or anions via ion-exchange sites that carry the opposite charge. However, the lack of selectivity between ions carrying the same charge still limits their use in separation processes where such selectivity is crucial.[4,5] In various practical applications, including fuel cells, resource recovery using ED and electro-membrane based batteries[6–10], the development of IEMs having excellent ion selectivity between monovalent and multivalent ions (*e.g.* Li^+/Mg^{2+}, Cl^-/SO_4^{2-}) or between ions with same valence (Cl^-/NO_3^-, Na^+/K^+) is urgently desirable.[11]

In general, the widely reported selectivities for specific ions by an IEM can be summarised in four categories: (1) tailor the permeation selectivities of the ions carrying the same charge on the basis of their mobility in the membrane matrix (*e.g.*, by their ion size and the structure of the membrane including pore size and porosity)[12], (2) the observed rejection of certain ions by surface modification of the IEM using a thin polyelectrolyte layer carrying a charge opposite to the charge of the IEM [13] or the build-up of a polyelectrolyte multilayer[14,15], and (3) the observed specific interactions of the ions to be separated with added functionalities present in the IEM [16,17] or in an added coating[18]. (4) A final category is based on recent research results[19,20] that points to the role of ion dehydration in the selective transport in IEMs. The use of selective IEMs for the separation of monovalent from divalent or multivalent ions have been reported [21–25]. Most widely used commercially available Neosepta, Fuji and Nafion cation ion membranes (CEMs) have a monovalent or monovalent over divalent cation selectivity ranging from 0.5-2.[26,27] In general, surface modification of standard CEMs improves the membrane cation selectivity.[28] Yang, et al.[17], reported that surface modification of the sulfonated polysulfone (SPSF) CEMs with crown ether improve the membrane K^+/Li^+ and K^+/Mg^{2+} selectivity to 3- and 6-fold, respectively. By the adsorption of

polyelectrolyte multilayers on the Nafion membrane, Zhu, et al.[26] reported an improved K^+/Mg^{2+} and Li^+/Co^{2+} selectivity by a factor 1000. However, it is still currently highly challenging to separate selectively two ions that have the same valence and have similar chemical properties, *i.e.* the separation of monovalent (K^+/Na^+) or divalent cations (Ca^{2+}/Mg^{2+}).

Previous studies from our lab were focused on the separation of alkali metal cations (especially K^+ from Na^+) using a supported liquid membrane (SLM) under ED conditions and its application in the field of element recovery, stimulated by the urgent need in the context of more severe legislation of salt discharges in the greenhouse industry.[20,29] In short, an SLM is made by filling the pores of an inert porous supporting membrane with an organic solvent containing a lipophilic salt to introduce the desired permselectivity.[30,31] The lipophilic salt also contributes to a reduction of the membrane electrical resistance.[32–34] In our earlier study we investigated cation-exchange membranes (CEMs), made by the introduction of lipophilic borate anions in the immobilised organic solvent (here, 2-nitrophenyl octyl ether, NPOE), and observed the selective permeation of K^+ relative to Na^+ and Li^+ [20]. The observed permeation selectivity of $K^+ > Na^+ > Li^+$ is in line with the order of increasing dehydration energy, *i.e.* $K^+ < Na^+ < Li^+$. The measured electrophoretic ion mobility increased in the order of $K^+ < Na^+ < Li^+$, implying that the smallest ion (Li^+) moves the fastest in the membrane. Overall, we concluded that despite the higher electrophoretic mobility of the Li^+ ion, the permeability of the K^+ is the highest because of the highest exchange selectivity, which, in turn, results from its low dehydration energy. The permeation selectivity is thus dominated by the dehydration energy of the ion species present.

The current study investigates the permeation selectivity for K^+ in relation to Ca^{2+} and Mg^{2+}, as well as the permeation selectivity for Ca^{2+} in relation to Mg^{2+}. Interpretation of the obtained results include the electrophoretic mobility of the investigated ions through the membrane, the extent of hydration of the exchanged cations and the ion-exchange selectivity at the water-membrane interface.

4.2 Materials and methods

4.2.1 Chemicals

All chemicals used were of analytical grade and used as received. The ACCUREL membrane support (polypropylene, thickness: 100 μm, pore size

(diameter): 0.1 μm) was purchased from MEMBRANA, the organic solvent 2-nitrophenyl-n-octyl ether (NPOE) and the lipophilic anion A: sodium tetrakis[3,5-bis(trifluoromethyl)phenyl]borate (NaBArF) for preparing the SLM were both purchased from Sigma-Aldrich. All salts for making the salt solutions (KCl, NaCl, CaCl$_2$, MgCl$_2$ and Na$_2$SO$_4$) were purchased from MERCK.

4.2.2 Membrane preparation

All experiments were performed with freshly prepared SLMs. The membrane support (ACCUREL) was cut into proper shape and, without any further pretreatment, submerged in the organic solution of 50 mM NaBArF in NPOE for 30 min at room temperature. Due to capillary forces, the ACCUREL pores are filled up with the solution. Before mounting the membrane in an ED cell (Section 4.2.3.1), excess of solvent was removed by gently wiping it with a tissue.

4.2.3 Membrane characterization

4.2.3.1 Electrodialysis (ED)

All studies regarding ion transport across the SLMs were performed under ED conditions. Experiments were carried out in a six-compartment cell that has been reported in our previous study with the configuration shown in Figure 4.1[20]. The membrane surface area and thickness of the SLMs were 10.15 cm^2 and 100 μm, respectively with a porosity $\Phi = 0.7$ and a tortuosity $\tau = 2.1$ (membrane property data are obtained from the manufacture and literature).[35,36] The mixed-salt experiments were carried out in equimolar 25 mM solutions of NaCl, KCl, CaCl$_2$ and MgCl$_2$ or in equimolar 50 mM binary ion solutions of KCl + CaCl$_2$, KCl + MgCl$_2$ or CaCl$_2$ + MgCl$_2$. The single-salt experiments were carried out using 0.1 M NaCl, KCl, CaCl$_2$ and MgCl$_2$ solutions. The buffer and electrolyte solutions were made with NaCl and Na$_2$SO$_4$ solutions, respectively, that have the same ionic strength as the testing solution. The testing solutions were all recirculated at a flow rate of 150 mL min^{-1} separately as feed and receiving phase in compartments A and B (Figure 4.1). Prior to use, SLMs were pre-conditioned for 24 h in the solution with the same ion composition and concentration as the test solution. Commercially available standard grade cation exchange membranes (CEMs) and anion exchange membranes (AEMs) from Neosepta were used in the six-compartment cell and pre-conditioned in the same way as the SLM. The temperature of all solutions was controlled at 25 ± 0.2 °C during

the experiment using a water bath. A potentiostat (Ivium Technologies, Vertex.One, Eindhoven, the Netherlands) was employed as power source for applying a constant current density. The presence of diffusion boundary layers at the membrane-solution interface can contribute to the total measured resistance. In order to minimize this effect, two Haber-Luggin capillaries were positioned directly adjacent (as close as possible) to the SLM surface and connected to two reservoirs containing 3M KCl filled Ag/AgCl reference electrodes (QM711X, QIS, the Netherlands) for monitoring the voltage drop over the membrane. For all ED experiments, a constant current of 10 mA (corresponding to a current density of 10 A·m^{-2}) was applied during a time-period of 24 h (for single-salt experiments) or 48 h (for all mixed-salt experiments).
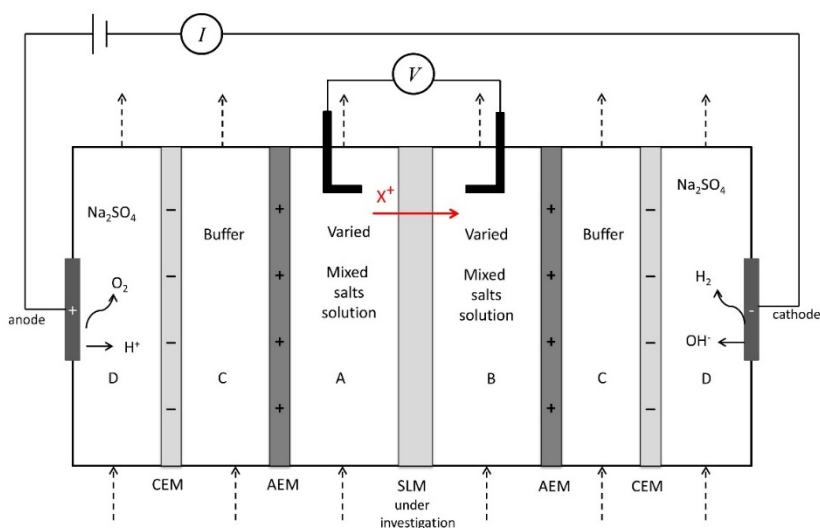
Figure 4.1 Schematic of the configuration of the six-compartment cell used during the electro-dialysis (ED) experiments. Compartment C and D as well as the position of the CEMs and AEMs prevent the concentration changes in the two inner testing compartments from any interferences. As a result, the concentration changes of the cation species of interest in compartments A and B is solely due to transport of the central SLM.

4.2.3.2 Transport numbers and mobility

Under ED conditions, the ion transport number represents the fraction of the current carried by that specific ion. The transport number of each ion can be derived from the concentration changes in compartments A and B. The (absolute) concentration change in compartment B (here an increase) is the same as the

(absolute) concentration change in compartment A (here a decrease), if both compartments have equal volume. Therefore, during the experiments, samples of 1 mL were taken from both compartments at a certain time interval. The ion concentrations were determined by ion chromatography (IC, Metrohm Compact IC 761), at a confidence level of > 95%.

The transport number t_i for ion species i is given by [37]:

$$t_i = \frac{zFV\frac{\Delta C}{\Delta t}}{I_{tot}A} \tag{4.1}$$

where z is the charge of the ion, F is the Faraday constant (96485 C·mol^{-1}), V is the volume (m^3) of the feed or receiving compartment, A represents the effective membrane surface area (m^2), and I_{tot} is the (constant) externally applied current density (A·m^{-2}). The number of moles of the ion i transferred over the SLM per unit time, $\Delta C/\Delta t$ (mol·m^{-3}·s^{-1}), was calculated from the concentration change in compartment A. Note that here the decrease in concentration in compartment A is the same with the increase of concentration in compartment B.

For ions moving through the membrane, the molar ion flux is expressed as:

$$J = -u_i c_i \frac{dE_m}{dx} \tag{4.2}$$

where u_i (m^2·V^{-1}·s^{-1}) is the electrophoretic mobility of the ion i in the membrane, c_i represents the ion concentration in the membrane (in mol·m^{-3}). The SLM is overall electro-neutral. Based on the overall electroneutrality of the SLM, the borate concentration determines the concentration of exchanged cations. For the monovalent cations that is equal to the borate concentration (50 mM) and for the divalent cations that is half of the borate concentration (25 mM). Because of the relatively high dielectric constant of NPOE ($\varepsilon=24$), intimate ion-pair formation between the borate and the cation is not considered.[38,39] By implication, the free, mobile cation concentration in the SLM equals the total cation concentration. dE_m/dx (V·m^{-1}) is defined as the electric field gradient.

Based on the electro-migration term in the Nernst-Planck equation, the current carried by ion species i is:

$$t_i I_{tot} = -zu_i c_i F \frac{dE_m}{dx} \tag{4.3}$$

I_{tot} represents the (total) current density. The effective membrane area is determined by the porosity Φ. In addition, the actual distance that the ion needs to travel through the SLM is larger than the membrane thickness, which is determined by the membrane tortuosity, τ. The electric field strength over the membrane should then be expressed as: $\frac{E_m}{\tau d}$, where E_m (V) is the recorded voltage drop over the membrane of thickness d (m). Therefore, Eq. 4.3 will be expressed as:

$$\frac{t_i I_{tot}}{\Phi} \times \tau = \varsigma t_i I_{tot} = zu_i c_i F \frac{E_m}{d} \tag{4.4}$$

Where ς is a correction factor determined by the porosity and tortuosity of the ACCUREL membrane support, here determined to be $\varsigma = \frac{\tau}{\Phi} = \frac{2.1}{0.7} = 3$.

The electrophoretic ion mobility u_i of ion species i in the membrane determined from single-salt ED experiments, can then be given by:

$$u_i = \varsigma \frac{t_i I_{tot}}{zc_i F \frac{E_m}{d}} \tag{4.5}$$

The concentration of counter ions in the membrane (c) equals the borate concentration (A^-) divided by the valence of the counter ion. After substituting $c = \frac{A^-}{z}$ in Eq. 4, the mobility ratio $\frac{u_1}{u_2}$ of two ion species as assessed in single-salt solutions scales with t_1/t_2 and $E_{m,2}/E_{m,1}$ and is independent of their charge z.

4.2.4 Karl Fischer titration

Karl Fisher titration (Metrohm 756 KF Coulometer) was employed for determining the water concentration present in the pure organic solvent phase (NPOE) and in the presence of the lipophilic borate anion and equilibration with the different investigated salt solutions at room temperature. First fixed volumes of pure NPOE and NPOE containing the lipophilic anion A as the sodium salt were equilibrated the same fixed volumes (0.5 mL) of aqueous salt solutions containing 100 mM of NaCl, KCl, CaCl$_2$ and MgCl$_2$. Equilibration with Milli-Q water was used as reference. After equilibration, a sample size of 50 μg of the organic solvent was taken for the

104

determination of the water content. The amount of water (g) in the sample can be calculated based on the wt% results from the measurements. All experiments were performed in triplicate and standard deviation (STD) of the measured samples were calculated to determine the accuracy of the measurements. Ion concentrations of the salt solutions were determined by IC for monitoring the extent of ion exchange.

4.3. Results & Discussion

4.3.1 Mass and charge balance

Ideally, when using the six-compartment cell shown in Figure 4.1, the concentration changes of the, in this case, cation species in the two inner compartments A and B can solely be ascribed to ion transport over the membrane under investigation. Therefore, the change in compartment B is of the same magnitude as the change in compartment A but of opposite sign. In addition, in order to retain electro-neutrality, the total charge in each compartment should add up to zero. The mass and charge balance for all measurements in this study, including using (1): single-salt solutions of 100 mM KCl, NaCl, $CaCl_2$ and $MgCl_2$, (2): binary salt solutions of equimolar (50 mM) KCl + $CaCl_2$, KCl + $MgCl_2$ or $CaCl_2$ + $MgCl_2$, and (3): four ion mixed-solution of equimolar (25 mM) KCl + NaCl + $CaCl_2$ + $MgCl_2$ were determined and detailed data can be found in the Supplementary Information. Indeed, in all three sets of ED tests, the mass and charge balance were essentially closed.

4.3.2 Ion exchange at the water-membrane interface

Consider the presence of ion species M_1 of valence z_1 in the water or feed phase (f) and ion species M_2 of valence z_2 in the membrane phase (m). The ion-exchange process at the water-membrane interface can be expressed by:

$$z_2 M_{1,f} + z_1 M_{2,m} \xrightleftharpoons{K_{ex}} z_2 M_{1,m} + z_1 M_{2,f} \qquad (4.6)$$
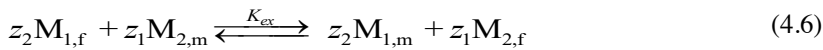
K_{ex} represents the ion exchange constant, given by:

$$K_{ex} = \frac{M_{1,m}^{z_2} \times M_{2,f}^{z_1}}{M_{1,f}^{z_2} \times M_{2,m}^{z_1}} \qquad (4.7)$$

Due to electroneutrality, the maximum total ion concentration in the membrane is determined by the impregnated lipophilic anion borate (A^-) concentration (50 mM). Therefore, the sum of positive charges from cations in the membrane equals the sum of negatively charges from the borate A^-:

$$z_1 M_{1,m} + z_2 M_{2,m} + z_A A = 0 \qquad (4.8)$$

with z_A the charge of the membrane-bound anion (-1).

The cation partitioning in the membrane relates to the Gibbs free energy required for the translocation of an ion species of charge z and crystal radius r (in Å) from phase 1 with permittivity ε_1 to phase 2 with permittivity ε_2, as given by the Born equation [40,41]:

$$\Delta G = \frac{N_A z^2 e^2}{8\pi\varepsilon_0 r}\left(\frac{1}{\varepsilon_2} - \frac{1}{\varepsilon_1}\right) \qquad (4.9)$$

with ΔG in kJ·Mol^{-1}, N_A Avogadro's number (6.02×10^{23}), e the elementary charge (1.6022×10^{-19} C) and ε_0 the permittivity of vacuum (8.854×10^{-12} F·m^{-1}). For transferring a monovalent cation ($z = 1$) from the aqueous phase ($\varepsilon_1 = 80$) into the NPOE/membrane phase ($\varepsilon_2 = 24$) [38,39] Eq. 4.9 can be simplified into $\Delta G = 20.3/r$. And for divalent cations ($z = 2$), this will be $\Delta G = 81.2/r$.

Table 1 lists the crystal radii and the calculated ΔG values for complete ion dehydration according to the Born equation of the two monovalent cations Na$^+$ and K$^+$ and for the two divalent cations Ca^{2+} and Mg^{2+} used in this study.

	Crystal radius (in Å) [42,43]	ΔG (in kJ mol^{-1})
Na$^+$	0.95	21.4
K$^+$	1.33	15.3
Mg^{2+}	0.65	124.9
Ca^{2+}	0.99	82.0

Table 4.1 Crystal radii (in Å) of Na$^+$, K$^+$, Ca^{2+} and Mg^{2+}, as well as the calculated Born ΔG (in kJ mol^{-1}) required for the transfer of the particular ionic species from the aqueous into the NPOE/membrane phase.

The partitioning of two ion species M_1 and M_2 over the water phase and the organic solvent membrane phase is defined by a Boltzmann distribution. Assuming

complete dehydration, the ion concentration ratio M_2 in the membrane, $M_{1,m}/M_{2,m}$ is defined as:

$$\frac{M_{1,m}}{M_{2,m}} = \frac{M_{1,f}}{M_{2,f}} \exp\left(\frac{\Delta G_{M_2} - \Delta G_{M_1}}{RT}\right)$$ (4.10)

with the ΔG values calculated according to the Born equation.

4.3.3 Ion mobility in single-salt solutions

Flux measurements in symmetrical 100 mM NaCl, KCl, $CaCl_2$ or $MgCl_2$ solutions were used to determine the electrophoretic mobility of each ion species in the SLM. Figure 4.2 shows the normalized Na^+, K^+, Ca^{2+} and Mg^{2+} concentration (the ratio of measured cation concentration and the initial cation concentration in the feed compartment A) over time and the linear fittings for all four ion species.
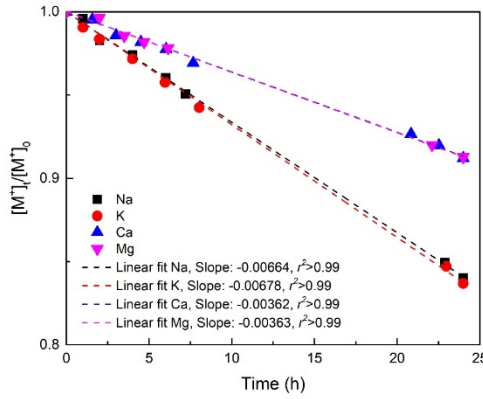
Figure 4.2 Normalized Na^+, K^+, Ca^{2+} and Mg^{2+} concentrations in the feed compartment A, recorded over time in symmetrical 100 mM NaCl, KCl, $CaCl_2$ or $MgCl_2$ solutions. Also indicated the linear fits of the data, including the slope and regression coefficient r^2.

For all four tested cation solutions, the normalized cation concentration exhibits a linear decrease over time that is similar for cations of the same valence, whereas the slope for monovalent cations Na^+ and K^+ are determined as -0.00664 and -0.00678, respectively and for divalent cations Ca^{2+} and Mg^{2+} are -0.00362 and -0.00363, respectively. Because of the charge difference of two and the same current density applied, the decrease in normalized concentration of divalent cations is half of that

found for the monovalent cations, which is also reflected by the ratio of the slopes of the plots.

The transport number of each ion (Eq. 4.1) can be derived from the data shown in Figure 4.2. The transport number and recorded voltage drop over the SLM (E_m/d) allow the calculation of ion mobility in the membrane (u), according to Eq. 4.5. The calculated ion mobility strongly depends on the accuracy of the recorded membrane potential, hence the reported standard deviation (SD) values. Table 4.2 summarizes the calculated ion transport number (t_{ion}), recorded membrane potential drop (E_m/d) and calculated ion mobility (u_i).

	t_{ion}	$E_m/d \times 10^{-4}$ (V·m⁻¹)	SD $E_m/d \times 10^{-4}$ (V·m⁻¹)	$u_i \times 10^{10}$ (m²·V⁻¹·s⁻¹)	SD $u_i \times 10^{10}$ (m²·V⁻¹·s⁻¹)
Na^+	0.97	1.6	0.04	3.60	0.09
K^+	0.93	2.8	0.12	2.17	0.09
Mg^{2+}	0.98	2.7	0.06	2.26	0.05
Ca^{2+}	0.98	4.0	0.17	1.52	0.06

Table 4.2 Transport numbers of Na^+, K^+, Mg^{2+} and Ca^{2+} (t_{ion}), recorded membrane potential drop (E_m/d) with SD, and the ion mobility in the membrane (u_i) with SD, all derived from single salt ED measurements.

As expected, and given that all transport numbers are close to unity (see Section 4.2.3.2), the mobility ratio of any couple of ions, u_1/u_2, (more or less) scales with the inverse of the corresponding measured membrane potentials, $E_{m,2}/E_{m,1}$. The electrophoretic mobility can also be expressed by [44]:

$$u_i = \frac{ez_i}{6\pi\eta r_i} \qquad\qquad (4.11)$$

Where e is the elementary charge, η (Pa·s) is the viscosity of the solvent and r_i (m) is the radius of the ion. As shown in Eq. 4.11, the electrophoretic mobility of an ion relates to its size, whether it is dehydrated or hydrated. If dehydrated, the mobility is expected to scale with the reciprocal ion crystal radius, if hydrated, with the reciprocal hydrated radius. According to Eq. 4.11, z/u is linear with r, with a slope of $e/6\pi\eta$ (in m³·V⁻¹·s⁻¹). As reported before [20], the mobility ratio of K^+ and Na^+ is rather close to the reciprocal ratio of their crystal radii, reflecting that these monovalent cations are present in the SLM essentially completely dehydrated. Figure 4.3 shows the

correlation of the ion crystal radius of K$^+$ and Na$^+$ with their charge and mobility (z/u) ratio (solid line), with the electrophoretic mobility values taken from Table 4.3. Based on theoretical considerations, the (extended) linear fit through the Na$^+$ and K$^+$ data points was forced to go through the origin. As remarked, Eq. 4.11 should hold irrespective the hydration state of the particular ion species. Therefore, the plot in Figure 4.3 has been extrapolated to z/u values of Ca^{2+} and Mg^{2+} (dotted line), again using the u values from Table 4.3. The in this way obtained radius of Ca^{2+} ($r_{p,Ca}$) and Mg^{2+} ($r_{p,Mg}$) is 2.68 Å and 3.96 Å, respectively, values clearly larger than the crystal radii listed in Table 4.1. However, the slope derived from Figure 4.3 is 3×10^{-20} m$^3 \cdot$V$^{-1} \cdot$s^{-1}, resulting in a viscosity η of the NPOE-borate system of 0.28 Pa·s, a value about 20 times higher than the reported value of 0.0137 Pa·s for pure NPOE [45]. Possible explanations for this observed difference include: (1) The actual concentration of free cations in the SLM. It is important to realize that all mobility calculations assume the cations to be present in the SLM as free, mobile charge carriers. For instance, given a borate concentration of 50 mM, the free cation concentration in the SLM was assumed to be 50 mM and 25 mM in pure NaCl or CaCl$_2$ solutions, respectively. We cannot rule out however that the borate interacts with the cations. The effect would be that at any moment in time only a fraction of the cations present contribute to the (constant) total applied current with the remaining fraction essentially temporarily immobilized. The extent of interaction may be cation species dependent. Even though this effect is expected to be more dominant for the divalent cations, their hydration shell, enlarging their effective radius, counteracts the higher charge regarding the electrostatic interaction with borate. One way to reconcile the high viscosity derived from Figure 4.3 and the much lower viscosity of pure NPOE is to assume that only 5% of the cations are free to move, implying an actual mobility 20 times higher than the ones calculated and listed in Table 4.2. This, in turn, results in a slope ($=r \times u/z$) of Figure 4.3 also 20 times higher and with that a 20 times lower viscosity (slope$=6\pi\eta/e$). (2) The actual viscosity of NPOE/borate is affected by an interaction with the membrane (Accurel) pore wall.

The data of Figure 4.3 indicate that, in contrast to monovalent cations, divalent cations are still partly hydrated while traversing the SLM. For that reason, next the amount of water taken up by the SLM was investigated, with the water present as hydration water of the divalent cations.
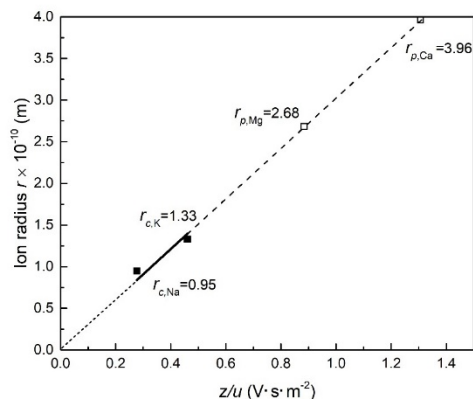
Figure 4.3 Correlation between the ion radius *r* and the ratio of charge and mobility (z/u) for K$^+$, Na$^+$, Ca^{2+} and Mg^{2+}. $r_{c,Na}$ and $r_{c,K}$ represent the crystal radius of Na$^+$ and K$^+$, $r_{p,Ca}$ and $r_{p,Mg}$ the predicted (partially hydrated) radius of Ca^{2+} and Mg^{2+}. The (extended) linear fit through the Na$^+$ and K$^+$ data points was forced to go through the origin because of theoretical considerations.

4.3.4 Water content in NPOE

Quantification of the water content in the organic solvents (NPOE or NPOE with lipophilic anion A) after equilibration with water or with different salt solutions was performed by using the standard coulometric Karl Fischer (KF) titration method. Measurements were performed in triplicate. As the lipophilic anion A$^-$ was impregnated in NPOE as a sodium salt, the same (calculated) amount of the Na$^+$ in the organic solvent was found in the aqueous solution after equilibration, indicating a full ion exchange of the cation species in the membrane. Tables 4.3 and 4.4 list the measured water content (wt%) in pure NPOE or NPOE containing lipophilic anion A$^-$, respectively, and the calculated amount of water C_{water} (in mM) for each sample. The SD values for all samples ≤0.02% indicates the rather high reproducibility of the KF measurements. Clearly, from Table 4.3, compared to the water content of the sample equilibrated in pure water, adding either 100 mM NaCl, KCl, CaCl2 or MgCl2 to the equilibration solution has no effect. The calculated amount of water in all samples is about the same (64-69 mM, based on 0.11-0.12 wt%)

110

Pure NPOE equilibrated with	C_{salt} (mM)	Measured Water (wt%)	SD	C_{water} (mM)
H_2O	0	0.12	0.01%	69
NaCl	100	0.12	0.00%	69
KCl	100	0.11	0.02%	64
$MgCl_2$	100	0.11	0.00%	69
$CaCl_2$	100	0.12	0.02%	64

Table 4.3 Measured mean water content (wt%) in pure NPOE after equilibration in pure water and in 100 mM NaCl, KCl, $MgCl_2$ and $CaCl_2$ solutions. Average values and standard deviations (SD) are based on measurements in triplicate.

As shown in Table 4.4, in pure water, adding A^- (present as Na^+ salt) to the NPOE doubles the water concentration in the SLM, from 69 to 137 mM. Adding either NaCl or KCl to the feed solution has no effect on the final water content of the NPOE. Apparently, either hydrated Na^+ from the feed is exchanged for hydrated Na^+ leaving the SLM or, alternatively, the exchange involves the two ions dehydrated. In both cases, the water content of the SLM remains the same. Based on this data alone we cannot distinct between these two scenarios. However, the mobility – ion radius relation makes us conclude that monovalent cations traverse the SLM in the dehydrated state. In contrast, with $MgCl_2$ or $CaCl_2$ present in the feed, the final water concentration almost doubles. Compared to the control of Table 4.3 and with A^- included in the SLM, the presence of $CaCl_2$ or $MgCl_2$ in the feed solution increased the water concentration of approximately 160 mM. Considering a Ca^{2+}/Mg^{2+} concentration of 25 mM (given the A^- of 50 mM), the (average) hydration number of each divalent cation-borate complex would be around 6.5. The increased water content due to the exchange of Mg^{2+} with Na^+ initially associated with the borates is 243-127=116 mM per 50 mM borate sites, and is slightly higher than Ca^{2+} of 220-127=93 mM per 50 mM borate site. This is also in line with stronger hydration by the smaller crystal radius of Mg^{2+}. Because the water involved in the hydration of A^- is ignored, this value is slightly overestimated. Considering the reported range of hydration numbers of Ca^{2+} and Mg^{2+} of 5-12 [37-40], this indicates that these divalent cations indeed have lost part of their water shell, consistent with the conclusion based on the relation mobility ratio and ion radius (Figure. 4.3).

NPOE+A⁻ equilibrated with	C_{salt} (mM)	MeasurednWater (wt%)	SD	C_{water} (mM)
H₂O	0	0.35	0.01%	137
NaCl	100	0.34	0.01%	127
KCl	100	0.33	0.02%	127
MgCl₂	100	0.53	0.00%	243
CaCl₂	100	0.50	0.02%	220

Table 4.4 Measured mean water content (wt%) in the NPOE in the presence of the lipophilic anion A⁻ (50 mM borate) after equilibration in pure water or 100 mM NaCl, KCl, MgCl₂ and CaCl₂ solutions. Average values and standard deviations (STD) are based on measurements in triplicate.

A final remark on the water content of NPOE concerns the presumed linearity between z/u and r, Eq. 4.11, a relationship constrained by a constant viscosity of the SLM. It is very well conceivable that the uptake of water alters the overall viscosity of the SLM system. However, given an NPOE concentration of approximately 4 M and water concentration differences in the order of 0.1 M, the assumption of constant viscosity seems justified.

4.3.5 Ion exchange

4.3.5.1 Determination of the ion-exchange selectivity constant in binary salt solutions

Ion permeation through an ion-exchange membrane by ED relates to both ion exchange of the particular ionic species over the biphasic water – membrane system and ion electrophoretic mobility through the membrane. The previous paragraphs addressed the extent of hydration on the electrophoretic ion mobility in single-salt experiments. This paragraph focusses on the electro dialysis of binary and multi-ion solutions to determine and understand the ion-exchange process.

As the total charge of the permeating cations in the membrane is equal to the charge carried by the present lipophilic anions, different cations will actually compete with each other to enter or to leave the SLM in the case of mixed-salt solutions in the feed phase.

Figure 4.4 shows how the ion concentrations in the feed compartment A change in time during 48 h starting with binary equimolar mixtures (50 mM each) of KCl and MgCl₂ (Figure 4.4a), KCl and CaCl₂ (Figure 4.4b), and CaCl₂ and MgCl₂ (Figure

4.4c). The changing ion concentrations are presented as normalized ion concentrations (left-hand axis). From the ion concentrations in the feed, the ionic current densities were calculated, which are also presented in Figure 4.4 (right-hand axis). The sum of the calculated transport numbers of the two cations involved in each series is 0.88 (Figure 4.4a), 1 (Figure 4.4b), and 0.98 (Figure 4.4c). These numbers indicate that under these conditions the current through the SLM is predominantly carried by the cations. For the binary mixture of KCl and $MgCl_2$, lower transport number of 0.88 was found, indicating that part of the current is carried in another way. The transport of protons was excluded because we did not detect a pH change in the feed and receiving phase compartments. It is speculated that, despite the cation-exchange properties of the SLM, some chloride might be counter transported. We have not investigated further this possibility.

Clearly, as seen from Figure 4.4a and 4.4b, K^+ is transported right from the start with the K^+ current gradually decreasing over time. In contrast, both the Mg^{2+} and Ca^{2+} transport is close to zero at the start and increased over time.

For a K^+/Mg^{2+} feed ratio of 0.2 (as observed after about 38 h; thus about 10 h earlier compared to the K^+/Ca^{2+} situation; see below), the current ratio is 5.8:3, reflecting a molar permeation ratio of 1:0.26. While for the mixture of K^+/Ca^{2+}, after 48 h, the K^+ current equals the Ca^{2+} current, indicating that at K^+/Ca^{2+} feed concentration ratio of about 0.2, the K^+/Ca^{2+} permeation ratio is about 1:0.5. By comparing these data, it is clear that Mg^{2+} is much less competitive compared to Ca^{2+} in the electro-dialysis with K^+. Also, in the combined Ca^{2+}/Mg^{2+} experiment (Figure 4.4c), we have observed a preference of Ca^{2+} permeation compared to Mg^{2+} permeation. This difference cannot be explained by the different mobilities of Mg^{2+} and Ca^{2+}, since we have observed (Table 4.2) that Mg^{2+} is more mobile compared to Ca^{2+}. Therefore, the difference originates from the difference in ion-exchange selectivity $K_{ex}(K^+/Mg^{2+})$ and $K_{ex}(K^+/Ca^{2+})$.

We will focus now on the extraction of the ion-exchange selectivity constants from our electro-dialysis data.

4
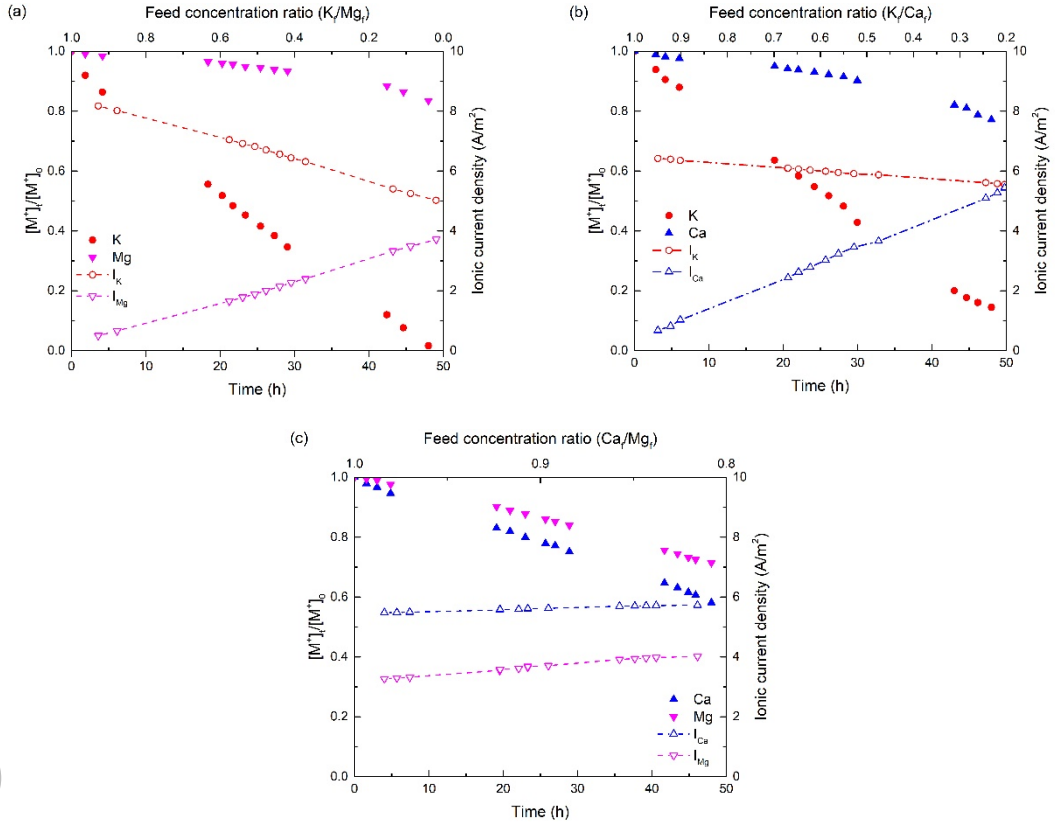
Figure 4.4 Normalized feed concentration ratios (left axis) and ionic currents (right axis) versus time as measured in symmetrical binary salt solutions of (a) 50 mM KCl + 50 mM CaCl$_2$, (b) 50 mM KCl + 50 mM MgCl$_2$ and (c) 50 mM CaCl$_2$ + 50 mM MgCl$_2$.

According to Eq. 4.4, the ratio of current carried by ion species M$_1$ and M$_2$ equals:

$$\frac{I_{M_1}}{I_{M_2}} = \frac{z_1 M_{1,m} u_{M_1}}{z_2 M_{2,m} u_{M_2}} \tag{4.12}$$

with M$_{1,m}$ and M$_{2,m}$ the concentrations of M$_1$ and M$_2$ in the membrane (mol·m^{-3}).

For experiments involving two monovalent or the two divalent cations, (*i.e.* $z_1 = z_2$), Eq. 4.12 equals:

$$\frac{M_{1,m}}{M_{2,m}} = \frac{I_{M_1}}{I_{M_2}} \times \frac{u_{M_2}}{u_{M_1}} \tag{4.13}$$

114

The general derived equation for the ion-exchange selectivity constant K_{ex} as given in Eq. 4.7 simplifies for two monovalent cations and for two divalent cations to:

$$K_{ex} = \frac{M_{1,m} \times M_{2,f}}{M_{1,f} \times M_{2,m}} = \frac{M_{1,m}}{M_{2,m}} \times \frac{M_{2,f}}{M_{1,f}}$$
(4.14)

Substituting Eq. 4.13 into Eq. 4.14 gives:

$$K_{ex} = \frac{I_{M_1}}{I_{M_2}} \times \frac{u_{M_2}}{u_{M_1}} \times \frac{M_{2,f}}{M_{1,f}}$$
(4.15)

In this case K_{ex} is dimensionless. The factor $\frac{I_{M_1}}{I_{M_2}} \times \frac{u_{M_2}}{u_{M_1}}$ is equal to $\frac{M_{1,m}}{M_{2,m}}$.

For a binary mixture containing one monovalent cation ($M_1=K^+$; $z_1=1$) and one divalent cation ($M_2=Ca^{2+}$ or Mg^{2+}; $z_2=2$), the situation is more complex. $M_{1,m}^{z2}/M_{2,m}^{z1}$ in Eq. 4.7 is expressed by:

$$\frac{M_{1,m}^2}{M_{2,m}} = \frac{I_{M_1}^2}{I_{M_2}} \times \frac{u_{M_2}}{u_{M_1}^2} \times \frac{2d}{FE_m}$$
(4.16)

Resulting in an expression of K_{ex} as a function of:

$$K_{ex} = \frac{M_{1,m}^2}{M_{2,m}} \times \frac{M_{2,f}}{M_{1,f}^2} = \frac{I_{M_1}^2}{I_{M_2}} \times \frac{u_{M_2}}{u_{M_1}^2} \times \frac{2d}{FE_m} \times \frac{M_{2,f}}{M_{1,f}^2}$$
(4.17)

According to Eq. 4.7, plotting $M_{1,m}^{z2}/M_{2,m}^{z1}$ as function of $M_{1,f}^{z2}/M_{2,f}^{z1}$ renders a graph with slope K_{ex}.

We have plotted our experimental data for the binary combinations K^+/Na^+ (earlier published by us[20]) and Ca^{2+}/Mg^{2+} according to Eq. 4.15. The results are shown in Figure 4.5a and 4.5b. For both combinations we observed, as expected, a linear fit. Based on theoretical considerations, the fit was forced to go through the origin. From the slopes of the plots we deduced the values for the ion-exchange selectivity constants $K_{ex}(K^+/Na^+) = 12.7$ and $K_{ex}(Ca^{2+}/Mg^{2+}) = 2.6$. As becomes clear by comparing Eqs. 4.10 and 4.14, the exponential term in Eq. 4.10 represents K_{ex}, thus providing, apart from Eq. 4.14/4.15, a second expression for K_{ex}, at least in the case of two monovalent cation species that require total dehydration. Indeed, the K_{ex} value

of 11.7 calculated from Eq. 4.10[20] nicely corresponds to the value of 12.7 after applying Eq. 4.15.
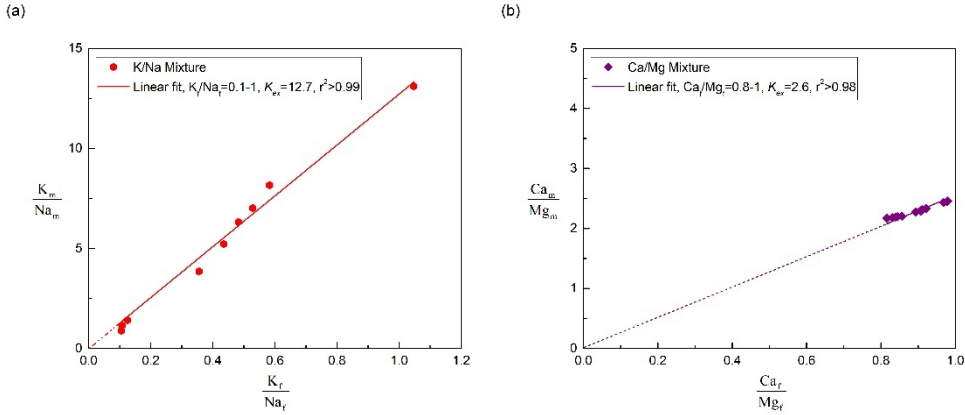
Figure 4.5 The ion-exchange selectivity constant of two ion species in binary ion solutions ($M_1=K^+$ or Ca^{2+} $M_2=Na^+$ or Mg^{2+}) determined as the slope by plotting $\frac{M_{1,m}}{M_{2,m}}$ versus $\frac{M_{1,f}}{M_{2,f}}$ and the regression coefficient r^2. Fits were forced to go through the origin.

Next, we plotted our experimental data for the binary combinations K^+/Mg^{2+} and K^+/Ca^{2+} according to Eq. 4.17 (Figure 4.6). We do indeed observe in both cases a linear plot (forced passing the origin) for $M_{1,f}^{z2}/M_{2,f}^{z1} < 25$. However, for the initial part of these experiments (where the feed ratios of K^+ to Mg^{2+} or to Ca^{2+} >0.6), $i.e.$ the upper right part in Figure 4.6a and 4.6b our data points deviate from the linear part. The use of K_{ex} values assumes chemical equilibrium. Therefore, this observed deviation may reflect that equilibrium has not (yet) established. For one thing, at the start of the experiment the concentration of divalent cations in the SLM will be virtually zero, implying that the exchange of $e.g.$ Ca^{2+} from the feed and Na^+ in the SLM occurs in one direction. In addition, it is well-known that membrane selectivity is not a fixed parameter but instead varies with changing ionic conditions in the feed and/or receiving solution, as is the case in a dynamic system as ours. From the linear part we first derived the ion-exchange selectivity constants of $K_{ex}(K^+/Mg^{2+}) = 10.6$ and $K_{ex}(K^+/Ca^{2+}) = 2.9$ from the slopes. From these two K_{ex} values, we can easily calculate and (expected) value of $K_{ex}(Ca^{2+}/Mg^{2+}) = 3.6$. This is very close to the obtained value of $K_{ex}(Ca^{2+}/Mg^{2+}) = 2.6$ from the experiment using the binary Ca^{2+}/Mg^{2+} mixture. This gives us confidence in the linear relation of the latter stage of the experiment. The data points strongly deviating from the linear plots $M_{1,f}^{z2}/M_{2,f}^{z1}$

> 35 are both related to the start of the experiments using feed mixtures containing K^+ and Mg^{2+} or Ca^{2+}. For some reasons in the initial stage of these experiments, the permeation through the membrane is much more favorable for K^+ compared to the later stage of the experiment. For now, we can only speculate about the reason causing this deviation. The calculation of K_{ex} is based on the assumption of chemical equilibrium. Apparently, during the first 5 hours or so of the experiment the equilibrium state is not reached yet. In addition, it might be that for some reason in ion mixtures involving both monovalent and divalent cations, K_{ex} is more sensitive to the K^+ concentration in the feed.
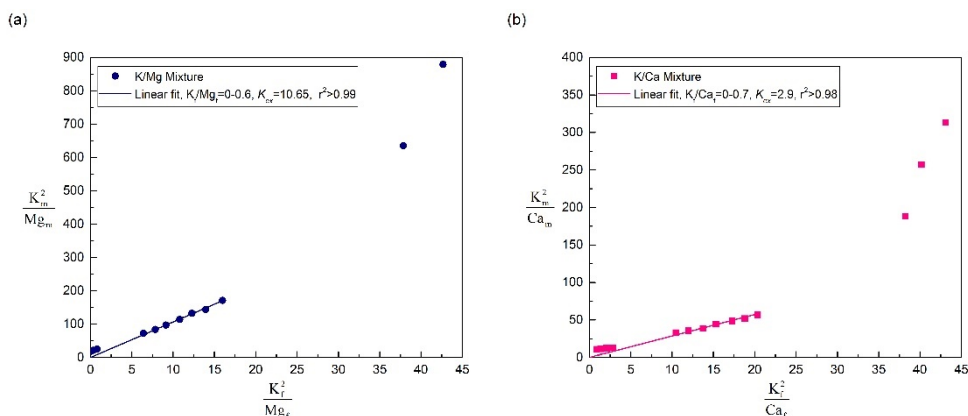

Figure 4.6 The ion-exchange selectivity constant of two ion species in binary ion solutions ($M_1=K^+$ or $M_2=Mg^{2+}$ or Ca^{2+}) determined as the slope by plotting $\frac{M_{1,m}^1}{M_{2,m}}$ versus $\frac{M_{1,f}^1}{M_{2,f}}$ and the regression coefficient r^2. Fits were forced to go through the origin.

In Table 4.5 the obtained ion-exchange selectivity constants are tabulated.

Ion exchange constant (K_{ex})	Binary mixture (Section 3.3.2)	Quaternary mixture (Section 3.3.3)
K^+/Na^+	12.6	11.3
Ca^{2+}/Mg^{2+}	2.6	3.3
K^+/Ca^{2+}	2.9	3.6
K^+/Mg^{2+}	10.6	12.8

Table 4.5 Determined ion-exchange selectivity constant for the ion combination of K^+/Na^+, Ca^{2+}/Mg^{2+}, K^+/Ca^{2+} and K^+/Mg^{2+} in binary ion mixture or the quaternary ion mixture.

4.3.3.3 Determination of the ion-exchange selectivity constant in quaternary solutions

Finally, we have investigated the electro-dialysis of an equimolar mixture (each at 25 mM) of NaCl, KCl, CaCl$_2$ and MgCl$_2$, to see if there is any cross-coupling effect between these different ions. This experiment was set up similarly as the experiments on the binary mixtures, discussed before.

Figure 4.7 shows how the ion concentrations in the feed compartment A change in time during 48 h starting with the quaternary equimolar mixture (25 mM each) of NaCl, KCl, MgCl2 and CaCl$_2$. The changing ion concentrations are presented as normalized ion concentrations (left-hand axis). From the changing ion concentrations in the feed, the ionic current densities were calculated and are also presented in Figure 4.7 (right-hand axis). The sum of the calculated transport numbers of the four cations involved is close to unity, and leads to the conclusion (as before) that under these conditions the current is predominantly carried by the cations.

It is observed that the dominant cation transported is K^+ and is followed by Na^+, Ca^{2+} and finally Mg^{2+}. This confirms the order observed before in the binary salt experiments, where K^+ is dialyzed in preference over Na^+ and where Ca^{2+} is dialyzed in preference over Mg^{2+}.
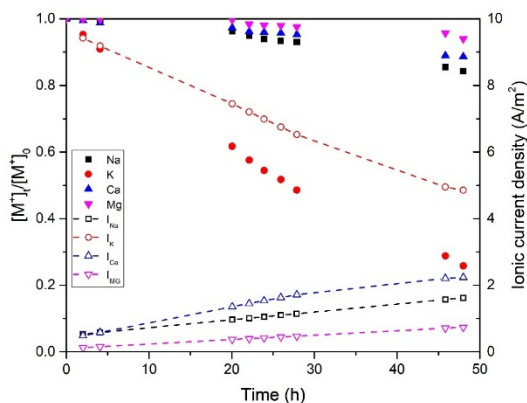
Figure 4.7 Normalized Na^+, K^+, Ca^{2+} and Mg^{2+} concentrations and ionic current over time in symmetrical equimolar (25 mM) mixed-salt solutions.

Similar to the analysis performed for the binary solutions, the K_{ex} values of the different ion combinations in the quaternary ion solution were determined and the results are shown in Figure 4.8. Comparing the combination of K^+/Na^+ and Ca^{2+}/Mg^{2+}, from Figure 4.8, we observed here a linear relation through the origin over the given entire concentration ratio range with the determined K_{ex} value of 11.3 and 3.3, respectively.
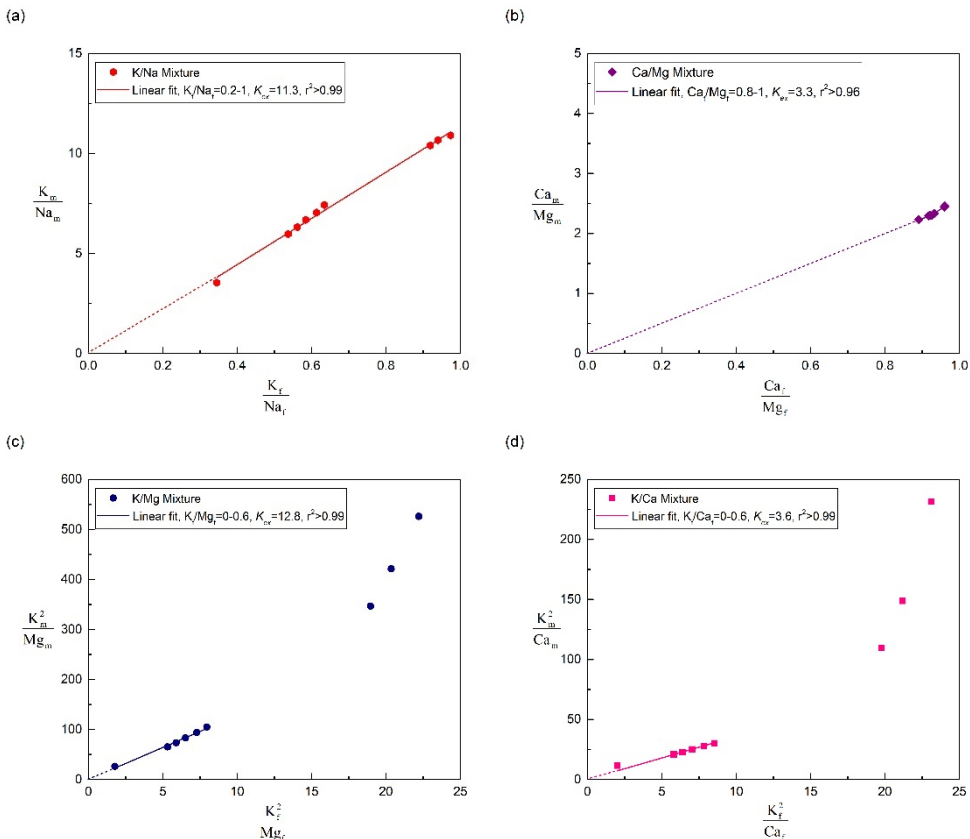
Figure 4.8 The ion-exchange selectivity constant of two ion species in four ion mixed solution ($M_1=K^+$, $M_2=Na^+$, Mg^{2+} or Ca^{2+}) determined as the slope by plotting $\dfrac{M_{1,m}^{Z_2}}{M_{2,m}^{Z_1}}$ versus $\dfrac{M_{1,f}^{Z_2}}{M_{2,f}^{Z_1}}$ and the regression coefficient r^2. Fits were forced to go through the origin.

For the combination K^+/Ca^{2+} and K^+/Mg^{2+}, we also made similar observations as in the binary salt experiments. The plotted lines (forced through the origin) relate only to the later stage of the experiment. Initially, also here a deviation from the linear plot was observed. The ion-exchange selectivity constants of $K_{ex}(K^+/Ca^{2+}) = 3.6$ and $K_{ex}(K^+/Mg^{2+}) = 12.8$ were obtained. All K_{ex} values obtained from the experiment using the quaternary salt mixture are also tabulated in Table 4.5 for comparison with the values obtained from the binary salt experiments. From this comparison it is remarkable to see the very good similarity of the obtained ion-exchange selectivity constant K_{ex} from both the binary and quaternary salt mixture experiments. This similarity shows that there is no interference between the different salts in that they

120

pass the membrane independently. The ion-exchange selectivity constant (K_{ex} relative to K_{ex} of K^+) increases in the order: $Ca^{2+} < Mg^{2+} \approx Na^+$.

4.4 Conclusions

This study investigated in detail the permeation of K^+, Ca^{2+} and Mg^{2+} under electro-dialysis conditions with constant current applied using a supported liquid membrane (SLM). Single-salt experiments identified an electro-phoretic mobility decreasing in the order: $Na^+ > K^+ > Mg^{2+} > Ca^{2+}$. The relative order between the monovalent ions (Na^+ and K^+) and also between the divalent ions (Mg^{2+} and Ca^{2+}) correlate with their ionic radii. However, such a correlation does not exist if we compare the monovalent and the divalent cations. From our earlier study on the permeation selectivity between Na^+ and K^+ [20], we had found that these ions enter the SLM in a dehydrated state. Clearly, that is not the situation for the divalent cations investigated here. From a correlation between z/u vs. r, where z is the valence of the cation, u the observed electro-phoretic mobility and r the radius of the migrating cation known for Na^+ and K^+, and unknown for Mg^{2+} and Ca^{2+}, we obtained the predicted radii of the divalent cations. These higher radii were interpreted as due to the presence of a (partial) hydration shell around that cation. The main difference in the hydration state between the mono- and divalent cations in the SLM is related to the much higher dehydration energy of the divalent ions compared to the monovalent cations. The electrophoretic mobility of the divalent cations is thus determined by the radius of their (partly) hydrated state. Karl Fisher titrations confirmed the presence of additional water in the SLM after equilibration with divalent cations compared to monovalent cations.

From the binary and quaternary salt experiments we found a permeation selectivity in the order of: $K^+ > Na^+ > Ca^{2+} > Mg^{2+}$. Clearly, this order does not correlate with the observed electro-phoretic mobilities from the single-salt experiments. The origin of this difference can be found in cation exchange occurring at the water/SLM interface. The different cations compete for the lipophilic borate sites in the SLM, quantified by an ion-exchange selectivity constant K_{ex} value. Analysis revealed values of K_{ex} following the order of: $K^+ > Ca^{2+} > Mg^{2+} \approx Na^+$. Both K_{ex} and the electro-phoretic mobility in the SLM contribute to the observed permeation selectivity of the different cation species.

4

121

Supporting information

4.S1 Mass and charge balance

In order to investigate whether the ion concentration changes in the two inner compartments of the six-compartment cell in Figure 4.2 can be exclusively ascribed to transport over the central membrane separating chambers A and B, mass and charge balances were set up. Ideally, the changes of one particular ionic species in both compartments are the same but of opposite sign; stated otherwise, their summation add up to zero. In addition, in order to retain electro neutrality, the total charge in each compartment also adds up to zero. Tables S1-3 show the mass and charge balance for all measurements in this study including using (1): single-salt solutions of 100 mM KCl, NaCl, $CaCl_2$ and $MgCl_2$, (2): binary salt solutions of equimolar (50 mM) KCl + $CaCl_2$, KCl + $MgCl_2$ or $CaCl_2$ + $MgCl_2$, and (3): quaternary mixed solution of equimolar (25 mM) KCl + NaCl + $CaCl_2$ + $MgCl_2$, respectively.

4

	Single KCl			Single NaCl		
	A	**B**	**Total**	**A**	**B**	**Total**
ΔK (mmol)	-8.39	8.26	-0.86	N/A	N/A	N/A
ΔNa (mmol)	N/A	N/A	-0.33	-8.16	8.11	-0.02
ΔCl (mmol)	-8.52	8.51	-1.09	-8.64	8.49	0.04
ΔSO$_4$ (mmol)	N/A	N/A	-0.03	N/A	N/A	-0.04
ΔCharge (mmol e)	0.01	0.00	-0.04	0.56	-0.61	0.01
	Single CaCl$_2$			Single MgCl$_2$		
	A	**B**	**Total**	**A**	**B**	**Total**
ΔNa (mmol)	N/A	N/A	-0.13	N/A	N/A	0.08
ΔCa (mmol)	-4.54	4.49	-0.07	N/A	N/A	N/A
ΔMg (mmol)	N/A	N/A	N/A	-4.69	4.58	-0.03
ΔCl (mmol)	-8.98	8.91	-0.31	-9.11	9.08	0.08
ΔSO$_4$ (mmol)	N/A	N/A	0.01	N/A	N/A	-0.01
ΔCharge (mmol e)	-0.10	0.07	0.02	-0.27	0.08	-0.04

Figure 4.S1 Mass and charge balance of Compartments A and B, where charge balance refers to the net charge of the solution after accounting for the measured ion concentration changes. The third column, labelled Total, refers to the balances including all compartments A, B, C and D. Balances were calculated from measurements in single salt of 100 mM KCl, NaCl, CaCl$_2$ and MgCl$_2$ solutions.

4

	Mixed KCl + CaCl$_2$			Mixed KCl + MgCl$_2$		
	A	B	Total	A	B	Total
ΔK (mmol)	-10.69	10.23	-0.21	-12.02	11.87	-0.15
ΔCa (mmol)	-3.38	3.29	-0.18	N/A	N/A	N/A
ΔMg (mmol)	N/A	N/A	N/A	-2.17	2.07	-0.2
ΔNa (mmol)	N/A	N/A	0.01	N/A	N/A	0.11
ΔSO$_4$ (mmol)	N/A	N/A	-0.02	N/A	N/A	0.03
ΔCl (mmol)	-17.42	16.91	-0.51	-16.39	15.98	-0.48
ΔCharge (mmol e)	-0.03	-0.1	-0.01	0.03	0.03	-0.02

	Mixed MgCl$_2$ + MgCl$_2$		
	A	B	Total
ΔK (mmol)	N/A	N/A	N/A
ΔCa (mmol)	-5.18	5.11	-0.14
ΔMg (mmol)	-3.53	3.47	-0.12
ΔNa (mmol)	N/A	N/A	0.17
ΔSO$_4$ (mmol)	N/A	N/A	0.01
ΔCl (mmol)	-17.71	17.43	-0.35
ΔCharge (mmol e)	0.29	-0.27	-0.02

Figure 4.S2 Mass and charge balance of Compartments A and B, where charge balance refers to the net charge of the solution after accounting for the measured ion concentration changes. The third column, labelled Total, refers to the balances including all compartments A, B, C and D. Balances were calculated from measurements in binary mixed salt solutions of equimolar (50 mM) KCl + CaCl$_2$, KCl + MgCl$_2$ or CaCl$_2$ + MgC

	Quaternary ion mixture		
	A	**B**	**Total**
ΔK (mmol)	-9.28	9.27	-0.03
ΔNa (mmol)	-1.97	1.92	0.04
ΔCa (mmol)	-1.33	1.29	-0.03
ΔMg (mmol)	-0.42	0.38	-0.03
ΔCl (mmol)	-16.30	16.27	-0.14
ΔSO$_4$ (mmol)	N/A	N/A	0.03
ΔCharge (mmol e)	1.55	-1.74	-0.03

Figure 4.S3 Mass and charge balance of Compartments A and B, where charge balance refers to the net charge of the solution after accounting for the measured ion concentration changes. The third column, labelled Total, refers to the balances including all compartments A, B, C and D. Balances were calculated from measurements in quaternary ion mixed solutions of equimolar (25 mM) KCl + NaCl + CaCl$_2$ + MgCl$_2$.

4

References

[1]   H. Strathmann, Electrodialysis, a mature technology with a multitude of new applications, Desalination. 264 (2010) 268–288. https://doi.org/10.1016/j.desal.2010.04.069.

[2]   A. Campione, L. Gurreri, M. Ciofalo, G. Micale, A. Tamburini, A. Cipollina, Electrodialysis for water desalination: A critical assessment of recent developments on process fundamentals, models and applications, Desalination. 434 (2018) 121–160. https://doi.org/10.1016/j.desal.2017.12.044.

[3]   S. Al-Amshawee, M.Y.B.M. Yunus, A.A.M. Azoddein, D.G. Hassell, I.H. Dakhil, H.A. Hasan, Electrodialysis desalination for water and wastewater: A review, Chem. Eng. J. 380 (2020) 122231. https://doi.org/10.1016/j.cej.2019.122231.

[4]   T. Sata, T. Sata, W. Yang, Studies on cation-exchange membranes having permselectivity between cations in electrodialysis, J. Memb. Sci. 206 (2002) 31–60. https://doi.org/10.1016/S0376-7388(01)00491-4.

[5]   T. Luo, S. Abdu, M. Wessling, Selectivity of ion exchange membranes: A review, J. Memb. Sci. 555 (2018) 429–454. https://doi.org/10.1016/j.memsci.2018.03.051.

[6]   H. Zhang, P.K. Shen, Advances in the high performance polymer electrolyte membranes for fuel cells, Chem. Soc. Rev. 41 (2012) 2382–2394. https://doi.org/10.1039/c2cs15269j.

[7]   M. Xie, H.K. Shon, S.R. Gray, M. Elimelech, Membrane-based processes for wastewater nutrient recovery: Technology, challenges, and future direction, Water Res. 89 (2016) 210–221. https://doi.org/10.1016/j.watres.2015.11.045.

[8]   J. Ran, L. Wu, Y. He, Z. Yang, Y. Wang, C. Jiang, L. Ge, E. Bakangura, T. Xu, Ion exchange membranes: New developments and applications, J. Memb. Sci. 522 (2017) 267–291. https://doi.org/10.1016/j.memsci.2016.09.033.

[9]   J.G. Hong, B. Zhang, S. Glabman, N. Uzal, X. Dou, H. Zhang, X. Wei, Y. Chen, Potential ion exchange membranes and system performance in reverse electrodialysis for power generation: A review, J. Memb. Sci. 486 (2015) 71–88. https://doi.org/10.1016/j.memsci.2015.02.039.

4

[10] A. Parasuraman, T.M. Lim, C. Menictas, M. Skyllas-Kazacos, Review of material research and development for vanadium redox flow battery applications, Electrochim. Acta. 101 (2013) 27–40. https://doi.org/10.1016/j.electacta.2012.09.067.

[11] L. Ge, B. Wu, D. Yu, A.N. Mondal, L. Hou, N.U. Afsar, Q. Li, T. Xu, J. Miao, T. Xu, Monovalent cation perm-selective membranes (MCPMs): New developments and perspectives, Chinese J. Chem. Eng. 25 (2017) 1606–1615. https://doi.org/10.1016/j.cjche.2017.06.002.

[12] F. Gallucci, Encyclopedia of Membranes, Springer Berlin Heidelberg, 2016. https://doi.org/10.1007/978-3-662-44324-8.

[13] Khoiruddin, D. Ariono, Subagjo, I.G. Wenten, Surface modification of ion-exchange membranes: Methods, characteristics, and performance, J. Appl. Polym. Sci. 134 (2017) 45540. https://doi.org/10.1002/app.45540.

[14] C. Cheng, N. White, H. Shi, M. Robson, M.L. Bruening, Cation separations in electrodialysis through membranes coated with polyelectrolyte multilayers, Polymer (Guildf). 55 (2014) 1397–1403. https://doi.org/10.1016/J.POLYMER.2013.12.002.

[15] T. Rijnaarts, D.M. Reurink, F. Radmanesh, W.M. de Vos, K. Nijmeijer, Layer-by-layer coatings on ion exchange membranes: Effect of multilayer charge and hydration on monovalent ion selectivities, J. Memb. Sci. 570–571 (2019) 513–521. https://doi.org/10.1016/J.MEMSCI.2018.10.074.

[16] S. Chaudhury, A. Bhattacharyya, A. Goswami, Electrodriven ion transport through crown ether-Nafion composite membrane: Enhanced selectivity of Cs+ over Na+ by ion gating at the surface, Ind. Eng. Chem. Res. 53 (2014) 8804–8809. https://doi.org/10.1021/ie500934v.

[17] S. Yang, Y. Liu, J. Liao, H. Liu, Y. Jiang, B. Van Der Bruggen, J. Shen, C. Gao, Codeposition Modification of Cation Exchange Membranes with Dopamine and Crown Ether to Achieve High K+ Electrodialysis Selectivity, ACS Appl. Mater. Interfaces. 11 (2019) 17730–17741. https://doi.org/10.1021/acsami.8b21031.

[18] L. Paltrinieri, E. Huerta, T. Puts, W. van Baak, A.B. Verver, E.J.R. Sudhölter, L.C.P.M. de Smet, Functionalized Anion-Exchange Membranes Facilitate Electrodialysis of Citrate and Phosphate from Model Dairy Wastewater, Environ. Sci. Technol. 53 (2018) 2396–2404. https://doi.org/10.1021/ACS.EST.8B05558.

[19] R. Epsztein, E. Shaulsky, M. Qin, M. Elimelech, Activation behavior for ion permeation in ion-exchange membranes: Role of ion dehydration in selective transport, J. Memb. Sci. 580 (2019) 316–326. https://doi.org/10.1016/j.memsci.2019.02.009.

4

[20]   Z. Qian, H. Miedema, S. Sahin, L.C.P.M. de Smet, E.J.R. Sudhölter, Separation of alkali metal cations by a supported liquid membrane (SLM) operating under electro dialysis (ED) conditions, Desalination. 495 (2020) 114631. https://doi.org/10.1016/j.desal.2020.114631.

[21]   M. Sadrzadeh, A. Razmi, T. Mohammadi, Separation of different ions from wastewater at various operating conditions using electrodialysis, Sep. Purif. Technol. 54 (2007) 147–156. https://doi.org/10.1016/j.seppur.2006.08.023.

[22]   A.H. Galama, G. Daubaras, O.S. Burheim, H.H.M. Rijnaarts, J.W. Post, Seawater electrodialysis with preferential removal of divalent ions, J. Memb. Sci. 452 (2014) 219–228. https://doi.org/10.1016/j.memsci.2013.10.050.

[23]   Y. Zhang, S. Paepen, L. Pinoy, B. Meesschaert, B. Van Der Bruggen, Selectrodialysis: Fractionation of divalent ions from monovalent ions in a novel electrodialysis stack, Sep. Purif. Technol. 88 (2012) 191–201. https://doi.org/10.1016/j.seppur.2011.12.017.

[24]   X.Y. Nie, S.Y. Sun, Z. Sun, X. Song, J.G. Yu, Ion-fractionation of lithium ions from magnesium ions by electrodialysis using monovalent selective ion-exchange membranes, Desalination. 403 (2017) 128–135. https://doi.org/10.1016/j.desal.2016.05.010.

[25]   M. Kumar, M.A. Khan, Z.A. AlOthman, M.R. Siddiqui, Polyaniline modified organic-inorganic hybrid cation-exchange membranes for the separation of monovalent and multivalent ions, Desalination. 325 (2013) 95–103. https://doi.org/10.1016/j.desal.2013.06.022.

[26]   Y. Zhu, M. Ahmad, L. Yang, M. Misovich, A. Yaroshchuk, M.L. Bruening, Adsorption of polyelectrolyte multilayers imparts high monovalent/divalent cation selectivity to aliphatic polyamide cation-exchange membranes, J. Memb. Sci. 537 (2017) 177–185. https://doi.org/10.1016/j.memsci.2017.05.043.

[27]   T. Luo, S. Abdu, M. Wessling, Selectivity of ion exchange membranes: A review, J. Memb. Sci. 555 (2018) 429–454. https://doi.org/10.1016/j.memsci.2018.03.051.

[28]   E.N. Durmaz, S. Sahin, E. Virga, S. de Beer, L.C.P.M. de Smet, W.M. de Vos, Polyelectrolytes as Building Blocks for Next-Generation Membranes with Advanced Functionalities, ACS Appl. Polym. Mater. 3 (2021) 4347–4374. https://doi.org/10.1021/ACSAPM.1C00654.

4

[29] Z. Qian, H. Miedema, L.C.P.M. de Smet, E.J.R. Sudhölter, Modelling the selective removal of sodium ions from greenhouse irrigation water using membrane technology, Chem. Eng. Res. Des. 134 (2018) 154–161. https://doi.org/10.1016/j.cherd.2018.03.040.

[30] N.M. Kocherginsky, Q. Yang, L. Seelam, Recent advances in supported liquid membrane technology, Sep. Purif. Technol. 53 (2007) 171–177. https://doi.org/10.1016/j.seppur.2006.06.022.

[31] P.K. Parhi, Supported Liquid Membrane Principle and Its Practices: A Short Review, J. Chem. 2013 (2013) 1–11. https://doi.org/10.1155/2013/618236.

[32] E. Bakker, E. Pretsch, Lipophilicity of tetraphenylborate derivatives as anionic sites in neutral carrier-based solvent polymeric membranes and lifetime of corresponding ion-selective electrochemical and optical sensors, Anal. Chim. Acta. 309 (1995) 7–17. https://doi.org/10.1016/0003-2670(95)00077-D.

[33] T. Rosatzin, E. Bakker, K. Suzuki, W. Simon, Lipophilic and immobilized anionic additives in solvent polymeric membranes of cation-selective chemical sensors, Anal. Chim. Acta. 280 (1993) 197–208. https://doi.org/10.1016/0003-2670(93)85122-Z.

[34] F.G. Bănică, Chemical Sensors and Biosensors: Fundamentals and Applications, John Wiley and Sons, Chichester, UK, 2012. https://doi.org/10.1002/9781118354162.

[35] H. Kreulen, C.A. Smolders, G.F. Versteeg, W.P.M. Van Swaaij, Determination of mass transfer rates in wetted and non-wetted microporous membranes, Chem. Eng. Sci. 48 (1993) 2093–2102. https://doi.org/10.1016/0009-2509(93)80084-4.

[36] M. Khayet, J.I. Mengual, G. Zakrzewska-Trznadel, Direct contact membrane distillation for nuclear desalination. Part I: Review of membranes used in membrane distillation and methods for their characterisation, 2005.

[37] Y. Tanaka, Ion Exchange Membranes, Fundamentals and Applications, 2nd ed., Elsevier, 2015. https://www.elsevier.com/books/ion-exchange-membranes/tanaka/978-0-444-63319-4.

[38] J.M. Zook, J. Langmaier, E. Lindner, Current-polarized ion-selective membranes: The influence of plasticizer and lipophilic background electrolyte on concentration profiles, resistance, and voltage transients, Sensors Actuators, B Chem. 136 (2009) 410–418. https://doi.org/10.1016/j.snb.2008.12.047.

[39] A. Kumar, P.S.H. Rizvi, A.M.S. Requena, Handbook of Membrane Separations: chemical, pharmaceutical, food, and biotechnological applications, 2nd ed., CRC Press, 2015.

4

[40]   Peter Atkins, Julio de Paula, James Keeler, Atkins' Physical Chemistry, Oxford University Press, 2006.

[41]   M. Born, Volumen und Hydratationswärme der Ionen, Zeitschrift Für Phys. 1 (1920) 45–48. https://doi.org/10.1007/BF01881023.

[42]   E.R. Nightingale, Phenomenological theory of ion solvation. Effective radii of hydrated ions, J. Phys. Chem. 63 (1959) 1381–1387. https://doi.org/10.1021/j150579a011.

[43]   R.A. Robinson, R.H. Stokes, Electrolyte Soutions: Second Revised Edition, Dover Publications, 2002.

[44]   L. Lizana, A.Y. Grosberg, Exact expressions for the mobility and electrophoretic mobility of a weakly charged sphere in a simple electrolyte, 2014.

[45]   Z. Samec, J. Langmaier, A. Trojánek, E. Samcová, J.Í. Málek, J. Heyrovsky´instituteheyrovsky´, Transfer of Protonated Anesthetics across the Water| o-Nitrophenyl Octyl Ether Interface: Effect of the Ion Structure on the Transfer Kinetics and Pharmacological Activity, 1998.

4

Chapter 5

Selective removal of sodium ions from greenhouse drainage water – a combined experimental and theoretical approach

Abstract

High Na^+ levels are detrimental for most crops. Selective membranes provide the possibility for the selective removal of Na^+ while preserving beneficial ion species. The challenge is to separate two ion species of the same charge. This study evaluates the implementation of an electrodialysis (ED) system equipped with a supported liquid membrane (SLM) and a commercially available monovalent cation-selective membrane (CIMS) in the treatment of greenhouse drainage water. The SLM shows a (minimum) K^+ over Na^+, Ca^{2+} and Mg^{2+} permeation selectivity of 9, 15 and 30, respectively. Whereas the CIMS holds a high K^+ over Ca^{2+} and Mg^{2+} permeation selectivity of 10 and 16, respectively, the K^+ over Na^+ permeation selectivity is just 1.3. With the experimentally obtained membrane characteristics at hand, the treatment of drainage water was simulated by a two-steps process with the two membrane types operating in series. Using real-life operational parameters, analysis revealed the optimal configuration and the ability to recover 96% of the K^+ and approximately 80% of the water, Ca^{2+} and Mg^{2+}. Summarized, this study not only shows the efficient separation of two ion species of the same valance but also the implementation of this technology in a real-life application.

5.1 Introduction

Greenhouse horticulture has become an increasingly important method in optimizing the production of crops all year round, also in high-latitude countries, by regulating climatic conditions and efficiently making use of land, nutrients and water resources. Water quality is essential to greenhouse operation. Greenhouse irrigation normally depends on natural water sources, particularly ground or surface water. In the Netherlands, the greenhouse horticulture covers nearly 10,000 hectares area, mainly in the western part of the country [1]. Compared to other Northwest European countries, both the total greenhouse area and the greenhouse density in the Netherlands are much larger [2]. However, in large parts of the Netherlands, ground and surface water quality does not meet the chemical and ecological standards as indicated by the EU Water Framework Directive [3]. Series of regulations have been released and implemented for improving water quality in greenhouse areas, with the controllable obligations for greenhouse growers for collection and reuse of drainage water and the permission to discharge drainage water only if crop-specific sodium (Na^+) levels in drain water are exceeded or in case of emergencies (*i.e.* outbreak of diseases) [2,4–7]. To further tackle the problem of drainage water quality, agreements were made between authorities and the growers' organization targeting (nearly) zero discharge regarding nutrients and plant protection products to surface waters in 2027.

In greenhouse cultivation, nutrients and water are supplied continuously to the irrigation water system to compensate for nutrient uptake by the plants and water loss due to evapotranspiration. A high Na^+ levels (*i.e.*, above the crop specific tolerance level) is one of the detrimental factors of irrigation water quality, as it inhibits plant growth directly or indirectly by hampering the uptake of other nutrients [8–11]. Due to its low uptake by plants, Na^+ is a typical example of an ion that builds up its concentration in the irrigation water over time [12]. Therefore, desalination is becoming an attractive method for the greenhouse drainage water treatment. Reverse osmosis (RO) belongs to one of the most widely used and most cost-effective desalination technologies [13]. RO is a membrane-based, pressure-driven process that employs size exclusion to effectively reject particles and ions including Na^+ and Cl^- to produce pure water [14]. While RO yields nearly pure water with a low concentration of ions, it also rejects other ions present, for instance K^+, Ca^{2+}, Mg^{2+} and SO_4^{2-}, all essential nutrients for crop growth [15,16]. This points to the need for ion-selective permeation approaches.

Electrodialysis (ED) is a membrane-based desalination processes using ion-exchange membranes (IEMs) and an electric field to drive the separation of the ions from the feed stream. Compared to RO, advantages of ED include high water recovery rates, long lifetime performance in desalination processes due to higher chemical and mechanical stability, less membrane fouling or scaling due to its process reversal operation, less raw water pretreatment and easier ways to adjust the separation process [17–19]. A large number of applications for ED can be found in industrial wastewater treatment [20], food and pharmaceutical industrial water treatments [21,22], portable water supply [23] and sea water desalination [24,25]. Preferential ion separation with selective IEMs for the separation of monovalent from divalent or multivalent ions have been reported [26–28]. The idea of partial desalination of the drainage water was recently proposed by monovalent ion-selective ED process for the separation of monovalent cations and divalent cations to reduce the need for adding Ca^{2+}, Mg^{2+} and SO_4^{2-} fertilizers [29]. However, it is still highly challenging to separate effectively and selectively two ionic species that share the same valence and have similar chemical properties. Within the context of greenhouse drainage water treatment, the separation of the monovalent cations K^+ and Na^+ is of utmost importance.

A previous study from our lab reports on the selective separation of K^+ from alkali metal cations [30] and divalent cations Ca^{2+} or Mg^{2+} using a supported liquid membrane (SLM) under ED conditions. The SLM is made by filling the pores of an inert porous supporting membrane with an organic solvent containing a lipophilic salt to invoke the desired membrane permselectivity [31–33]. Preferential separation of the ions was found to follow the order of $K^+>Na^+>Li^+$ for alkali cations and $K^+>Na^+>Ca^{2+}>Mg^{2+}$ in multi-ion mixtures. The selectivity of the SLM relies on the difference of ion dehydration energy during the ion exchange/partitioning at the water-membrane interface. Different from the SLM, commercially available special grade monovalent cation-exchange membranes (CIMS) are dense membranes with fixed negatively charged groups to the polymeric backbone (they have typically an ion-exchange capacity about 1.5-1.8 mEq·g^{-1} [34,35]) and a polycation layer on top, allowing the monovalent cations predominantly to permeate [36–38].

A key challenge in working towards closed loop greenhouse irrigation is dealing with the Na^+ accumulation problem. In other words: how to selectively remove Na^+ while keeping the level of other ions high, especially the one of the nutrient ion K^+. Membrane permeation selectivity is a term for defining the preferential permeation of certain ionic species through the membrane. In the literature, membranes showing a

high Na$^+$ over K$^+$ permeation selectivity have not been reported so far. However, by combining the SLM, which holds a high K$^+$ over Na$^+$ permeation selectivity, with a monovalent cation-selective membrane (CIMS), Na$^+$ can be selectivity removed employing a 2-step separation process that separate K$^+$ from Na$^+$ and divalent cations with SLM then Na$^+$ separation from divalent cations with CIMS (Figure 5.1a) or monovalent cation separation from divalents with CIMS followed by K$^+$ and Na$^+$ separation with the SLM (Figure 5.1b). In this study, we, first, assessed the properties of SLM and CIMS membranes. With the membrane characteristics at hand, we simulated a system with the two membrane types in tandem schemes as shown in Figure 5.1. By employing a 2-step ED process, the ability to selectively separate Na$^+$ from greenhouse drainage water is investigated.
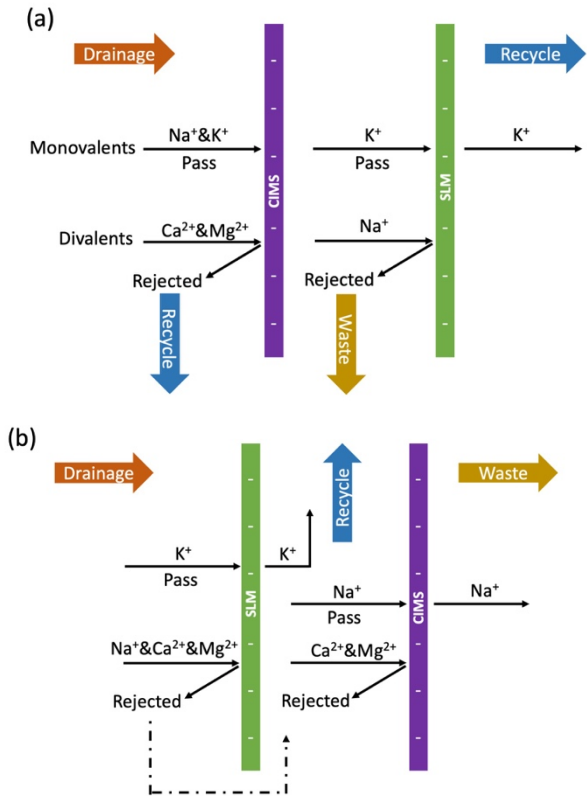

Figure 5.1 Schematic outline of the two-steps treatment process with (a). a first treatment by the CIMS, followed by the SLM and (b). a first treatment by the SLM, followed by the CIMS.

5.2 Materials and methods

5.2.1 Materials and chemicals

All chemicals used were of analytical grade. The ACCUREL support (polypropylene, thickness: 100 μm, pore size: 0.1 μm) was purchased from MEMBRANA. The following ion-exchange membranes have been used: standard grade Neosepta cation-exchange membrane (CMX), standard grade Neosepta anion-exchange membrane (AMX) and Neosepta monovalent selective cation-exchange membrane (CIMS). All Neosepta membranes were purchased from Eurodia. All other chemicals were purchased from Sigma-Aldrich: the organic solvent used for impregnating the ACCUREL support, 2-nitrophenly-n-octyl ether (NPOE); the lipophilic anion sodium tetrakis[3,5-bis(trifluoromethyl)phenyl]borate (NaBArF) and the salts, KCl, NaCl, $CaCl_2 \cdot 2H_2O$, $MgCl_2 \cdot 6H_2O$ and Na_2SO_4. Greenhouse drainage water samples were provided by Van der Knaap, Wateringen, The Netherlands. The cation composition of these sample were obtained by Inductively Coupled Plasma Mass Spectrometry (ICP-MS). All greenhouse drainage water received was filtered with a membrane filter (0.45 μm) to remove all solid particles before their use in ED experiments.

5.2.2 Membrane preparation

All experiments involving SLMs were performed with freshly prepared membranes. The organic solvent mixture for impregnating the SLM was prepared by dissolving the NaBArF into the NPOE to a fixed concentration of 0.05 M. The porous membrane support ACCUREL was then submerged in the organic solvent mixture for 30 min at room temperature. The organic solvent quickly filled into the pores due to capillary forces.

5.2.3 Electrodialysis with equimolar salt solutions

Ion transport over the SLM and CIMS were first evaluated separately under ED conditions. All experiments were carried out in a six-compartment cell equipped with a platinum electrode (54 mm in diameter), as shown in Figure 5.2. By using a six-compartment cell containing two Buffer compartments (compartments C), it is ensured that possible redox reactions occurring in the two outer compartments

(compartments D) will not influence the composition of the ion species present in the two inner compartments (compartments A and B).

The position of cation-exchange membranes (CMX) and anion-exchange membranes (AMX) is according to the scheme shown in Figure 5.2 [30]. Changes in concentration in the two inner compartments can be attributed exclusively to ion transport over the SLM or CIMS.
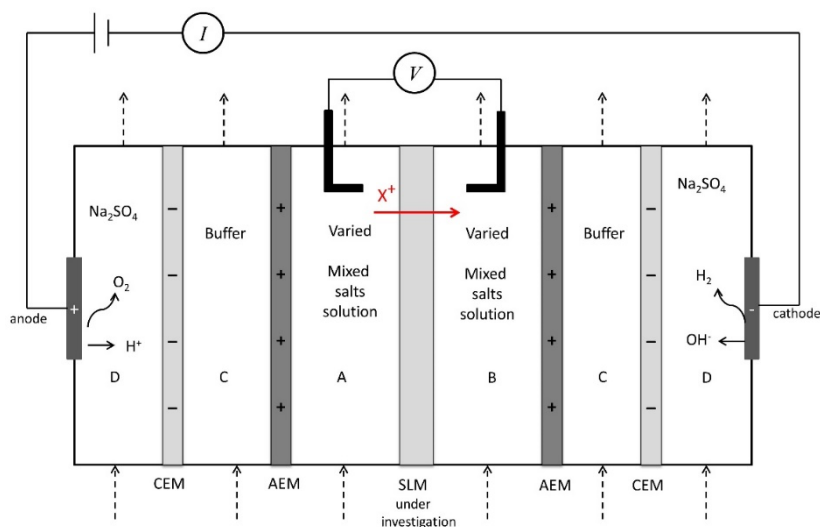
Figure 5.2 Schematic showing the configuration of the six-compartment cell used during the electro dialysis experiments. Compartments C and D as well as the position of the CEM and AEM ensure that the concentration changes in the two inner measuring compartments arise solely from ion fluxes over the SLM.[30]

The SLMs and CIMS under investigation was placed into the cell with a polytetrafluoroethylene membrane holder and the effective membrane surface areas were 10 cm² in both cases. The thickness of the SLMs and CIMS are 100 μm and 150 μm, respectively. The membrane transport study was performed with the feed compartment A and receiving compartment B recirculating with an equimolar mixture of KCl, NaCl, $CaCl_2$ and $MgCl_2$ solution of which each cation concentration was 0.025 M with a total volume of 500 mL. In the two middle compartments C a buffer solution containing 0.2 M NaCl solution with the volume of 1 L was recirculated, while. an electrolyte solution containing 0.1 M Na_2SO_4 solution with a volume of 1 L was recirculated in the two outer compartments D. The flow rates in all compartments

were set to 150 mL·min^{-1}. Prior to the experiments, all membranes were pre-conditioned for 24 h in the measuring solution. The temperature of all solutions was controlled at 25 ± 0.2 °C. A potentiostat (Ivium Technologies, Vertex One, Eindhoven, The Netherlands) was employed as power source for applying a constant current density. A constant current of 10 mA (corresponding to a current density of 10 A·m^{-2}) was applied during a time period of 48 h. Samples of 1 mL were taken periodically during the experiment from all compartments during the experiment and the concentration of all ion species were determined using ion chromatography (IC, Metrohm compact IC 761).

5.2.4 Electrodialysis with greenhouse drainage water

Evaluation of the performance of the SLM and CIMS under ED conditions using the six-compartment cell was done using greenhouse drainage water provided by Van der Knaap. Table 5.1 shows the composition of the main cations K$^+$, Na$^+$, Ca^{2+} and Mg^{2+} of the received drainage water and the greenhouse stock irrigation water (stock irrigation water is pre-made high concentration irrigation water containing necessary ions and nutrients that can be diluted to the target value). In each of the compartment A and B 500 mL of this water was recirculated. In the two middle compartments C a buffer solution containing 0.05 M NaCl solution was circulated, while an electrolyte solution containing 0.05 M Na$_2$SO$_4$ solution was recirculated in compartments D. Prior to the experiments, all membranes were pre-conditioned for 24 h in the filtered greenhouse drainage water. All other experimental conditions and procedures were described in Section 5.2.2.

Cations	K$^+$	Na$^+$	Ca^{2+}	Mg^{2+}
Drainage concentration (mM)	13	10.7	10.1	5.7
Stock irrigation concentration (mM)	9.5	0	7.0	3.0

Table 5.1 Greenhouse drainage and stock irrigation water cation composition.

5.2.5 Determination of limiting current density (LCD)

Due to concentration polarization and the depletion of ions at the membrane surface, the current density during ED will approach a limiting value, regardless any further increase of potential[39,40]. Operation in the so-called over-limiting current density regime can cause water splitting and producing protons and hydroxide ions which serve as additional charge carriers. This needs to be avoided because it lowers the efficiency of ED regarding the ion species of interest. Therefore, the limiting current density (LCD) for both the SLM and the CIMS was determined by recording current-voltage (*i-V*) curves using the six-compartment cell shown in Figure 5.2, with the two inner compartments filled with 0.02 M NaCl solution. The flow rate in all compartments was 150 mL/min and the membrane surface area 10 cm^2. While applying a voltage swipe across the membrane, the potential difference between the two Haber-Luggin capillaries was measured step-wise as a function of the electric current passing through the membrane. The *i-V* curves can be divided into an ohmic, a limiting and an over-limiting regime [41–43], as observed in Figure 5.3, at least in case of the CIMS. The ohmic regime represents a linear relation between current and voltage. The limiting region indicates ion depletion at the membrane interface reflected by a plateau, *i.e.*, a constant voltage over the membrane despite an increase of applied current density. In the over-limiting regime the voltage again increases upon an increase of current density. The LCD is defined as the current magnitude at the intersection of extrapolated slope lines of the ohmic and limiting regime. As shown, the CIMS and SLM curves are essentially different in shape with the SLM lacking a limiting regime. This difference may reflect differences in transport mechanisms between the two entirely different types of membranes.

Figure 5.3 shows the *i-V* curves of the SLM and CIMS. The LCD value of SLM and CIMS are determined to be about 17 A·m^{-2} and 27 A·m^{-2}, respectively. Note that both curves do not exactly originate at zero, as expected. This deviation is most likely due to a small offset in the recorded transmembrane voltage using Haber-Luggin capillaries. During the experiments as well as for the simulations, the applied current density was always set below these LCD values (see *e.g.* Table 5.2).
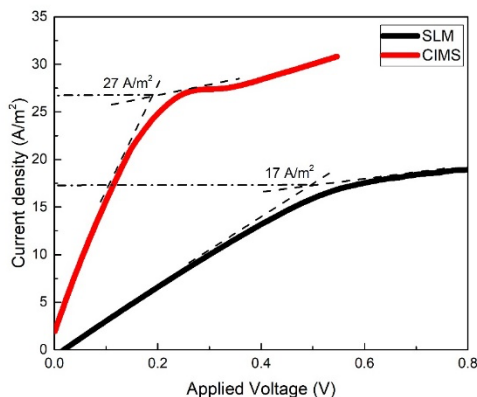
Figure 5.3 *i-V* curves of the SLM and CIMS obtained at 0.02 mol NaCl to determine the Limiting current density.

5.3 Results and discussion

5.3.1 Membrane characterization

5.3.1.1 Ion transport in equimolar salt solutions containing K⁺, Na⁺, Ca²⁺ and Mg²⁺

To determine the membrane cation permeation selectivity K^+/Na^+, K^+/Ca^{2+} and K^+/Mg^{2+}, ED experiments with both the SLM and the CIMS were performed, in symmetrical equimolar (25 mM) solutions containing all four cation species. Figure 5.4 shows the comparison between the SLM and CIMS regarding the normalized ion concentrations in feed compartment A and flux changes over a time span of 48 h. The normalized concentration is defined as the ratio of measured cation concentration at any time *t* and the initial cation concentration in compartment A.

As can be observed in Figure 5.4a, during the first 10 h, the SLM transports preferably K^+, with the concentrations of the other three ion species (Na^+, Ca^{2+} and Mg^{2+}) decreasing only marginally. In all cases, the ion concentration and flux change (Figure 5.4b) more or less linearly with time. Even though at a more prolonged time scale (up to 48 h), the other three ion species are transported at higher rates, K^+ transport remains dominant as reflected in the higher slope of the K^+ concentration over time. Note that the K^+ flux, as shown in Figure 5.4b gradually decreases over

140

time, form 10×10^{-6} to 6×10^{-6} mol cm^{-2} s^{-1}. These observations confirm previously reported data [30,44].

As anticipated, the CIMS shows a clear monovalent cation over divalent cation selectivity due to the polycation modification on the surface. Compared with the SLM, the CIMS shows much less preference of K$^+$ over Na$^+$. Actually, over time and with the Na$^+$ flux gradually increasing, the difference in transport rates between K$^+$ and Na$^+$ halves over time, from an initial 1.2×10^{-6} mol cm^{-2} s^{-1} at the start to 0.6×10^{-6} mol cm^{-2} s^{-1} at the end of the experiment. Note the difference in flux scale in Figure 5.4b, due to the fact that with the CIMS the (constant) applied current density is more equally distributed over K$^+$ and Na$^+$. These observations are in very close agreement with reported data in the literature [45,46].

For both the SLM and the CIMS, the summed transport numbers of all four ions are close to unity, *i.e.* 0.98 and 0.99, respectively, indicating that under the given experimental conditions, with an applied current density of 10 A m^{-2}, the current is by far predominantly carried by cations. In addition, the CIMS as well as the SLM shows a permeation preference for monovalent cations.
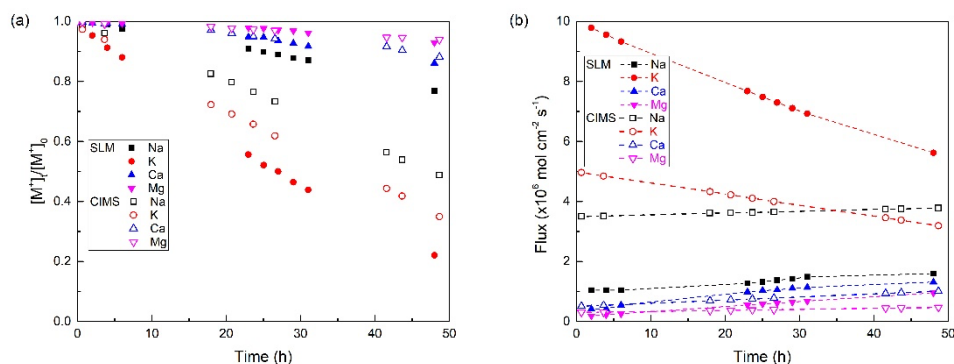
Figure 5.4 Comparison between the SLM regarding (a) normalized K$^+$, Na$^+$, Ca^{2+} and Mg^{2+} concentration in the feed phase and (b) ion flux across the membrane. Unconnected data points refer to concentration, dotted lines to flux. Data have been obtained by experiments in equimolar (25 mM) salt solutions containing K$^+$, Na$^+$, Ca^{2+} and Mg^{2+}.

5.3.1.2 Mass and charge balance

To investigate whether the cation concentration changes in the two inner compartments of the six-compartment cell can be exclusively ascribed to transport over the central membrane mass and charge balances were set up. Theoretically, the (absolute) change of a certain cation species in each compartment should be the same in magnitude and their summation should add up to zero. Furthermore, for retaining electro neutrality, the total charge in each compartment should also add up to zero. The mass and charge balance for the equimolar four ion mixed solutions for both the SLM and the CIMS are indeed essentially closed; detailed data can be found in the supplementary information (Table 5.S1). The same holds for the 'Total' balance taking into account all six compartments. After careful evaluation, it is concluded that any deviation, *i.e.*, any non-zero value, falls in the error-range of ion concentration measurement by IC or ICP, typically ±5% and are not due to ion accumulation inside the membrane.

5

5.3.1.3 Permeation selectivity in binary salt solutions

Next, the permeation selectivity of the SLM and the CIMS were assessed in equimolar binary salt solutions. Following Sata [46] and Tanaka [47], the membrane permeation selectivity of ion species B over ion species A can be expressed as:

$$P_A^B = \frac{J_B}{J_A} \times \frac{C_A}{C_B} \tag{5.1}$$

where J represents the ion flux (mol·m^{-2}·s^{-1}) cross the membrane and C the ion concentration (mol·L^{-1}) in the feed. In the current study, B represents K$^+$ and A represents Na$^+$, Ca^{2+} or Mg^{2+}. Note that Eq. 5.1 represents the permeation selectivity, expressed in terms of fluxes, normalized for the particular ion concentrations in the feed. Figure 5.5 shows the calculated membrane selectivity of the SLM and CIMS at different feed ratios, starting (at the left) from equimolar binary salt solutions, *i.e.* a feed ratio of unity.
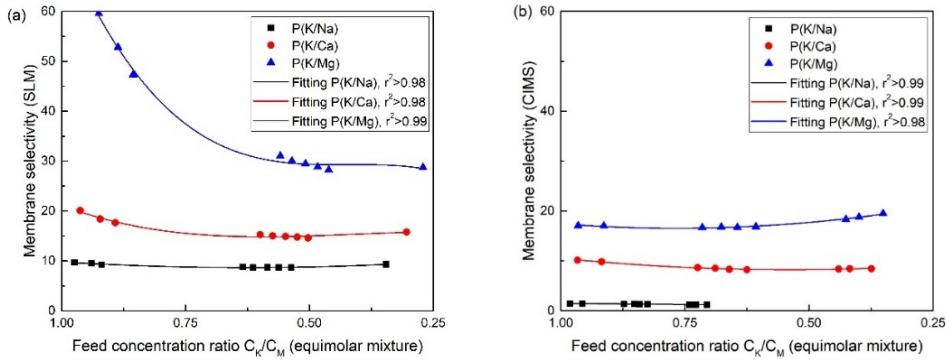
Figure 5.5 Calculated membrane permeation selectivity P(K/Na), P(K/Ca) and P(K/Mg) of the SLM (left) and the CIMS (right). Data has been fitted by 3rd order polynomials in order to obtain the perm selectivity at any given feed ratio, used for simulations performed later on. Data has been obtained by experiments in binary salt solutions.

In general, the SLM shows a rather high K$^+$ over Na$^+$, K$^+$ over Ca^{2+} and K$^+$ over Mg^{2+} selectivity of 9, 15 and 30, respectively, even at rather low feed concentration ratios (K$^+$/X$^+$). As anticipated, the monovalent cation over divalent cation selectivity of the CIMS is lower but still substantial, 10 and 20 for the K$^+$ over Ca^{2+} and K$^+$ over Mg^{2+} selectivity, respectively. However, the CIMS hardly discriminates between K$^+$

and Na$^+$, reflected in a K$^+$ over Na$^+$ selectivity of just 1.3. The permeation selectivity of SLM mainly comes from the difference in required ion dehydration energy upon entering the membrane, thus the SLM showed good discrimination between the monovalent and divalent cations as well as between Na$^+$ and K$^+$ which have the same valence without any additional (surface) modification as present in the used commercial CIMS. In addition, the CIMS has a high IEC, leading to aggregation of the fixed anionic groups into reversed micellar structures and channels filled with water. The cations transported are therefore likely hydrated. This situation is completely different compared to the SLM, where the IEC is much lower and the anionic sites are most likely not clustered into domains. In this way it is understandable that cation dehydration energies play an important role only in SLM and not in CIMS. Both membranes share in common that the K$^+$ over Na$^+$ and K$^+$ over Ca^{2+} selectivity is relatively constant over the entire feed concentration ratio studied. Both membrane types differ most in respect to the K$^+$/Mg^{2+} selectivity. As for the SLM, though the K$^+$/Mg$^+$ selectivity starts high, it rapidly declines to a constant value around 30. In contrast, for the CIMS, the starting value is much lower, around 17, and remains relatively constant, gradually increases to a value around 20.

In our previous study [30,44] and from literature [48–52], we can conclude that permeation selectivity depends on the partitioning of the ion species over the water and membrane phase, the ion electrophoretic mobility and the interaction between the ions and the immobile charged groups in the membrane. Ion (de)hydration plays a role in all three aspects. In partitioning, in terms of (de)hydration energy, in mobility, in terms of ion radius and in interaction, in terms of electrostatics. In case partitioning dominates, it is expected that selectivity becomes (more or less) independent of the feed concentration ratio. In the more hydrophilic CIMS [53–55], cations are less dehydrated than in the SLM. By implication, the interaction between these hydrated cations and the immobile charged moieties in the membrane is less than between the more dehydrated cations and the borate moieties in the SLM. This probably explains the different selectivity behavior in relation to the feed concentration ratio, as shown in Figure 5.5. Apparently, at lower K$^+$/Mg^{2+} feed ratios, the interaction between Mg^{2+} and borate starts to affect the perm selectivity of the SLM. Noteworthy, a feed concentration ratio-dependent selectivity is not uncommon, for example, for ion channels, membrane embedded proteins mediating the (selective) ion transport over biological membranes [56].

In terms of current density, Eq. 5.1 can be expressed as:

$$P_A^B = \frac{z_A I_B}{z_B I_A} \times \frac{C_A}{C_B} \tag{5.2}$$

where z_i and I_i (in A m^{-2}) are the charge the current density of ion species i, respectively. Fitting the data of Figure 5.4 renders the permeability of each ion species relative to that of K$^+$ at any given feed ratio.

The current carried by Na$^+$, Ca^{2+} and Mg^{2+} and expressed in terms of I_K follows directly from Eq. 5.2 and is given by:

$$I_i = I_K \frac{1}{P_i^K} \frac{z_i C_i}{z_K C_K} \tag{5.3}$$

with i representing Na$^+$, Ca^{2+} or Mg^{2+}. Ignoring the possible contribution of any other ion species (*i.e.*, H$^+$ and Cl$^-$), the applied current density (I) in the equimolar mixed solution equals:

$$I = I_K + I_{Na} + I_{Ca} + I_{Mg} \tag{5.4}$$

Combining Eqs. 5.3 and 5.4 gives:

$$I_K = \frac{I_{tot}}{(1 + \dfrac{1}{P_{Na}^K} \dfrac{C_{Na}}{C_K} + \dfrac{2}{P_{Ca}^K} \dfrac{C_{Ca}}{C_K} + \dfrac{2}{P_{Mg}^K} \dfrac{C_{Mg}}{C_K})} \tag{5.5}$$

The initial feed concentrations (ratios) of all four ion species are known. The data fitting of Figure 5.5 renders the permeation selectivity of each ion species relative to that of K$^+$ at any given feed ratio. Using Eq. 5.5, I_k (at $t=0, t_0$) can be calculated. Once I_k is known, Eq. 5.3 allows the calculation of the other three ion currents. Using Eq. 5.6, these calculated currents serve as input to calculate the feed concentration (in M) at time t_1 after which the currents at t_1 are calculated and from that the feed concentrations at t_2.

$$\Delta C_i = \frac{A z_i I_i \Delta t}{FV} \tag{5.6}$$

where F is the Faraday constant (96485 C·mol^{-1}), A the (effective) membrane surface area (m^2) and V the volume of feed compartment (L). Given the initial feed composition, the applied current density, the perm selectivity and transport numbers of the SLM and CIMS, this procedure simulates the ion concentration changes over

time. In the next section, the same calculation will be used to simulate the treatment of (synthetic) irrigation water containing four cation species.

5.3.2 Transport in synthetic greenhouse drainage water

The performance of the SLM and CIMS were tested in synthetic greenhouse drainage water containing K^+, Na^+, Ca^{2+} and Mg^{2+}, all in concentrations as indicated in Table 5.1. Figure 5.6 show the comparison between the experimentally obtained ion concentration changes and the simulated values based on the membrane permeation selectivity calculated from the equimolar binary salt solutions, as outlined in section 5.3.1.3. The summed cation transport numbers for SLM and CIMS are 0.94 and 0.98, respectively, indicating that also under these given experimental condition the current is predominantly carried by cation species. As expected, with the K^+ selective SLM (Figure 5.6a), K^+ was preferably being removed from the feed solution, with the concentration decreasing from 13 mM to 3.5 mM. With the monovalent cation-selective CIMS (Figure 5.6b), Na^+ and K^+ were both being removed from the feed solution with a concentration decrease from 10.7 mM and 13 mM to 0.5 and 0.3 mM, respectively.
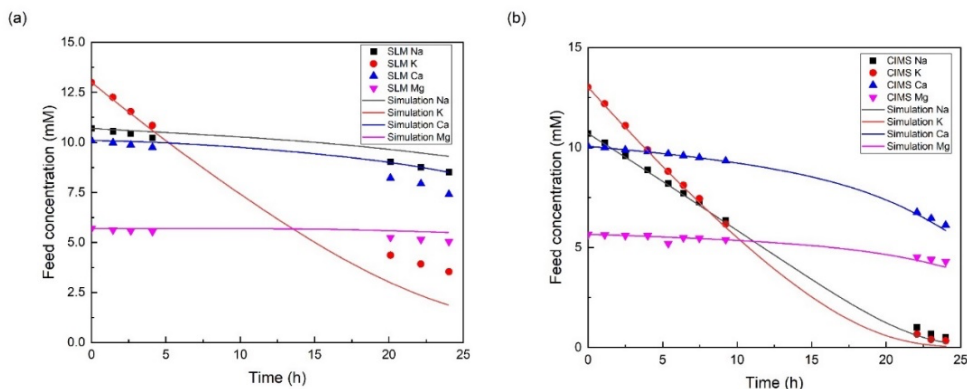
Figure 5.6 Experimental (symbols) and simulated (solid lines) feed cation concentrations as obtained in synthetic greenhouse water with initial composition as presented in Table 5.1 and using either the SLM (left) or the CIMS (right). The simulations are based on the selectivity determined in binary salt solutions, shown in Figure 5.4.

The simulations of the ion concentrations, represented as solid lines in Figure 5.6, are fairly close to the experimental results for both membranes. In the case of SLM,

the simulation underestimates the K^+ concentration at low feed concentration ratios. By implication and because of the constant current density applied, the concentrations of the other three ion species are slightly overestimated. Apparently, the selectivity as obtained in binary mixtures (Figure 5.4) slightly deviates from the selectivity shown in mixtures containing four different cation species instead. This may not come as a surprise given the observation that even in a binary mixture selectivity depends, to a more or lesser extent, on the feed concentration ratio, notably the K^+/Mg^{2+} selectivity of the SLM.

The next step is to simulate a system with the two membrane types in series and investigate the Na^+ removal ability of such a system as well as the recovery of the three other cation species. In addition, water loss and energy consumption will be briefly discussed as well.

5.4 Implementation of the membrane-based ED system

5.4.1 Process design

Obviously, from a practical, experimental point of view, a membrane with a high Na^+ over K^+ selectivity would be by far the best or at least most straightforward option to selectively remove Na^+. However, as discussed in the previous sections, our SLM shows an inverse selectivity, *i.e.* a high K^+ over Na^+ permeation selectivity. For that reason, the Na^+ separation technology to be developed is bound to a two-step process with the SLM (separating K^+) and CIMS (separating Na^+ from Ca^{2+} and Mg^{2+}) operating in two different tandem schemes shown in Figure 5.1.

One can imagine the tandem schemes shown in Figure 5.1 into two treatment scenarios (Figure 5.7). Figure 5.7a outlines scenario 1 with the separation of divalent and monovalent cations using the CIMS in the first step, followed by the separation of K^+ and Na^+ using the SLM. Figure 5.7b illustrates scenario 2 with the separation of Na^+ and divalent cations from K^+ using the SLM in first step, followed by the separation of Na^+ and divalent cations using the CIMS. Apart from positioning the SLM and CIMS in different order, the identity of the dilute and concentrate streams for either the SLM or the CIMS differ as well as the point where fresh irrigation water (IR) and stock solution enters the process stream. In scenario 1, IR water and stock solution enters the greenhouse directly. The drainage water leaving the greenhouse and entering the SLM functions both as dilute and concentrate stream. In the first step of scenario 2, the dilute stream of the SLM is, as in scenario 1, made up by drainage

water leaving the greenhouse. However, in this case an irrigation stock solution with the ionic composition shown in Table 5.1 is introduced as the concentrate stream. With the volumetric flow of dilute and concentrate stream the same, the SLM step is also the point where IR water enters the system. In scenario 1, the concentrate stream leaving the CIMS functions as the dilute stream for the SLM in step 2. In scenario 2, the concentrate leaving the SLM is directly fed back to the greenhouse. As shown in Figure 5.7a, in scenario 1, the volumetric flow leaving the greenhouse (Φ_V) is, before entering the CIMS, distributed over two streams $Q_{d,s1}$ and $Q_{c,s1}$. Later on in step 2, $Q_{c,s1}$ becomes the dilute stream for the SLM, $Q_{d,s2}$. The streams $Q_{d,s1}$ and $Q_{d,s2}$ are not independent (if, for example, $Q_{d,s1}=20\%\Phi_V$ then $Q_{d,s2}=80\%\Phi_V$), and their ratio has a direct and significant effect on the entire separation and recovery process. We therefore performed a sensitivity test to calculate the effect of the distribution ratio at point A. The (arbitrary) chosen $Q_{d,s1}/Q_{d,s2}$ ratios were 20/80, 50/50 and 80/20. As for scenario 2, here $Q_{d,s1}$ and $Q_{d,s2}$ are independent. $Q_{d,s1}$ equals the total volumetric flow leaving the greenhouse. At point B the outlet from $Q_{d,s2}$, can take any value between 0 and Q_v and with that determines for a large extent the total water loss of the system.

Detailed information regarding the sensitivity study and the simulation data can be found in the supplementary information (Table 5.S2). Here we suffice by giving the final result, *i.e.*, the optimal volumetric flow rates turned out to be: $Q_{d,s1}=80\%\Phi_V$ and $Q_{d,s2}=20\%\Phi_V$ for scenario 1 and $Q_{d,s2}=80\%\Phi_V$ for scenario 2.

5
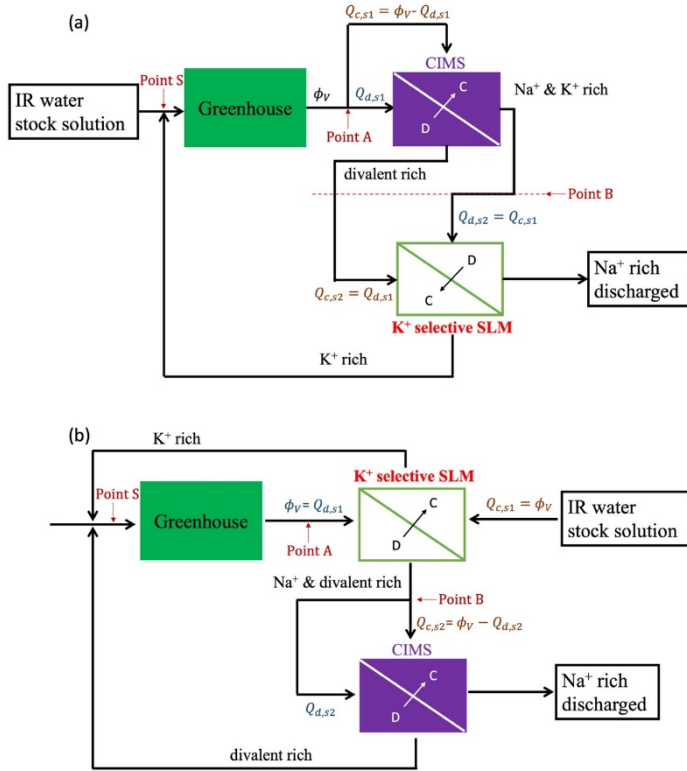
Figure 5.7 Two-step treatment of greenhouse drainage water for the selective removal of Na$^+$ with a combination of the SLM and CIMS in ED system, (a) scenario 1 and (b) scenario 2. $Q_{d,s1}$ or $Q_{d,s2}$ indicate the volumetric flow of the dilute stream in step 1 and step 2, respectively. $Q_{c,s1}$ or $Q_{c,s2}$ indicate the volumetric flow of the concentrate stream in step 1 and step 2, respectively. D and C indicate the dilute and concentrate stream, respectively. The ionic current from D to C is composed of K$^+$, in the case of the SLM, or K$^+$ + Na$^+$, in the case of the CIMS.

5.4.2 Optimal membrane surface area and K$^+$, Ca^{2+} and Mg^{2+} recovery rates

The required total membrane surface area (A) is a key operational parameter. The calculation of A requires the input of several other parameters. Eq. 5.7 gives the required value of A as a function of ion transport number (t_i), ion concentration difference between the dilute stream entering and leaving the membrane module ΔC_i,

the applied current density I (A·m^{-2}), the Faraday constant F (96485 C·mol^{-1}) and volumetric flow of the dilute through the membrane module Q_d (m^3·h^{-1}) [57].

$$A = \frac{Q_d \times F \times \Delta C_i}{I \times t_i} \tag{5.7}$$

Note that in this study Eq. 5.7 is exclusively used for monovalent cations, therefore the charge of the ion (+1) is not specified explicitly.

Table 5.2 summarizes a number of operational parameters including Q_d (m^3's^{-1}), based on the sensitivity study discussed previously, I (A·m^{-2}), based on the LCD analysis, ΔC (mol·m^{-3}), based on greenhouse requirements, t_i, based on the experimentally obtained membrane selectivity properties and, finally, A (m^2), calculated according to Eq. 5.7, all for both membrane types (*i.e.*, for step 1 and step 2) and for both scenarios.

As for the ion concentration changes, two requirements were at the base of the calculation. First, the Na$^+$ level of the water entering the greenhouse (point S in Figure 5.6) should remain below the threshold value of 4 mM. Secondly, the aim to recover as much K$^+$ as possible. This combined aim determines, together with the composition of the water leaving the greenhouse and the added stock solution/fresh IR water, the ΔC values for of K$^+$, Na$^+$ and K$^+$+ Na$^+$. Once these ΔC values are known and together with Q_d, I_{tot} and t_i values, A can be calculated, of both the SLM and the CIMS and for both scenarios. As for scenario 1, the required membrane surface areas for the CIMS in step 1 and the SLM in step 2 turn out to be 48 m^2 and 52 m^2, respectively. As for scenario 2, the calculated surface area of the SLM in step 1 is 57 m^2 and of the CIMS in step 2, 6 m^2.

Note that the transport number t_i listed in Table 5.2 represents either the ion or the sum of the ions of choice. Given the cation selectivity of both the SLM and the CIMS, the unaccounted part of the transport number that deviates from unity represents a charge carried by divalent cations.

5

Scenario 1			
Step 1: CIMS		**Step 2: SLM**	
Q_d (m³·h⁻¹)	80%Φ_V	Q_d (m³·h⁻¹)	20%Φ_V
	1.18		0.30
I (A m⁻²)	20.00	I (A m⁻²)	15.00
$\Delta C_{(Na+K)}$ (mol·m⁻³)	21.33	$\Delta C_{(Na)}$ (mol·m⁻³)	15.63
$t_{(Na+K)}$	0.70	$t_{(Na)}$	0.16
A_1 (m²)	48	A_2 (m²)	52
Scenario 2			
Step 1: SLM		**Step 2: CIMS**	
Q_d (m³·h⁻¹)	100%Φ_V	Q_d (m³·h⁻¹)	80%Φ_V
	1.48		1.18
I (A m⁻²)	15.00	I (A m⁻²)	20.00
$\Delta C_{(K)}$ (mol·m⁻³)	13.00	$\Delta C_{(Na)}$ (mol·m⁻³)	2.55
$t_{(K)}$	0.60	$t_{(Na)}$	0.70
A_1 (m²)	57	A_2 (m²)	6

Table 5.2 Operational parameters employed in scenario 1 and 2, including the volumetric flow rate Q_d (m³·h⁻¹) of the dilute stream, applied current density I (A·m⁻²), ion concentration change ΔC (mol·m⁻³), ion transport number t of the given membrane (calculated from the equimolar mixed salt ED test) and the calculated required membrane surface area A (m²). Note that Q_d is expressed in terms of the total volumetric flow, Q_V.

With the membrane surface areas calculated, all relevant parameters of the SLM and CIMS are defined. Table 5.3 summarizes the recovery rates of K^+, Ca^{2+} and Mg^{2+} as well as of water. Based on these numbers, scenario 2 performs slightly better, notably regarding the recovery of Ca^{2+} and Mg^{2+}.

	Recovery			
	K^+	Ca^{2+}	Mg^{2+}	Water
Scenario 1	97%	63%	68%	80%
Scenario 2	96%	79%	79%	80%

Table 5.3 Summary of the recovery rates of K^+, Ca^{2+} and Mg^{2+} as well as of water when applying either scenario 1 or 2.

5.4.3. Outlook

Any potential real-life application of the system outlined here depends on its competitiveness with currently existing technology. The economics of the SLM-based technology, in turn, will depend (to a more or lesser extent) on the life-time of the SLM. In order to investigate its stability in terms of both mechanical strength and functionality, the SLM was exposed to the same experimental conditions as applied before (Table 5.2) but for a period of 20 days. Figure 5.8 shows the ionic fluxes over the SLM in equimolar mixed salt solutions containing Na^+, K^+, Ca^{2+} and Mg^{2+} during 20 days of continuous operation with the solution refreshed every two days. Figure 5.8 allows two conclusions. Firstly, the selectivity shown is in line with the selectivity seen in Figures 5.4-5.6, with a selectivity order of K^+>Na^+>Ca^{2+}>Mg^{2+}. Secondly, the functionality of the SLM, regarding both selectivity and flux magnitude, remains fairly constant over the 20 days period
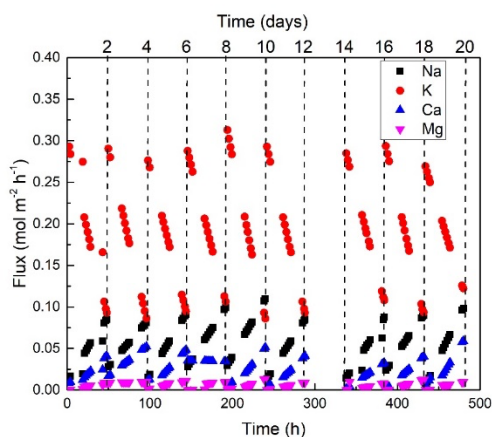
Figure 5.8 SLM mediated ionic fluxes carried by Na^+, K^+, Ca^{2+} and Mg^{2+} under ED conditions during 20 days of continuous operation with the solution refreshed every two days.

Addition to the membrane lifetime, another hurdle to take on the way to application is lowering the membrane resistance of the SLM and with that the ED energy consumption. As evident from Figure 5.3, for any applied current density, the recorded voltage over the membrane is higher for the SLM than for the CIMS, indicating the higher SLM resistance. A factor of 6 can be calculated from the slope from Figure 5.3 between the resistance of SLM and CIMS. This is mainly due to the lower IEC of the SLM. The maximal solubility of the Na^+ borate salt used here in

NPOE is 50 mM, equivalent to an IEC of 0.085 mEq·g^{-1}. With a reported IEC of 1.5-1.8 mEq.g^{-1}, the IEC of the CIMS is approximately 20 times higher. The difference of the observed ratio of 6 from LCDs for membrane resistance in comparison to the ratio of 20 as deduced from the IEC, likely points to differences in ionic aggregation and the formation of intimate ion-pairs between anionic charged groups and cations that has been described in literature [58]. There are essentially two ways to lower the SLM resistance. Firstly, increasing the IEC of the SLM by a different combination of salt and organic solvent. Secondly, a reduction of the membrane thickness from 100 um, preferably to the <10 um range, possibly in combination with a porous support rendering the necessary mechanical strength.

5.5 Conclusion

As determined in binary equimolar salt solutions, the SLM shows a K$^+$ over Na$^+$, K$^+$ over Ca^{2+} and K$^+$ over Mg^{2+} selectivity of 9, 15 and 30, respectively, even at rather low K$^+$ feed concentrations and low feed ratios. When extrapolated to solutions containing K$^+$, Na$^+$, Ca^{2+} and Mg^{2+}, these binary selectivities predict quite well the experimentally observed concentrations changes over time of all four cation species. Because the SLM demonstrates a permeation preference of K$^+$ over Na$^+$, the selective removal of Na$^+$ from greenhouse irrigation water requires a two-step process implying the SLM operating in series with a (generic commercially available) CIMS with a monovalent cation over divalent cation selectivity. Based on the permeation characteristics of both the SLM and the CIMS, this two-step process has been simulated using real-life operational input parameters. Starting point of the simulation was the (mandatory) requirement to keep the Na$^+$ concentration below its (toxic) threshold of 4 mM, while recovering as much K$^+$ as possible. With nearly all K$^+$ recovered (96%), the recovery of Ca^{2+}, Mg^{2+} and water turned out to be around 80%, indicating the efficiency of the novel tandem technology presented here.

Supporting information

5.S1 Mass and charge balance

In order to investigate whether the ion concentration changes in the two inner compartments of the six-compartment cell in Figure 5.2 can be exclusively ascribed to transport over the central membrane separating chambers A and B, mass and charge balances were set up. Ideally, the changes of one particular ionic species in both compartments are the same but of opposite sign; stated otherwise, their summation add up to zero. In addition, in order to retain electro neutrality, the total charge in each compartment also adds up to zero. Tables 5.S1 shows the mass and charge balance for all equimolar quaternary ion mixed solution using (25 mM) KCl + NaCl + CaCl$_2$ + MgCl$_2$.

	SLM			CIMS		
	A	B	Total	A	B	Total
ΔK (mmol)	-5.73	5.77	0.04	-6.66	6.66	0
ΔNa (mmol)	-2.19	2.17	-0.97	-8.38	8.36	-0.26
ΔCa (mmol)	-2.84	2.83	-0.01	-1.31	1.29	-0.02
ΔMg (mmol)	-1.28	1.27	-0.01	-0.42	0.41	-0.01
ΔCl (mmol)	-16.21	16.2	-0.99	-18.4	18.3	-0.3
Δcharge	0.05	-0.06	0.02	-0.1	0.12	-0.02

Table 5.S1 Mass and charge balance of compartments A and B, where charge balance refers to the net charge of the solution after accounting for the measured ion concentration changes. The column labeled Total, refers to the balance including all compartments A, B, C and D.

5.S2 Simulation of the ion concentration changes

Simulated ion concentration changes in the dilute and concentrate streams of the SLM and CIMS are based on the experimentally obtained membrane selectivities in binary solutions and the operational parameters listed in section 5.4. Table 5.S2 summarizes the concentration of each ion species in the dilute and concentrated stream of both membrane modules. As indicated in Figure 5.7, at point A (scenario 1) and at point B (scenario 2) the volumetric flow splits. The distribution ratio over the two streams affects the overall recovery rates. In order to quantify this effect, calculations were performed at three different distribution ratios, with Q_d/ϕ_v equal to 20%, 50% and 80%.

$Q_d = 20\%\Phi_V = 0.3$ (m³ h⁻¹)								

Scenario 1								
Concentration(mol·m⁻³)	Step 1: CIMS				Step 2: SLM			
	Dilute		Concentrate		Dilute		Concentrate	
	t=0	t=24	t=0	t=24	t=0	t=24	t=0	t=24
K^+	13.0	0.7	13.0	16.1	16.1	0.3	0.7	64.0
Na^+	10.7	1.2	10.7	13.1	13.1	8.7	1.1	18.8
Ca^{2+}	10.1	7.0	10.1	10.8	10.8	7.7	8.4	16.6
Mg^{2+}	5.7	4.7	5.7	5.9	5.9	5.2	4.7	7.4
Scenario 2								
Concentration(mol·m⁻³)	Step 1: SLM				Step 2: CIMS			
	Dilute		Concentrate		Dilute		Concentrate	
	t=0	t=24	t=0	t=24	t=0	t=24	t=0	t=24
K^+	13.0	0.5	9.5	22.0	0.5	0.3	0.5	0.5
Na^+	10.7	7.6	0.0	3.1	7.6	6.0	7.6	8.0
Ca^{2+}	10.1	8.2	7.0	8.9	8.2	7.9	8.2	8.3
Mg^{2+}	5.7	5.2	5.1	3.5	5.2	5.1	5.2	5.2

5

$Q_d= 50\%\Phi_V = 0.74$ (m^3 h^{-1})								
Scenario 1								
Concentration(mol·m^{-3})	Step 1: CIMS				Step 2: SLM			
	Dilute		Concentrate		Dilute		Concentrate	
	t=0	t=24	t=0	t=24	t=0	t=24	t=0	t=24
K$^+$	13.0	0.7	13.0	25.3	25.3	0.4	0.7	25.6
Na$^+$	10.7	1.2	10.7	20.2	20.2	13.5	1.2	7.9
Ca^{2+}	10.1	7.0	10.1	13.1	13.1	10.4	7.0	9.7
Mg^{2+}	5.7	4.7	5.7	6.6	6.6	5.9	4.7	5.4
Scenario 2								
Concentration(mol·m^{-3})	Step 1: SLM				Step 2: CIMS			
	Dilute		Concentrate		Dilute		Concentrate	
	t=0	t=24	t=0	t=24	t=0	t=24	t=0	t=24
K$^+$	13.0	0.5	9.5	22.0	0.5	0.3	0.5	0.6
Na$^+$	10.7	7.6	0.0	3.1	7.6	5.1	7.6	10.0
Ca^{2+}	10.1	8.2	7.0	8.9	8.2	7.7	8.2	8.7
Mg^{2+}	5.7	5.2	5.1	3.5	5.2	5.0	5.2	5.4

5

$Q_d = 80\%\Phi_V = 1.18$ (m³ h⁻¹)								
Scenario 1								
Concentration(mol·m⁻³)	Step 1: CIMS				Step 2: SLM			
	Dilute		Concentrate		Dilute		Concentrate	
	t=0	t=24	t=0	t=24	t=0	t=24	t=0	t=24
K^+	13.0	0.7	13.0	62.2	62.2	1.3	0.7	15.8
Na^+	10.7	1.1	10.7	48.9	48.9	33.1	1.1	4.9
Ca^{2+}	10.1	7.0	10.1	22.3	22.3	18.3	7.0	7.9
Mg^{2+}	5.7	4.7	5.7	9.4	9.4	8.9	4.7	4.9
Scenario 2								
Concentration(mol·m⁻³)	Step 1: SLM				Step 2: CIMS			
	Dilute		Concentrate		Dilute		Concentrate	
	t=0	t=24	t=0	t=24	t=0	t=24	t=0	t=24
K^+	13.0	0.5	9.5	22.0	0.5	0.2	0.5	1.3
Na^+	10.7	7.6	0.0	3.1	7.6	4.8	7.6	18.9
Ca^{2+}	10.1	8.2	7.0	8.9	8.2	7.6	8.2	10.6
Mg^{2+}	5.7	5.2	5.1	3.5	5.2	5.0	5.2	6.0

Table 5.S2 Ion concentration change at the start (t=0) and after the treatment (t=24 h) in the dilute and concentrate streams in each step of the two proposed treatment scenarios with different set parameters of dilute stream volumetric flow rate.

The overall recovery for K^+, Ca^{2+} and Mg^{2+} according to Table 5.S2 are calculated and listed in Table 5.S3. As show, setting Q_d at a the volumetric flow rate of 1.18 m³ h⁻¹ ($80\%\Phi_V$) renders the best performance in the overall ion recovery.

Recovery	Q_d=0.3 (m³ h⁻¹)		Q_d=0.74 (m³ h⁻¹)		Q_d=1.18 (m³ h⁻¹)	
	Scenario 1	Scenario 2	Scenario 1	Scenario 2	Scenario 1	Scenario 2
K^+	98%	96%	98%	96%	97%	96%
Ca^{2+}	33%	34%	48%	57%	63%	79%
Mg^{2+}	26%	27%	47%	53%	68%	79%

Table 5.S3 Overall recovery rates of K^+, Ca^{2+} and Mg^{2+} based on the simulation results of the ion concentration changes shown in Table 5.S2, calculated at three different Q_d values.

5.S3 Cost evaluation of the 2 scenarios

The key parameters governing the overall costs of a water treatment system using ED can be summarized into three categories: nutrient costs (including fertilizer supplied, nutrients recovered and net water usage), energy consumption (including electric power used for both ED and pumping), and membrane module costs (based on purchase or synthesis prices and membrane life time) [59]. Here we suffice by briefly commenting on nutrient and membrane costs. Energy consumption is already briefly addressed in the main text, notably in the context of the implications of the high resistance of the SLM.

Table 5.S4 shows the recovery of nutrients and water and the estimated membrane cost for both scenarios. Based on the higher recovery rates of K^+, Ca^{2+} and Mg^{2+}, scenario 2 clearly is the better option. Current practice is that greenhouse drainage water in the Netherlands is collected and discharged or, in some cases, used for the irrigation of salt resistant crops. The water recovery under optimal operational conditions for both scenarios is 80%, a value that translates to an estimated annual water saving of 5168 m^3/hectare/year.

	Recovery			Water saving	Membrane cost
	K^+	Ca^{2+}	Mg^{2+}	(m^3/hectare/year)	(€/day)
Scenario 1	97%	63%	68%	5168	65
Scenario 2	96%	79%	79%	5168	64

Table 5.S4 Comparison of nutrient and water recovery rates for the two scenarios given an optimal Q_d of 1.18 m^3 h^{-1}.

The ability of ED system to preferentially remove Na^+ over K^+, Ca^{2+} and Mg^{2+} also leads to fertilizer savings. Currently, greenhouses using a desalination treatment system, including RO and ED, need to add significant amounts of salt fertilizers to obtain the desired composition of their nutrient water [60]. Ca^{2+} and Mg^{2+}-containing salts contribute to the annual fertilizer costs by a factor of about 1/3rd. Values regarding K^+ salts are less clear. Therefore, the estimation of fertilizer savings were solely based Ca^{2+} and Mg^{2+} use and recovery. Considering the unaccounted contribution from K^+, this estimation represents a lower limit value. Based on the amount of added fertilizer in greenhouses using a desalination system, typical fertilizer costs are 30000 €/hectare [60]. With Ca^{2+} and Mg^{2+} recovery rates of about

158

65% and 79%, annual fertilizer savings add up to 6500 €/hectare and 7900 €/hectare, for scenario 1 and 2, respectively.

As for the costs related to the membrane modules, we only consider the costs of the membrane themselves, not the manufacturing of the module. The calculated total membrane capital costs are based on the purchase price of the CIMS and the producing costs of the SLM. As for the CIMS, we assumed a purchase price per m^2 of 300 €. The lifetime of monovalent-cation selective membranes for high salinity water treatment is reported to be 7 years [60,61]. The calculated costs of the SLM per m^2 of 800 € is based on the purchase price of the chemicals from Sigma Aldrich and the membrane support from MEMBRANA. Reported prices in this study reflect upper limit values. At the current stage, it is still difficult to estimate the expected lifetime of the SLM. Given optimal operational conditions and assuming a life time of 5 and 2 years for the CIMS and SLM, respectively, the membrane costs per day are estimated to be 65 €/day and 64 €/day for the two different scenarios.

5

References

[1]   M. Raaphorst, Quantitative Information for Greenhouse Horticulture, Report
        GTB-5154, Wageningen, 2017.

[2]   C. van der Salm, W. Voogt, E. Beerling, J. van Ruijven, E. van Os,
        Minimising emissions to water bodies from NW European greenhouses;
        with focus on Dutch vegetable cultivation, Agricultural Water Management.
        242 (2020). https://doi.org/10.1016/j.agwat.2020.106398.

[3]   EU-WFD, Water Framework Directive, Directive 2000/60/EC of the
        European Parliament and of the Council of 23 October 2000 establishing a
        framework for Community action in the field of water policy, Official
        Journal of the European Communities. L327/1-72 (2000).

[4]   G.B.K. Roos-Schalij, M.P. Leunissen, K. Krijt, Lozingenbesluit WVO
        Glastuinbouw, the Hague, 1994.

[5]   EU-ND, Nitrate Directive, Council Directive of 12 December 1991
        concerning the protection of waters against pollution caused by nitrates from
        agricultural sources (91/676/EEC), Official Journal of the European
        Communities. L 375/1-8 (1992).

[6]   Besluit Glastuinbouw, Regulation Greenhouse Horticulture, (2002).
        https://wetten.overheid.nl/BWBR0013430/2012-01-01.

[7]   E.A.M. Beerling, C. Blok, A.A. Van Der Maas, E.A. Van Os, Closing the
        water and nutrient cycles in soilless cultivation systems, Acta Horticulturae.
        1034 (2014) 49–55. https://doi.org/10.17660/ActaHortic.2014.1034.4.

[8]   J.L. Zhang, T.J. Flowers, S.M. Wang, Mechanisms of sodium uptake by
        roots of higher plants, Plant and Soil. 326 (2010) 45–60.
        https://doi.org/10.1007/s11104-009-0076-0.

[9]   A.D. Blaylock, Cooperative Extension Service Soil Salinity, Salt Tolerance,
        and Growth Potential of Horticultural and Landscape Plants, 1994.

[10]   A. Läuchli, S.R. Grattan, Plant growth and development under salinity
        stress, in: Advances in Molecular Breeding Toward Drought and Salt
        Tolerant Crops, Springer Netherlands, 2007: pp. 1–32.
        https://doi.org/10.1007/978-1-4020-5578-2_1.

[11]   T.B. Kinraide, Interactions among Ca2+, Na+ and K+ in salinity toxicity:
        quantitative resolution of multiple toxic and ameliorative effects, Journal of
        Experimental Botany. 50 (1999) 1495–1505.
        https://doi.org/10.1093/jxb/50.338.1495.

5

160

[12]   A.M.S. Abdul Qados, Effect of salt stress on plant growth and metabolism of bean plant Vicia faba (L.), Journal of the Saudi Society of Agricultural Sciences. 10 (2011) 7–15. https://doi.org/10.1016/j.jssas.2010.06.002.

[13]   S. Burn, M. Hoang, D. Zarzo, F. Olewniak, E. Campos, B. Bolto, O. Barron, Desalination techniques - A review of the opportunities for desalination in agriculture, Desalination. 364 (2015) 2–16. https://doi.org/10.1016/j.desal.2015.01.041.

[14]   C. Fritzmann, J. Löwenberg, T. Wintgens, T. Melin, State-of-the-art of reverse osmosis desalination, Desalination. 216 (2007) 1–76. https://doi.org/10.1016/j.desal.2006.12.009.

[15]   D. Cohen-Tanugi, J.C. Grossman, Water desalination across nanoporous graphene, Nano Letters. 12 (2012) 3602–3608. https://doi.org/10.1021/nl3012853.

[16]   U. Yermiyahu, A. Tal, A. Ben-Gal, A. Bar-Tal, J. Tarchitzky, O. Lahav, Rethinking desalinated water quality and agriculture, Science. 318 (2007) 920–921. https://doi.org/10.1126/science.1146339.

[17]   H. Strathmann, Electrodialysis, a mature technology with a multitude of new applications, Desalination. 264 (2010) 268–288. https://doi.org/10.1016/j.desal.2010.04.069.

[18]   T. Scarazzato, K.S. Barros, T. Benvenuti, M.A.S. Rodrigues, D.C.R. Espinosa, A.M.B. Bernardes, F.D.R. Amado, V. Pérez-Herranz, Achievements in electrodialysis processes for wastewater and water treatment, in: Current Trends and Future Developments on (Bio-) Membranes, Elsevier, 2020: pp. 127–160. https://doi.org/10.1016/b978-0-12-817378-7.00005-7.

[19]   L. Ge, B. Wu, D. Yu, A.N. Mondal, L. Hou, N.U. Afsar, Q. Li, T. Xu, J. Miao, T. Xu, Monovalent cation perm-selective membranes (MCPMs): New developments and perspectives, Chinese Journal of Chemical Engineering. 25 (2017) 1606–1615. https://doi.org/10.1016/j.cjche.2017.06.002.

[20]   T. Benvenuti, M.A. Siqueira Rodrigues, A.M. Bernardes, J. Zoppas-Ferreira, Closing the loop in the electroplating industry by electrodialysis, Journal of Cleaner Production. 155 (2017) 130–138. https://doi.org/10.1016/j.jclepro.2016.05.139.

[21]   Y.V.L. Ravikumar, S. Sridhar, S. V. Satyanarayana, Development of an electrodialysis-distillation integrated process for separation of hazardous sodium azide to recover valuable DMSO solvent from pharmaceutical effluent, Separation and Purification Technology. 110 (2013) 20–30. https://doi.org/10.1016/j.seppur.2013.02.031.

5

[22]   E. Vera, J. Ruales, M. Dornier, J. Sandeaux, R. Sandeaux, G. Pourcelly, Deacidification of clarified passion fruit juice using different configurations of electrodialysis, Journal of Chemical Technology & Biotechnology. 78 (2003) 918–925. https://doi.org/10.1002/jctb.827.

[23]   K.G. Nayar, P. Sundararaman, C.L. O'Connor, J.D. Schacherl, M.L. Heath, M.O. Gabriel, S.R. Shah, N.C. Wright, A.G. Winter, V, Feasibility study of an electrodialysis system for in-home water desalination in urban India, Development Engineering. 2 (2016) 38–46. https://doi.org/10.1016/j.deveng.2016.12.001.

[24]   M. Sadrzadeh, T. Mohammadi, Sea water desalination using electrodialysis, Desalination. 221 (2008) 440–447. https://doi.org/10.1016/J.DESAL.2007.01.103.

[25]   G. Doornbusch, H. Swart, M. Tedesco, J. Post, Z. Borneman, K. Nijmeijer, Current utilization in electrodialysis: Electrode segmentation as alternative for multistaging, Desalination. 480 (2020) 114243. https://doi.org/10.1016/j.desal.2019.114243.

[26]   M. Sadrzadeh, A. Razmi, T. Mohammadi, Separation of different ions from wastewater at various operating conditions using electrodialysis, Separation and Purification Technology. 54 (2007) 147–156. https://doi.org/10.1016/j.seppur.2006.08.023.

[27]   A.H. Galama, G. Daubaras, O.S. Burheim, H.H.M. Rijnaarts, J.W. Post, Seawater electrodialysis with preferential removal of divalent ions, Journal of Membrane Science. 452 (2014) 219–228. https://doi.org/10.1016/j.memsci.2013.10.050.

[28]   Y. Zhang, S. Paepen, L. Pinoy, B. Meesschaert, B. Van Der Bruggen, Selectrodialysis: Fractionation of divalent ions from monovalent ions in a novel electrodialysis stack, Separation and Purification Technology. 88 (2012) 191–201. https://doi.org/10.1016/j.seppur.2011.12.017.

[29]   B. Cohen, N. Lazarovitch, J. Gilron, Upgrading groundwater for irrigation using monovalent selective electrodialysis, Desalination. 431 (2018) 126–139. https://doi.org/10.1016/j.desal.2017.10.030.

[30]   Z. Qian, H. Miedema, S. Sahin, L.C.P.M. de Smet, E.J.R. Sudhölter, Separation of alkali metal cations by a supported liquid membrane (SLM) operating under electro dialysis (ED) conditions, Desalination. 495 (2020) 114631. https://doi.org/10.1016/j.desal.2020.114631.

[31]   N.M. Kocherginsky, Q. Yang, L. Seelam, Recent advances in supported liquid membrane technology, Separation and Purification Technology. 53 (2007) 171–177. https://doi.org/10.1016/j.seppur.2006.06.022.

[32]   A. Šlampová, P. Kubáň, P. Boček, Fine-tuning of electromembrane extraction selectivity using 18-crown-6 ethers as supported liquid membrane modifiers, ELECTROPHORESIS. 35 (2014) 3317–3320. https://doi.org/10.1002/elps.201400372.

[33]   P.K. Parhi, Supported liquid membrane principle and its practices: A short review, Journal of Chemistry. (2013). https://doi.org/10.1155/2013/618236.

[34]   Y. Asensio, C.M. Fernandez-Marchante, J. Lobato, P. Cañizares, M.A. Rodrigo, Influence of the ion-exchange membrane on the performance of double-compartment microbial fuel cells, (n.d.).

[35]   Jingwei Zhou, Han Kuang, Wei Zhuang, Yong Chen, Dong Liu, Hanjie Ying, Jinglan Wu, Application of electrodialysis to extract 5′-ribonucleotides from hydrolysate: efficient decolorization and membrane fouling, RSC Advances. 8 (2018) 29115–29128. https://doi.org/10.1039/C8RA02550A.

[36]   S. Sahin, J.E. Dykstra, H. Zuilhof, R.L. Zornitta, L.C.P.M. De Smet, Modification of cation-exchange membranes with polyelectrolyte multilayers to tune ion selectivity in capacitive deionization, ACS Applied Materials and Interfaces. 12 (2020) 34746–34754. https://doi.org/10.1021/ACSAMI.0C05664.

[37]   T. Sata, R. Izuo, Modification of the transport properties of ion exchange membranes. XII. Ionic composition in cation exchange membranes with and without a cationic polyelectrolyte layer at equilibrium and during electrodialysis, Journal of Membrane Science. 45 (1989) 209–224. https://doi.org/10.1016/S0376-7388(00)80515-3.

[38]   G. Saracco, Transport properties of monovalent-ion-permselective membranes, Chemical Engineering Science. 52 (1997) 3019–3031. https://doi.org/10.1016/S0009-2509(97)00107-3.

[39]   B.A. Cooke, Concentration polarization in electrodialysis-I. The electrometric measurement of interfacial concentration, Electrochimica Acta. 3 (1961) 307–317. https://doi.org/10.1016/0013-4686(61)85007-X.

[40]   I. Rubinstein, Theory of concentration polarization effects in electrodialysis on counter-ion selectivity of ion-exchange membranes with differing counter-ion distribution coefficients, Journal of the Chemical Society, Faraday Transactions. 86 (1990) 1857–1861. https://doi.org/10.1039/FT9908601857.

[41]   X. Xiao, M.A. Shehzad, A. Yasmin, Z. Ge, X. Liang, F. Sheng, W. Ji, X. Ge, L. Wu, T. Xu, Anion permselective membranes with chemically-bound carboxylic polymer layer for fast anion separation, Journal of Membrane Science. 614 (2020). https://doi.org/10.1016/j.memsci.2020.118553.

5

[42]   J.C. de Valenca, Overlimiting current properties at ion exchange
        membranes, University of Twente, 2017.
        https://doi.org/10.3990/1.9789036543149.

[43]   A. Uzdenova, M. Urtenov, Potentiodynamic and galvanodynamic regimes
        of mass transfer in flow-through electrodialysis membrane systems:
        Numerical simulation of electroconvection and current-voltage curve,
        Membranes. 10 (2020). https://doi.org/10.3390/membranes10030049.

[44]   Z. Qian, H. Miedema, L.C.P.M. de Smet, E.J.R. Sudhölter, Permeation
        selectivity in the electro-dialysis of mono- and divalent cations using
        supported liquid membranes, Desalination. 521 (2022) 115398.
        https://doi.org/10.1016/j.desal.2021.115398.

[45]   Y.D. Ahdab, D. Rehman, G. Schücking, M. Barbosa, V. John H. Lienhard,
        Treating Irrigation Water Using High-Performance Membranes for
        Monovalent Selective Electrodialysis, ACS ES&T Water. 1 (2020) 117–
        124. https://doi.org/10.1021/ACSESTWATER.0C00012.

[46]   T. Sata, Theory of Membrane Phenomena in Ion Exchange Membranes, in:
        Ion Exchange Membranes, Royal Society of Chemistry, 2007: pp. 7–34.
        https://doi.org/10.1039/9781847551177-00007.

[47]   Y. Tanaka, Fundamental Properties of Ion Exchange Membranes, in: Ion
        Exchange Membranes, Elsevier, 2015: pp. 29–65.
        https://doi.org/10.1016/b978-0-444-63319-4.00002-x.

[48]   B. Tansel, Significance of thermodynamic and physical characteristics on
        permeation of ions during membrane separation: Hydrated radius, hydration
        free energy and viscous effects, Separation and Purification Technology. 86
        (2012) 119–126. https://doi.org/10.1016/j.seppur.2011.10.033.

[49]   L. Ge, B. Wu, D. Yu, A.N. Mondal, L. Hou, N.U. Afsar, Q. Li, T. Xu, J.
        Miao, T. Xu, Monovalent cation perm-selective membranes (MCPMs): New
        developments and perspectives, Chinese Journal of Chemical Engineering.
        25 (2017) 1606–1615. https://doi.org/10.1016/j.cjche.2017.06.002.

[50]   T. Sata, T. Sata, W. Yang, Studies on cation-exchange membranes having
        permselectivity between cations in electrodialysis, Journal of Membrane
        Science. 206 (2002) 31–60. https://doi.org/10.1016/S0376-7388(01)00491-
        4.

[51]   T. Luo, F. Roghmans, M. Wessling, Ion mobility and partition determine the
        counter-ion selectivity of ion exchange membranes, Journal of Membrane
        Science. 597 (2020) 117645. https://doi.org/10.1016/j.memsci.2019.117645.

[52]   T. Luo, S. Abdu, M. Wessling, Selectivity of ion exchange membranes: A
        review, Journal of Membrane Science. 555 (2018) 429–454.
        https://doi.org/10.1016/j.memsci.2018.03.051.

164

[53]   I. Stenina, D. Golubenko, V. Nikonenko, A. Yaroslavtsev, Selectivity of transport processes in ion-exchange membranes: Relationship with the structure and methods for its improvement, International Journal of Molecular Sciences. 21 (2020) 1–33. https://doi.org/10.3390/ijms21155517.

[54]   I.A. Stenina, A.B. Yaroslavtsev, Ionic mobility in ion-exchange membranes, Membranes. 11 (2021). https://doi.org/10.3390/membranes11030198.

[55]   K.J. Kim, M. Shahinpoor, Effective diffusivity of nanoscale ion–water clusters within ion-exchange membranes determined by a novel mechano-electrical technique, International Journal of Hydrogen Energy. 28 (2003) 99–104. https://doi.org/10.1016/S0360-3199(02)00026-5.

[56]   B. Hille, Ion channels of excitable membranes, Sinauer, 2001.

[57]   H. Strathmann, Electrodialysis, a mature technology with a multitude of new applications, Desalination. 264 (2010) 268–288. https://doi.org/10.1016/j.desal.2010.04.069.

[58]   M. Li, A. Ju, X. Li, M. Ge, Electrochemical determination of ionization constants of tetrabutylammonium salt in acetonitrile and o-nitrophenyloctylether, Ionics. 12 (2014) 1777–1782. https://doi.org/10.1007/S11581-014-1117-0.

[59]   L.J. Andrés, F.A. Riera, R. Alvarez, Recovery and concentration by electrodialysis of tartaric acid from fruit juice industries waste waters, Journal of Chemical Technology & Biotechnology. 70 (1997) 247–252. https://doi.org/10.1002/(SICI)1097-4660(199711)70:3<247::AID-JCTB763>3.0.CO;2-8.

[60]   K.G. Nayar, J.H. Lienhard V, Brackish water desalination for greenhouse agriculture: Comparing the costs of RO, CCRO, EDR, and monovalent-selective EDR, Desalination. 475 (2020). https://doi.org/10.1016/j.desal.2019.114188.

[61]   K.G. Nayar, J. Fernandes, R.K. McGovern, B.S. Al-Anzi, J.H. Lienhard, Cost and energy needs of RO-ED-crystallizer systems for zero brine discharge seawater desalination, Desalination. 457 (2019) 115–132. https://doi.org/10.1016/j.desal.2019.01.015.

5

Chapter 6

Conclusions and outlook

This final chapter summarizes the conclusions from the preceding chapters (Section 6.1). In addition, new research directions for further improvement of the system outlined in this thesis, are briefly discussed (Section 6.2).

6.1 Conclusions

The prime aim of this PhD project was to develop a membrane system for the selective removal of Na^+ from greenhouse drainage water to facilitate its re-use as irrigation water and reduce waste. Along the way, we aimed for a better understanding of the key mechanisms playing a role in the membrane separation process, in particular in the case of ion species carrying the same charge.

<u>Chapter 2</u> presents a model of the greenhouse irrigation water system, essentially based on mass and charge balances. The simulations were used to explore the (minimum) required Na^+/K^+ selectively of the membrane-based water treatment system. Despite the detrimental effects on growth, plants have a certain limited tolerance towards Na^+. Consequently, and dependent on the plant species, not all Na^+ needs to be removed from the drainage water. All that needs to be achieved is to maintain the Na^+ level below a crop-specific threshold. The outcome of this analysis, based on real-life operational parameters, was that a Na^+ over K^+ permeation selectivity of 6 suffices to maintain the Na^+ below the, for tomatoes, threshold of 4 mM. We therefore proposed a closed-loop irrigation water system including a membrane-based module to remove the excess of Na^+ while preserving K^+ and other valuable nutrients as much as possible.

In <u>Chapter 3</u>, the concept of the supported liquid membrane (SLM) is introduced. An SLM consists of a microporous support impregnated with an organic phase (1-(2-nitrophenoxy)octane, NPOE), doped with 50 mM of a lipophilic salt, a Na-borate derivative. Here we start out to investigate the ability of the SLM to separate two ion species that are very similar in both charge and size, under electrodialysis (ED) conditions. The SLM exhibits excellent performance reflected in a high separation efficiency (up to ~90% for K^+ over Na^+ and up to ~100% for K^+ over Li^+), even in the absence of traditional, highly selective carrier molecules like crown ethers. Actually, adding crown ethers hardly affected the selectivity but considerably slowed down the K^+ transport. For that reason, the initial idea to include crown ethers was abandoned at this stage. Given the two ion species of interest have the same valence, the working mechanism of the NPOE-borate-based SLM is entirely determined by the differences in ion radius. This parameter affects the dehydration energy, which, in turn, affects

the partitioning over the biphasic water/membrane system, as well as the electro-phoretic ion mobility. The relative permittivity (dielectric constant) of NPOE is significantly lower than the permittivity of water (40 *vs*. 80). Consequently, prior to entering the hydrophobic NPOE-based membrane, ions need to be (partly) dehydrated. The dehydration energy is governed by the Born equation, accounting for the valence and radius of the ion and the permittivity difference between the two phases. According to the Born equation, the larger the crystal ion radius, the lower the required dehydration energy. The actual partitioning of an ion species over the two phases is dictated by a Boltzmann distribution, implying that the partitioning ratio of two ion species scales exponentially with the difference in dehydration energy. Although the largest ion species has the lower mobility, the dehydration/partitioning effect dominates the overall permeation selectivity of the SLM. The SLM favors the largest ion species, *i.e.* K^+ over Na^+. Chapter 3 validates the behavior of the SLM according to these basic physico-chemical principles. As shown, the combination of Born and Boltzmann predicts perfectly well the measured K^+ over Na^+ permeation selectivity of the SLM. Here, Born refers to the energy required for complete dehydration. Apparently, for these two monovalent cation species to pass the water/NPOE interface requires the surrounding water shell to be completely removed.

Chapter 4 extends the investigation of the SLM separation behavior to divalent cations. The electrophoretic mobility decreased in the order of $Na^+ > K^+ > Mg^{2+} > Ca^{2+}$. Given that the crystal radius of Mg^{2+} is by far the smallest, this result points out that the divalent cations, in contrast to their monovalent counterparts, are still partly hydrated when passing the SLM. This hypothesis was confirmed by water uptake measurements. As the divalent cations require only partly dehydration, Born/Boltzmann failed to adequately predict the monovalent over divalent cation distribution, and with that, the selectivity of the SLM. The ion-exchange selectivity constant K_{ex} was used to quantify and compare the affinity of the SLM for these different ion species. Analysis revealed that K_{ex} values follow the order of $K^+ > Ca^{2+} > Mg^{2+} \approx Na^+$. The observed membrane permeation selectivity ($K^+ > Na^+ > Ca^{2+} > Mg^{2+}$), as obtained in an equimolar solution containing all four ion species, reflects the combined contribution of K_{ex} and the electrophoretic mobility in the SLM. Comparison of the reported viscosity of NPOE and the one calculated from a Stokes-like relation, made us conclude that only 20% of the cations present in the SLM are actually free to move, thereby contributing to the measured conductance. The

remaining 80% is temporarily immobilized by an electrostatic interaction with the negatively charged borate moieties in the SLM.

Chapter 5 outlines a process for irrigation water treatment. The leading principle of the design was two-fold, retain the Na^+ level below the tomato threshold of 4 mM and recover water and other nutrients as much as possible. The study combines an experimental and theoretical approach. As our SLM shows a K^+ over Na^+ selectivity, the removal of Na^+ requires a two-step process. One step to separate K^+ (by the SLM) and one to separate Na^+ from the divalent cations (by a monovalent cation-selective membrane. Based on the permeation characteristics of the SLM, as described in the previous chapters and the properties of a commercially available monovalent cation ion-exchange membrane (CIMS), typically showing a monovalent over divalent cation selectivity, the operation of these two membranes in series was simulated. The simulation showed K^+, Ca^{2+} and Mg^{2+} recovery amounts of 96%, 79% and 79%, respectively, as well as 80% water savings, while keeping the Na^+ level below the threshold of 4 mM.

6.2 Outlook

In this section several research directions to further improve the SLM-ED system outlined are briefly addressed and discussed.

6.2.1 Improving SLM stability

The SLM consists of a microporous support (ACCUREL) impregnated with NPOE, which is constraint in the (hydrophobic) ACCUREL pores by capillary forces. However, in terms of industrial demands, the loss of the organic liquid membrane phase remains one of the major limitations in scaling up the SLM-ED system. Loss of the organic phase may be due to mechanical shear forces acting on the system, which not only pollutes the environment, but eventually also leads to a reduced SLM performance.[1–3] To improve the lifetime and stability of the SLM, a commonly reported method is to coat both sides of the SLM with a thin polymer layer.[4] Surface coating can be achieved by a variety of techniques such as dip coating, gelation, UV photo grafting and interfacial polymerization.[2,5–11] Organic polymers such as polyvinyl chloride and polyamines have been reported to improve the stability of SLMs applied for the removal or separation of anionic compounds such as nitrates.[3,5] Wijers, *et al*.[7] suggested the use of a negatively charged polymer for

6

improving the stability of SLM in transporting cations. It has been reported that an improved stability of the SLM in the recovery of Cu^{2+} was achieved by means of a surface modification by sulfonated polyether ether ketone (sPEEK). Based on these reports, sPEEK as a coating material seems an attractive direction to improve SLM stability, hopefully also under ED conditions. sPEEK has a high ion-exchange capacity, is chemically stable and has good mechanical properties[12–14]. We therefore conducted preliminary research of SLM surface coating with sPEEK.

6.2.1.1 SLM-sPEEK composite membrane

The preparation of the composite membrane is achieved by dip coating the ACCUREL support in a 15 wt.% sPEEK solution (sPEEK polymer fibers with sulfonate ion-exchanging groups, with an IEC around 1.9 mEq·g^{-1} according to the specification of te supplier). Coating of the ACCUREL support is performed prior to impregnating with NPOE. Figure 6.1 schematically illustrates the preparation of the composite membrane. The ACCUREL membrane support is dipped into the coating solution 3-4 times with both sides exposed to the sPEEK solution. A small area is left uncoated and used for the impregnation with NPOE later on. The membrane is dried in an oven under a nitrogen atmosphere for 24 h at a temperature of 70 °C. After coating and drying, the sPEEK-ACCUREL membrane is soaked in the NPOE solution, containing 50 mM of sodium tetrakis[3,5-bis(trifluoromethyl)phenyl]borate (NaBArF) for 48 h to allow full impregnation. The excess of organic solution is gently wiped off using tissue paper and prepared for characterization and ED testing. The pores of the ACCUREL membrane support were determined to be more or less completely filled by NPOE by measuring the weight increase after the impregnation with NPOE, the NPOE density, and the void volume.
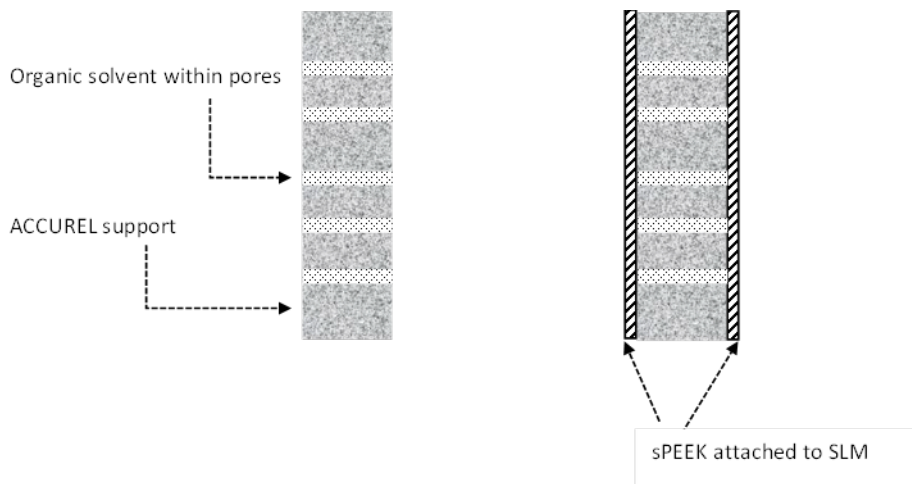
6

Figure 6.1 Schematic illustration of the composite membrane.

6.2.1.2 Morphology of sPEEK-SLM composite membrane

The morphology of the membranes was studied using scanning electron microscopy (SEM). Figure 6.2 shows the cross-sectional SEM images of the ACCUREL membrane support and sPEEK-ACCUREL composite membrane at a magnification of 2,500×.
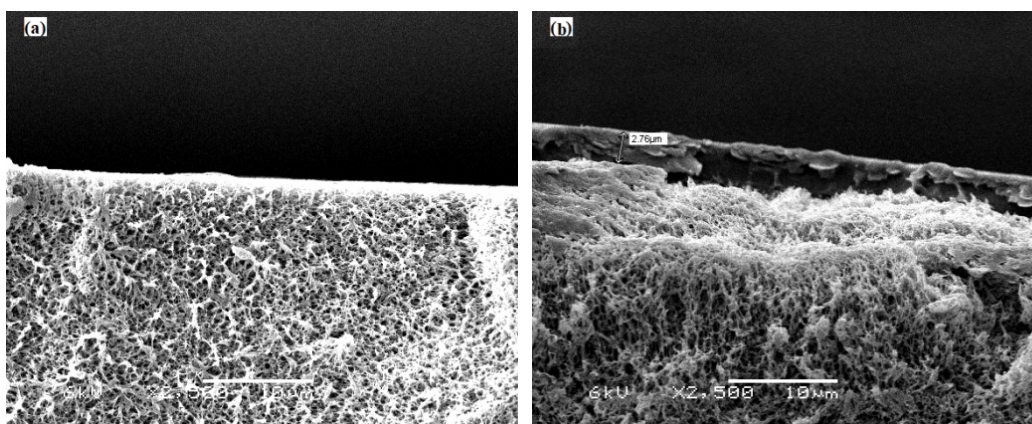

Figure 6.2 SLM images of (a) ACCUREL membrane support and (b) sPEEK-ACCUREL composite membrane at magnification of.

The pores of the membrane support in both images are uniformly distributed across the entire cross section, and represent the region where organic solvent is impregnated. The top layer in Figure 6.2(b) is the successfully coated sPEEK layer. The thickness of the sPEEK layer ranges between 1.8-2.9 μm (thickness of the ACCUREL membrane support is 100 μm). The coating thickness observed under SEM is consistent with the ones reported by Wijers *et al*.[15] for dip coating and Kemperman[16] for interfacial polymerization.

6.2.1.3 Membrane stability preliminary testing

The long-term membrane stability under ED conditions of the sPEEK-SLM was monitored during 10 consecutive experiments of 48 h each, in equimolar (25 mM) mixed salt solutions. The testing solutions were refreshed after each ED experiment. All other experimental conditions were the same as previously stated (Chapters 4 and 5). Figure 6.3 shows the flux changes over time of Na^+, K^+ and Ca^{2+}. During long-term ED operation, the preference of ion permeation was in the order of $K^+ > Ca^{2+} > Na^+$ and remained the same during all 10 experiments. The (time course of the) fluxes of K^+, Na^+ and Ca^{2+} were stable and found to be in the range of 0.1-0.25, 0.025-0.05 and 0.025-0.1 mol·m^{-2}·h^{-1}, respectively over a total time period of 480 hrs. Comparison Figure 6.3 with Figure 5.8 (Chapter 5), representing the data for the uncoated SLM, shows a similar stable membrane selectivity and more or less the same stable flux magnitudes. For example, the initial K^+ flux in the uncoated SLM is around 0.30 mol·m^{-2}·h^{-1} versus 0.25 mol m^{-2}·h^{-1} in the coated SLM as all experiments were carried out under constant current mode. However, a higher cross membrane potential was needed for the sPEEK-SLM compared to the uncoated SLM to maintain the set fixed current density conditions.
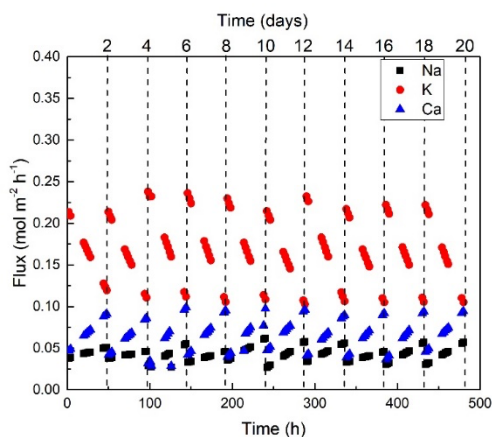
Figure 6.3 Fluxes carried by Na$^+$, K$^+$ and Ca^{2+} through the sPEEK-coated SLM under ED conditions during 20 days of operation.

The stability, in terms of NPOE content, of the SLM and sPEEK-SLM was also checked by means of measuring the weight of the membrane before and after one ED measurement of 10 hrs. Before checking the weight, the membrane was first dried in the vacuum oven at 40 °C overnight. A weight decrease of 9.9 g (about 3.7% of the original NPOE content) was found for the SLM while for the sPEEK-SLM the weight change was below 0.7 g (about 0.3% of the original NPOE content). In other words, the weight loss decreased by a factor of ≈12 upon the addition of sPEEK-SLM coating.

From these preliminary coating experiments, we conclude that coating does not, or at least hardly, compromise SLM functioning. Based on the weight loss reduction after coating, due to retaining the NPOE more effectively inside the ACCUREL support, we conclude that coating improves the stability and with that the life-time of the SLM. During the 480 h stability ED experiment, no indication that the additional sPEEK layer detached from the SLM was observed.

6.2.2 Membrane development

Compared with the data shown in Table 1.1 (Chapter 1), the SLM developed here shows a promising permeation selectivity among monovalent and divalent cations. Nevertheless, the SLM suffers, as all other membrane types do as well, from a principle generally known as the 'trade off' effect in membrane technology.[17] This

175

principle holds that, in general, a high selectivity pairs with low fluxes and *vice versa*. Figure 6.4 summarizes ion fluxes in relation to the membrane mono-/divalent cation selectivity or mono-/monovalent cation selectivity of cation-exchange membranes reported in the literature, as well as those of the SLM presented in this study.[18,19,28,20–27] The "trade-off" effect can be clearly observed. Ideal membrane performance combines high selectivity with high fluxes, which in Figure 6.4 would be represented as a data point in the top right corner. Note that all data points are positioned left of a barrier, indicated here by the dotted line, the so-called upper bound.[17] Crossing the upper bound still remains a key challenge of current membrane development. When focusing specifically on selectivity amongst monovalent cations (K^+/Li^+ and K^+/Na^+), it can be seen that our SLM shows relatively high selectivity but low flux magnitudes.
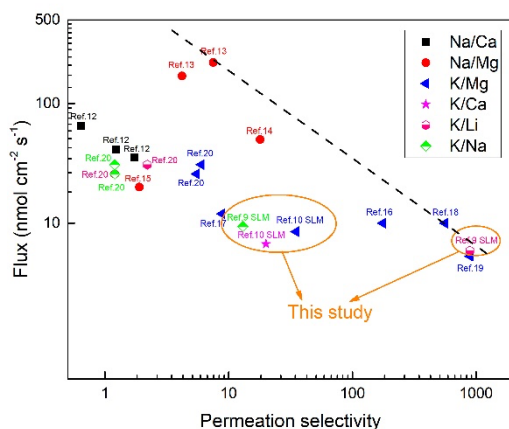

Figure 6.4 Upper bound relationship for mono-/monovalent and mono-/divalent cation separation. Data collected from references [18,19,28,20–27].

Generally, ion exchange between the water and membrane phase depends on ion partitioning, ion pair formation with the ion-exchange sites (the borate sites in case of the SLM) and ion electrophoretic mobility of the free (*i.e.*, non-complexed) ions in the membrane. In general, ion selectivity of ion-exchange membrane can be achieved by: 1) improving the sieving effects or electrostatic barrier effects of the membrane by a thin, dense layer on top of the membrane or by changing the membrane polymer itself; 2) change the nature of the charged groups in the membrane; 3) adding a

176

chelating agent to the feed, and 4) differences in dehydration energy between ion species entering the membrane.[29,30]

In Chapters 3 and 4, the importance of ion dehydration was addressed. Given the difference in relative dielectric constant between NPOE (24) and the one of water (80), differences in dehydration energy can be exploited to turn the SLM in a selective membrane. As shown in this thesis, this effect is strong enough to separate two ion species of the same valance, *e.g.* K⁺ and Na⁺. The inclusion of negatively charged borate moieties in the NPOE serves two goals, 1) to improve the cation over anion selectivity, and 2) to increase the cation content of the SLM, thereby lowering the membrane resistance, a topic closely related to the discussion in the next section.

6.2.3 Energy consumption in ED process for water treatment

A hurdle to take on the way of the implementation of this type of SLMs in real-life applications, is to lower the membrane resistance because this is a key parameter directly linked to energy consumption. Chapter 5 presents two potential tandem schemes by combining an SLM and a CIMS for greenhouse water treatment. Our simulation study shows high recovery rates of water, K⁺, Ca²⁺ and Mg²⁺. As an extension to Chapter 5, here we address the energy consumption solely related to ED, for both scenarios, *i.e.* a CIMS followed by an SLM and the other way around. All simulations were performed by assuming membrane stacks with a surface area of each individual membrane of 1 m². Each cell pair consists of an anion-exchange membrane (AEM), a cation-exchange membrane (in this case the SLM or the CIMS), and two spacer channels. Operational parameters are as defined in Table 5.2.

The cell potential V over the entire stack is the product of the potential over a single cell pair (V_c) and the number of cell pairs (N), $V=N{\times}V_c$. The power consumption of ED, expressed per m³ of treated water, is[31]:

$$P_{ED} = N\frac{V_c I A_c}{Q_{d,c}} = \frac{VIA}{Q_d} \tag{6.1}$$

with P_{ED} in kWh/m³. V_c, A_c and $Q_{d,c}$ represent the voltage per cell pair, the surface area of a single membrane and the dilute volumetric flow per cell pair, respectively. Note that P_{ED} is independent of the design of the stack, *i.e.* independent of N but just

depends on the total voltage over the stack (V), the total membrane surface area (A) and the total dilute volumetric flow (Q_d), at any given current density.

The (average) cell pair potentials V_c were obtained from measurements using the six-compartment cell, and were 3.2 V and 9 V for the CIMS and SLM, respectively. According to Eq. 6.1, P_{ED} values for both scenarios fall in the range of 300-400 kWh·m^{-3}. Typical values found in the literature range from 0.1-2 kWh·m^{-3}, depending on the salt concentration and the extent of desalination.[31] The main reason for the exceptional high value we calculate is the high resistance and consequently high voltage drop over the SLM. Ways to lower the SLM resistance include: (1) increasing the IEC by a different combination of salt and organic solvent, (2) reduction of the membrane thickness from 100 μm, preferably to the <10 μm range, possibly in combination with a porous support rendering the necessary mechanical strength.

The high membrane resistance of the SLM is caused by the low IEC of the membrane (0.085 mEq·g^{-1}) and, as described in Chapter 4, the (electrostatic) interaction between the cations passing the membrane and the borate sites, resulting in a reduction of the mobile charge carrier density.

The challenge of any SLM application is to combine opposing requirements, as the choice of the impregnated solvent has an effect on the extent of hydration/dehydration of the entering ions, lower solvent permittivity requires higher extent of dehydration, and in this way on the ion permeation selectivity. A low membrane resistance requires a high IEC and a high mobile charge density. The relation between these two parameters and the permittivity of the solvent is less obvious. It is expected that the solubility of a lipophilic salt like the Na-borate derivate used in this study shows an optimum as function of the permittivity of the solvent, implying the permittivity should not be too low. On the other hand, a too high permittivity compromises the charge selectivity of the SLM because the Donnan exclusion mechanism is less effective in keeping anions out, even at higher borate densities and especially at higher salt concentrations of the embedding solution.

A final word on membrane resistance relates to the so-called percolation theory. One can envision essentially two ways an ion can move through the SLM. Given the Na- or K-borate complex is electroneutral, and with that insensitive to the electric field, one way is by migration as free, dissociated ion. The alternative is a mechanism based on hopping from one borate site to another. Tongwen *et al*.[32] provided a general percolation model applicable to all ionomeric systems. They showed that only when the IEC exceeds a certain threshold value, ions start to flow through the

membrane. An increase of charge density, just from 1.02 to 1.1 g·cm^{-3} (*i.e.* ≈8 % increase), increased the membrane conductance more than 220,000 times. With an SLM Na-borate concentration of 50 mM, the charge density of the SLM is about 0.044 g·cm^{-3}, which is a factor of 25 lower than the abovementioned value that resulted in a significant conductance difference. Even though we compare two entirely different membrane systems, the percolation theory may hint to a possibly attractive way to substantially lower the resistance of future SLM designs.

6.3 Concluding remarks

The initial aim of this thesis was to develop a membrane with a high Na$^+$ permeation selectivity. However, even after inclusion of a, according to the literature, Na$^+$-selective crown ether (<u>Chapter 3</u>), the SLM still exhibited a preference for permeating K$^+$. The only effect of the crown ether was an inhibition of the K$^+$ flux. The reason for this comes from the low free Na$^+$ concentration in the membrane compared to the high K$^+$ concentration. Despite the complexation constant for Na$^+$ is higher than for K$^+$, more K$^+$-crown ether complexes are formed. As a result, we ended up with a K$^+$-selective SLM, solely containing NPOE and a Na-borate derivative. The underlying working mechanism of the SLM is a combination of differences in dehydration energy and electrophoretic mobility of the ion species involved. As the SLM shows K$^+$ permeation selectivity, the selective removal of Na$^+$ requires a two-step process. While using the experimentally obtained permeation characteristics of the SLM and the commercially available CIMS, a simulation study shows promising results with most K$^+$, Ca^{2+} and Mg^{2+} recovered and the Na$^+$ level kept below the set threshold. Directions to further improve the long-term stability of the SLM are provided. Future research should also focus on lowering the membrane resistance, which can be achieved by increasing the charge density of lipophilic salt used and/or reducing the membrane thickness.

6

References

[1]   A.M. Neplenbroek, D. Bargeman, C.A. Smolders, Mechanism of supported liquid membrane degradation: emulsion formation, J. Memb. Sci. 67 (1992) 133–148. https://doi.org/10.1016/0376-7388(92)80021-B.

[2]   R.N.R. Sulaiman, N. Jusoh, N. Othman, N.F.M. Noah, M.B. Rosly, H.A. Rahman, Supported liquid membrane extraction of nickel using stable composite SPEEK/PVDF support impregnated with a sustainable liquid membrane, J. Hazard. Mater. 380 (2019) 120895. https://doi.org/10.1016/J.JHAZMAT.2019.120895.

[3]   M.C. Wijers, M. Wessling, H. Strathmann, Limitations of the lifetime stabilization of supported liquid membrane by polyamides layers, Sep. Purif. Technol. 17 (1999) 147–157. https://doi.org/10.1016/S1383-5866(99)00036-2.

[4]   H. Strathmann, Membrane separation processes: Current relevance and future opportunities, AIChE J. 47 (2001) 1077–1087. https://doi.org/10.1002/aic.690470514.

[5]   A.J.B. Kemperman, H.H.M. Rolevink, D. Bargeman, T. Van Den Boomgaard, H. Strathmann, Stabilization of supported liquid membranes by interfacial polymerization top layers, J. Memb. Sci. 138 (1998) 43–55. https://doi.org/10.1016/S0376-7388(97)00202-0.

[6]   T. Jin, J. Song, J. Zhu, L.D. Nghiem, B. Zhao, X.M. Li, T. He, The role of the surfactant sodium dodecyl sulfate to dynamically reduce mass transfer resistance of SPEEK coated membrane for oil-in-water emulsion treatment, J. Memb. Sci. 541 (2017) 9–18. https://doi.org/10.1016/J.MEMSCI.2017.06.079.

[7]   M.C. Wijers, M. Jin, M. Wessling, H. Strathmann, Supported liquid membranes modification with sulphonated poly(ether ether ketone): Permeability, selectivity and stability, J. Memb. Sci. 147 (1998) 117–130. https://doi.org/10.1016/S0376-7388(98)00131-8.

[8]   T. He, Towards stabilization of supported liquid membranes: preparation and characterization of polysulfone support and sulfonated poly (ether ether ketone) coated composite hollow fiber membranes, Desalination. 225 (2008) 82–94. https://doi.org/10.1016/J.DESAL.2007.04.090.

[9]   T. He, L.A.M. Versteeg, M.H.V. Mulder, M. Wessling, Composite hollow fiber membranes for organic solvent-based liquid–liquid extraction, J. Memb. Sci. 234 (2004) 1–10. https://doi.org/10.1016/J.MEMSCI.2003.12.015.

6

[10]   Y. Wang, F.M. Doyle, Formation of epoxy skin layers on the surface of supported liquid membranes containing polyamines, J. Memb. Sci. 159 (1999) 167–175. https://doi.org/10.1016/S0376-7388(99)00047-2.

[11]   Y. Wang, Y.S. Thio, F. M. Doyle, Formation of semi-permeable polyamide skin layers on the surface of supported liquid membranes, J. Memb. Sci. 147 (1998) 109–116. https://doi.org/10.1016/S0376-7388(98)00129-X.

[12]   C. He, M.D. Guiver, F. Mighri, S. Kaliaguine, Surface orientation of hydrophilic groups in sulfonated poly(ether ether ketone) membranes, J. Colloid Interface Sci. 409 (2013) 193–203. https://doi.org/10.1016/J.JCIS.2013.06.063.

[13]   J. Xi, W. Dai, L. Yu, Polydopamine coated SPEEK membrane for a vanadium redox flow battery, RSC Adv. 5 (2015) 33400–33406. https://doi.org/10.1039/C5RA01486G.

[14]   S. Sonpingkam, D. Pattavarakorn, Mechanical Properties of Sulfonated Poly (Ether Ether Ketone) Nanocomposite Membranes, Undefined. 5 (2014) 181–185. https://doi.org/10.7763/IJCEA.2014.V5.374.

[15]   M.C. Wijers, M. Jin, M. Wessling, H. Strathmann, Supported liquid membranes modification with sulphonated poly(ether ether ketone). Permeability, selectivity and stability, J. Memb. Sci. 1998 (1998) 117–130. https://doi.org/10.1016/S0376-7388(98)00131-8.

[16]   A.J.B. Kemperman, H.H.M. Rolevink, D. Bargeman, T. Van Den Boomgaard, H. Strathmann, Stabilization of supported liquid membranes by interfacial polymerization top layers, J. Memb. Sci. 138 (1998) 43–55. https://doi.org/10.1016/S0376-7388(97)00202-0.

[17]   L. Ge, B. Wu, D. Yu, A.N. Mondal, L. Hou, N.U. Afsar, Q. Li, T. Xu, J. Miao, T. Xu, Monovalent cation perm-selective membranes (MCPMs): New developments and perspectives, Chinese J. Chem. Eng. 25 (2017) 1606–1615. https://doi.org/10.1016/j.cjche.2017.06.002.

[18]   Z. Qian, H. Miedema, S. Sahin, L.C.P.M. de Smet, E.J.R. Sudhölter, Separation of alkali metal cations by a supported liquid membrane (SLM) operating under electro dialysis (ED) conditions, Desalination. 495 (2020) 114631. https://doi.org/10.1016/j.desal.2020.114631.

[19]   Z. Qian, H. Miedema, L.C.P.M. de Smet, E.J.R. Sudhölter, Permeation selectivity in the electro-dialysis of mono- and divalent cations using supported liquid membranes, Desalination. 521 (2022) 115398. https://doi.org/10.1016/j.desal.2021.115398.

6

[20]   S. Abdu, M.-C. Martí-Calatayud, J.E. Wong, M. García-Gabaldón, M. Wessling, Layer-by-Layer Modification of Cation Exchange Membranes Controls Ion Selectivity and Water Splitting, ACS Appl. Mater. Interfaces. 6 (2014) 1843–1854. https://doi.org/10.1021/AM4048317.

[21]   L. Ge, B. Wu, Q. Li, Y. Wang, D. Yu, L. Wu, J. Pan, J. Miao, T. Xu, Electrodialysis with nanofiltration membrane (EDNF) for high-efficiency cations fractionation, J. Memb. Sci. 498 (2016) 192–200. https://doi.org/10.1016/J.MEMSCI.2015.10.001.

[22]   H. Farrokhzad, M.R. Moghbeli, T. Van Gerven, B. Van Der Bruggen, Surface modification of composite ion exchange membranes by polyaniline, React. Funct. Polym. 86 (2015) 161–167. https://doi.org/10.1016/J.REACTFUNCTPOLYM.2014.08.003.

[23]   H. Farrokhzad, S. Darvishmanesh, G. Genduso, T. Van Gerven, B. Van Der Bruggen, Development of bivalent cation selective ion exchange membranes by varying molecular weight of polyaniline, Electrochim. Acta. 158 (2015) 64–72. https://doi.org/10.1016/J.ELECTACTA.2015.01.062.

[24]   N. White, M. Misovich, A. Yaroshchuk, M.L. Bruening, Coating of Nafion Membranes with Polyelectrolyte Multilayers to Achieve High Monovalent/Divalent Cation Electrodialysis Selectivities, ACS Appl. Mater. Interfaces. 7 (2015) 6620–6628. https://doi.org/10.1021/AM508945P.

[25]   G.S. Gohil, V. V. Binsu, V.K. Shahi, Preparation and characterization of mono-valent ion selective polypyrrole composite ion-exchange membranes, J. Memb. Sci. 280 (2006) 210–218. https://doi.org/10.1016/J.MEMSCI.2006.01.020.

[26]   A. Chapotot, G. Pourcelly, C. Gavach, Transport competition between monovalent and divalent cations through cation-exchange membranes. Exchange isotherms and kinetic concepts, J. Memb. Sci. 96 (1994) 167–181. https://doi.org/10.1016/0376-7388(94)00107-3.

[27]   S. Yang, Y. Liu, J. Liao, H. Liu, Y. Jiang, B. Van Der Bruggen, J. Shen, C. Gao, Codeposition Modification of Cation Exchange Membranes with Dopamine and Crown Ether to Achieve High K+ Electrodialysis Selectivity, ACS Appl. Mater. Interfaces. 11 (2019) 17730–17741. https://doi.org/10.1021/acsami.8b21031.

[28]   Y. Zhu, M. Ahmad, L. Yang, M. Misovich, A. Yaroshchuk, M.L. Bruening, Adsorption of polyelectrolyte multilayers imparts high monovalent/divalent cation selectivity to aliphatic polyamide cation-exchange membranes, J. Memb. Sci. 537 (2017) 177–185. https://doi.org/10.1016/j.memsci.2017.05.043.

6

[29]   T. Sata, Studies on ion exchange membranes with permselectivity for specific ions in electrodialysis, J. Memb. Sci. 93 (1994) 117–135. https://doi.org/10.1016/0376-7388(94)80001-4.

[30]   L. Ge, B. Wu, D. Yu, A.N. Mondal, L. Hou, N.U. Afsar, Q. Li, T. Xu, J. Miao, T. Xu, Monovalent cation perm-selective membranes (MCPMs): New developments and perspectives, Chinese J. Chem. Eng. 25 (2017) 1606–1615. https://doi.org/10.1016/j.cjche.2017.06.002.

[31]   S.K. Patel, P. Maarten Biesheuvel, M. Elimelech, Energy Consumption of Brackish Water Desalination: Identifying the Sweet Spots for Electrodialysis and Reverse Osmosis, (2021). https://doi.org/10.1021/acsestengg.0c00192.

[32]   X. Tongwen, Y. Weihua, H. Binglin, Ionic conductivity threshold in sulfonated poly (phenylene oxide) matrices: A combination of three-phase model and percolation theory, Chem. Eng. Sci. 56 (2001) 5343–5350. https://doi.org/10.1016/S0009-2509(01)00242-1.

6

Acknowledgment

Thank you
Bedankt
谢谢

"Life is like a box of chocolates, you never know what you're gonna to get." Five years ago, before coming to the Netherlands, I had never imagined that I would live, study and work in Europe. But here I am, at the end of my PhD journey, and just started a new job and have a family. It wouldn't be possible for me to reach to these milestones without everyone who has played an important part in my project and in my life.

The chairman and members of the **Doctoral Committee**. Thank you for all the time and efforts you have put into reading this dissertation, the critical evaluation of it, and becoming a part of my defense.

My sincere appreciation goes to my **supervision team** Ernst Sudhölter (1st promoter), Louis de Smet (co-promoter) and Henk Miedema (co-promoter and Wetsus supervisor). **Ernst**, I would like to thank you for all your support and guidance during all those years. You are always positive and constructive. Your expertise in organic chemistry, membranes and electrochemistry contributed significantly to my project. Our talks always brought new insights for my research. **Louis**, I would like to thank you for all your support along the way of my project. I would never complete all the complicated organic synthesis without your kindness offer of doing it at WUR-ORC. I also learned a lot from you in scientific writing and presenting my work. All this made me better qualified as a researcher. **Henk**, when I started the project, I know very little about electrochemistry and desalination processes, but you guided me through the learning process and gave me all the freedom on exploring this attracting field. I showed you a huge amount of results over the years, a mixture of (initially) confusing and interesting, and instructive ones. You taught me no results are ever bad. With the nice discussions we had, there were always new ideas or insights I could find. The PhD journey can sometime be difficult and challenging, but you were always there to encourage me. Thank you for all the support and supervision. It is a great experience to work with you!

Wetsus. Wetsus is an amazing place to do research. The expertise, resources and support brings up the maximized that all researchers can do. Thank you **Cees, Bert and Johannes** for making – and keeping – all this possible.

Desalination Theme. Many thanks to all the participants and fellow PhDs of our research theme for the nice and fruitful discussions and their financial support. Special thanks to **Van der Knaap** and **Yara**, partners of this project, for the support and information you gave for the past years. It was a great pleasure to have the chance working together with you.

I would also like to give my gratitude to my beloved **family**. 感谢我的**妈妈**，你为了我的成长和发展，在过去的几十年中，牺牲很多，付出了极大的心血。你给予我了无私的爱，并且尽最大程度的让我接受最好的教育。竭尽所能的给予我精神和经济上的支持和帮助。因为你，我的成长和求学道路更加轻松顺畅。**Mia**，我最亲爱的豆豆宝贝。你是妈妈人生中可以获得的最好的礼物。因为你的到来，让生活中的一切都变得更有意义，也让妈妈成为了更好的自己。感谢我其他的**家人**，你们对我的爱和支持，是在我人生道路中可以获得的最好的馈赠。在我在外求学的这十几年中，虽然跟你们聚少离多，但是你们一直在默默的支持我。没有所有家人的理解和支持，我也无法顺利完成我的博士学习。Diego, thank you for all the love and support; without you, it would never have been possible for me to have the second family here in the Netherlands. Nadia and Dario, thank you for your support and the nice reunions we had in the Netherlands, Italy and Germany.

Thank you, my office mates from the **office of happiness**: Antoine, Casper, Enas, Ilse, Jorrit, Louis, Naghme, Suyash, Sofia, Tania, Yin, Olga, Nandini, Rita, and Edwin. All of you together created a great atmosphere in the office, making my daily work much enjoyable.

To my other **Wetsus colleagues and friends**: Hakan, Paulina, Rose, Gijs, Yujia, Xiaoxia, Qingdian, Gaofeng, Yanyue, Bingnan, Yang, Danielle, and all other friends, thank you for the nice time we spent together.

Many thanks to the **Wetsus analytical team**. I could never achieve what I have achieved now without the efforts you made for analyzing the huge amount of samples I made.

Thanks to the **Wetsus technicians**. **Harm**, as the assigned technician to my project, thank you for your technical supports and helping me with building up my setup and keep it running.

I would also like to thank the **ORC group** from Wageningen University. **Sevil**, thank you for your warm welcome and help during my time in Wageningen. All the synthesis works would have been much more difficult without your help. **Kaustub,** thank you for being a nice friend and neighbor. I enjoyed all our little discussions and it was great experience to see all the assumptions from those discussions became true. **Barend**, thank you for your help with all the analyses you have done for me.

Last but not the least, for all the people I forgot to mention: thank you!

About the author

Zexin Qian was born on July 5, 1992 in Xi'an, China. After finishing her high school degree in 2010, she started studying *Chemical Engineering and Technology* at Sichuan University. This BSc study was completed with a thesis on removal of Cu^{2+} ions using multiwalled nanotubes as a novel nanosorbent.
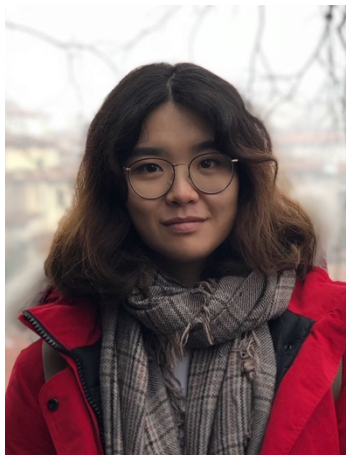
Zexin continued with an MSc study in Chemical Engineering, at University of Cincinnati, United States in 2014. This study was completed with a thesis on the topic of "*the impact of humidity on an optical chemical sensing device for non-invasive exhaled gas monitoring*".

In December 2016, Zexin started as a PhD candidate in the Organic Materials & Interfaces group at Delft University of Technology, performing her research activities at Wetsus, Leeuwarden. The research focused on selective ion separation using supported liquid membranes. The results are presented in this thesis.

List of publications

Journal articles:

Qian, Z., Miedema, H., de Smet, L.C.P.M. and Sudhŏlter, E.J.R., 2018. Modelling the selective removal of sodium ions from greenhouse irrigation water using membrane technology. *Chemical Engineering Research and Design*, *134*, p.154-161.

Singh, K., Qian, Z., Biesheuvel, P.M., Zuilhof, H, Porada, S., de Smet, L.C.P.M., 2020. Nickel hexacyanoferrate electrodes for high mono/divalent ion-selectivity in capacitive deionization. *Desalination, 481,* 114346.

Qian, Z., Miedema, H., Sahin, S., de Smet, L.C.P.M. and Sudhŏlter, E.J.R., 2020. Separation of alkali metal cations by a supported liquid membrane (SLM) operating under electro dialysis (ED) conditions. *Desalination*, *459*, 114631.

Xu, S., Song, J., Bi, Q., Chen, Q., Zhang, W., Qian, Z., Zhang, L., Xu, S., Tang, N., He, T., 2021. Extraction of lithium from Chinese salt-lake brines by membranes: Design and practice. *Journal of Membrane Science, 635,* 119441.

Qian, Z., Miedema, H., de Smet, L.C.P.M. and Sudhŏlter, E.J.R., 2022. Permeation selectivity in the electro-dialysis of mono- and divalent cations using supported liquid membranes. *Desalination*, *521*, 115398.

Qian, Z., Miedema, H., Pintossi D., Ouma M. and Sudhŏlter, E.J.R., Selective removal of sodium ions from greenhouse drainage water – a combined experimental and theoretical approach. [Submitted to *Desalination*]

Other contributions:

Oral presentation at the 4th International Conference on Desalination using Membrane Technology, 2019. (3rd prize)

Oral presentation at the International Congress on Membrane & Membrane Processes, 2020.

Propositions

1. Selective desalination by electrodialysis is a promising approach to exploit a variety of water resources.

This proposition pertains to this dissertation.

2. Supported liquid membranes offer new possibilities for ion-selective desalination.

This proposition pertains to this dissertation.

3. The exchange of ions over the water – supported liquid membrane interface is dominated by ion dehydration energy.

This proposition pertains to this dissertation.

4. The balance between membrane permeation selectivity, transport rate and electrical resistance determines the optimal performance of ion-selective supported liquid membranes.

This proposition pertains to this dissertation.

5. Guts to innovate cannot be missed in doing groundbreaking research.

6. In trying to solve problems, a little help from my friends makes wonders.

7. The unknown is always full of surprises and often gives birth to charming feelings.

8. Dedicated analysis of complex experimental data sets needs a framework.

9. There are no such things like waste, there are only resources.

10. Cycling is a beloved Dutch tradition, no matter how the weather is.